Indonesian climate investigations using stable isotopic data from modern, Holocene and Pliocene corals

Submitted in partial fulfilment of the requirements for the degree of Master of Science in Geology

at the University of Canterbury

By Louise Dawn Moody

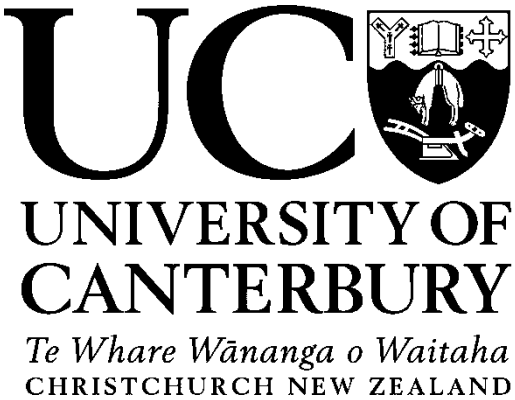

2012

Frontispiece

Coastal scene looking south to the Timor Sea.

Dedication

To Oma, whose adventurous spirit will always be with us.

Thesis Abstract

Earth's climate system has experienced significant changes throughout its history. Tropical, glacial and interglacial conditions have persisted across the globe during the Tertiary, and the present interglacial period with strong seasonality and episodes of warming and cooling has existed for the last several thousand years. However, rapid warming during the last century has highlighted the importance of understanding past climate behaviour, in order to predict the likely effects of such warming on our future climate. This has led to the use of proxies, such as sediment cores, tree rings, ice and carbonates, which provide high resolution palaeoclimate archives. Studies using a variety of proxies from around the globe have developed a network of site specific climate information, offering insights of climate fluctuations on a millennial scale, and identifying changing oceanic conditions as a major influence on global climate change. Coral skeletons are particularly sensitive recorders of ambient seawater conditions as they record fluctuations of oxygen and carbon in their aragonitic skeletons, which are caused by perturbations of sea surface temperature (SST) and sea surface salinity (SSS). Therefore, tropical oceans themselves provide a crucial record of climate change. Many of the coupled atmospheric-oceanographic processes that drive the global climate system occur in the Indo-Pacific, making it a particularly important region for data collection. *Porites* corals from the Indo-Pacific have been studied in detail and have revealed high resolution SST and SSS records, yet comprehensive investigations using other coral species are minimal. This study expands upon the current understanding of coral proxies by investigating three coral species of different ages, and provides new insights into the palaeoclimate history of the Indo-Pacific.

Goniastrea retiformis, *Platygyra pini* and *Platygyra lamellina* corals have been retrieved from Timor Leste in the Indo-Pacific, and analysed using stable and radiogenic isotopic techniques. Sclerochronology was used to determine that the 4.5 year old, modern *G. retiformis* coral was living from 2006-mid 2010. Uranium-thorium (U/Th) analysis provided a mid Holocene age of 4.5 ± 0.092 (2σ) ka for the fossil *P. pini*. Uranium-lead (U/Pb) techniques were used to obtain a 2.7 ± 0.34 (2σ) Ma age for the fossil *P. lamellina.* A rigorous diagenetic screening process of X-ray diffraction (XRD), petrographic analysis of thin sections, and scanning electron microscopy (SEM) has been carried out to ascertain the extent of preservation in each coral. X-ray images allow annual density bands to be located

and unique micromilling paths were developed for the three samples. This enabled us to obtain the first $\delta^{18}O$ and $\delta^{13}C$ stable isotope results for a *G. retiformis* coral, and the first fossil coral results for the *Platygyra* genus. Cross spectral analysis has been used to verify the periodicity of seasonal fluctuations visible in the data, and confirmed that these coral species are suitable for use as climate proxies.

G. retiformis is an abundant reef coral distributed throughout the tropical Pacific, and has a robust skeletal configuration making it suitable for use as a climate proxy. The 4.5 year long record has revealed that $\delta^{18}O$ and $\delta^{13}C$ values range from -4.62‰ ± 0.03‰ (2σ) to -6.11‰ ± 0.02‰ (2σ), and 1.57‰ to -2.53‰, with means of -5.35‰ and -1.02‰, respectively. These values are in agreement with the average $\delta^{18}O$ range of -5.1 to -5.6‰ in modern corals throughout the Indo-Pacific, predominantly of the *Porites* genus. Statistical analysis of the isotopic data has revealed a quasi-biennial signal in *G. retiformis*, typical of the temporal interaction between El Niño Southern Oscillation (ENSO) and the South Asian monsoon. Results have also been compared to the Southern Oscillation Index (SOI) in order to assess potential relationships between coral isotopes and ENSO. This has shown an accurate record of El Niño and La Niña events for the first half of the ~ 4.5 year record, from 2006 to mid 2008. Climate processes such as local rainfall and the Indian Ocean Dipole (IOD) are also reflected in the record, to varying extents.

The use of *Platygyra* corals as climate proxies is limited to three investigations using modern samples, despite the fact that this genus has a much broader latitudinal range than the extensively studied *Porites* genus. This thesis provides the first examination of fossil samples, and provides analysis of both pristine and altered specimens. The 4.5 ka *P. pini* coral has allowed investigation of the palaeoclimate record in a sample that has been exposed to diagenesis. XRD, petrographic and SEM analyses have revealed widespread secondary aragonite growth, dissolution and secondary calcite within the coral, which would have occurred due to marine and freshwater diagenesis. However, primary growth textures have been retained in some areas of the coral. $\delta^{18}O$ and $\delta^{13}C$ values range from -3.47‰ ± 0.03‰ (2σ) to -5.45‰ ± 0.02‰ (2σ), and 3.43‰ to -0.49‰, with means of -4.82‰ and 1.12‰, respectively. These values are significantly more positive that the mean $\delta^{18}O$ of four *Platygyra* corals from the Pacific region, which range from -4.82‰ to -5.10‰. There are two reasonable explanations for this. Secondary aragonite, which is detected throughout the

milled section of coral, causes positive shifts in coral $\delta^{18}O$, an effect which is likely to have altered the geochemical record of this particular coral. But the fact that SST in the southern Indo Pacific Warm Pool (IPWP) during the mid Holocene were 1.2° C cooler than present must also be acknowledged, as cooler temperatures also impart a shift toward higher $\delta^{18}O$, due to equilibrium fractionation processes. SST reconstruction using the temperature dependence equation from a modern *Platygyra* coral reveals an SST range of 18.5-27.6° C, and mean of 24.7° C. The present day mean annual SST of 28° C suggests that mid Holocene temperatures less than 26.8° C are unrealistically cool, highlighting the fact that isotopic fractionation during diagenesis has affected coral chemistry. However, the presence of interannual periodicity indicates that ENSO was operating, and the magnitude of isotopic fluctuation through the 10 year record is similar to that found in modern and other Holocene corals. We suggest that although absolute isotopic and SST values are unreliable, prohibiting the extraction of high resolution climate records, insights into the behaviour of broad scale, seasonal and interannual climate processes may still be obtained.

A strong annual periodicity has been detected when analysing the stable isotopic values recorded in the 2.7 Ma *P. lamellina* coral. This indicates that seasonal SST fluctuations were the dominant influence on this coral. Ranges of -4.67‰ ± 0.03‰ (2σ) to -5.48‰ ± 0.02‰ (2σ) and 0.88‰ to -1.12‰ for $\delta^{18}O$ and $\delta^{13}C$, respectively, are similar to modern *Platygyra* coral results, suggesting that this coral has been preserved in pristine condition. Palaeo-SSTs have been reconstructed using a modern *Platygyra* temperature dependence equation, providing a range of 24-27.7° C and a mean of 25.9° C. Foraminiferal data from sediment cores in the greater Indo-Pacific suggest that mean annual SSTs at this time were ~ 2-3° C cooler than present. The coral record I present supports this statement, providing new insights into our understanding of tropical palaeoclimates. This coral has been entrained within a turbidite deposit on the sea floor that has subsequently been uplifted during the emergence of Timor, with U/Pb dating allowing further constraints of the stratigraphic age of the deposit. Tectonic narrowing is postulated to have caused major changes to the Indonesian Throughflow (ITF) from 4-2 Ma, and been a driver of major global climate change beginning in the late Pliocene. This means that fossil *Platygyra* corals Timor Leste could provide unique time slices of information about this important time in global climate history.

This study confirms that *G. retiformis*, *P. pini* and *P. lamellina* corals are excellent candidates for further, detailed investigations. They provide the opportunity to develop new coral proxies which are both abundant throughout the tropics and distributed over a wide latitudinal range. Their prevalence in both modern and fossil reefs means that once modern samples of each species have been calibrated against modern SST and SSS, these corals will provide reliable, quantitative palaeoclimate proxies, with potential for data capture throughout the Indo-Pacific and mid latitudes. Geochemical coral archives are a crucial tool in the study of climate processes, and we believe that these species are ideally suited to enhancing and refining our current understanding of earth's climate system.

Acknowledgements

First and foremost I would like to thank Mark Quigley for giving me the opportunity to undertake this exciting yet challenging research. I have appreciated the freedom you have given me to explore the topic as I saw best, and relied upon your positivity and enthusiasm throughout. Not to mention piggy backing me through the river when I was plagued with trench foot! The experiences I have had during this thesis, especially the month of fieldwork in Timor Leste, have been an unexpected and extremely rewarding time in my life. Thanks to Mark, Brendan Duffy, Jamie Shulmeister, Lamberto Fernandes, Jhony dos Reis, Jhony Soares, Atino Varela and Nabe for sharing an intrepid field season in 2010, which although "not ideal", was a very memorable and unique experience.

This research could not have been carried out without the generous financial support of the Marsden Grant which is gratefully acknowledged.

I am indebted to the NIWA crew of Helen Neil, Peter (Chazz) Marriot and Alan Orpin, whose tireless lab assistance and sample analysis meant that this project could truly take flight. This project would have been impossible without the technical assistance of Kerry Swanson, Rob Spiers, Chris Grimshaw, Stephen Brown, Catherine Brown, and Mike Flaws from the University of Canterbury, and John Futter from GNS Science. Thanks to Kate Bromfield for coming to the rescue and identifying all of my corals! Janet Warbuton assisted me with all the paper work and administration, and a special mention must go to Pat Roberts who greeted my endless requests with a smile, no matter how busy she was. I am very grateful for time spent with Helen McGregor (University of Wollongong), Nerilie Abram (ANU), Jessica Carilli (ANSTO), and Jody Webster (University of Sydney), for their counsel and expert advice when difficulties arose. Thanks to Jon Woodhead and John Hellstrom from the University of Melbourne who dated the corals and provided expert radiogenic isotope advice. The data analysis and quasi-banter sessions with Travis Horton, Josh Blackstock and Tom Brookman were crucial in the final stages of write up, and Travis has also helped me to improve the final manuscript.

To my fellow postgraduate students and friends, you have all been a great network of fun and support. Particular thanks to Lizzie Wandrag, Sophie Bainbridge, Courtney Hutchison, Louise Vick and Lauren Foote for listening to my rants and giving me help when I needed it.

Mum, Dad and Brent – your continual support and trips to Christchurch have been so important to me throughout my university career. It has been fantastic to share so much of this experience with you, and I have never felt far from home.

Lastly, thank you Tom for the dozens of pep talks, encouragement, and fun you've shared with me along the way.

Table of Contents

PROLOGUE TO THE THESIS

SCIENTIFIC CONTEXT

This study has been undertaken in an attempt to increase the temporal and spatial resolution of climate data capture throughout tropical and mid latitude oceans. Previously, *Porites* corals have provided most of the modern and palaeoclimate data from the Indo-Pacfic and central Pacific regions. This genus offers reliable data, but is not the only abundant tropical coral, and is not prolific is mid latitude regions where mean annual SSTs are cooler. Detailed studies using modern, Holocene and Pliocene age corals have provided promising results that these three species are also useful climate proxies. Similar to *Porites,* climate processes such as seasonal variability of SST, ENSO, and monsoon rainfall have been detected in the three geochemical records.

Although there have been many modern coral investigations throughout the Pacific (e.g. Asami et al., 2004; Chiang et al., 2010; Gagan et al., 1994; McGregor et al., 2011), the number of studies using fossil corals is relatively few, and mostly from sites in Papua New Guinea (PNG) and Indonesia (e.g. Gagan et al., 2004; Hughen et al., 1999; McGregor and Gagan, 2004; Tudhope et al., 1995). Only one investigation has been undertaken in West Timor, Indonesia, using a modern *Porites* coral (Cahyarini et al., 2008), and no previous studies using corals from Timor Leste have occurred. The Indo-Pacific is a particularly significant region in the palaeoclimate field as it is the area of highest coral species diversity in the world, giving rise to some of the most detailed climate records available. Over 700 species are located in the region, which is bounded by Sumatra and Java in the southwest, Sabah and the Phillipines in the northwest, and the Phillipines and PNG in the southeast. To the east of this region, coral diversification decreases significantly as proximity to the IPWP reduces. Investigation of the modern *G. retiformis* is important, as it provides the basis for development of this species as a new climate proxy, enabling increased sampling density throughout the tropics.

Pioneering work by Weber and Woodhead (1972), Shen et al., (1987), and Lea et al., (1989) demonstrates that the variability of chemical element compositions in coral skeletons quantitatively reflects past surface chemistry of the oceans, and the fact that coralline aragonite may be altered by both biological and diagenetic processes. During precipitation of

skeletal aragonite, coral metabolic activity ('vital effects') may cause large compositional deviations from thermodynamic equilibrium and compromise geochemical reliability of climate tracers such as SST and SSS (e.g. Montaggioni and Braithwaite, 2009). As a consequence, rigorous diagenetic screening methods for modern and fossil corals have been developed to avoid using altered corals which result in marked biases in both climate reconstruction and age determination using radiometric techniques (e.g. Allison et al., 2007; Hendy et al., 2007; McGregor and Abram, 2008; Scholz and Mangini, 2007). To address the inherent problems with obtaining reliable geochemical data from diagenetically altered corals, a mid Holocene *P. pini* has been selected for investigation. This coral has been subject to diagenetic alteration causing the growth of secondary aragonite, calcite and skeletal dissolution through marine and freshwater processes. A thorough examination of isotopic results has provided new interpretations of the role that diagenetically altered corals may provide as climate proxies.

A geologically young island, Timor can provide important information on the evolution of the Indonesian Seaway, with palynology indicating Timor has only been emergent since the latest Miocene (Nguyen et al., In prep). Therefore, corals living between ~ 5 Ma and the present, such as the 2.7 Ma *P. lamellina*, will have recorded changes in ambient seawater conditions in the Indonesian region. The need for a coral record such as this is revealed when considering the provocative hypothesis presented by Cane and Molnar (2001). They suggest that global climate change beginning 3-4 Myr ago was initiated due to tectonic closure of the Indonesian seaway, with subsequent cooling of the Indian Ocean leading to East African aridification and hominid evolution. This tectonic alteration caused a switch in the source waters of the ITF whereby the cooler, fresher North Pacific water became the dominant source, lowering the Indian Ocean SST and SSS. The shut-off of formerly through flowing waters of the warmer, saltier South Pacific provides a mechanism for terminating the Pliocene 'permanent El Niño'(Molnar and Cane, 2007), and creating the modern ENSO (Gordon et al., 2003; Schott and McCreary, 2001). Pliocene fossil corals contained in marine sedimentary rocks of the Viqueque Megasequence (VM) now exposed on the island of Timor Leste were entrained in turbidite debris flows during storm- and/or seismic-triggered events during the last several million years (Quigley et al., 2012). This sudden entrainment into a turbidite deposit during catastrophic events has meant exceptional preservation of the original, pristine aragonitic coral skeletons. Unlike most corals of similar age around the

world, these particular fossil corals have not undergone extensive weathering to calcite. Therefore, geochemical records contained in Pliocene Indonesian corals provide an excellent proxy for the sequence of events leading to hominid evolution, and the development of the ENSO cycle in the Southern Hemisphere.

The use of corals as climate proxies is demonstrated by a relatively dense network of coral records across the tropical Pacific, which has shown the key role of Pacific-centred ENSO in global climate variability (Gagan et al., 2000). Montaggioni and Braithwaite (2009) explain that climate reconstructions from modern corals in this region indicate a long-term trend of decreasing $\delta^{18}O$ of about 0.17‰ V-PDB, corresponding to a warming of about 0.8°C since the middle of the 19th century. This appears to have started throughout the tropics at the end of the Little Ice Age (LIA) in the mid-18th century and continues throughout the entire tropical Pacific, from the westernmost to the easternmost areas. Given that the coral $\delta^{18}O$ signal is a composite of SST and SSS, the decrease in $\delta^{18}O$ may also incorporate a seawater freshening signal (Cole, 1996). In the western tropical Pacific, SST and SSS have shown interdecadal variations for the last two centuries, in relation to variations in the position of the South Pacific Convergence Zone (SPCZ) and ENSO events (Juillet-Leclerc et al., 2006). The compilation of all coral studies in this and other regions are gradually showing the past trends in climate behaviour which will improve our understanding for future climatic change. The corals studied in this thesis have been selected in the hope of expanding the palaeoclimate proxy network throughout the Indo-Pacific, and revealing new climate data from the terminal Pliocene to present through further investigation of these species.

THESIS STRUCTURE

This thesis is devoted to improving the field of coral palaeoclimate proxies through the investigation of three relatively unstudied corals. As such, the thesis has been divided into three main chapters focusing on each individual coral. Each chapter has been written in the form of a self contained paper with the aim to submit each for peer-reviewed publication upon submission of the thesis. Although separate papers, their unifying aspect is that they each focus on the investigation of a different coral species as a climate proxy from a different period in geological time.

Chapter 1 provides an extensive literature review, beginning with the application of corals as climate proxies, their geochemical behaviour and a thorough guide to analysing stable isotopic data from corals. A discussion of the study area in terms of geologic and climatic parameters through time prepares the reader for more detailed analysis of climatic trends during the time period relevant to each coral record.

Chapter 2 presents the investigation of the modern coral *Goniastrea retiformis* as a new climate proxy for the Indo-Pacific. Stable isotope results of a 4.5 year period from 2006 to mid 2010 indicate that this species is capable of recording ENSO and monsoon interaction, with the recognition of quasi-biennial periodicity. Climate processes such as local rainfall and the IOD are also reflected in the record. This pilot investigation provides evidence that this species is capable of recording geochemical signals of local and regional climate processes, and due to its abundance and skeletal robustness is an ideal candidate for development into a reliable climate proxy.

Chapter 3 presents the investigation of a diagentetically altered 4.5 ka, mid Holocene *Platygyra pini* coral. Extreme isotopic fluctuation in distinct zones of the coral provide unrealistic SSTs of as low as 18.5° C, consistent with "cool" artifacts created by secondary aragonite and dissolution. However, interannual periodicity of 4 and 8.75 years suggests that ENSO is operating, and temporal isotopic fluctuations of ~ 0.4‰ are consistent with other low latitude coral records, an indicator that diagenesis has not obliterated the magnitude of seasonal variation. The preservation of these features within the geochemical record means that climate behaviour can still be analysed. This study shows that although diagenesis masks absolute SST information, altered corals can in fact be used to provide qualitative insights of palaeoclimate processes.

Chapter 4 presents the investigation of the 2.7 Ma *Platygyra lamellina* coral, which offers the oldest seasonal coral record from the southern Indo-Pacific. Isotopic analysis allows the first palaeo-SST interpretation from the terminal Pliocene in the southwest IPWP, with a range of 24.0-27.7° C and mean of 25.9° C consistent with foraminiferal isotopic records, indicating cool anomalies of 2-3° C relative to modern mean annual SSTs. Spectral analysis shows that annual periodicity is dominant in the five year record, suggesting seasonal SST variability is the key climate parameter affecting the geochemical signal. The U/Pb date of this pristine coral also provides the opportunity to improve the temporal resolution of marine

chronostratigraphic records, giving further constraints to the uplift of the turbidite sequence in which the coral is entrained. These oceanographic and tectonic implications outline the importance of detailed investigations using fossil *Platygyra* corals from Timor Leste to increase our understanding of the dynamic processes occurring in the Indonesian Seaway during the terminal Pliocene.

Chapter 5 outlines the conclusions of the thesis, that these three species will play an important role in the collection of climate data from coral proxies.

1 LITERATURE REVIEW

1.1 CORAL AS CLIMATE PROXIES

The state of the global climate system is a topic at the forefront of scientific research since it was noted in the late 20th century that our climate was undergoing changes at an unprecedented rate (IPCC, 2007). Global average temperature is one of the most cited indicators of global climate change, and shows an increase of 0.8°C since the early 20th century (NOAA, 2012). Other ways in which climate change is manifest is in perturbations of precipitation, sea surface temperature (SST) and sea surface salinity (SSS). Such fluctuations are often minute, however can be clearly recorded by entities which incorporate isotopes into their matter. Corals, tree rings, ice, and sedimentary sequences provide palaeoclimatic archives that can, in some instances, be used to reconstruct past climate variability in annual resolution (Felis and Paetzold, 2003). Because instrumental records of climate change are relatively short (~100 years), proxies such as these are important tools for climate research. In particular, corals have emerged as key climate proxies in this field since pioneering studies realised their geochemical potential (Fairbanks and Dodge, 1979; Hudson et al., 1976; Oomori et al., 1983; Swart and Coleman, 1980; Weber and Woodhead, 1970, 1972). Coupled with the fact that they occupy clear, warm shallow-water environments and occur in equatorial and mid latitude oceans around the world (Dullo, 2005), their ability to record geochemical changes in sea water means they are ideally located to record interactions between atmospheric and oceanic processes that occur in the tropics. Due to the favourable year-round water temperatures (26-28°C), the tropical oceans are home to a wealth of coral species. Massive scleractinian corals, such as *Goniastrea*, *Porites*, and *Diploastrea*, grow at rates of millimetres to centimetres per year (Felis and Paetzold, 2003), and produce annual density bands in their aragonitic ($CaCO_3$) skeleton. These bands can be used for the development of chronologies with clear seasonal resolution. Within their annual bands, corals incorporate isotopic and elemental tracers reflecting the environmental conditions in the ambient seawater during their growth, thus offering a rich archive of past climate variability in tropical ocean regions where such instrumental data is particularly limited, and where our knowledge of multi-decadal climate sensitivity is incomplete (Corrège, 2006; Druffel, 1997; Gagan et al., 2000; Wara et al., 2005).

Dunbar and Cole (1999) explain that corals are capable of revealing subtle changes in SST, rainfall and evaporation within the annual cycle, and can provide clues about how seasonal climate responds to large scale forcing and background changes. Also, because many reef sequences in the tropics span millennia, they represent climate conditions during times of very different boundary conditions (Fairbanks et al., 1997). Significant palaeoclimate work on Quarternary fossil corals has been carried out in the Pacific (e.g. Cobb et al., 2003), Australian (e.g. Gagan et al., 1994; Watanabe et al., 2003) and Indonesian regions (e.g. Hughen et al., 1999; Qu, 2007; Sun et al., 2005; Tudhope et al., 2001). Many studies in these regions have used massive corals of the *Porites* genus, which provide useful palaeoclimate archives due to their wide distribution throughout the tropics (Fig. 1.1), their ability to be accurately dated, and because they contain a wide range of geochemical tracers within their skeletons (Dunbar and Cole, 1999; Gagan et al., 2000). Their dense skeletons and rapid growth rates (~1 cm/year) means they are ideally suited for sub-annual sampling. Watanabe et al. (2003) also found that *Diploastrea* records interannual climate variability as clearly as *Porites*, thus also yielding a dependable palaeoclimate signal. With global climate change a dominant issue in the scientific realm, it is necessary to provide as much verification as possible of incremental climate change throughout the last decades, centuries and millennia. Coral provide an excellent tool for this, and the analysis of new species means that data capture throughout the world's tropical oceans can be maximised.

1.1.1 Corals through time

Scleractinian corals such as *Goniastrea* and *Porites* first became important to reef systems in the shallow seas of the Tethys during the Mesozoic, with most modern families and genera present by the middle Cenozoic (Bromfield and Pandolfi, 2011). Closure of the Tethys during the Oligocene (~34-23 Ma) created the division of original Tethyan fauna into the two unique faunas currently prevailing in the tropical Atlantic and Indo-Pacific regions. Three major extinction events, occurring at the Eocene-Oligocene, Oligocene-Miocene and Plio-Pleistocene boundaries served as faunal turnover events (Edinger and Risk, 1994). The Plio-Pleistocene event occurred between 4-1 Ma, with Atlantic communities undergoing a severe restriction event meaning that many genera now extinct in the Caribbean Ocean are extant in modern day Indo-Pacific reefs. Palaeontological data shows that modern reefs prevailing today are a reasonably accurate representation of how reefs have existed for over 25 Ma (mid-late Tertiary) (Boekschoten et al., 1989), therefore studies using modern corals are not

only applicable to modern climate reconstruction, but can also be used in a palaeoclimate sense when a fossil coral of the same genus or species is analysed.

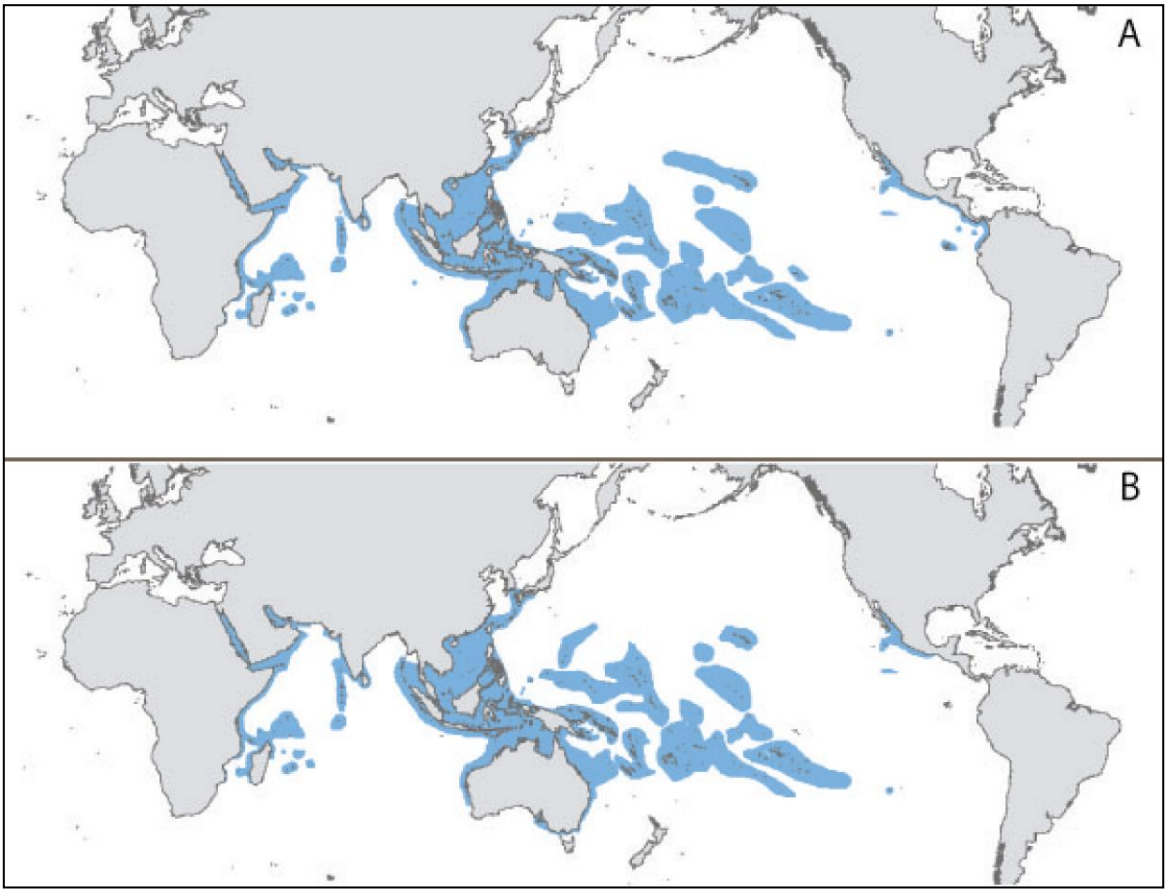

Fig. 1.1 Global distribution of *Porites lobata* (A) and *Porites lutea* (B). Images sourced from Veron, 2000.

1.1.2 Climate records in corals

The region around Timor Leste is especially important from a climate perspective. The tropical western Pacific provides the largest of three major global tropical heat sources, which contributes significantly to climate variability in the Pacific region (the two other major heat sources reside over the Amazon and Africa) (Wang, 2002). The southwest Pacific is also affected by key climate parameters El Niño Southern Oscillation (ENSO), the Asian-Australian monsoon, and the Indian Ocean Dipole (IOD). These parameters all influence the Indo-Pacific Warm Pool (IPWP) which is a primary component of the global coupled ocean-atmosphere system (Gagan et al., 2004). Variations in these climate processes influence SST, SSS, and precipitation in equatorial regions. It has also been realised that the industrial revolution has significantly influenced the natural state of our global system, with rapid

increases in atmospheric gas levels raising concern in regards to how the natural system will respond to these anthropogenically induced changes. Some scientists believe that through the injection of fossil fuel CO_2 into the atmosphere, modern SST, natural temperature and climate variability, and coupled ocean-atmosphere phenomenon such as El Niño/La Niña, have already been influenced (Fairbanks et al., 1997). The authors argue for increased severity and frequency of El Niño events since the 1970s. Hughen et al. (1999) explains that this coincides with a time of rapidly increasing global temperatures, which may be linked to human-induced greenhouse forcing. On the other hand, a coral record from the Galápagos Islands has recorded an abrupt and synchronous shift in ^{14}C and SST following the El Niño event of 1976 in the eastern tropical Pacific (Guilderson and Schrag, 1998), and the authors conclude that such alteration to the vertical thermal structure may be responsible for the increased and intensified El Niño behaviour thereafter. The extent to which these changes reflect natural variability versus anthropogenic input requires a better understanding of annual climate records over geological time scales. A vital aspect of understanding the possible future trends of the global climate system begins with gaining an understanding of palaeoclimate trends, and tropical corals are particularly sensitive recorders of this.

1.2 Coral geochemistry

Massive, hermatypic corals, such as *Goniastrea*, *Porites*, and *Diploastrea*, have desirable morphology for use as climate proxies. This is because massive corals form round, wave-resistant structures that can include hundreds of years of uninterrupted growth, and also their calcium carbonate accretion rate is higher than deep water coral species. Annual density bands represent changes in both the rate of linear skeletal extension and calcification, and have been used to detect variations in growth rates during certain years as the result of ENSO events. Optimal growth conditions for hermatypic corals include temperatures within the range of 20^0-26^0C, low sediment load, growth at 5-15 m depth to ensure sufficient light penetration through the water column, normal ocean salinities (25-40‰), and relatively protected water bodies where energy levels are low (Druffel, 1997). These conditions yield an optimum vertical growth rate of 10-15 mm/yr for massive, modern species (Veron, 2000)

1.2.1 Stable isotopes

Coral aragonite records ambient seawater conditions which can be resolved using geochemical techniques. Attributes that control coral chemistry include water temperature,

salinity, isotopic composition, turbidity, runoff, and upwelling intensity. Therefore, examining $\delta^{18}O$ and $\delta^{13}C$ ratios within a coral may provide detailed insights into the prevailing palaeoceanographic and atmospheric conditions. For example, higher (more positive) $\delta^{18}O$ values indicate colder a climate with greater global ice volume, so the general trend over time toward lower (more negative) $\delta^{18}O$ values at numerous sites in the world's tropical oceans suggests a gradual warming and/or freshening of the surface ocean over the past century (Druffel, 1997). Fig. 1.2 summarises the expected relationships between environmental conditions and coral $\delta^{18}O$ (as explained by Felis and Paetzold, 2003), showing that increases in temperature, precipitation and runoff all result in more negative $\delta^{18}O$ values. In contrast, increased evaporation results in more positive coral $\delta^{18}O$. Increased precipitation and runoff also serve to freshen local and regional SSS conditions, whereas increased evaporation causes heightened salinities.

SST and SSS varies according to ENSO phases, meaning that ENSO behaviour is recorded in corals living in the equatorial Pacific basin and central Indian Ocean (Dunbar and Cole, 1999). It has been found that the cool, dry conditions experienced in the western Pacific during an El Niño phase of ENSO result in deposition of isotopically heavy skeletal oxygen (more positive $\delta^{18}O$), whereas the warm, wet conditions of La Niña result in an isotopically light coral skeleton (more negative $\delta^{18}O$) (Tudhope et al., 2001; Tudhope et al., 1995). This relationship is not only relevant in the modern but also in the Holocene, as McGregor and Gagan (2004) found that seven $\delta^{18}O$ records from Holocene *Porites* from PNG show decreases in SST and precipitation similar to modern ENSO behaviour, from a time period spanning 7.6-5.4 ka. Positive $\delta^{18}O$ anomalies were also seen in 14 out of 16 El Niño events from modern coral records at the same site. The coupling of changes in SST and the amount of $\delta^{18}O$-depleted rainfall in the tropical southwest Pacific makes sites such as PNG, Indonesia and Timor particularly sensitive recorders of ENSO variability.

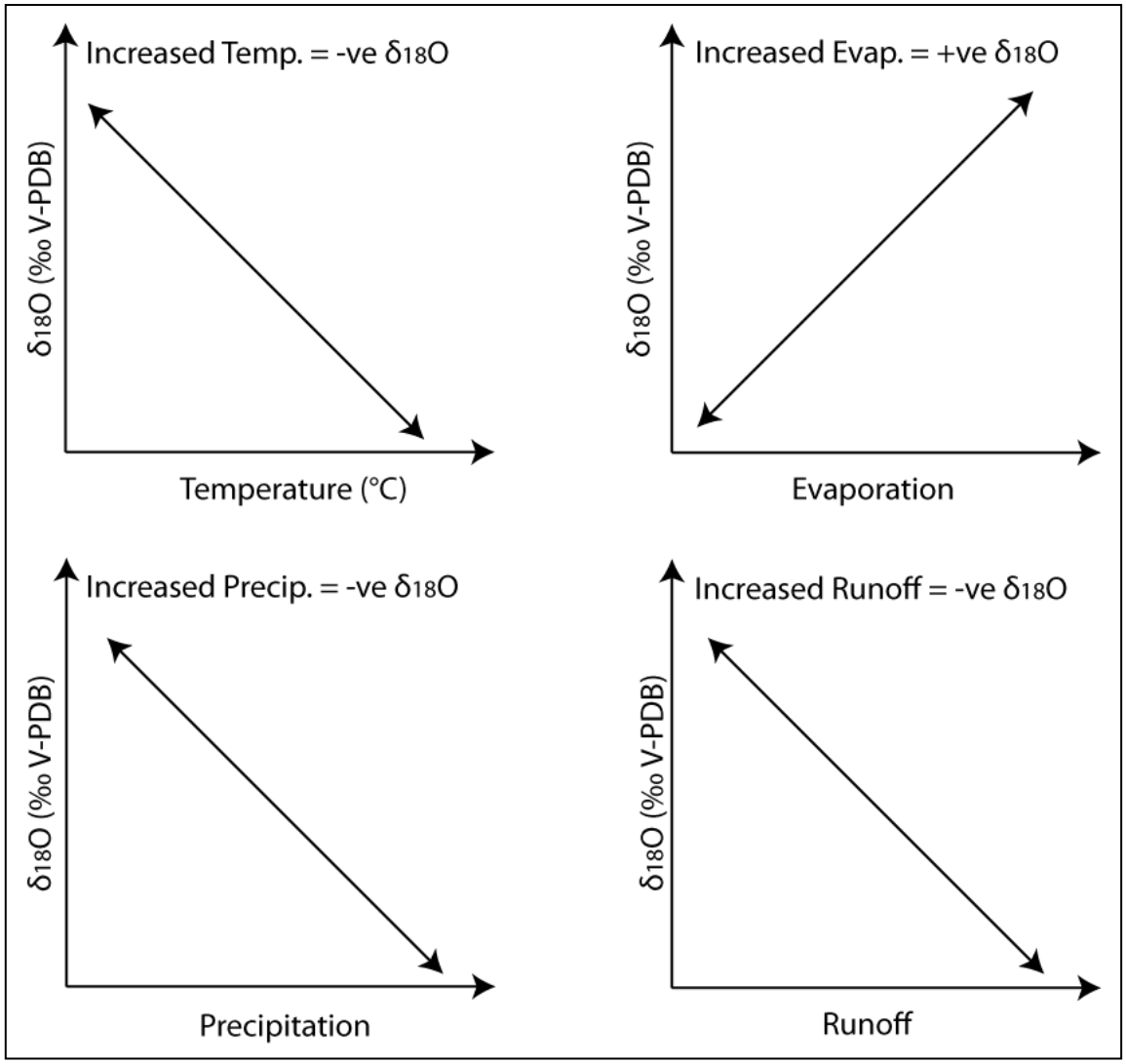

Fig. 1.2 Relationships between changing environmental conditions and $\delta^{18}O$ composition of seawater.

1.2.2 Sr/Ca

Strontium-calcium (Sr/Ca) ratios in corals have been shown to provide a promising proxy for water temperature variation, with calibrations suggesting a temperature dependence of 0.062mmol/mol per 1^0C (Gagan et al., 2000). Unlike $\delta^{18}O$, which is influenced by both SST and $\delta^{18}O$ of seawater ($\delta^{18}O_{sw}$) , coral Sr/Ca is a reliable proxy purely for SST (Cahyarini et al., 2008). The coupled Sr/Ca-$\delta^{18}O$ technique makes it possible to reconstruct not only $\delta^{18}O_{sw}$, but also SST, by removal of the temperature component of the $\delta^{18}O$ signal (McCulloch et al., 1994). Information about precipitation, evaporation, and water mass transport can also be inferred. This technique has been successfully used in nine sites in the Pacific and Indian Oceans using fossil *Porites* corals, however its high sensitivity to very

minor amounts of diagenesis (as outlined below) has meant that this analysis is beyond the scope of this particular study.

1.2.3 Coral diagenesis

Diagenesis of biominerals occurs frequently in the marine realm, and coralline aragonite is not exempt to this. Corals are subject to post depositional diagenetic alteration in both marine and freshwater phreatic and vadose environments (McGregor and Abram, 2008) (Table 1.1). Diagenesis within these zones can have three possible outcomes – 1) the precipitation of secondary aragonite or calcite in skeletal voids, 2) the replacement of skeletal aragonite, usually with calcite, or 3) dissolution of the primary aragonite skeleton (Bathurst, 1975). Dissolution in water-saturated areas causes "chalky zones" in the skeletal aragonite, often developed in association with precipitation of single-crystal calcite, where dissolution occurs at a greater rate than calcite precipitation (McGregor and Gagan, 2003). These zones show increased leaching particularly at calcification centres. If diagenesis occurs in the vadose zone, corals are most likely to transform to calcite. Characteristic vadose zone diagenetic sequence begins with leaching of primary aragonite and overgrowths of fine calcite, transitional to calcite void filling and neomorphic, fabric sleeve replacement of the coral skeleton. Neomorphism occurs when aragonite is replaced with calcite without destroying the gross coral morphology.

Table 1.1 Types of diagenesis that occur in corals situated in different diagenetic zones

Diagenetic zone	*Characteristic features of zone*	*Diagenesis*
Marine phreatic zone	Pore spaces completely saturated with seawater	Secondary aragnonite Dissolution
Freshwater phreatic zone	Pore spaces completely saturated with freshwater	Calcite Dissolution
Marine vadose zone	Pore spaces filled with mix of air and seawater	Secondary aragonite Calcite (subaerial exposure) Dissolution
Freshwater vadose zone	Pore spaces filled with mix of air freshwater	Calcite (subaerial exposure) Dissolution

When using corals for palaeoclimate research, they must either be pristine or their level of diagenesis precisely known in order for the isotopic and elemental signals to be meaningful. If meteoric water is present during recrystallisation of aragonite into calcite, the stable isotopic and elemental time series may be affected. McGregor and Abram (2008) outline the

influences of diagenetic material on SST reconstructions, with results from their own study of modern and fossil *Porites* from PNG supportive of previous investigations (e.g. Allison et al., 2007; Bar-Matthews et al., 1993; Hendy et al., 2007; McGregor and Gagan, 2003). They explain that secondary aragonite growth in modern corals creates "cool" SST artifacts, secondary calcite growth in both modern and fossil corals leads to "warm" SST artifacts, and dissolution is shown to create "cool" anomalies in a range of trace element SST proxies. These temperature shifts can also be explained in terms of positive or negative shifts in the stable isotope and Sr/Ca values. Secondary aragonite growth as a result of early marine diagenesis would bring on significant *positive shift* in coral $\delta^{18}O$, $\delta^{13}C$ and Sr/Ca values relative to pristine corals. In contrast, diagenetic transformation of primary aragonite to calcite, or addition of calcite cements in environments with meteroric water, involves a *negative shift* in the $\delta^{18}O$, $\delta^{13}C$ and Sr/Ca composition of the diagenetically altered corals. Therefore, the effect that diagenetically altered coral geochemical signals have on the palaeoclimate record is significant. Sr/Ca signals have been found to have nearly 2.5 times the sensitivity of $\delta^{18}O$ ratios to the same degree of alteration, and McGregor and Gagan (2004) have found that lower Sr/Ca and $\delta^{18}O$ in diagenetically altered coral would produce 1.1 to $1.5^{0}C$ and -0.2 to $0.2^{0}C$ warmer SST artifacts for palaeotemperature reconstruction, respectively. The influence of secondary aragonite is particularly strong, with 20% of secondary aragonite forcing a shift to 0.5‰ higher $\delta^{18}O$ (Qu, 2007). This means that sensitivity of coral $\delta^{18}O$ and $\delta^{13}C$ to subtle infilling and replacement of the original coral matrix by secondary aragonite can create significant geochemical variations that may be independent of any climatic or environmental change. Because of this, an extensive diagenetic screening process has been carried out to determine levels of diagenesis in corals from Timor Leste.

1.2.4 Limitations

Coral skeletons are depleted in ^{18}O and ^{13}C with respect to isoptopic equilibrium with the ambient seawater (Felis and Paetzold, 2003), which has been attributed to a kinetic ("vital") effect that takes place during hydration and hydroxylation of CO_2. This is known as "disequilibrium". However, the disequilibrium does appear to be constant over time along the major growth axis of an individual coral colony where growth and calcification rates are at their maximum (McConnaughey, 1989). Hence coral microsamples are always milled along the major axis of coral growth following single fans of corallites. A problem for

palaeoclimate reconstruction is that mean isotopic disequilibrium offset from seawater can vary significantly for individual corals living in the same environment (Guilderson and Schrag, 1998), which means that quantitative comparison of mean climatic conditions being drawn from $\delta^{18}O$ records of corals growing in different locations or during different time periods must be treated with caution. It seems that coral $\delta^{18}O$ provides an excellent proxy for variability but should not be considered an absolute proxy for SST or $\delta^{18}O_{sw}$, as the reported differences of 0.2 to 0.4‰ for coral $\delta^{18}O$ equal 1-2^{0}C in terms of temperature interpretation (Felis and Paetzold, 2003).

Although coral Sr/Ca ratios also have a vital effect that produces disequilibrium with the ambient seawater, it appears the temperature calibrations do not vary significantly for individual corals living in the same environment, nor between different species (of *Porites*) and colonies with different growth and calcification rates, provided sampling follows optimal growth regions (Alibert and McCulloch, 1997). Therefore, Sr/Ca ratios could yield more reliable results than $\delta^{18}O_c$ when attempting to delineate changes in absolute mean temperatures at a given location. The average of 0.062mmol/mol per 1^{0}C from several corals sampled by Gagan et al. (2000) is certainly useful, but it is unknown whether this relationship is generally valid for *Porites*. It is also important to acknowledge that glacial conditions may have significantly altered the seawater Sr/Ca ratio due to weathering and dissolution of Sr-enriched carbonates exposed on the continental shelves (Stoll and Schrag, 1998). The key message to be taken from this research is that analytical errors can be reduced when a multi-proxy approach is used for palaeoclimate reconstructions.

1.3 Dating of corals

There are four reliable ways to numerically date corals; (1) sclerochronology, (2) ^{14}C dating (3) uranium-thorium (U/Th) dating, and (4) uranium-lead (U/Pb) dating. This study employed all of these techniques except ^{14}C dating. Sclerochronology involves counting annual density bands and is most effective when the sample is collected from a living specimen, meaning counting can work backwards from the age of the uppermost, youngest annual density band. U/Th techniques are useful for fossil corals as they allow dates of a few years to ~ 500 ka to be obtained. This record can be extended much further, up to many millions of years, using the U/Pb decay scheme (Woodhead et al., 2006). Accuracy using U/Th ranges from ± 5 years (2 σ) for a 180 year old coral, ± 44 years at 8,294 years, and ±

1.1 thousand years at 123.1 ka (Edwards et al., 1987). U/Pb has a minimum uncertainty of 1‰ associated with the half-life of ^{234}U (Denniston et al., 2008). However, a limitation of U/Pb dating of fossil corals is the susceptibility of their porous and metastable aragonite skeletons to diagenetic alteration (Denniston et al., 2008). Fortunately, measurement of $^{234}U/^{238}U$ and $^{230}Th/^{238}U$ can be a powerful diagnostic test for post-depositional mobility of U-series nuclides, as where either of these ratios has departed from secular equilibrium it can be assumed that the sample has not behaved as a closed system (i.e. is diagenetically altered) for all of the last ~1 Ma (for ^{234}U) or ~ 500 ka (for ^{230}Th) (Quigley et al., 2012). A combined dating technique using both U/Pb and U/Th to determine whether the coral age is within secular equilibrium has allowed for the highest precision of the 2.7 Ma terminal Pliocene coral age. Since the Holocene corals are within the age range of 500 ka, U/Th was the sole technique used to obtain the two 4.5 ka dates, while sclerochronology was applied to the modern coral.

1.3.1 Applications of dated corals

Denniston et al. (2008) completed the first successful dating of a pre-Quaternary coral using U/Pb techniques, recognising the suitability of corals for refining the chronologies of late Cenozoic marine sedimentary sequences. A date of 5.52 ± 0.15 Ma was obtained, and is the only study of a pre-Quaternary coral which has employed U/Pb dating until this study and previous reconnaissance studies of Pliocene corals found in the uplifted VM in Timor Leste (Quigley et al., 2012). Denniston et al. (2008) acknowledged that the limitations to prior coral studies has been insufficient age control on some fossil-bearing lithologies, whereas U/Pb dating introduces reliable dates under the right circumstances. Corals younger than Pliocene age have also been dated. Two mid Pleistocene corals have been obtained using U/Pb and U/Th techniques, providing ages of 1.02 ± 0.07 Ma and 1.288 ± 0.034 Ma (Getty et al., 2001). These ages, combined with shallow-marine sequence dates, have been used to define rates of marine invertebrate evolution, tectonic uplift and palaeoclimate change in the Caribbean Basin. Other palaeoclimate studies using fossil corals of Tertiary age have used stratigraphic sequencing to provide approximate ages of corals (Brachert et al., 2006; Ivany et al., 2004; Mackenzie et al., 1997; Roulier and Quinn, 1995). A study that is extremely well correlated to the use of detrital corals from Timor Leste is that of Brachert et al. (2006), which uses 10 Ma *Porites* corals from Crete to provide insights into late Miocene seasonal and interannual climate variability. These exceptionally well preserved, massive coral

skeletons were retrieved from a coral buildup and analysed for isotope fluctuations. From this it was ascertained that climate dynamics in the eastern Mediterranean reflect atmospheric variability related to the Icelandic Low 10 Myr ago. Although dating of fossil corals can be somewhat difficult, using a combined technique of coupled U/Pb and U/Th dating along with reference to biostratigraphic ages, uncertainties can be largely minimised.

1.4 Study area – Timor Leste

1.4.1 Geographical setting

The island of Timor is located within maritime southeast Asia, and is the largest and easternmost of the Lesser Sunda Islands (Fig. 1.3). Situated approximately 640 km northwest of Australia, Timor represents the southern arm of the outer Banda Arc. The Banda Sea, Ombai Strait, and Wetar Strait extend northward, the Timor Sea to the south, while to the west lies the Indonesian Province of East Nusa Tenggara. The island of Timor is divided in two, West (Pulau Timor) and East (Timor Leste), along a 100 km north-south political boundary in roughly the centre of the island, from which Timor Leste extends 250 km eastward. Elevation increases rapidly from the coast inland in Timor Leste, and peaks at 2,963 m (Mt. Ramelau) along a roughly west-east trending mountain range which is highest in the west.

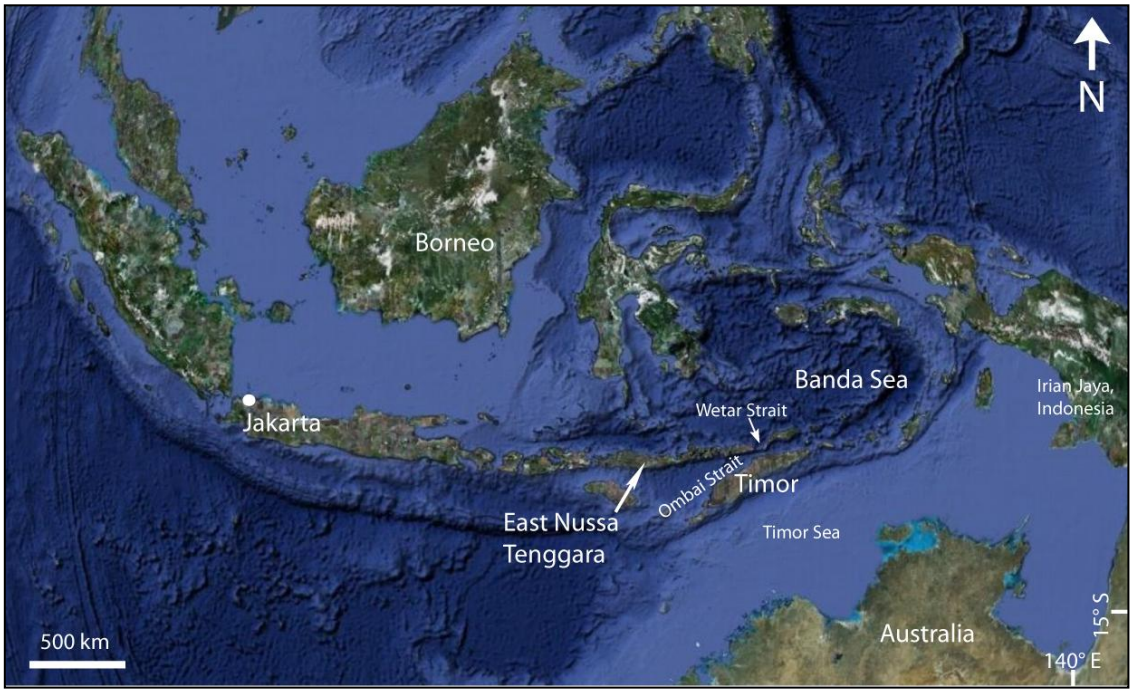

Fig. 1.3 Location of Timor within maritime southeast Asia.

1.4.2 Geological setting

Tectonic narrowing of the Indonesian Seaway occurred due to NNE-directed movement of the Australian continent at ~ 70 mm yr^{-1} relative to the Sunda Shelf (DeMets et al., 1994), resulting in collision of the leading continental margin with the Banda Arc by the Miocene to early Pliocene (Audley-Charles, 2011; Rutherford et al., 2001). Tectonic processes including the accretion of the Banda Arc to the Australian continental crust (Bock et al., 2003; Nugroho et al., 2009) and the detachment of the downgoing slab from the Australia Plate lead to the uplift of the island of Timor (Audley-Charles, 1968a; Harris, 1991; Price and Audley-Charles, 1987; Sandiford, 2008). The timing of arc-continent collision in Timor remains poorly constrained and controversial, varying from ca. 3.5 Ma (Carter et al., 1976) to 5.5-9.8 Ma (Haig and McCartain, 2007; Keep and Haig, 2010). The uplift of Timor reorganised oceanic pathways so that the proto-Timor-Sea was divided in two as parts of Timor rose from mid-bathyal depths in the terminal Miocene to terrestrial environments in the late Pliocene or early Pleistocene (Haig and McCartain, 2007; van Marle, 1991). The island is surrounded by >3000 m deep basins in both the forearc and foreland regions of the orogen (Audley-Charles, 1986; Kenyon, 1974) that serve as pathways between the Pacific and Indian Oceans through the Indonesian Seaway. The Wetar Strait north of Timor is a young, retro-foreland basin associated with movement on the Wetar Suture that locked up around 2 Ma (Harris, 1991; Price and Audley-Charles, 1983, 1987) and foraminiferal evidence shows that the Timor Trough axis south of Timor has migrated 60-80 km south of Timor since 4.5 Ma (Veevers et al., 1978). This migration was accompanied the shortening and thickening of the Timor orogen, which partially blocked the Indonesian Seaway and uplifted the Viqueque Megasequence (VM) beginning in the Early Pliocene (Keep and Haig, 2010). As such, the exhumed VM provides a geologic archive relevant to understanding Indonesian Seaway evolution, as changes in salinity and temperature will be recorded in skeletons of pristine fossil corals retrieved from the sedimentary VM, discussed further in Chapter 4. The present tectonic configuration of Timor is displayed in Fig. 1.4.

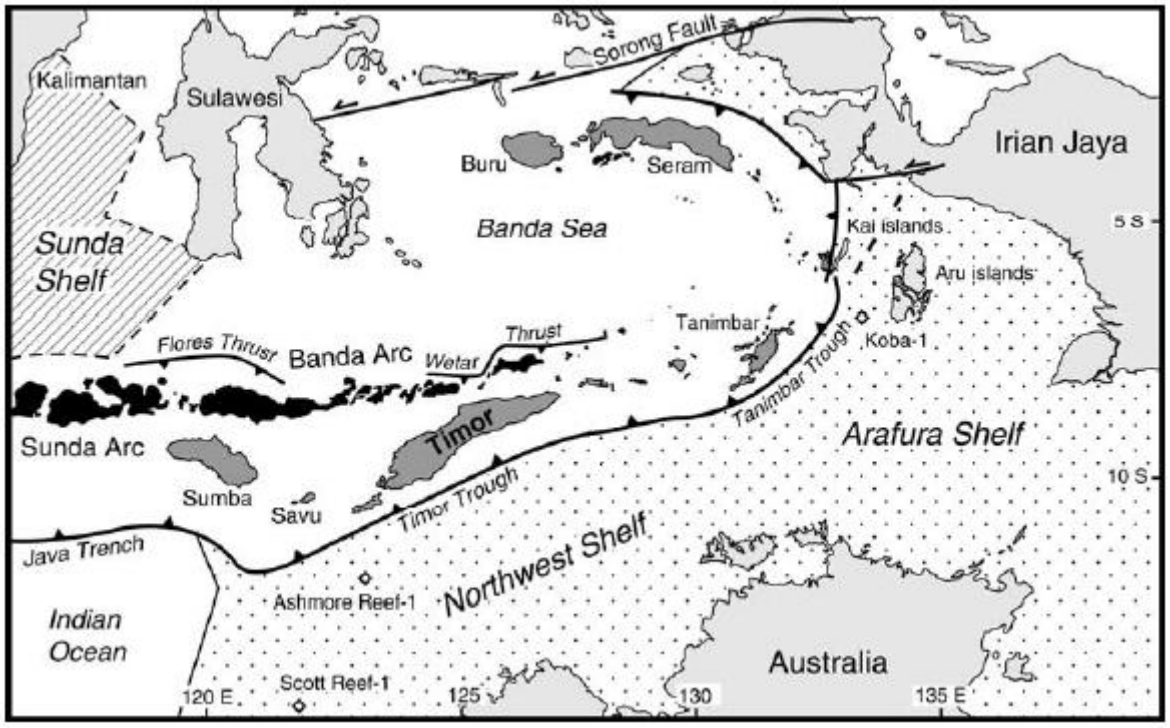

Fig. 1.4 Location of Timor relative to Australia and the Banda Arc. Volcanic islands are shaded black, forearc islands are shaded intermediate grey. The offshore Australian and Sundaland continental shelves are represented by the dotted and hatched patterns, respectively. Sourced from Charlton, 2002a.

1.5 Indo-Pacific climate

When attempting to relate $\delta^{18}O$ and $\delta^{13}C$ records from corals to climate fluctuations, it is important to understand all climate processes which affect the region from which the coral is retrieved. The Indo-Pacific climate is controlled by a complex interaction of atmospheric and oceanic processes which have evolved through time. Although the modern climate is constrained by historical data collection and the creation of climate models, the Holocene and Pliocene climate parameters are less clearly defined. Information from a network of climate proxies across the region that extend back several millions of years has helped to create a general idea of prevailing conditions through time, however more data from a range of proxies is needed in order to further clarify these interpretations.

1.5.1 Modern climate

The key oceanic feature of the southwest Pacific region is the IPWP (Fig. 1.5). It is the warmest body of open-ocean water on Earth with a mean SST of greater than 28^0C (Abram et al., 2009), and precipitation that exceeds evaporation by ~2 m within the 28^0C isopleth

(Gagan et al., 2004). As such, it is believed to play a vital role in global climate change through its interaction with major climate systems, and due to the vigorous convection that occurs above it and subsequent distribution of heat and water vapour. There are several main atmospheric processes which interact over the Indo-Pacific; the Indian Ocean Diople (IOD), the Indo-Pacific monsoon, and ENSO. The IOD is an irregular oscillation of SSTs in which the western Indian Ocean becomes alternately warmer (cooler) than the eastern part of the ocean, with positive (negative) anomalies causing drought (flood) conditions in over Indonesia and Australia. The monsoon season brings peak temperature and precipitation from September to February. The ENSO phenomenon in particular has a dominant effect on the climate in the southwest Pacific due to its influence on the IPWP. El Niño and La Niña are officially defined as sustained SST anomalies of >0.5°C across the central tropical Pacific Ocean. When the +0.5°C (-0.5°C) condition is met for a period of less than five months, it is classified as El Niño (La Niña) *conditions*. If the anomaly persists for five months or longer, it is classified as an El Niño (La Niña) *episode*. During El Niño the Indonesian region becomes cooler and drier as the IPWP shrinks and moves eastward as the result of weaker trade winds, causing negative SST anomalies and less precipitation. In contrast, stronger trade winds during La Niña push the IPWP westward, bringing positive SST anomalies and greater levels of precipitation. Fig. 1.6 illustrates the alterations to normal Pacific conditions that occur during El Niño and La Niña. These three climate processes are inherently related, with recent studies showing that positive feedbacks exist between strengthened Asian monsoon rainfall and IOD events (Abram et al., 2009), meaning that when negative events coincide with peak monsoon rainfall there is the potential for much greater than average rainfall.

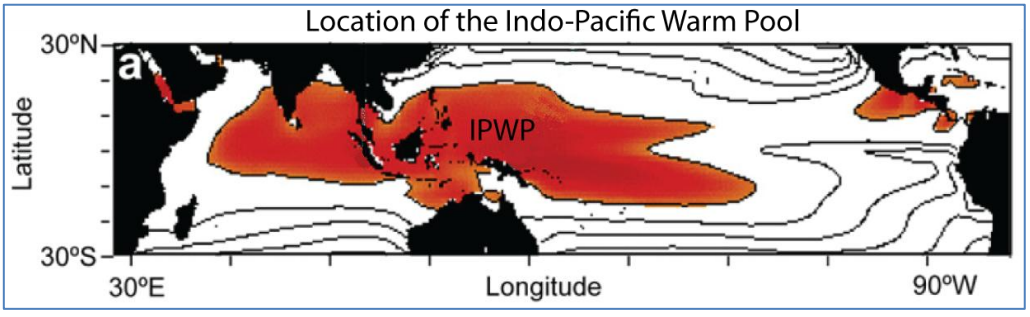

Fig. 1.5 Location of the Indo-Pacific Warm Pool, which spans the western Pacific to the eastern Indian Ocean. Mean annual SST map depicts 2° C contour interval, with shaded area >28° C. Modified from Abram et al., 2009.

Atmospheric circulation above the equatorial southwest Pacific is also important in determining the global and regional climate. Thermally driven global atmospheric circulation cells, the Walker and Hadley cells, are associated with ENSO and located in the tropics. Both are conceptual models to explain how parcels of air follow a closed circulation in the zonal and vertical directions (Walker cell) and meridional direction (Hadley cell). Walker cell circulation is characterised as the air ascending in the equatorial western Pacific, flowing eastward in the upper troposphere, sinking in the equatorial Pacific, and returning to the equatorial western Pacific in the lower troposphere (Wang, 2002). During El Niño this convection cell is weakened. The tropical Hadley cell is intimately related to the trade winds, tropical rainbelts, subtropical deserts and the jetstreams, with heated tropical air rising and flowing aloft towards the subtropical region where it cools, sinks, and flows back to the tropical region (Wang, 2002). During El Niño the western Pacific Hadley cell shows an anticlockwise rotation with anomalous descending motion in the tropics an anomalous ascending motion in the subtropics (Wang, 2002). Therefore, both the Walker and Hadley cells are recognized as playing an important role in the evolution of ENSO. SST itself is known to be an important factor in climate dynamics, due to the nonlinearity of the relationship between SST and heat transfer to the atmosphere meaning that even small changes in tropical SST ($0.5 – 1.0^{0}$C) can have large effects on the patterns of rainfall, storm tracks and intensities, and indeed on the overall general atmospheric circulation (Beck et al., 1997). This distinguishes SST as an essential boundary condition to be considered in any modelling of past or future climate. It is apparent that the location of coral reefs in such areas of principal circulation processes means that isotopic and elemental records from skeletal primary aragonite has the potential to delineate incremental changes in the global climate system, at higher resolution and over broader time spans than many other records.

Fig. 1.6 (Next page) Illustrations of western Pacific conditions resulting from the El Niño and La Niña phenomenon. During normal conditions, equatorial winds push the WPWP westward, causing the upwelling of cold water along the South American coast. During El Niño, the WPWP approaches the South American coast to instigate warming, while the western Pacific becomes relatively cool and dry. During La Niña, the WPWP extends towards the west, causing relatively warm and wet conditions in the western Pacific. Images sourced from NOAA.

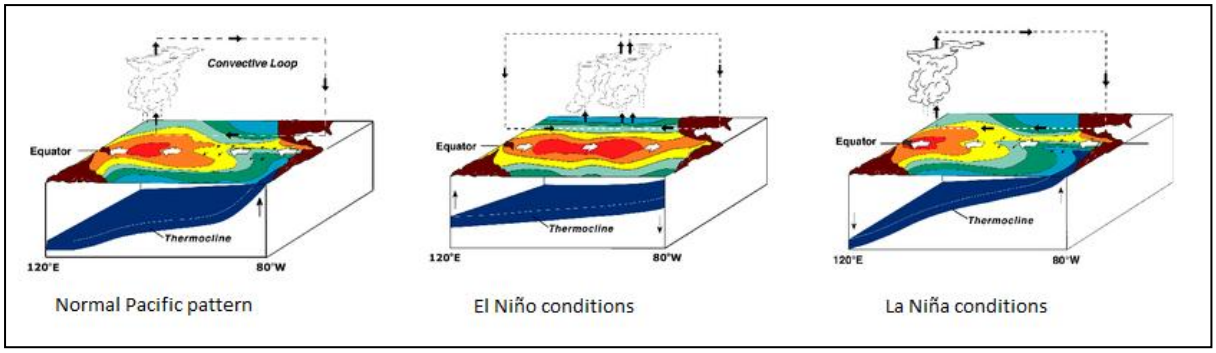

1.5.2 Holocene climate

The Indo-Pacific has been a key area for palaeoclimate delineation in the last several decades, with many studies using fossil *Porites* corals and foraminifera from sediment cores as proxies to provide a window to climate conditions at various times throughout the Holocene. Together these records have allowed scientists to piece together a general understanding of climate history in this region since ~ 10 ka.

1.5.2.1 Holocene Sea surface temperature

SSTs in the IPWP were ~ 3^0C cooler than present during the Last Glacial Maximum (LGM) (~ 26-19 ka), but the central IPWP experienced a rapid post-glacial SST rise which triggered deglaciation by ~ 3 ka later, producing near-modern SSTs by the early Holocene (Gagan et al., 2004). Both coral and sediment core records show a decrease in $\delta^{18}O_{sw}$ of 0.5‰ relative to modern seawater since the early to mid Holocene, equating to a 1^0C drop in tropical SSTs (Gagan et al., 1998; Stott et al., 2004). At higher temporal resolution, Sr/Ca analyses of a suite of 48 *Porites* corals from PNG and Indonesia have shown fluctuations in southeastern and southwestern IPWP SSTs during the Holocene. The coral records indicate that these regions of the IPWP were cooler than present between ~ 5.5-4.3 ka, (~ 1.2^0C ± 0.3^0C), and were similarly cool before ~ 6.8 ka (Abram et al., 2009). The results also elucidate a short-lived shift to mean SSTs that were warmer than at present between ~ 6.6-6.3 ka. This means there was a brief, mid-Holocene temperature peak, which is similar to the conditions that are thought to have prevailed after ~ 4.3 ka. The authors suggest that the mid-Holocene cooling at the study sites was related to contractions of the southeastern and southwestern margins of the IPWP, associated with the more northerly position of the Inter-tropical Convergence Zone (ITCZ) that accompanied mid-Holocene strengthening of the Asian summer monsoon. In turn, warming is predicted to be the result of a more southerly position of the ITCZ coupled with a weakening monsoon. This suggestion further strengthens the case for dynamic

relationships between the coupled ocean-atmospheric climate system in the tropics being drivers for SST and SSS fluctuations. Beck et al. (1997) uses *Porites* Sr/Ca ratios to examine the SSTs from Espiritu Santo, Vanuatu, revealing a depression of as much as 6.5^0C below modern values at ~ 10.35 ka, followed by an abrupt temperature rise during the following 1.5 ka. McCulloch et al. (1996) have high precision (near weekly) Sr/Ca ratios from uplifted coral terraces dated at ~ 9 ka and ~ 7.5 ka from the Huon Peninsula, PNG, which support previous findings. (Abram et al., 2009; Beck et al., 1997). U/Th dating provided these early Holocene ages for the *Porites* cores, with results giving a minimum of $2\text{-}3^0$C cooler than modern SSTs in the equatorial western Pacific, which is also consistent with late glacial coral records from the Caribbean indicating lower (~ 6^0C) SSTs for the equatorial oceans (Beck et al., 1997).

1.5.2.2 Holocene Sea surface salinity

The decline in SSS in this region is supported in the sediment core record, as shown by deep sea drilling core foraminiferal results from Indonesia. Isotopic data provided by the examination of *Globigerinoides ruber*, at multi-decadal to centennial temporal resolution throughout the Holocene, shows that a decrease in $\delta^{18}O_{sw}$ of 0.5‰ reflects a decrease in SSS of 1-1.5 practical salinity units (psu), causing ocean freshening. This observation implies that in the early Holocene, tropical western Pacific surface water was as salty as the surface water in the south central equatorial Pacific today (> 35.2 psu) (Stott et al., 2004). Therefore, if SSSs across the Pacific are stable, the salinity gradient that currently exists was either absent or significantly reduced in the early to mid Holocene. It has also been noted that Holocene-age groundwater from the Phillipines has the same $\delta^{18}O_{SMOW}$ (standard mean ocean water) as modern rainwater, indicating not only that the moisture source to the region has remained unchanged during this time, but also that there has been a persistent and strong monsoon system throughout the Holocene (Stott et al., 2004). The decrease in SSS is supported by a 54-year long, high resolution *Porites* record (~ 15 samples per year) from the South China Sea, which has allowed an insight into monsoon variability and ENSO behaviour during summer and winter at ~ 4.4 ka. Higher summer rainfall and cooler winter SSTs due to greater Northern Hemisphere insolation is recorded through $\delta^{18}O$ fluctuations in this coral, contributing to mounting evidence for recent freshening of the tropical western Pacific (Sun et al., 2005). $\delta^{18}O$ and Sr/Ca records from corals have shown that surface waters in the western Pacific and South China Sea were probably 0.5-1.0°C warmer and more salty than

present during the Holocene Climatic Optimum (~ 7-6 ka) (Montaggioni and Braithwaite, 2009).

1.5.2.3 ENSO in the Holocene

Spectral analysis of winter SSTs reveals a strong ENSO cycle, suggesting the influence of ENSO on winter SSTs in southeast Asia was well established by ~ 4.4 ka (Sun et al., 2005). However, this is not observed in summer SSTs, leading to suggestions that teleconnections between ENSO and summer monsoon rainfall were restricted at this time. The cause of the differences in ENSO behaviour during the early–middle Holocene is likely to have been differences in the earth's orbital configuration (Cane, 2005). This idea is strengthened by Gagan et al. (2004) who find that the onset of modern ENSO periodicities are identified by palaeo-ENSO records throughout the tropical Pacific region ~ 5 ka, with an abrupt increase in ENSO magnitude ~ 3 ka. Mid Holocene coral records show subdued precipitation in response to El Niño temperature anomalies, but this abruptly changes in the late Holocene due to enhanced interaction between the Southern Oscillation and ITCZ. Yet ENSO is believed to have been active long prior to this. Hughen et al. (1999) have discovered robust ENSO activity during the last interglacial when global climate was slightly warmer than present. The interannual variability seen in the Pleistocene $\delta^{18}O$ record of an individual *Porites* coral from North Sulawesi, Indonesia, dated at 124,000 ka, shows similar frequency and behaviour to modern instrumental records prior to the mid-1970s increase in frequency and severity of ENSO events. This is further confirmed by Tudhope et al. (2001) who examine $\delta^{18}O$ in 14 fossil *Porites* corals from PNG, spanning seven distinct age time periods spanning 2-130 ka, as well as three modern samples. Their findings suggest that ENSO has been prevalent in the Indo-Pacific since at least 130 ka, and is stronger now than at any other time.

1.5.3 Pliocene climate

Global Pliocene climate conditions had several key similarities to the present day, notably the intensity of sunlight incidence, global geography, and the atmospheric concentration of carbon dioxide (Fedorov et al., 2006; Wara et al., 2005). However, substantially higher global average temperatures (~ 3^0C) meant there was an absence of continental glaciers in the Northern Hemisphere, and subsequently sea levels were ~ 25 m higher than today (Ravelo et al., 2004). Two key drivers for global climate change are postulated to have

occurred during the Pliocene (5.8-2.6 Ma), the joining of North and South America by the Panama Isthmus, and closure of the Indonesian Seaway. The latter is believed to be instrumental in Indian Ocean cooling and subsequent aridification of East Africa during the Pleistocene, prompting the development of open grasslands and major evolution of hominids (deMenocal, 2004; Reed, 1997; Wynn, 2004). The current debate as to whether the Pliocene was a time of permanent El Niño (Wara et al., 2005) or of regular ENSO cycles (Watanabe et al., 2011) is not yet resolved.

1.5.3.1 The Indonesian Throughflow

The Indonesian Throughflow (ITF) plays a unique role as the only open pathway between two major ocean basins, the Pacific to Indian Oceans, and tropical latitudes. Described as a 'valve' by Wright (2001), its route winds past numerous islands and through narrow straits before reaching the Indian basin (Fig. 1.7), forming a warm surface water route for the global thermohaline circulation. This means it has a strong influence on the regional and global climate system. Its driving force is the pressure gradient between the western Pacific and the Indian Ocean, established by the easterlies in the equatorial Pacific (Morey et al., 1999). This pressure gradient varies in magnitude with the seasonal reversal of the monsoons, being weakest during the northwest monsoon (boreal winter) and strongest during the southeast monsoon (boreal summer). The reversing annual wind patterns associated with the Asian-Australia monsoon system cause large seasonal variation in the circulation and transport patterns within the Indonesian seas (Sprintall et al., 2009). This seasonal circulation change alters the proportion of North Pacific and South Pacific water within the Indonesian archipelago, leading to variations in SSTs and salinity and thus strongly influencing regional rainfall patterns. Morey et al. (1999) state that the majority of the water entering the Indian Ocean from the ITF is transported through the Timor Strait, with lesser amounts travelling through the Savu Sea and Lombok Strait. This means that corals living in coastal waters north and south of Timor during the Pliocene would have been exposed to SST or SSS fluctuations of the ITF.

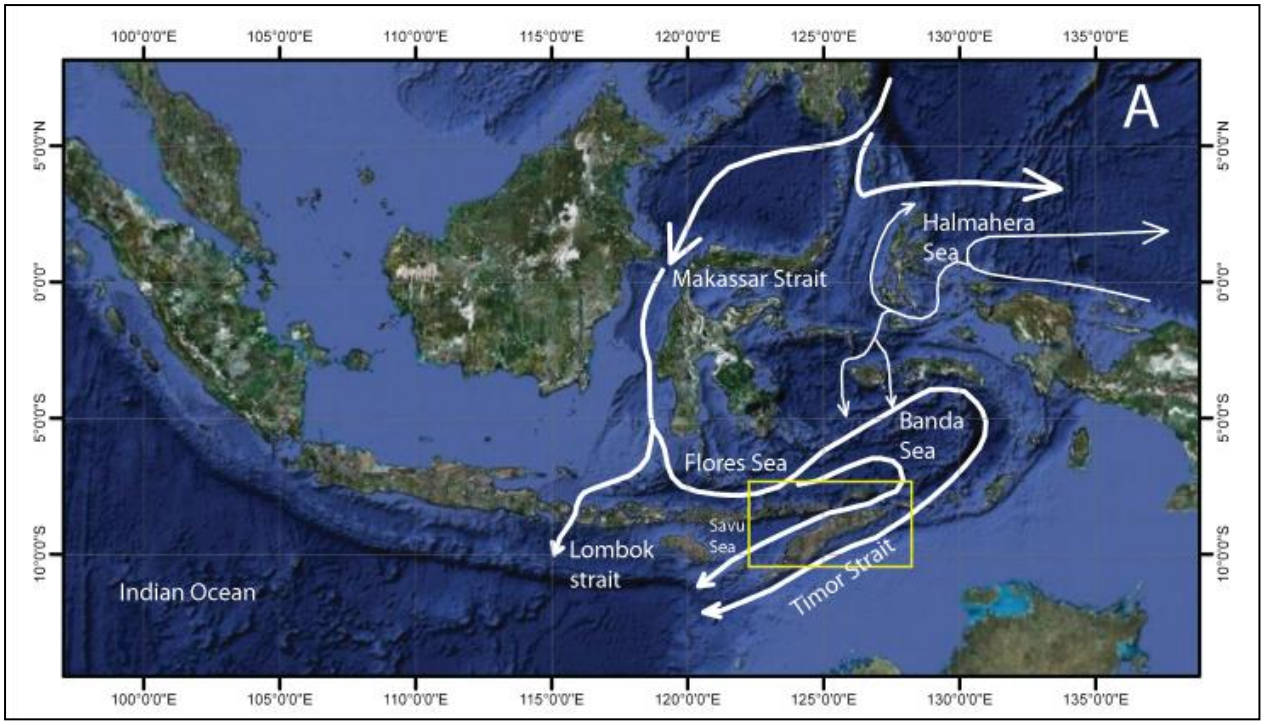

Fig. 1.7 Pathways of the ITF. Thick white lines represent main pathways, thin white lines represent minor pathways (as described by Gordon and Fine, 1996). Yellow box indicates location of Timor within the Indo-Pacific.

1.5.3.2 PLIOCENE CHANGES TO THE ITF

Cane and Molnar (2001) state that prior to ~ 5 Ma, the Indonesian passage was wider, deeper, and located further to the south that it is at present. Tectonic collision of Australia with the Banda Arc lead to the emergence of Halmahera, an equatorial island situated on the margin of the Celebes Sea (or Sulawesi Sea) and Pacific Ocean. The narrowing of the Indonesian seaway and the uplift of Halmahera is postulated to have had a major impact on the source and flow path of the ITF. When the majority the island was submerged, it would have allowed a flux of warm South Pacific water into the Indian Ocean, maintaining higher SSTs and precipitating a rainier climate in East Africa. However, since ~ 5 Ma it has been acting as a blockade and limiting the mixing of South Pacific waters into the ITF, changing the throughflow composition in the surface layer from ~ 69% North Pacific and 31% South Pacific to 92% and 8%, respectively (Morey et al., 1999). This is because it prevents the flow of southern water into the Celebes Sea and also diverts some of it southward through the Seram and Banda Seas. Planktonic foraminiferal $\delta^{18}O$ and Mg/Ca data from the tropical eastern Indian Ocean Deep Sea Drilling Project (DSDP) record gradual SST and SSS

freshening from 5.5-2 Ma, before commencement of a distinct cooling episode of ~ 4^0C and freshening of subsurface waters between 3.5-3 Ma (Karas et al., 2009). This shows that the Indian Ocean has undergone a considerable transformation to cooler, fresher waters since the Pliocene.

1.5.3.3 ENSO in the Pliocene

Jochum et al. (2009) describes how ENSO would have been weaker and more irregular prior to seaway narrowing. The northward movement of New Guinea and subsequent increased flow of North Pacific waters into the ITF, combined with eastward transport of warm and fresh North Pacific surface waters along the equator to the central equatorial Pacific resulted in a shift of the ITCZ. Its new location further from the equator and a reduction in the early Pliocene eastern extent of the Western Pacific Warm Pool (WPWP), the warmest part of the IPWP, are the processes believed to have lead to the present state of strong, regular ENSO cycles. This suggests a weaker, more irregular ENSO cycle prior to Indonesian Seaway narrowing at ~ 3 Ma. However, as outlined above, the extent of the reduced ENSO signal is debated in the literature. The case for permanent El Niño-like conditions during the Pliocene (Ravelo et al., 2004; Wara et al., 2005) has been questioned by recent evidence from spectral analysis of *Porites* corals from the Phillipines (Watanabe et al., 2011). The SST and SSS results from two 35 year long, monthly resolved δ^{18}O records reveals variability that is similar to present ENSO variation. The authors suggest that prior research advocating a permanent El Niño state may have been limited by the coarse resolution of many SST proxies, and maintain that this new coral-based analysis identifies climate variability at the temporal scale required to firmly resolve ENSO structure. Wara et al. (2005) used δ^{18}O and Mg/Ca ratios from foraminiferal shells at temporal intervals of ~ 10 ka from 5.3 Ma to present, gathering over 400 data points. Several key features in the results showed that the Pliocene maintained permanent El Niño-like conditions. (1) Relative to today, the equatorial upwelling region of the eastern equatorial Pacific (EEP) was warmer (by ~ 2^0C than modern SSTs), (2) the west-east SST difference along the equator was reduced, (3) the thermocline in the EEP was deeper, and (4) subsurface conditions were more symmetric across the tropical Pacific. The alteration of these conditions may be the cause of the much stronger and more frequent cycles of El Niño experienced today. On the other hand, the fossil *Porites* records from the Philippines resemble a modern, living *Porites* record from the study site which correlates with modern ENSO variability, and negative δ^{18}O events in the fossil corals closely

resemble the decreases in $\delta^{18}O$ seen in the living, modern coral during El Niño events. Obviously further research is needed in order to confirm whether or not the Pliocene was indeed a time of permanent El Niño-like conditions.

1.6 Conclusion

It is apparent that corals represent an essential tool for analysing climate change on a range of timescales and resolutions. The Indo-Pacific, which is home to the greatest diversity of coral species, is a region of dynamic climate interactions, many of which dictate the behaviour of the entire global climate system. The range of coral species used as climate proxies is relatively narrow at present. *Porites* and *Diploastrea* are the two genera from this region which are best understood in terms of the reliability of their geochemical signal. This thesis provides pioneering studies using a modern *Goniastrea retiformis* coral and fossil *Platygyra pini* and *Platygyra lamellina* corals, offering the first detailed study of such species in the Indo-Pacific. Discussions draw on climate information gathered during previous studies and provide new and unprecedented insights into climate conditions in the Indonesian region.

2 *Goniastrea retiformis*, investigations of a new climate proxy for the Indo-Pacific

2.1 Abstract

A modern *Goniastrea retiformis* coral was retrieved from an intertidal reef on the north coast of Timor Leste. Skeletal $\delta^{18}O$ and $\delta^{13}C$ show clear seasonal records that correspond to changes in local sea surface temperature (SST). This is the first detailed investigation using this coral species and confirms that *G. retiformis* shows promise as a palaeoclimate proxy. Its abundance throughout the Pacific and Indian Oceans since the middle Cenozoic, intermediate growth rate and dense skeleton emphasise that this species is an ideal candidate. Analyses of stable isotopes $\delta^{18}O$ and $\delta^{13}C$ have revealed mean values of -5.35‰ ± 0.03‰ (2σ) and -1.02‰ ± 0.02‰ (2σ), respectively, and range from -4.62 to -6.11‰ and 1.57 to -2.53‰. $\delta^{18}O$ and $\delta^{13}C$ are in phase, suggesting that a common kinetic or metabolic mechanism is affecting the isotope ratios of both elements. The record spans ~ 4.5 years, and when plotted against the Southern Oscillation Index (SOI) is seen to emulate El Niño Southern Oscillation (ENSO) cycles throughout the 2006-2008 study period, but becomes out of phase during the mid 2008-2010 period. This may be due to a local climate effect overprinting the isotopic signal of the regional ENSO phenomenon. Local SST data has been modelled using the Met Office Hadley Centre's HadISST1 data set, with positive (negative) $\delta^{18}O$ values corresponding with SST troughs (peaks), as expected. *G. retiformis* $\delta^{18}O$ data is compared with a modern *Porites* coral from West Timor, enabling comparison with a well understood coral genus from the same region. The *Porites* $\delta^{18}O$ ranges from -4.07 to -5.94‰, with a mean of -5.31‰ which is only 0.04‰ more positive than *G. retiformis* mean $\delta^{18}O$. $\delta^{18}O$ is also consistent with mean regional values of -5.1‰ to -5.6‰ found in *Porites* corals. Spectral analaysis and sinusoidal modelling of isotopes has revealed quasi-biennial periodicity, representative of the interaction between ENSO and the South Asian monsoon, which is manifest at low latitudes as tropical biennial oscillation (TBO). These results suggest that with further investigation this species will become a robust climate proxy for both modern and palaeoclimates throughout the Indo-Pacific region.

2.2 Introduction

Modern corals from the tropical south west Pacific have been recognised as important tools for climate research. Coral records have had a major contribution to the current understanding of climate change on geological timescales, as isotopic analysis of their aragonite skeletons provides detailed incremental fluctuations in oxygen and carbon isotopes. A thorough geochemical understanding of *Porites* corals has meant that this genus is most commonly used, with many studies providing robust evidence for a strong corroboration between coral $\delta^{18}O$ and regional SST and sea surface salinity (SSS) data (e.g. Asami et al., 2004; Cahyarini et al., 2008; Guilderson and Schrag, 1999). Annual periodicity is typically recorded in modern *Porites* corals (e.g. Al-Rousan et al., 2007; Cahyarini et al., 2008; McGregor et al., 2011), which is indicative of seasonal SST and SSS fluctuations. However this is not the only periodicity that can be recorded, with a quasi-biennial signal visible in some *Porites* corals (Charles et al., 1997). This phenomenon is explained by Meehl (1994), who describes that coupled climate interactions between the ocean and atmosphere contribute to a mechanism that produces TBO in the troposphere and upper ocean in the tropical Indian and Pacific Ocean regions. Research has linked the biennial component of variability to ENSO, whereby TBO is associated with modulations of the seasonal cycle, with maxima in the TBO manifested as temperature extremes (El Niño and La Niña) in the tropical Pacific (Meehl, 1987). Of pertinence to this study, links between the South Asian monsoon and ENSO have been shown to have a biennial tendency (e.g. Rasmusson and Carpenter, 1983; Webster and Yang, 1992), driving SST and surface wind variations.

Porites are not the only abundant corals found in the Indo-Pacific. *Goniastrea retiformis* corals are prolific throughout the Indo-Pacific, an area of particular interest to climate change scientists due to the region's major influence on global climate behaviour (Qu et al., 2005). This species has been selected for a pilot study to assess its ability to accurately record climate fluctuations in the southern Indo-Pacific. *G. retiformis* colonies are massive, hemispherical, flat or columnar, often over one metre across and generally occur between 1-15m water depth (Veron, 2000). Similar to *Porites*, this species flourishes throughout the Indo-Pacific and extends to the coastline of east Africa and the Red Sea (Fig. 2.1). Growth rate investigation of a colony at Enetewak (Marshall Islands, North Pacific) showed maximum annual growth rates of 10.0 mm, 9.5 mm, and 6.0 mm for depths of 0-5 m, 6-15 m, and 16-25 m, respectively (Dullo, 2005; Highsmith, 1979). This species is also described as

having an intermediate growth rate compared to *Favia pallida* and *Porites lutea*, as well as the densest skeleton of all three (Highsmith, 1979). These skeletal features make it a suitable coral for using X-ray analysis to determine annual density bands, and provides a robust skeleton allowing high resolution micromilling. This sample was collected from a natural, intertidal reef setting on the north coast of Timor Leste (125° 34' E/08° 29' S), in close proximity to Indonesian Throughflow currents flowing through Ombai Strait (Fig. 2.2). After thorough screening for diagenesis, involving X-ray diffraction (XRD), petrographic analysis and scanning electron microscopy (SEM), a section of the coral has been micromilled to create aragonite powders collected for stable isotope analysis. $\delta^{18}O$ and $\delta^{13}C$ results from this ~ 4.5 year old coral are in phase, suggesting that a combination of kinetic and metabolic isotope effects acting upon and within the coral are causing this covariant relationship. Statistical analysis has been carried out using the programme Palaeontological Statistics (PAST). Spectral analysis and sinusoidal models of $\delta^{18}O$ and $\delta^{13}C$ are used to identify periodicity within the data. Comparison with regional climate records has allowed investigation of specific climate events recorded by the coral, but unfortunately historical climate data for Timor Leste is limited.

Expanding the application of coral proxies beyond *Porites* will enable increased data capture throughout the tropics, and provide increasingly detailed insights into modern and historical climate variability. Timor Leste is a prime setting for such research as it is located within the Indo Pacific Warm Pool (IPWP), where the interaction of atmospheric and oceanic processes control the regional climate. In spite of this, there have been no previous efforts to establish coral proxy records in this location. Our findings suggest that further analyses of *G. retiformis* corals will yield additional positive results for the calibration of this coral species as a climate proxy.

2.2.1 Modern coral studies

A thorough understanding of isotope and elemental dynamics in the *Porites* genus has meant that detailed insights of not only modern climate but also Holocene climate behaviour throughout the Indo-Pacific has been revealed, due to the excellent preservation and abundance of *Porites* corals in raised reefs. To a lesser extent, modern *Montastrea* (Swart et al., 1996; Watanabe et al., 2002; Winter et al., 2000), *Diploastrea* (Watanabe et al., 2003), and *Platygyra* (Weber and Woodhead, 1972) have also been studied. Watanabe et al. (2003)

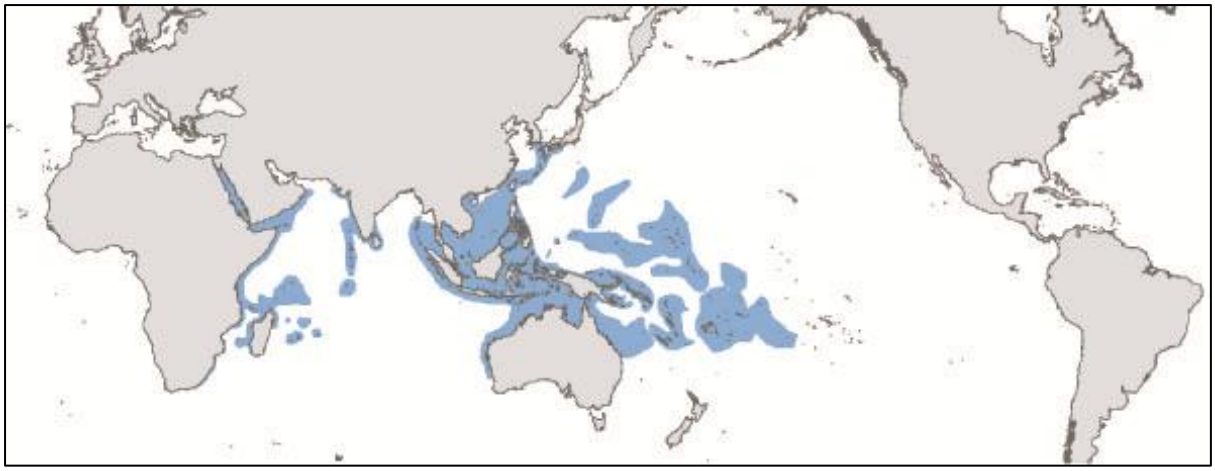

Fig. 2.1 Global distribution of *Goniastrea retiformis*. Image sourced from Veron, 2000.

examined the geochemical systematics of the robust, slow growing (2 to 6mm/yr) *Diploastrea heliopora,* which is distributed throughout the Indo-Pacific. In contrast with the rapidly growing *Porites* (8 to 24mm/yr), the slow growing nature and long fossil history of *D. heliopora* means it has the potential to yield continuous palaeoclimate records spanning up to 1000 years in the IPWP (Watanabe et al., 2003). This unique feature of *D. heliopora* is highlighted by the discovery by Dunbar et al. (1994) that *Pavona* from the eastern equatorial Pacific has the same barrier as *Porites* and *Montastrea*, with continuous geochemical records limited to ~300-400 years B.P. However, coral calibrations are not restricted to the Caribbean and Pacific. The discovery of significant correlations between Sr/Ca ratios and SST records in the non-tropical *Cladocora caespitosa* from the north-western Mediterranean Sea (Silenzi et al., 2005) suggests the feasibility of using this coral as a new climate proxy for the region. Similarly with the Indo-Pacific region, the only possibility to extend beyond the historical climate database in the Mediterranean Sea is to use well-dated natural archives of climate variability.

Of significance to this study, a modern *Porites* calibration for West Timor using paired coral $\delta^{18}O$ and Sr/Ca measurements to determine $\delta^{18}O_{sw}$ and SSS has been completed by Cahyarini et al. (2008). A drill core sampled along the main growth axis of the coral provides the paired record spanning 1985-2004 years (Fig. 2.3). The $\delta^{18}O$ and Sr/Ca records both display strong seasonal variation. The isotopic and elemental results were compared with SSS data from the Simple Ocean Dada Assimilation (SODA) model prepared by Carton et al. (2000a; 2000b) which provides monthly averages of SST and SSS data extending back until 1950

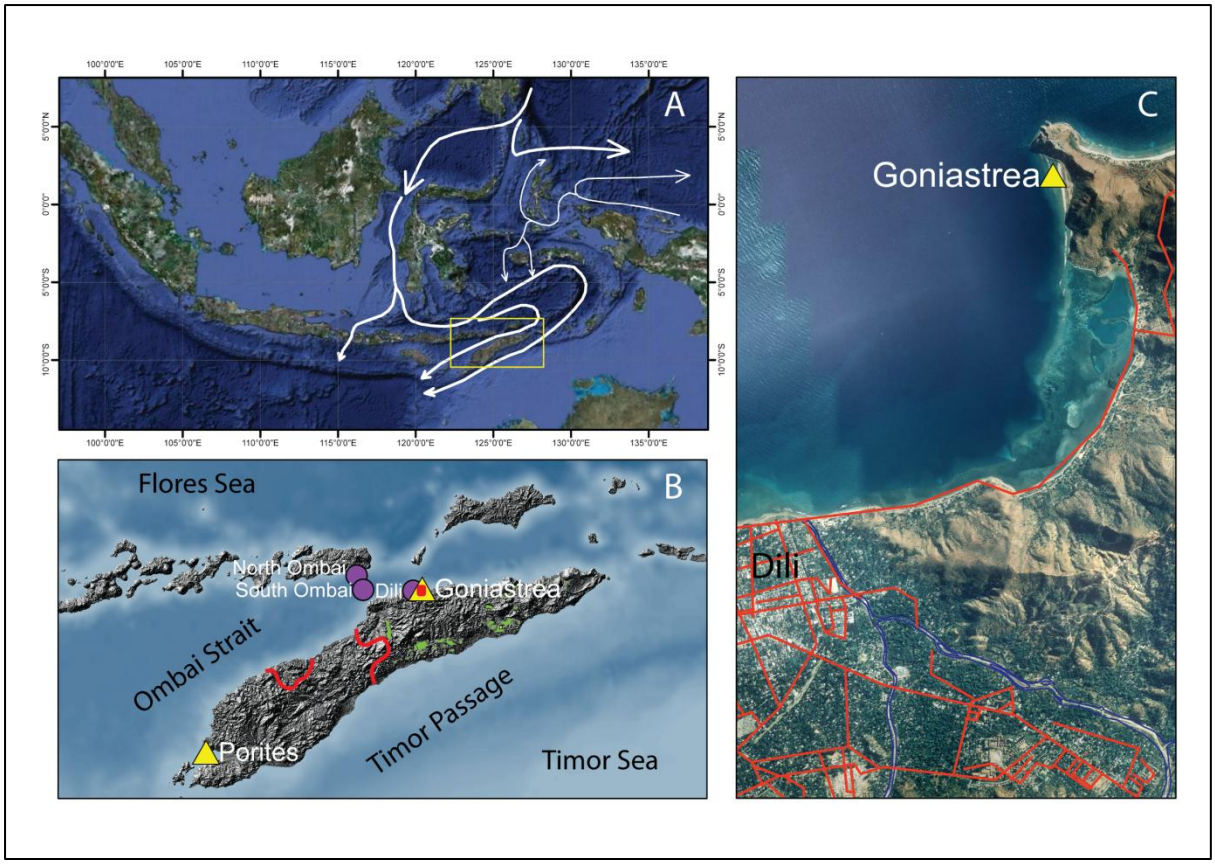

Fig. 2.2 (A) Location of Timor within southwest Pacific (yellow box). Thick white lines represent main pathways of the Indonesian Throughflow (ITF), thin white lines represent minor pathways of the ITF, as shown by Gordon and Fine (1996). (B) Larger image of Timor, with red lines indicating the roughly north-south boundary of Timor Leste with West Timor, and red line within West Timor indicating the enclave of Oecussi, part of Timor Leste. Modern *Goniastrea* coral site and modern *Porites* site depicted by yellow triangles. Climate data collection points depicted by purple circles. Green shaded areas in Timor Leste indicate the extent of the Viqueque Megasequence. Red square indicates where map (C) is located. (C) Shows the intertidal reef location of the modern *Goniastrea retiformis* coral.

over a 0.5^0 by 0.5^0 grid. A gradual freshening was detected in annual mean $\delta^{18}O_{sw}$ throughout the study period. However, it is acknowledged that the SODA data may underestimate the variance of the SSS record, with higher SSS variance revealed in the coral record. As historical instrumental records from the Timor region are limited, Cahyarini et al. (2008) acknowledged that long term monitoring programmes would greatly reduce the uncertainties of quantitative $\delta^{18}O_{sw}$ and SSS reconstructions from corals in this region and significantly improve the reliability of results. This issue of limited historical climate data is

also true for Timor Leste, and the suggestion for the initiation of more long term monitoring programmes to aid scientific research applies throughout the entire island of Timor.

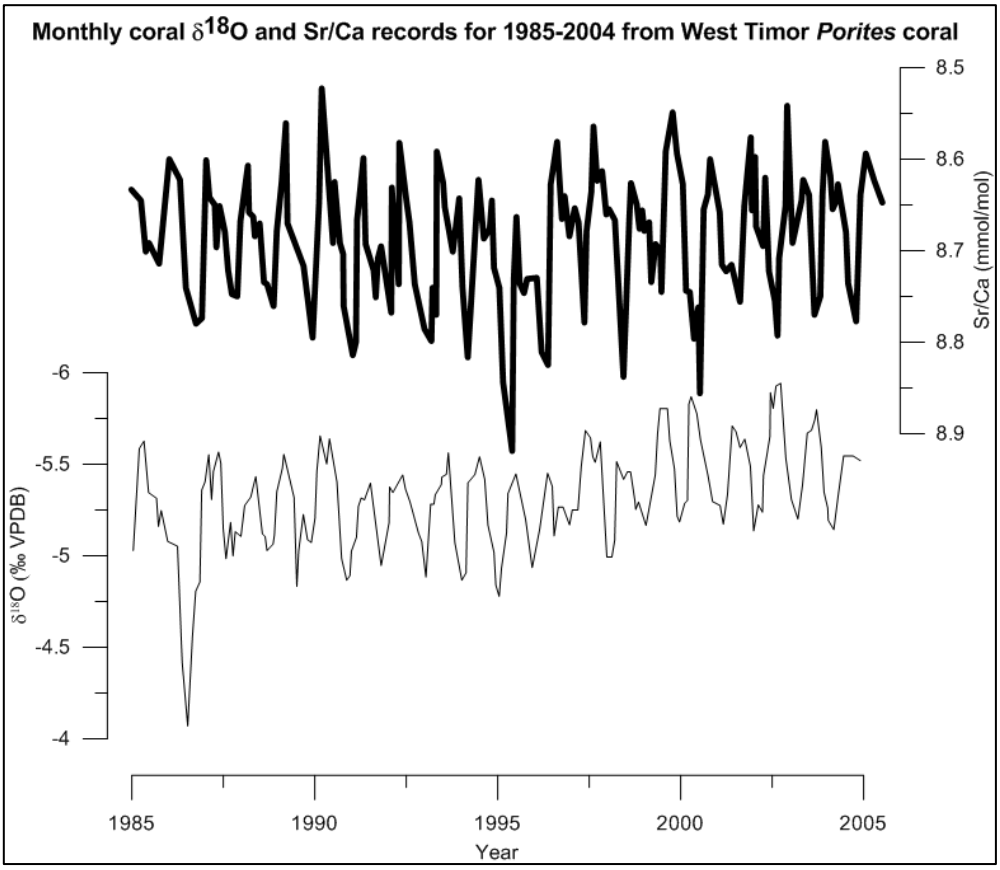

Fig. 2.3 Monthly coral $\delta^{18}O$ (thin line) and Sr/Ca (thick line) records for the time period 1985-2004 for a *Porites* coral from West Timor. Modified from Cahyarini et al., 2008.

In order to gain an understanding of the isotopic range of a variety of modern corals from within the Indo-Pacific and beyond, coral $\delta^{18}O$ data from similar studies has been amalgamated into a table (Table 2.1). This shows that overall mean values for the Indo-Pacific are -5.1 to -5.6‰, -4.3 to -5.0‰ in the central Pacific, and -4.3 to -5.7‰ in the South China Sea. These values provide a relevant reference frame to compare with the *G. retiformis* $\delta^{18}O$ results.

Table 2.1 Mean $\delta^{18}O$ range for modern corals sampled from the Indo-Pacific, central Pacific, South China Sea, Caribbean Sea, Mediterranean Sea and Red Sea.

Coral species	Location	Mean $\delta^{18}O$ range (‰ VPDB)	Record length (years)	Time period	Publication
Porites sp.	West Timor, Indonesia	-5.0 to -6.0	19	1985-2004	(Cahyarini et al., 2008)
Porites sp.	Alor, Indonesia	-5.4 to -5.6	14	1985-1999	(Watanabe et al., 2003)
Diploastrea heliopora	Alor, Indonesia	-5.0 to -5.4	19	1980-1999	(Watanabe et al., 2003)
Porites lobata	Double Reef, Guam	-5.0 to -5.5	20	1980-2000	(Asami et al., 2004)
Porites sp.	Nauru Island	-4.5 to -5.5	103	1896-1999	(Guilderson and Schrag, 1999)
Platygyra lamellina	Espirito Santo Island, Vanuatu	-4.5 to -5.5	173	1806-1979	(Quinn et al., 1993)
Porites sp.	New Caledonia	-4.4 to -4.5	12	1980-1992	(Watanabe et al., 2003)
Diploastrea heliopora	New Caledonia	-3.8 to -4.3	16	1980-1996	(Watanabe et al., 2003)
Porites lutea	Pandora Reef, Great Barrier Reef	-3.8 to -5.2	6	1978-1984	(Gagan et al., 1994)
Porites sp.	Christmas Island, Central Pacific	-4.8 to -5.2	29	1978-2007	(McGregor et al., 2011)
Porites lobata	Nanwan Bay, Taiwan	-4.4 to -5.6	12	1992-2003	(Chiang et al., 2010)
Platygyra sp.	Ishigaki Island, Japan	-4.5 to -6.0	10	1995-2005	(Shimamura et al., 2008)
Porites sp.	Ishigaki Island, Japan	-4.2 to -5.5	10	1995-2005	(Shimamura et al., 2008)
Montastrea faveolata	Biscayne National Park, South Florida	-3.2 to -4.4	24	1962-1986	(Swart et al., 1996)
Cladocara caespitose	Mediterranean Sea	-1.0 to -2.0	95	1906-2001	(Silenzi et al., 2005)
Porites lutea	Gulf of Aqaba, Red Sea	-2.2 to -3.0	18	1988-2005	(Al-Rousan et al., 2007)
Porites lobata	Gulf of Aqaba, Red Sea	-2.2 to -3.2	14	1991-2005	(Al-Rousan et al., 2007)

2.2.2 Modern climatic setting

Timor Leste has a climate typical of the Asian tropics, with little temperature variation throughout the year and relatively high annual rainfall. It experiences the effects of both the Indo-Australian monsoon system and ENSO, and is located within the warmest part of the IPWP, (i.e. the Western Pacific Warm Pool, WPWP), which encompasses the region east of Indonesia where the SST is > 29^0C (Linsley et al., 2010). Strong seasonal variations are caused through changes in prevailing winds, which control the wet and dry seasons. NW winds from December through March bring heavy rains during the wet season, and the change to SE-NE winds from May to October brings a dry season to all localities, except the south coast and southern slopes where rainfall generally continues until July. Average annual rainfall increases with altitude, from approximately 565mm at Manatuto (10 to 20 m a.s.l.) on the northern coast, to 2837mm at Lolotoi in the central western mountains (Kirono, 2010). Temperature also exhibits this spatial pattern. Average temperatures of 27^0C are recorded at sea level, dipping to 25^0C in the highlands, and a dramatic decrease to 14^0C at 2000 m elevation (Barnett et al., 2003; Kirono, 2010). During the wet season, SST in the waters around Timor range between ~28.5^0 and 30^0C, and low salinity waters from the South China Sea are pushed into the Makassar Strait, a main passage of the Indonesian Throughflow (ITF) (Cahyarini et al., 2008). In the dry season, SST ranges between ~26^0 and 29^0C, with low salinity waters found further to the east in the Banda Sea (Gordon et al., 2004). In order to determine the amplitude of seasonal changes in SST and SSS in Timor, SODA data has been used to create a graph showing average values over two years (Fig. 2.4). The SODA reanalysis project is ongoing, beginning in the mid 1990s, with the aim to reconstruct historical ocean climate variability, providing monthly averages of SST and SSS data extending back until 1950. Version 1.4.2 extends from 1958 to 2001 and includes data relevant for Timor. When plotted, both SST and SSS show a clear seasonal cycle and positively co-vary, with maximum (minimum) SST coinciding with maximum (minimum) SSS. SST ranges from 26.8°C in August to 30°C in December. SSS ranges from 34 practical salinity units (psu) in July to 34.4 psu in January. Timor Leste has been defined as having three climatic zones based on rainfall and temperature characteristics; a relatively warm and dry northern coast, a warm and wet southern coast, and a cool and very wet mountain zone. Barnett (2003) explains that Timor also experiences two distinct rainfall patterns; Northern Monomodal Rainfall Pattern (NMRP) and Southern Bimodal Rainfall Pattern (SBRP).

NMRP is a 4 to 6 month wet season beginning in December, affecting most of the northern side of the country and tapers to the east. In contrast, SBRP is a longer, 7 to 9 month wet season with two rainfall peaks which begin in December and May, affecting the southern side of the country. Total annual rainfall and mean temperature data from locations around Timor Leste (Fig. 2.5) represents the aforementioned rainfall patterns (Fig. 2.6). Mean annual temperature and precipitation records from Dili which span the lifetime of the *G. retiformis* coral (2006-2010) are shown in Fig. 2.7 and Fig. 2.8, respectively. A maximum temperature fluctuation of 1.4°C is observed in the temperature data. ENSO episodes have been indicated in the Timor Leste rainfall figures, showing that distinct rainfall peaks (troughs) have been recorded throughout the country during La Nina (El Niño) years. Timor has a dynamic climate due to the interactions between multiple climate systems and its location within the central part of the tropics.

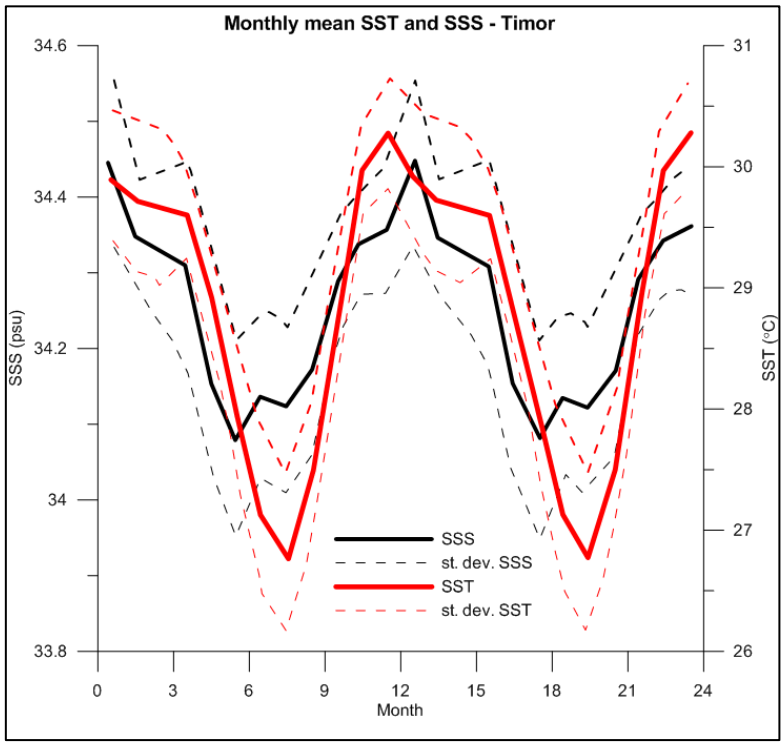

Fig. 2.4 Monthly mean SST (solid red line) and SSS (solid black line) data for Timor. The climatology is calculated over the period 1958-2004, with average monthly values being displayed over a two year period with month 1 being January, month 12 December, and month 24 the following December. Two distinct annual cycles are visible, with a strong covariance between SST and SSS. Dashed lines are standard deviation (1σ) of monthly mean SST and SSS data. SST and SSS are obtained from SODA v. 1.4.2. (Carton et al., 2002a). Modified from Cahyarini et al., (2008).

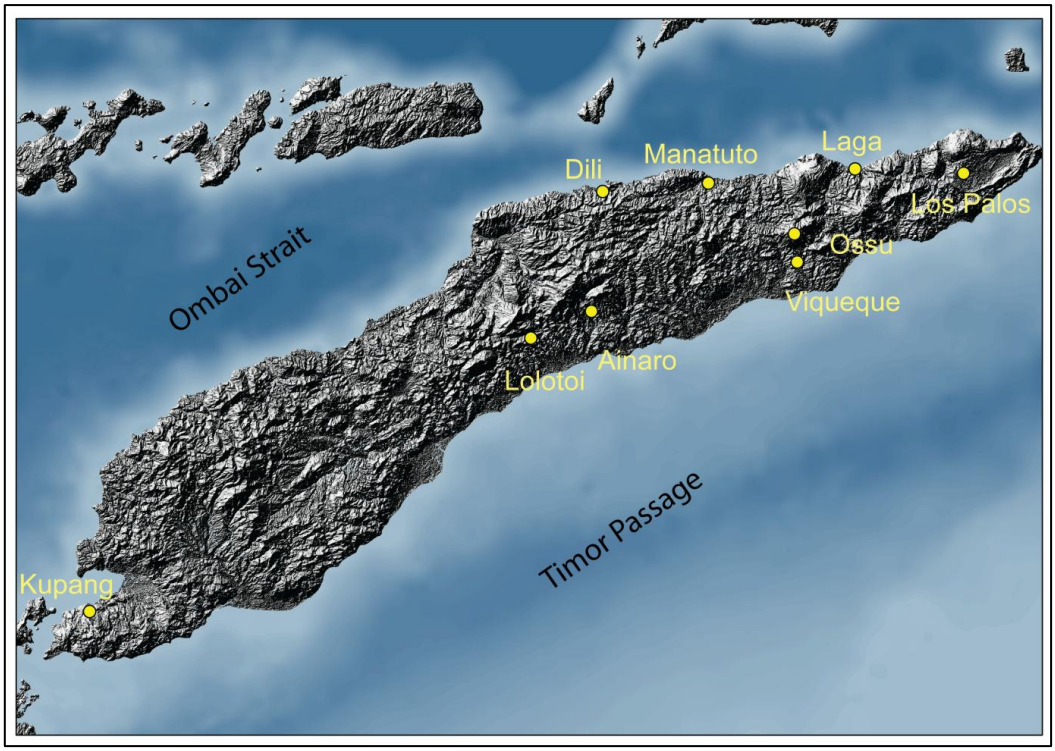

Fig. 2.5 Locations of rainfall and temperature data from Timor Leste and West Timor.

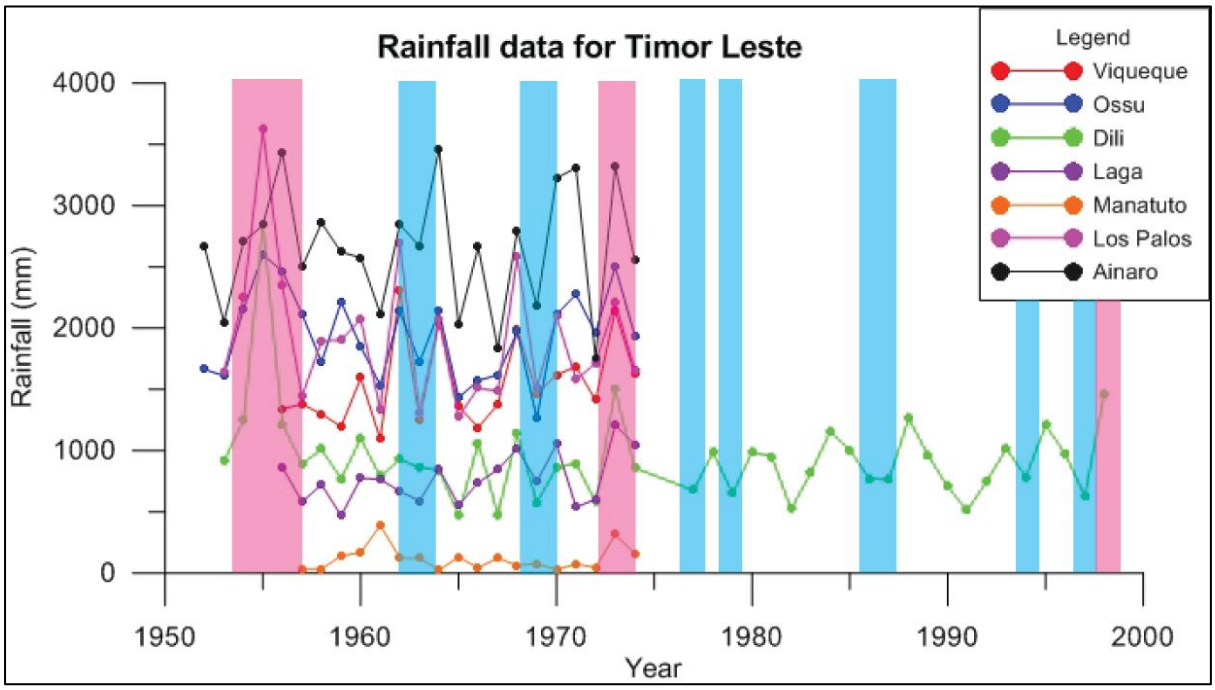

Fig. 2.6 Total annual rainfall data for Timor Leste, from 1952-1999 (Dili) and 1952-1989 for all other locations, showing the distinct pattern of higher rainfall in the southern and mountainous zones, and drier conditions in the northern lowlands. Blue bars indicate El Niño episodes, pink bars indicate La Niña episodes (NOAA data). Rainfall data sourced from the Timor Leste Meteorological Survey (Meteorologia de Timor Leste).

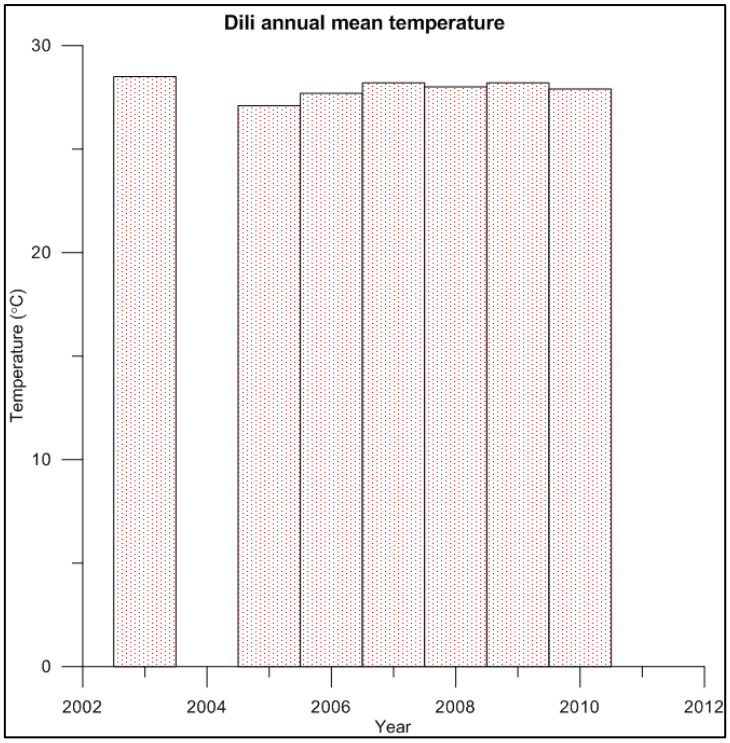

Fig. 2.7 Mean annual temperature for Dili Airport data collection site, 2003-2010, displaying a maximum fluctuation of 1.4°C. No data available for 2004. Data sourced from Australian Bureau of Meteorology.

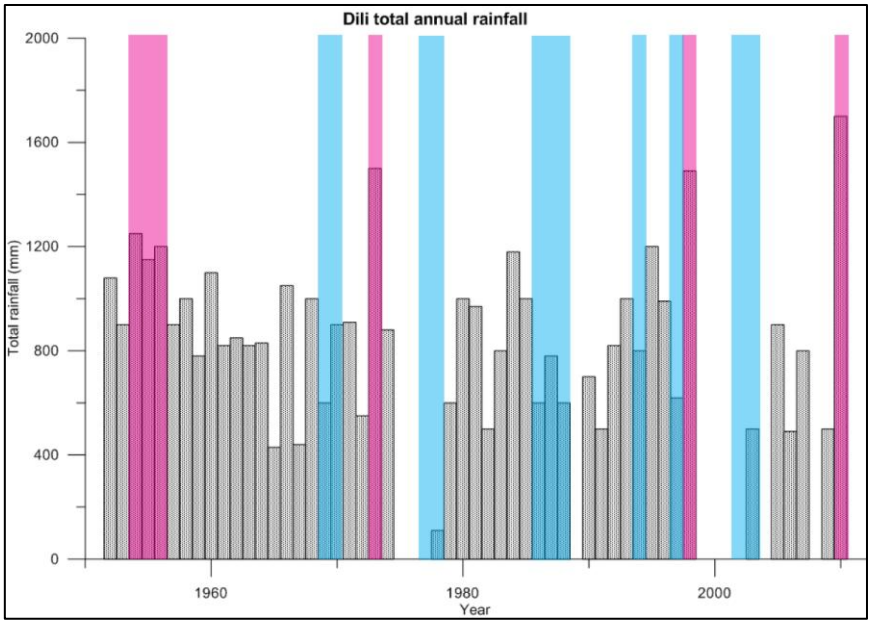

Fig. 2.8 Total annual rainfall for Dili Airport data collection site, 1952-2010. Blue bars indicate El Niño episodes, pink bars indicate La Niña episodes (NOAA data). Rainfall data sourced from the Australian Bureau of Meteorology.

2.3 Methodology

The *G. retiformis* coral was retrieved with hammer and chisel from an intertidal reef at 2 m depth at high tide, approximately 50 m offshore off the coast near Dili in July 2010 (Fig. 2.2 C). Initially, two 7mm slabs were cut from the centre of the robust coral skeleton with a diamond wafer saw, cleaned with an ultrasonic probe to remove loose particles and surface contaminants, then X-rayed to identify annual density bands (Fig. 2.9). These bands revealed approximately 4.5 years of growth, meaning that the coral was living from early 2006 until July 2010. This also allows growth rates to be determined, with a rate of ~ 5 mm/year identified in this sample, which is slower than growth rates identified in a *G. retiformis* colony in Enetewak (Dullo, 2005; Highsmith, 1979).

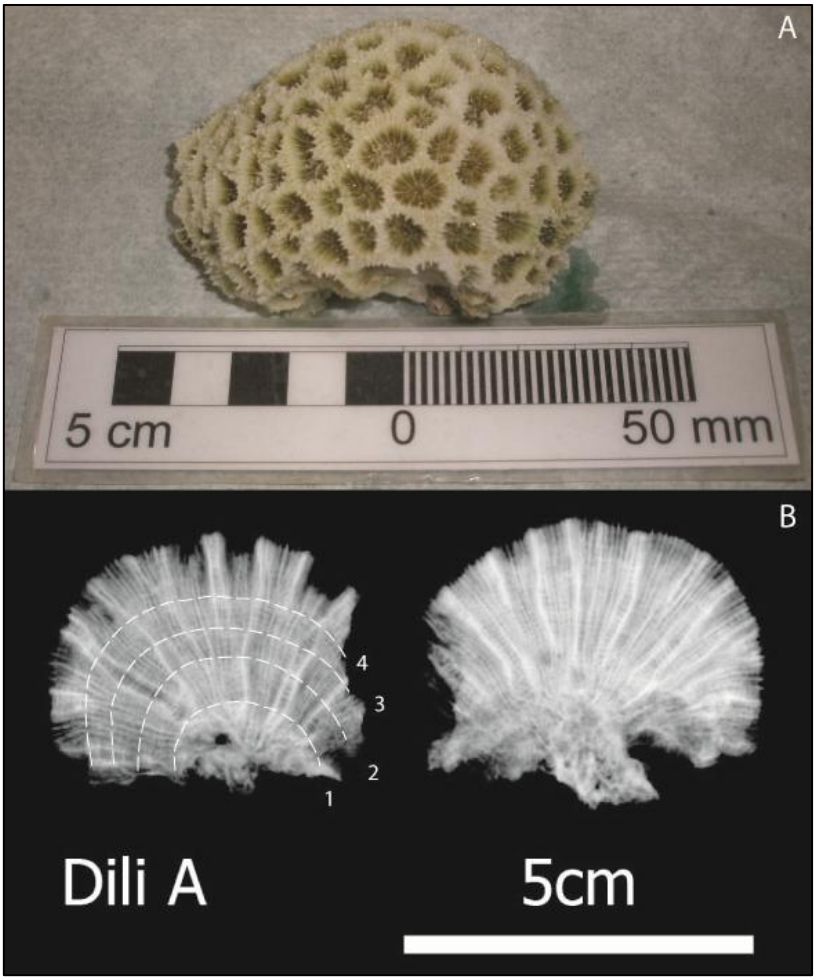

Fig. 2.9 (A) *G. retiformis* coral specimen shortly after retrieval from living position in shallow reef, (B) X-ray image of two 7mm slabs with visible high and low density couplets indicating ~ 4.5 years growth. Dashed white lines on X-ray image indicate location of annual growth bands, with number representing years of growth.

2.3.1 Screening for diagenesis

2.3.1.1 XRD

The cut face adjacent to the two 7mm X-rayed slabs was used to create samples for analysis by XRD and SEM. Coral samples were collected from the basal, middle and uppermost zones of the coral (Fig. 2.10), and were cleaned with ultra-pure compressed air prior to sampling in order to remove any loose particles, and coral chunks collected with tweezers or hand dremel. Tweezers were cleaned with ethanol and dremel bit cleaned on a piece of granite between each sample to avoid cross contamination between samples. Samples were then crushed into powder using an agate mortar and pestle which was cleaned with ethanol between samples. During the XRD screening procedure samples were scanned from 2θ of 3^0 to 50^0 using a Philips XRD at the University of Canterbury, providing a 100% aragonite result (Table 2.2). However, the first set of results gave trace calcite in the basal sample Dili A_A, which indicated the presence of a calcite below the specific detection threshold of 5%. Following this result, the coral was re-sampled in the same zones, but each sample was covered in ethanol prior to being crushed to powder with mortar and pestle, as secondary calcite can sometimes be artificially created during the process of sample crushing. The second set of results showed 100% aragonite with 0% calcite, indicating the during the initial XRD screening, secondary calcite had indeed been inadvertently produced. Diffractograms of all samples exhibit the aragonite peaks observed in the six individual samples (Refer to Appendix Figure 1 and Appendix Figure 2), and the trace calcite present in Sample Dili A_A. After passing this initial screening test, petrographic and SEM analyses were conducted.

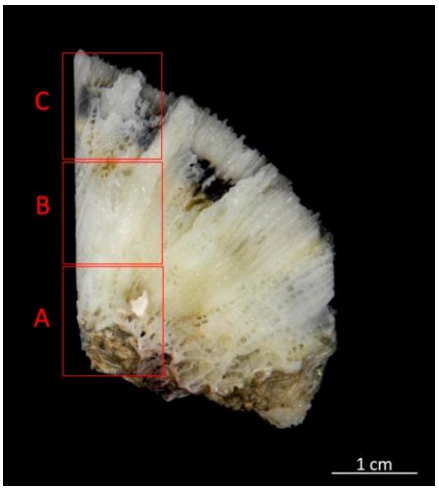

Fig. 2.10 Cut face of Dili A exhibiting location of XRD samples

Table 2.2 XRD results from first and second run of coral samples

XRD run	Coral sample	Aragonite (%)	Calcite (%)
1st	Dili A_A	100	trace
1st	Dili A_B	100	0
1st	Dili A_C	100	0
2nd	Dili A_a	100	0
2nd	Dili A_b	100	0
2nd	Dili A_c	100	0

2.3.1.2 PETROGRAPHIC ANALYSIS

One of the X-rayed 7 mm slabs was set in epoxy resin, and standard 0.03 mm thick, 60 x 20 mm petrographic thin sections were prepared. These revealed primary aragonitic textures as described by McGregor and Abram (2008) and provided the most compelling evidence of pristine aragonite, with radiating sclerodermites, centres of calcification and dissepiments visible, and minimal algal borings or leaching observed (Fig. 2.11 and Fig. 2.12). Sclerodermites are the basic building blocks of all parts of all coral skeletons and consist of fine aragonite crystals or fibers arranged in three dimensional fans about a calcification centre (Cohen and McConnaughey, 2003), thus represent an unaltered coralline skeleton when visible. Petrographic analysis is an imperative technique, as it allows secondary aragonite to be distinguished from primary aragonite due to their different crystal structure, whereas both give the same pattern in XRD. Additionally, the XRD detection limit is around 1% calcite at best, and even calcite levels as low as this have been shown to cause significant alteration of coral proxy climate signals (McGregor and Abram, 2008). This highlights the importance of petrographic analysis in any coral screening programme.

2.3.1.3 SEM

SEM analysis required that chunks of coral were mounted onto stubs to allow investigation of both polished and broken surfaces (Fig. 2.13). Hendy et al., (2007) show the results of diagenesis visible under SEM, with pristine coral being smooth and having good preservation of pore spaces and dissepiments without any overgrowths. They describe secondary aragonite as having a fibrous, needle-like texture and dissolution causing a "melted"

appearance. The three main textures indicative of diageneis are (1) exposure of fasciculi bundles and an etched appearance of the skeletal wall surface, (2) pitting or a melted appearance of individual crystals, and (3) the loss of the granular microcrystalline coating, indicative of early marine dissolution. SEM analysis of the chunks of *G. retiformis* shows mostly very good preservation, with minor presence of what appear to be worm tubes visible in some pore spaces (Fig. 2.13 D).

2.3.2 Micromilling

After screening for diagenesis and determining that the preservation of this coral meets the standards required for isotope analysis, two new 7mm slabs were cut from the coral and prepared for micromilling. This involved cleaning with an ultrasonic probe and X-raying to determine the exact location of the annual density band couplets on these two slabs. A hand dremel was used to cut away the skeleton to the very edge of a solid septal wall, along which a milling path was set up using a New Wave Micromill (Fig. 2.14). Due to the size of the coral, approximately fortnightly sampling (0.02 mm spacing) was the maximum resolution attained over three density band couplets in the centre of the coral. This provided ~ 26 samples per year. The basal and uppermost density band couplets were milled at approximately monthly resolution, providing ~ 12 samples (0.04 mm spacing) from the basal density band and ~ 6 samples (0.04 mm spacing) from the uppermost density band. Samples were reacted with three drops of 103% H_3PO_4 at 75°C in an automated individual-carbonate reaction device (Kiel III). $\delta^{18}O$ and $\delta^{13}C$ of CO_2 liberated by the acid-carbonate reaction was determined on a Finnigan MAT252 mass spectrometer coupled to the Kiel III at the National Institute of Water and Atmospheric Research (NIWA), Wellington.

.

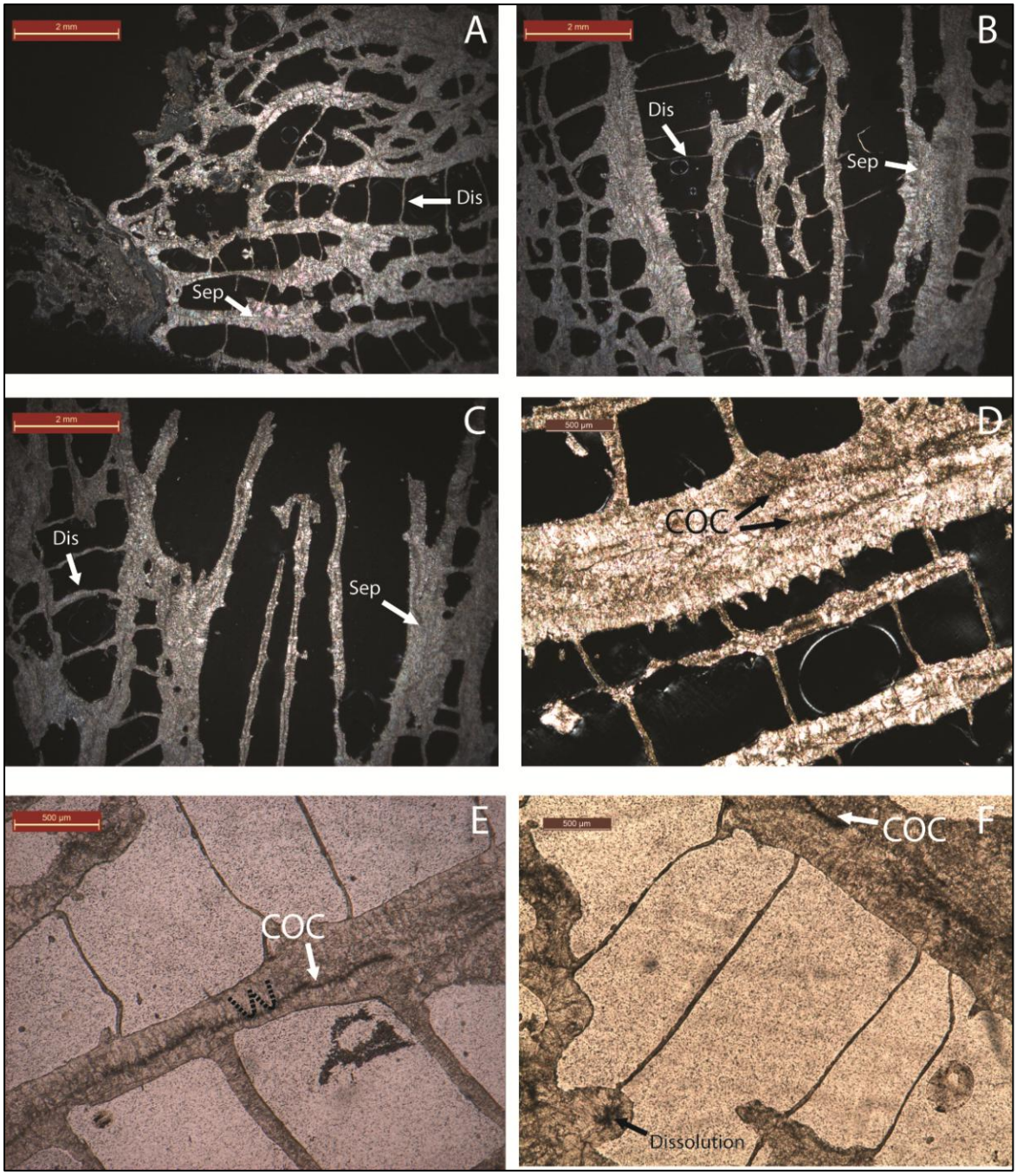

Fig. 2.11 Thin section micrographs of pristine modern coral aragonite in *Goniastrea retiformis* sample Dili A. (A) Cross polarised light (CPL) image of basal section of coral with arrows pointing to well preserved septae (Sep) and dissepiments (Dis). (B) CPL image of middle section of coral showing well preserved septae and dissepiments. (C) CPL image of uppermost section of coral showing well preserved septae and dissepiments. (D) Increased magnification CPL image showing well preserved dark, linear centres of calcification (COCs), no visible boring, dissolution or micritic infilling. (E) PPL image showing dark, linear COCs, sclerodermites (U-shaped dashed lines), and no visible boring,

dissolution or micritic infilling. (F) PPL image with minor dissolution visible, but otherwise well preserved COCs and dissepiments.

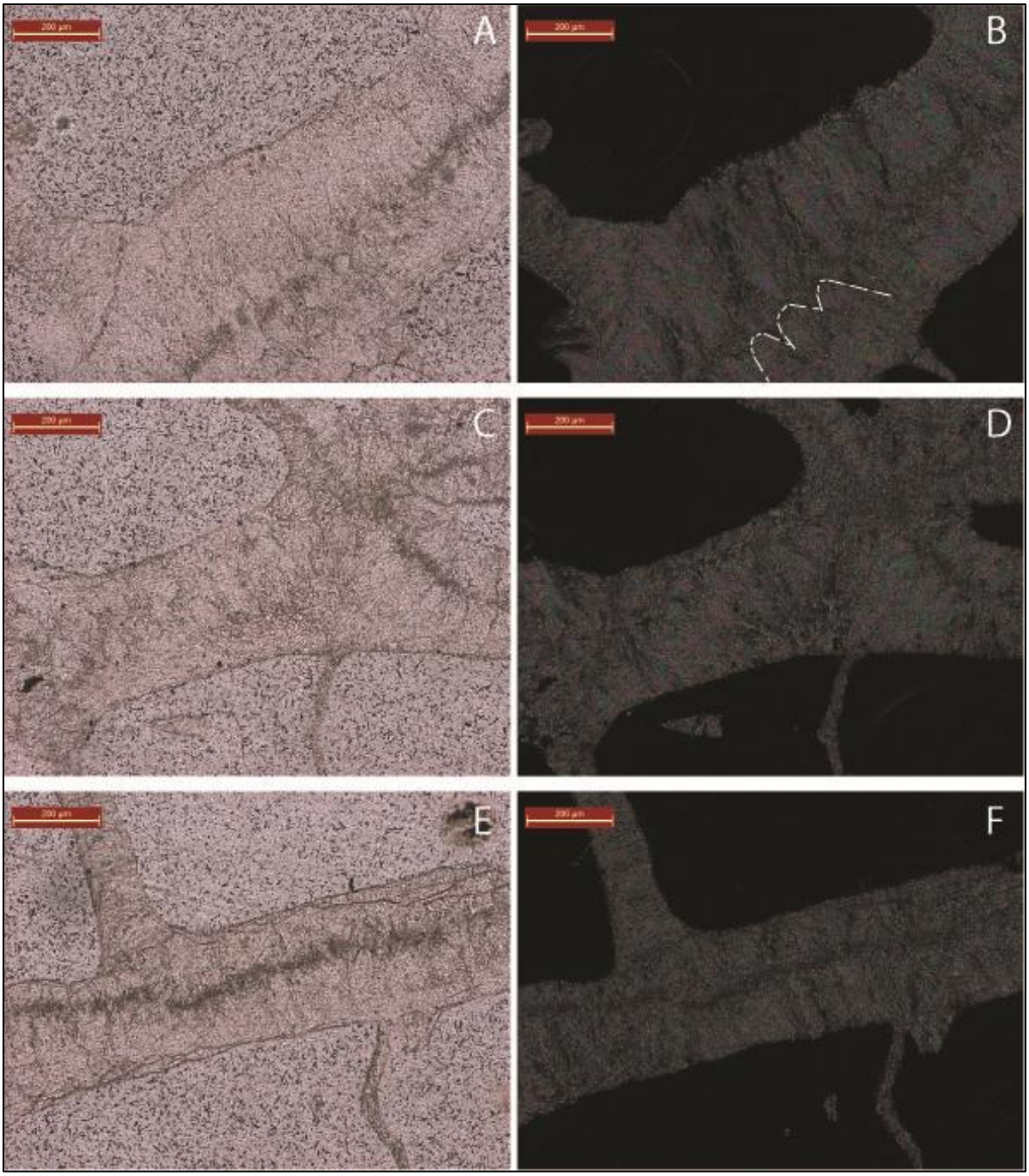

Fig. 2.12 Thin section micrographs of Dili A with images A, C and E shown in PPL, and images B, D and F shown in CPL. Well preserved dark, linear COCs visible in all images, no boring or micritic infilling of pores, edges of septae and dissepiments well preserved with no overgrowths. Dashed lines in (B) indicate sclerodermites.

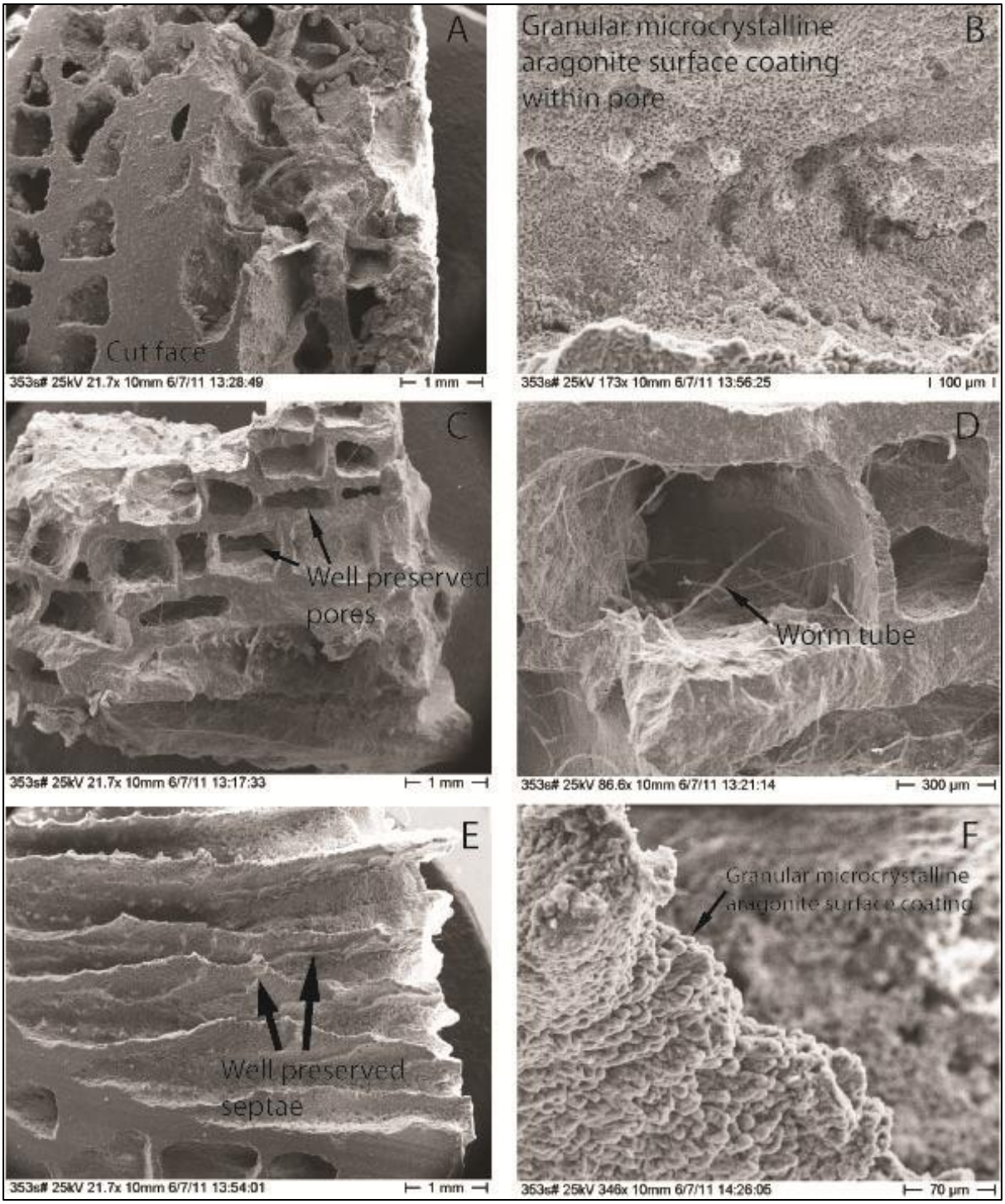

Fig. 2.13 Scanning electron microscopy (SEM) images of Dili A. Images (A) and (B) are basal zone, (C) and (D) are middle zone, (E) and (F) are uppermost zone. A) Overview of coral sample A with cut face providing cross sectional view of septae and dissepiments. (B) Close up of interskeletal pore from Sample A. (C) Overview of coral sample B with cut face providing cross sectional view of septae and dissepiments. (D) Close up of interskeletal pore from Sample B with visible worm tubes. These may have a minor amount of calcite but not enough to contribute towards any error in stable

isotope values. (E) Overview of coral sample C at the very top of the coral with a profile view of septae visible. (F) Close up of septa with primary aragonite crystals visible.

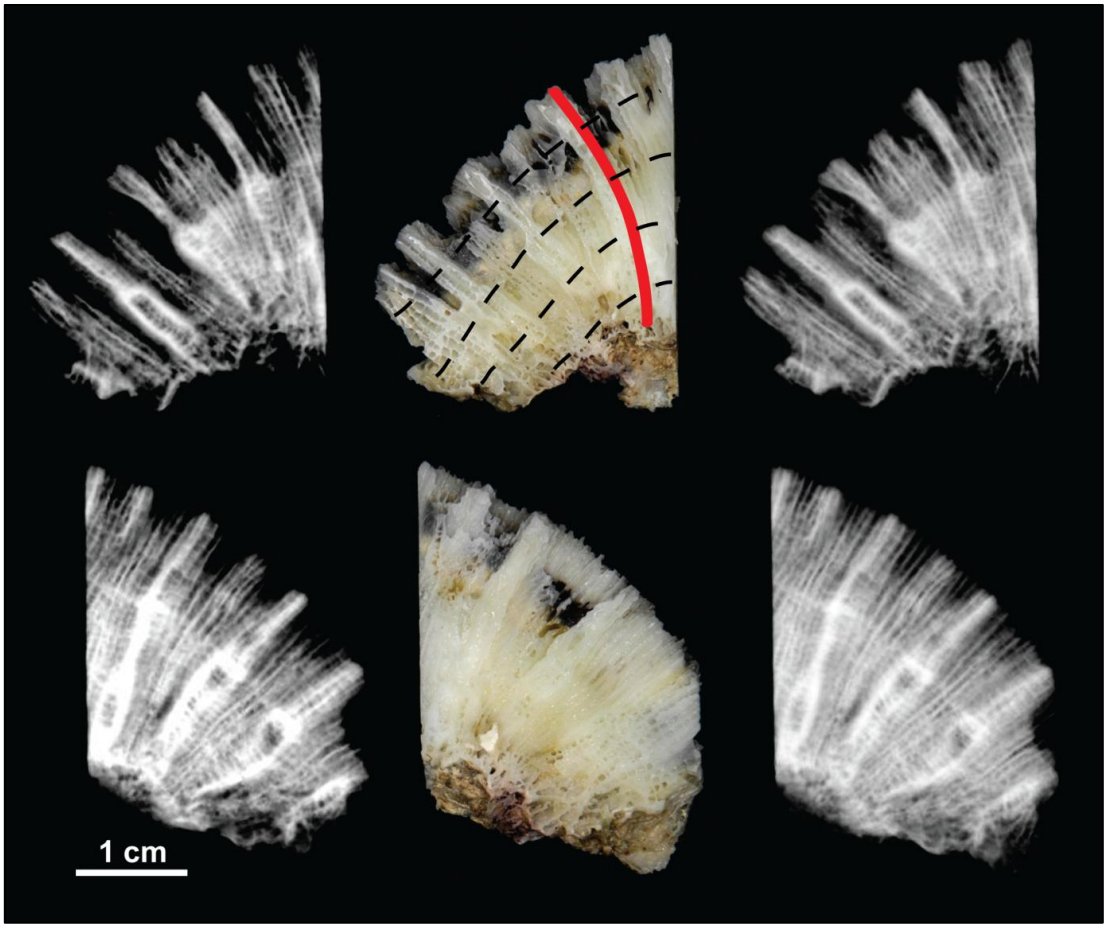

Fig. 2.14 Composite image showing two 7 mm slabs and X-ray images of *G. retiformis*. Micromill path shown in red. Material to right of red micromill path cut away with hand dremel prior to milling. Dashed lines indicate annual growth lines.

2.4 Results

Analyses of stable isotopes $\delta^{18}O$ and $\delta^{13}C$ have revealed mean values of -5.35‰ and -1.02‰, respectively, ranging from -4.62 to -6.11‰ and 1.57 to -2.53‰ (refer to Appendix Table 1). Raw isotopic data is presented in Fig. 2.15, with sample number in the x-axis and isotopic values on the y-axis. The coral powder samples collected between 60 and 70 were of minimal size due to changing polyp structure and therefore these results may not be a true representation of the isotopic ratios within this section of the coral. Sample numbers 58, 61, 66 and 68 are absent from the raw data as they were combined with their preceding sample in order to form the powder volume required for the mass spectrometer. Sample number 67

shows an anomalous positive peak in the $\delta^{18}O$ data set, reaching a value of -4.62‰. The next most positive value is -4.90‰. $\delta^{13}C$ also has a peak at sample 67, however this is not anomalous as there are multiple values of -0.34‰ or higher throughout this data set, which has greater amplitude fluctuations that the $\delta^{18}O$ results. Generally, the magnitude of fluctuations is greater in the $\delta^{13}C$ results than $\delta^{18}O$, except between sample numbers 60-70. A covariant relationship between $\delta^{18}O$ and $\delta^{13}C$ seen in Fig. 2.15 is investigated further using a correlation plot (Fig. 2.16), giving an R^2 value of 0.48.

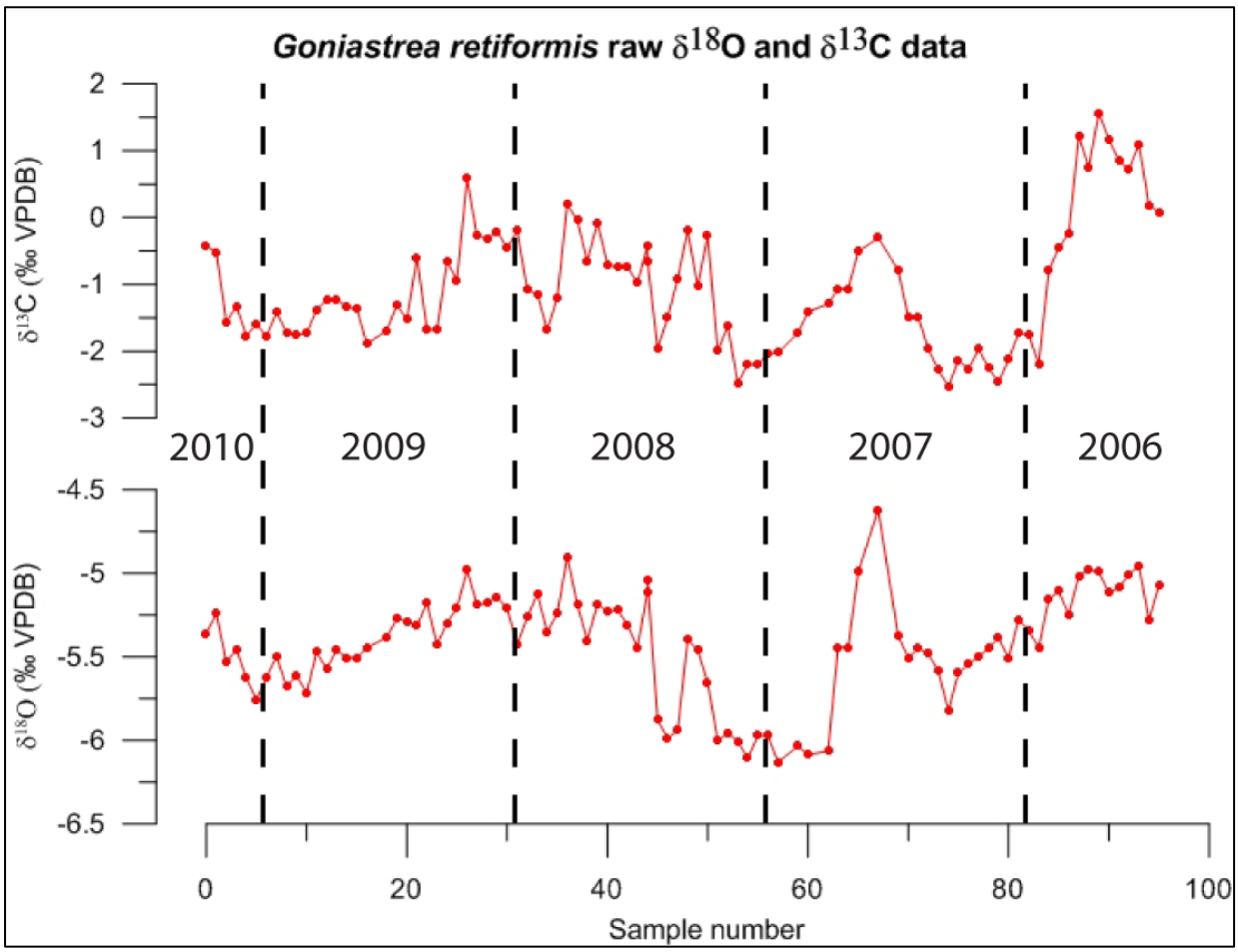

Fig. 2.15 Raw $\delta^{18}O$ and $\delta^{13}C$ data for *G. retiformis.* A distinct positive peak of -4.62‰ is visible at sample 67 of $\delta^{18}O$ plot. Dashed lines indicate years of coral growth which samples have been milled from.

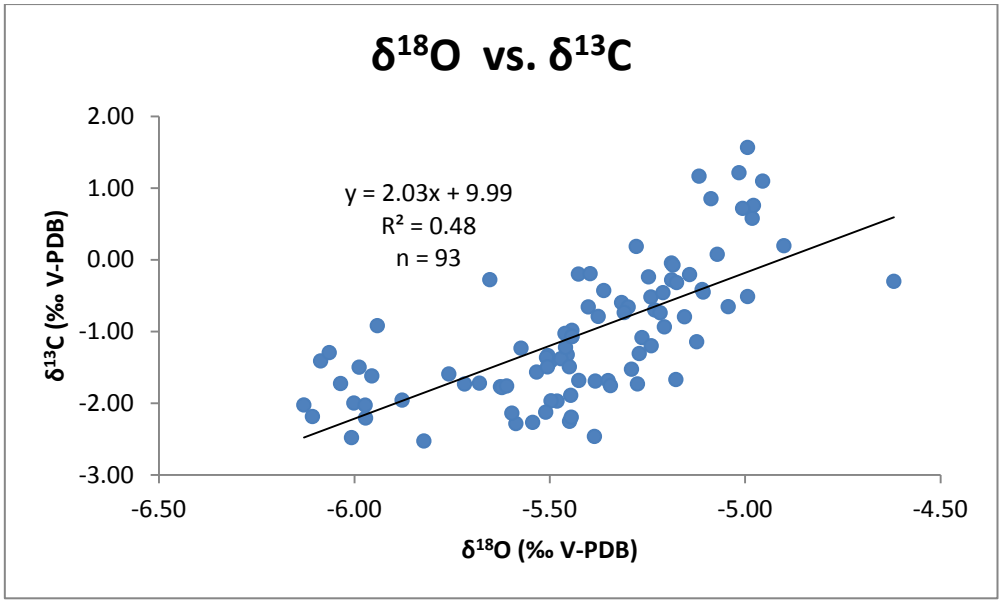

Fig. 2.16 $\delta^{18}O$ versus $\delta^{13}C$ scatter plot for all aragonite powders analysed. Covariance gives an R^2 value of 0.48 from 93 data points.

Raw $\delta^{18}O$ and $\delta^{13}C$ values are also displayed in time, with the period of coral growth (2006-2010) in the x-axis (Fig. 2.17). It must be noted that due to the coral being milled from the top to the base, Fig. 2.15 presents the data getting older to the right, whereas Fig. 2.17 shows younging to the right. In this figure, each year is separated with a dashed line to aid identification of periodicity in the data set. Annual cycles are not obvious within this coral, however it appears that there is some periodicity on a biennial scale. This is further analysed using PAST to create spectral analysis and sinusoidal fits to gain statistical insights into the data. As the purpose of spectral analysis is to estimate the power of periodic components at all possible frequencies, this form of analysis is exceptionally well suited to analysing this data set. Fig. 2.18 uses the Lomb periodogram to display spectral analysis of monthly $\delta^{18}O$. PAST requires data to be evenly spaced through the time series, therefore alterations to the raw data needed to be made in order to perform these statistical analyses. Monthly resolution was the lowest resolution recorded across the entire coral sample, so the three years of fortnightly resolved data (Years 2, 3 and 4) were modified to attain monthly values. This was achieved by using the mean value of every two fortnightly couples to provide a monthly mean value for each month of the three year period. The frequency of the strongest peak in the spectrum is reported as 0.03009 cycles per month. The equation used to convert peak frequency into a periodicity is as follows;

$$Periodicity = \frac{1}{0.03009}$$

$$Periodicity = 33.233\ months\ per\ cycle$$

Therefore, the strongest periodicity recorded in this coral is a 33 month cycle. This is significantly longer than the 12 month (annual) cycle recorded in modern *Porites* corals (e.g. Cahyarini et al., 2008). There are no other statistically significant peaks at either the $p<0.01$ or $p<0.05$ confidence levels. This interpretation is further supported by applying a sinusoidal fit to the data (Fig. 2.19), with one sine curve fitting the 33 month frequency seen in spectral analysis. Spectral analysis for $\delta^{13}C$ (Fig. 2.20) revealed similar results;

$$Periodicity = \frac{1}{0.03704}$$

$$Periodicity = 26.997\ months\ per\ cycle$$

This 27 month cycle is seen in when the time series is plotted as a sinusoidal graph (Fig. 2.21).

It is important to compare the isotopic data with recorded climate indices from the time period 2006 to mid 2010. In order to compare the coral data with ENSO, Southern Oscillation Index (SOI) data has been sourced from the Australian Bureau of Meteorology (BoM), which documents ENSO behaviour through time. This information is presented in a graph which overlays $\delta^{18}O$ and SOI data, showing the correlation of the *G. retiformis* $\delta^{18}O$ signal with ENSO cycles from 2006 to mid 2010 (Fig. 2.22). Sustained negative (positive) SOI values of greater than -8 (+8) are indicative of El Niño (La Niña) events. The effect of ENSO on $\delta^{18}O$ of *Porites* corals has been determined as a positive shift during El Niño and negative shift during La Niña (Abram et al., 2009), therefore the $\delta^{18}O$ axis has been oriented accordingly, with negative (positive) SOI values and more positive (negative) $\delta^{18}O$ values signifying El Niño (La Niña). Coral $\delta^{18}O$ is aligned with ENSO during the first half of the 4.5 year record, from early 2006 to mid 2008. However, from mid 2008 to mid 2010 the stable isotope values display the opposite of what is expected during El Niño and La Niña phases.

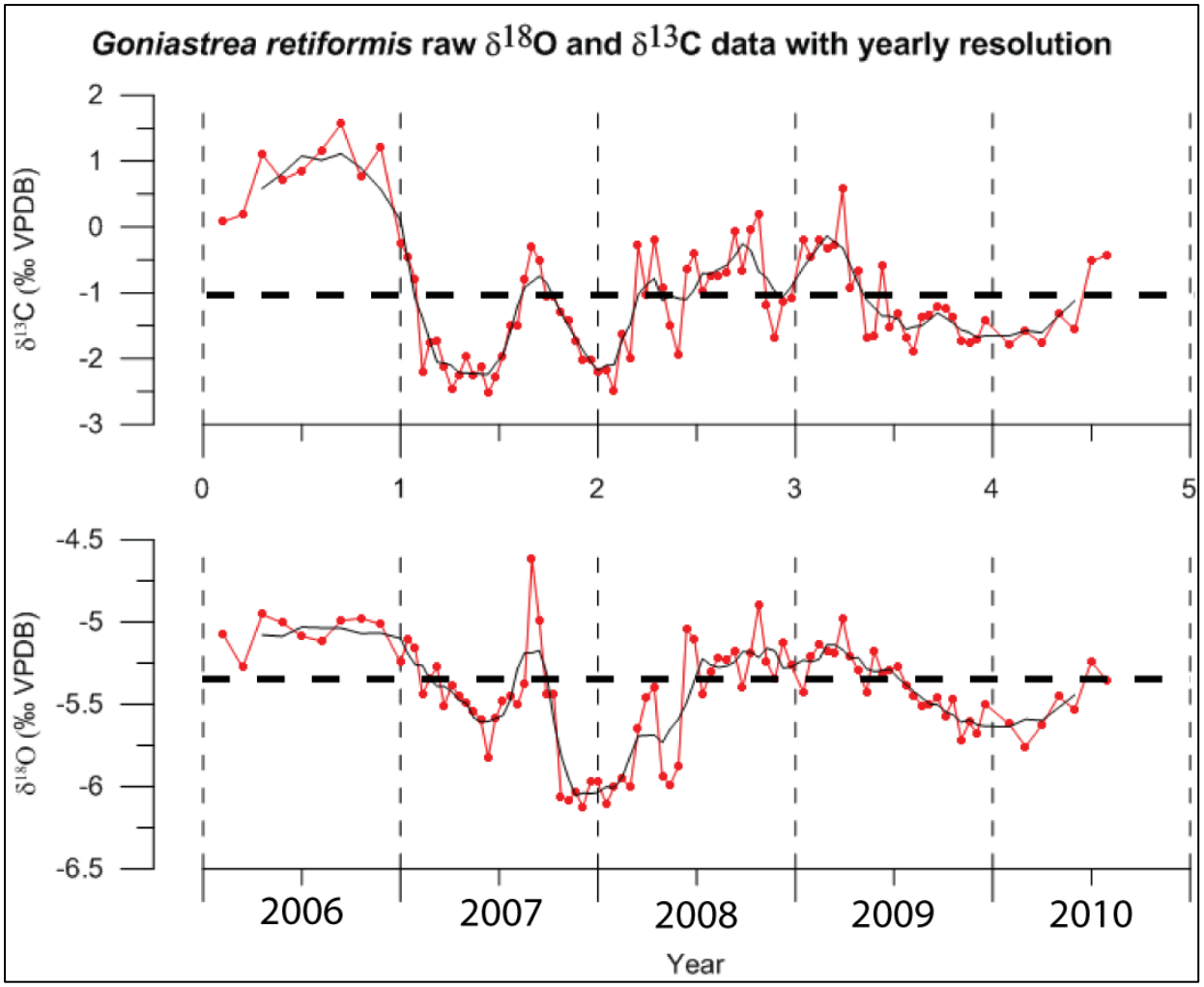

Fig. 2.17 *G. retiformis* stable isotope data as sampled through time (2006-2010). Running average shown by thin black line. Vertical dashed lines indicate yearly boundaries. Horizontal dashed lines represent mean $\delta^{18}O$ of -5.35‰ and mean $\delta^{13}C$ of -1.02‰.

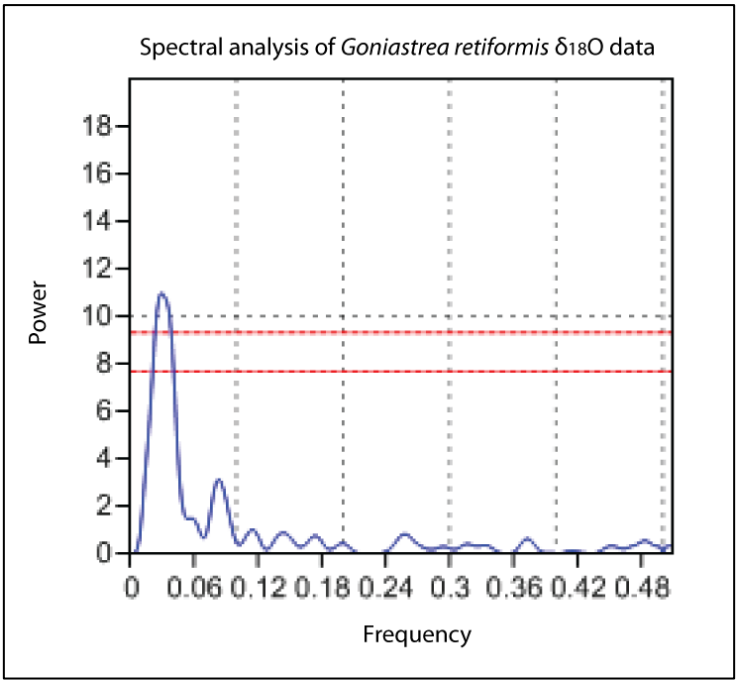

Fig. 2.18 Spectral analysis of monthly *G. retiformis* $\delta^{18}O$ data. The strongest peak in the spectrum is reported as 0.03009. The two dashed red lines are significance levels; the upper is $p<0.01$ and lower is $p<0.05$, with respect to white, uncorrelated noise.

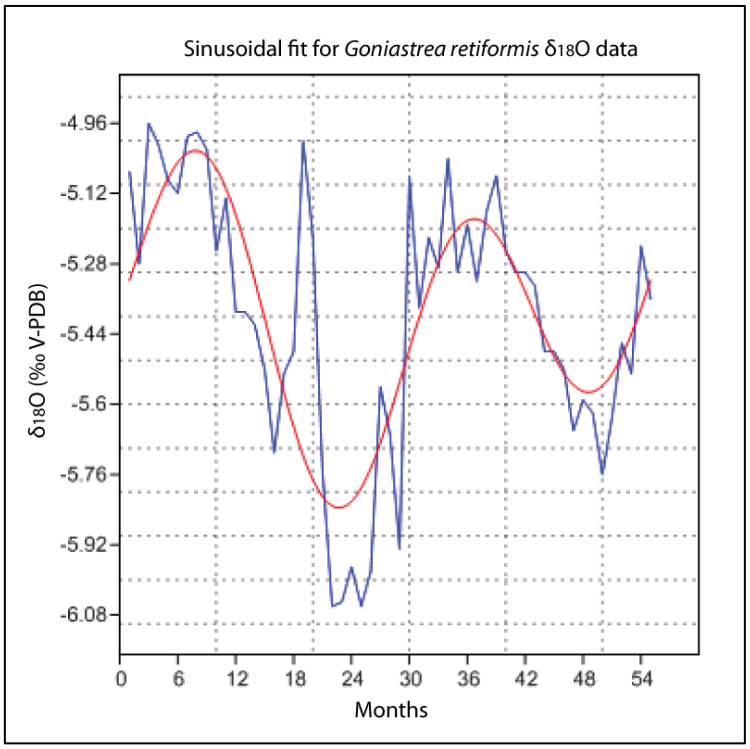

Fig. 2.19 Sinusoidal fit of monthly *G. retiformis* $\delta^{18}O$ data. $\delta^{18}O$ data represented by blue line is, sinusoid represented by red line. One sine curve is seen to correlate with 33 months.

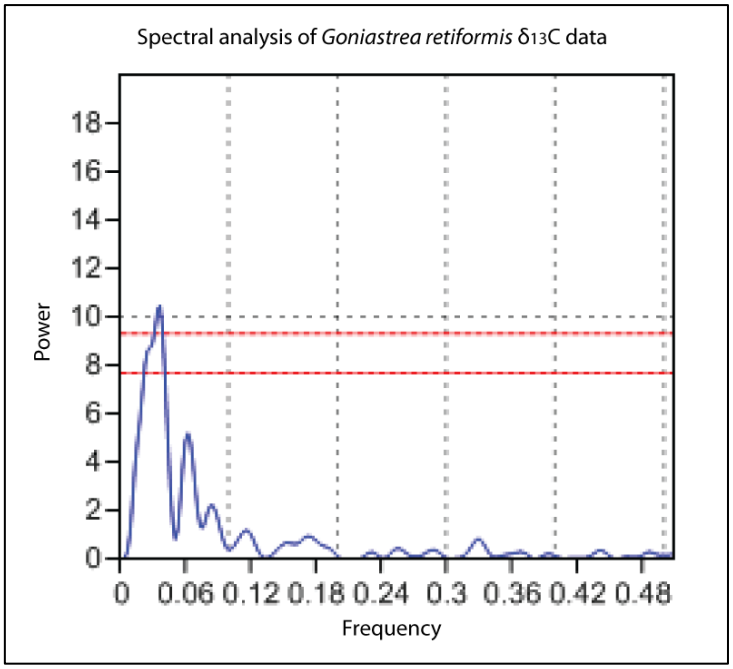

Fig. 2.20 Spectral analysis of monthly *G. retiformis* $\delta^{13}C$ data. The strongest peak in the spectrum is reported as 0.03704. The two dashed red lines are significance levels; the upper is $p<0.01$ and lower is $p<0.05$, with respect to white, uncorrelated noise.

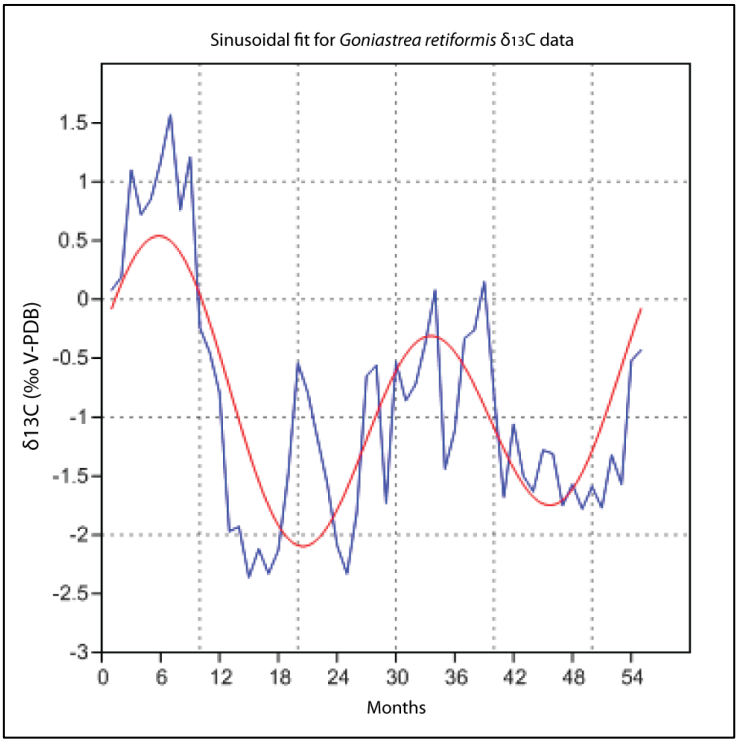

Fig. 2.21 Sinusoidal fit of monthly *G. retiformis* $\delta^{13}C$ data. $\delta^{13}C$ data is represented by blue line, sinusoid represented by red line. One sine curve is seen to correlate with 27 months.

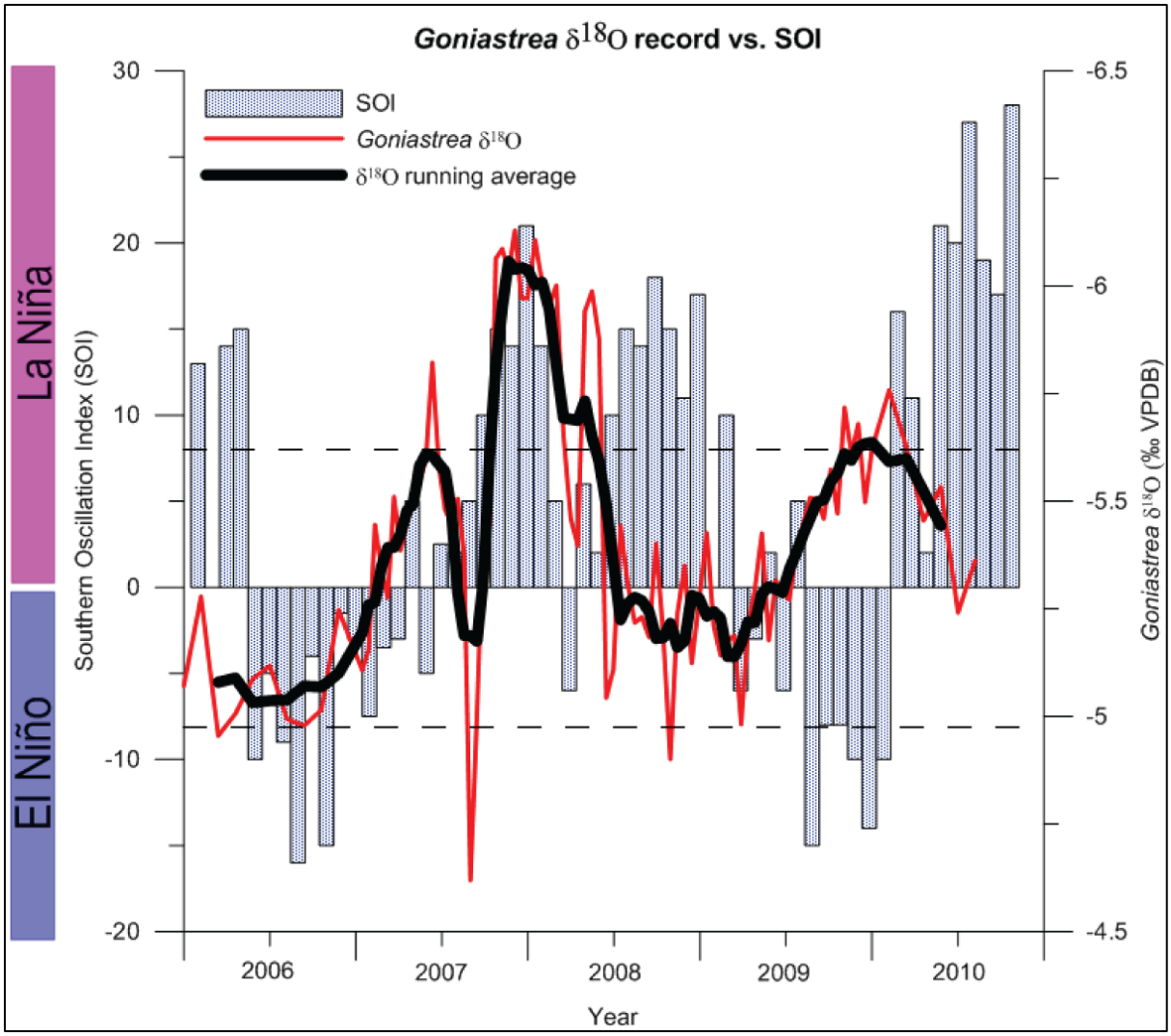

Fig. 2.22 *G. retiformis* $\delta^{18}O$ record plotted against SOI. Sustained negative values of > −8 indicate El Niño episodes, sustained postive values of > +8 indicate La Niña episodes. The dashed black lines indicate these thresholds. Red line represents raw $\delta^{18}O$ data, black line represents the running average. SOI data has been obtained from the BoM website.

SST data for the period 2005-2011 has been sourced from HadISST1 data set; a unique combination of monthly globally complete fields of SST and sea ice concentration on a 1° latitude-longitude grid from 1871. HadISST compares well with other published analysis, capturing trends in global, hemispheric and regional SST well, containing SST field with more uniform variance through time and better month to month persistence that those in the global sea ice and sea surface temperature data set (Rayner et al., 2003). This SST data has been plotted against *G. retiformis* $\delta^{18}O$ data (Fig. 2.23) and shows that isotope data from years 2006, 2007, 2008 and 2010 all represent the local SST fluctuations. A trough is

observed during the summer-time SST peak in 2009, showing that the isotope and SST data is not in phase during this period. Fig. 2.24 depicts the location of the 124-126°E to 08-09°S grid of SST generation.

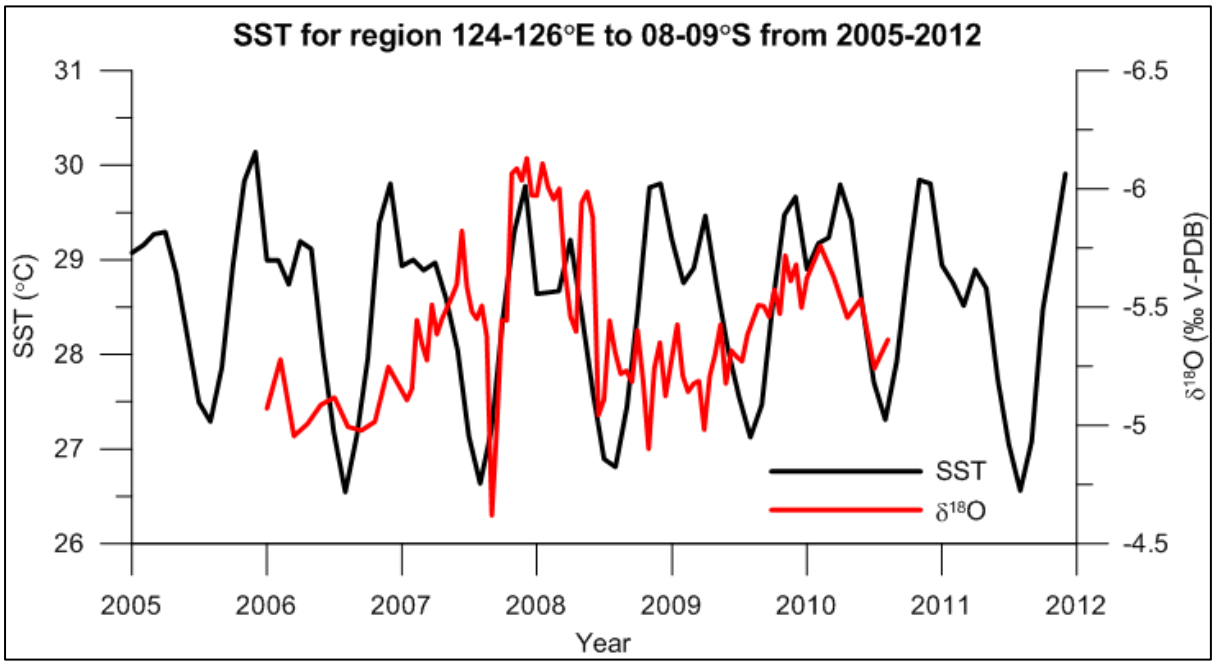

Fig. 2.23 *G. retiformis* $\delta^{18}O$ data plotted against SST for the region 8-9°S and 124-126°E. Collection site of *G. retiformis* is 08°29'S/125°34'E. SST generated by HadISST1 dataset. Isotope values have been plotted in a descending manner, as this correlates with the effect of increasing temperature causing more negative $\delta^{18}O$ values in coral.

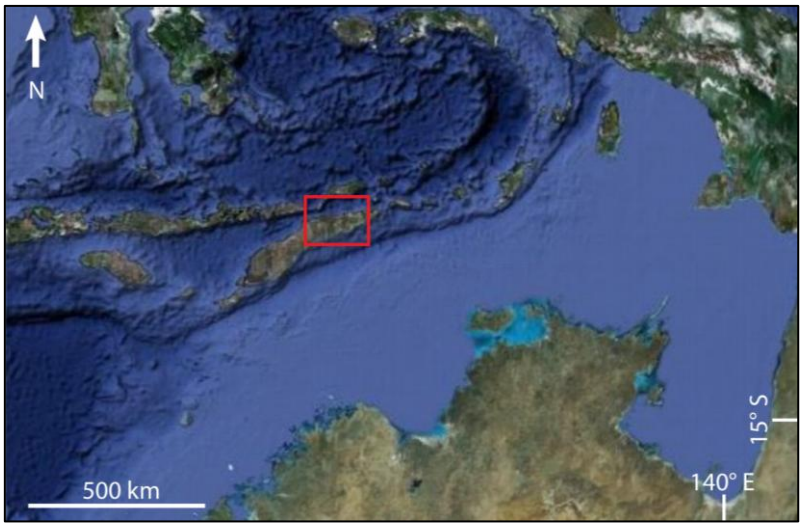

Fig. 2.24 Map showing location of HadISST1 data generation (red box) at latitude 124-126° E and longitude 08-09° S.

A comparison of the *G. retiformis* record against a *Porites* $\delta^{18}O$ record from West Timor (Cahyarini et al., 2008) is plotted in Fig. 2.25. This comparison is relevant as it is the closest study site and uses the well understood *Porites* genus, providing a robust data set with a mean $\delta^{18}O$ value of -5.31‰, ranging from -4.07 to -5.94‰. These two records to do not cover the same time span, with the *Porites* record from 1999 to 2004, so they are not expected to be in phase. However, the similar range and mean $\delta^{18}O$ values implies that *G. retiformis* is capable of recording local ambient seawater conditions, such as SST and SSS, in a similar manner to the *Porites* coral from West Timor. These two sites are only 275 km apart and 1.7° of latitude different, and subjected to the same flow of the ITF travelling through the Ombai Strait. The SST and SSS conditions are modelled over four 0.5° grids using SODA v. 1.4.2.

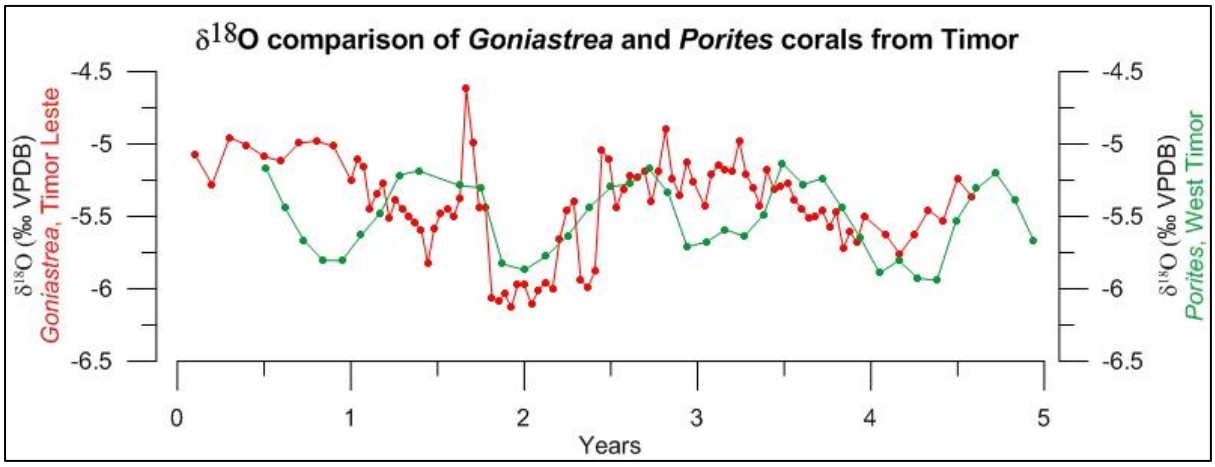

Fig. 2.25 Comparison of *G. retiformis* from Timor Leste and *Porites* from West Timor, exhibiting the similar range of $\delta^{18}O$ values seen in both samples. N.B. Records are from different time periods (*G. retiformis* from 2006-2010 and *Porites* from 1995-1999) so are not expected to be in-phase.

To verify that the *Porites* $\delta^{18}O$ record from West Timor was in fact recording SST and SSS fluctuations, these three variables have been plotted on the same time axis (Fig. 2.26). This graph displays monthly recorded SST and SSS values between December 1995 and April 1999 from North and South Ombai Strait (Sprintall et al., 2003) against near-monthly resolution $\delta^{18}O$ from the West Timor *Porites* over the same time. Best fit lines of SST and SSS data are well reflected in the $\delta^{18}O$ record, with peaks and troughs displaying covariance throughout the time series. This means that corals living in waters surrounding Timor have the ability to accurately record climate signals, which is important to verify as the Cahyarini (2008) study provides the only coral data from Timor preceding this thesis.

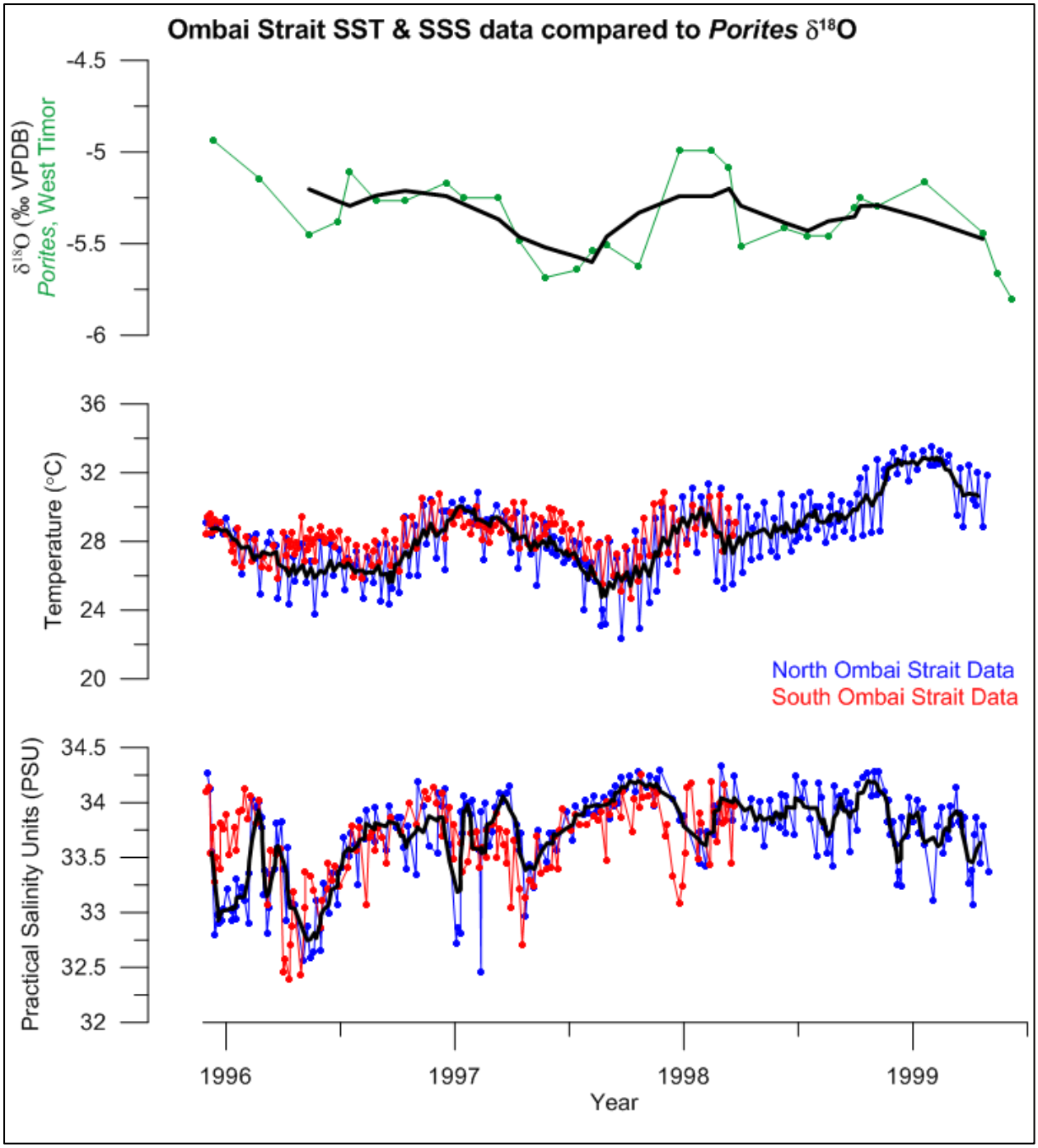

Fig. 2.26 Comparison of sea surface temperature (SST) and sea surface salinity (SSS) data for North and South Ombai Strait (data from Sprintall et al., 2003) and *Porites* $\delta^{18}O$ record (data from Cahyarini et al., 2008) from December 1995 to March 1998 (South Ombai Strait) and April 1999 (North Ombai Strait). Black lines indicate running means of each data set.

2.5 Discussion

2.5.1 Oxygen isotopes and local SST

A variety of climate and isotope data is presented with the aim of delineating the significance of the *G. retiformis* isotope data, in the context of its ability to record local and regional climate events and its reliability compared to *Porites* studies. The acknowledgement that the $\delta^{18}O$ results fit well within the mean range of -5.1‰ to -5.6‰ for the Indo-Pacific is the first step in confirming the reliability of the results. $\delta^{18}O$ recorded by *G. retiformis* is also representative of the regional mean of $\delta^{18}O$ in precipitation, which has been discovered through the interpolation of ~ 700 global precipitation monitoring sites undertaken by the International Atomic Energy Agency (IAEA) and World Meteorological Organisation (WMO) (Fig. 2.27). This project, the Global Network of Isotopes in Precipitation, provides annual means of ^{18}O content in precipitation for all areas across the globe. The annual mean for Timor is ~ -6‰, which is similar to the results of the Timor corals. Comparison to the modern *Porites* record from West Timor provides additional support for the robustness of our results. The significance of the similarity in oxygen isotopes recorded by these two corals is that the calibrated *Porites* coral from West Timor exhibits mean $\delta^{18}O$ values from regional *Porites* records, and therefore the similarity of *G. retiformis* results indicates this species is likely to be recording the local ambient $\delta^{18}O_{sw}$ signature accurately. Confirming exact SST and SSS fluctuations from coastal Timor ocean waters is hampered by the sparse collection of historical climate data. Fortunately, Cahyarini et al. (2008) were able to use SST and SSS data from Ombai Strait sampling sites (Sprintall et al., 2003) which provides a reference with which to directly compare with the *Porites* $\delta^{18}O$ records from late 1995 to mid 1999 (Fig. 2.26). The best fit lines through each of the three variables (SST, SSS and $\delta^{18}O$) show clearly that $\delta^{18}O$ is recording SST and SSS fluctuations. A similar evaluation has been made using the HadISST1 data set to model local SST conditions during the period of *G. retiformis* sampling. The SST model has provided accurate temperature fluctuations to those described as typical by Carton et al. (2000a) in the SODA version 1.4.2 data set. SST peaks occur during the wet season (December – March) and troughs during the dry season (May – October), consistent with local climate descriptions (Barnett et al., 2003; Kirono, 2010). This local SST and $\delta^{18}O$ comparison has demonstrated that all years of the record, except 2009, are compatible with the SST signal. The SST peaks (troughs) correspond with more negative (positive) $\delta^{18}O$ values, which is the expected relationship. The excursion from the SST

record in 2009 may be due to local climate conditions overprinting the temperature-dependent signal, resulting in more positive $\delta^{18}O$ values. This could be explained through the event of an abnormally dry period causing increased evaporation relative to the typical wet season conditions during the summers of 2006, 2007, 2008 and 2010. This is a plausible theory, as the SOI graph shows that a strong El Niño episode was in fact occurring during the latter half of 2009. Annual rainfall measured at the Dili airport site (Fig. 2.8) shows total rainfall of 450 mm in 2009 compared to 400 mm in 2006, 800 mm in 2007, and 1700 mm in 2010. Unfortunately there no data was collected from the site in 2008.

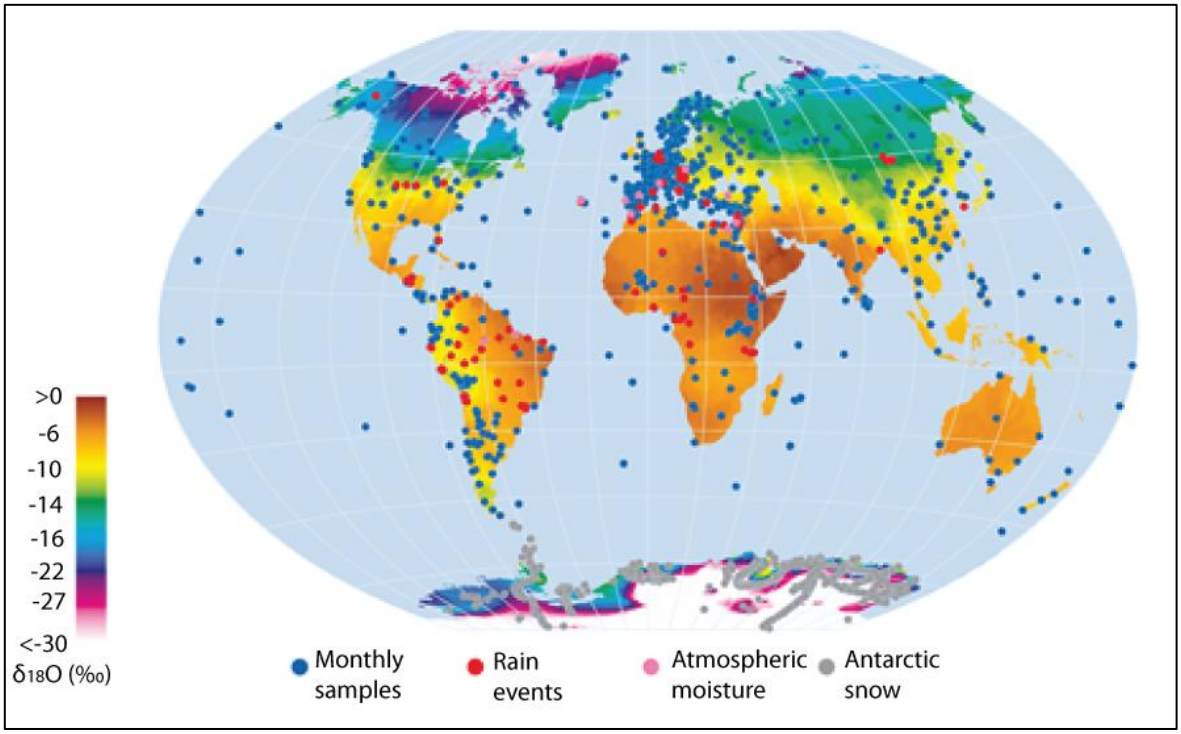

Fig. 2.27 Global distribution of δ18O (‰) in precipitation produced by interpolation of long-term annual means from about 700 GNIP stations. Figure sourced from the International Atomic Energy Agency (IAEA) and World Meteorological Organization (WMO) joint network.

2.5.2 ENSO

The ~ 4.5 year long $\delta^{18}O$ record appears to correlate reasonably well with ENSO cyclicity as reported by the National Oceanic and Atmospheric Administration (NOAA) and the Australian BoM. Fig. 2.22 provides a visual comparison of $\delta^{18}O$ data from 2006 – 2010 with recorded ENSO events and the SOI. The SOI gives an indication of the development and

intensity of El Niño or La Niña events in the Pacific Ocean, and is calculated using the sea level pressure (SLP) differences between Tahiti and Darwin;

$$SOI = \frac{Standardised\ Tahiti - Standardised\ Darwin}{Monthly\ standard\ deviation\ (MSD)}$$

Standardised values are derived by subtracting mean SLP from actual SLP, and dividing this number by the standard deviation of the site (Tahiti or Darwin). This provides a particularly useful reference frame for climate conditions in Timor Leste due to the proximity to Darwin. Fig. 2.17 shows that compared to the mean $\delta^{18}O$ value of -5.35‰, a positive $\delta^{18}O$ excursion reaching -4.98‰ is seen during the El Niño event of September 2006 – early 2007, and a strongly negative $\delta^{18}O$ excursion with a peak of -6.11‰ during the June 2007 – late 2008 La Niña event. These stable isotope values fit well with what is expected during such ENSO cycles. From here the $\delta^{18}O$ excursions are more loosely correlated to the reported ENSO cycles, but with an El Niño peak of -4.98‰ at the beginning of the June 2009 – May 2010 El Niño. The moderately negative excursion from mid 2009 to mid 2010 may be the result of local environmental conditions, such as increased temperature, precipitation, or runoff from a local weather anomaly causing an overprinting the regional ENSO signal. The skeleton measured by the final data point might have been capturing the effects of and the onset of a La Niña event in June 2010. This is represented by a negative shift of 0.12‰ (-5.24‰ in May 2010 to -5.36‰ in June 2010) which would correlate well with the extremely wet conditions experienced during the June 2010 field season. This is also seen in Fig. 2.22, with the best fit $\delta^{18}O$ data aligning with SOI from 2006 to 2008, then becoming out of phase during the latter half of the record.

2.5.3 Indian Ocean Dipole and local rainfall patterns

No negative Indian Ocean Dipole (IOD) events have occurred from 1992 until a strong event in late 2010. This means the IOD and monsoon system did not coincide during the time sampled by our coral. However, two consecutive, positive IOD events occurred from 2006-2008. Positive conditions cause negative SSTs and drier conditions, which may be a driving factor for the distinct negative $\delta^{18}O$ values occurring from late 2007 to early 2008.

From a local perspective, the influence of NMRP, which brings increased precipitation to the northern coast for 4-6 months beginning in December, is predicted to result in more negative

coral $\delta^{18}O$. A pattern that could be capturing this is seen by the two similar negative shifts that begin in late 2006/early 2007, and late 2008/early 2010 (Fig. 2.22). These two periods display a steady decrease from ~ -5.1‰ to ~ -5.6‰ over a 6 month period, with both events followed by a rapid switch towards more positive values.

2.5.4 Tropical biennial oscillation

Temporal fluctuations in the $\delta^{18}O$ and $\delta^{13}C$ ratios are recorded in the coralline aragonite, determined using spectral analysis. Yet the peak frequency does not depict the clear annual oscillation seen in *Porites*, rather periodicity that is closer to biennial cyclicity. Spectral analysis is a fundamental technique used in many coral investigations (e.g. Brachert et al., 2006; Hughen et al., 1999; Quinn et al., 1996; Tudhope et al., 2001) due to its ability to distinguish periodicity in a time series, thus is an important method for analysing the *G. retiformis* data. Using spectral analysis in PAST, the statistically strongest periodicities are 33 month ($\delta^{18}O$) and 27 month cycles ($\delta^{13}C$). Sine curves in the sinusoidal models also depict the 33 and 27 month periods. These correspond to 2.75 and 2.25 years, respectively, meaning the cycle is slightly longer than biennial. This contrasts with the periodicities recorded in *Porites* corals, which are commonly documented as annual or seasonal (e.g. Al-Rousan et al., 2007; Cahyarini et al., 2008; McGregor et al., 2011). However, this is not the first detection of a quasi-biennial cycle in the coral record. Cross spectral analysis of $\delta^{18}O$ and $\delta^{13}C$ records from a *Platygyra lamellina* coral head in Vanuatu indicates a strong concentration of variance at the quasi-biennial frequency band and ENSO (~ 4-5 years) (Quinn et al., 1993). These frequencies have also been recorded in a 150 year long $\delta^{18}O$ record from *Porites lutea* coral cores in the Seychelles, eastern Indian Ocean, which has provided an index of the relationship between ENSO and the Asian monsoon (Charles et al., 1997). ENSO was represented in the coral time series by interannual cycles, yet decadal variability characteristic of the monsoon system was also dominant in the record. Within this decadal variability, a 2.4 year frequency band was detected and seen to be modulated by the decadal monsoon cycle. The dominant form of variability in the Asian monsoon has been identified as quasi-biennial (Meehl, 1994), and throughout the tropics is seen to have a similar geographic expression to that of ENSO (Charles et al., 1997). The interaction between ENSO and the Asian monsoon has traditionally been identified as one process affecting the other (i.e. ENSO affecting monsoon, or vice versa), but this coral record

suggests otherwise. If the quasi-biennial cycle is part of the ENSO phenomenon, its decadal amplitude modulation may represent the clearest example of monsoon processes influencing interannual climate variability in the topics, implying an active rather than passive role of the Asian monsoon (Charles et al., 1997). It was observed in the Seychelles coral record that negative $\delta^{18}O$ (warm SST) anomalies corresponded with weak monsoons, and positive anomalies (cool SST) followed strong monsoons. This relationship has not yet been observed in an Indo-Pacific coral, but provides an exogenous mechanism for the quasi-biennial signal recorded in *G. retiformis* $\delta^{18}O$. This does not rule out the possibility that an endogenous control may also be an influential mechanism, which could be determined with further geochemical understanding of the species.

2.5.5 $\delta^{18}O$ and $\delta^{13}C$ covariance

It is apparent that $\delta^{18}O$ and $\delta^{13}C$ are in phase (Fig. 2.15). This is not unexpected, as covariance has also been identified in *Tubastrea* (McConnaughey, 1989) and *Platygyra lamellina* (Quinn et al., 1993). McConnaughey (1989) describes the phenomenon as being caused through a combination of "kinetic" and "metabolic" isotope effects, with Quinn et. al (1993) defining this further with the suggestion that the relation is due to the influence of cloud cover on photosynthesis, and hence the $\delta^{13}C$ record. The kinetic effect is attributed to slower CO_2 hydration and hydroxylation reactions by molecules enriched in the heavier isotopes ^{13}C and ^{18}O (Spero et al., 1997). In contrast, metabolic effects can be attributed to the incorporation of ^{13}C-depleted respired CO_2 (Spero et al., 1997). Without a detailed geochemical study it is difficult to ascertain at present the exact cause of the isotopic covariance seen in this particular *G. retiformis* coral.

2.6 Conclusion and implications

G. retiformis, an abundant hermatypic coral, collected from an intertidal location on the north coast of Timor Leste, shows promise as a climate proxy. Stable isotopic data provides evidence that this species has the ability to record the effect ENSO on local SST and SSS, positive IOD events, and local rainfall patterns. Periodicity has been identified as quasi-biennial, which was unexpected given the well documented annual and seasonal periodicities seen in tropical *Porites* corals. However, TBO is a recognised effect of the interaction between ENSO and the monsoon system, both of which are primary climatic drivers in this region. Therefore it is realistic that the isotopic variations as a result of this interaction have

been recorded by the coral. Stable isotope results, assessment of $\delta^{18}O$ variations during the oscillation of multiple climate processes, and comparison to a modern *Porites* record from West Timor, display that this *G. retiformis* coral was influenced by local and regional climate processes.

The habitat and longevity of *G. retiformis* means that once it has been calibrated to become a reliable climate proxy it could be used as a key species in tracing regional and local climate conditions throughout the Holocene, and perhaps as far back as the Pliocene. This would encompass the time period over which modern-day ENSO has developed, and possibly provide insights into the changes in temperature and salinity of the ITF as tectonic narrowing triggered a switch from warm, salty to cooler, fresher ITF source waters. The location of Timor Leste within the IPWP and region strongly influenced by ENSO, Asian-Australian monsoon and IOD means it is an appropriate and desirable site for the calibration of modern corals for such palaeoclimate investigations.

2.6.1 Future work

Further investigations of this coral species are required to determine the extent to which larger scale phenomena are recorded in its isotopic record. This would require the collection of multiple living *G. retiformis* corals from coastal Timor and throughout the Indo-Pacific region. Procedures such as diagenetic screening and micromilling as conducted during this study would need to be carried out on all samples. Following this, a $\delta^{18}O$ -temperature dependence equation for determining absolute SST and SSS values from $\delta^{18}O$ could be developed. Conducting a detailed study to confirm the theory that *G. retiformis* and *Porites* record isotopic fluctuations in a similar manner would also be beneficial. If living samples of each of the corals were collected from the same location and sampling carried out at the same resolution (e.g. fortnightly), this would allow for calibration of *G. retiformis* data against a *Porites* coral recording the same ambient seawater conditions, thus the differences between each genus would become clear (Chivas, 2012 Pers. Comm.). A raised reef on Huon Peninsula containing an array of Holocene aged (125 ka) *G. retiformis* corals across the upper reef slope (Montaggioni and Braithwaite, 2009) provides an ideal location to instigate fossil studies. Extensive research using *Porites* corals from this peninsula has already occurred, providing a detailed insight into Holocene SST and SSS from this location, and a reference point against which to examine *G. retiformis* results. As well as stable isotopes, trace

elements such as Sr/Ca should also be analysed if the corals are pristine. This method of combined analyses would improve the reliability of climate interpretations, which is extremely important when attempting to determine absolute SST and SSS values using climate proxies.

3 Expanding palaeoclimate data capture using diagenetically altered fossil corals

3.1 Abstract

A *Platygyra pini* coral was collected from a raised reef on the north coast of Timor Leste and dated using U/Th techniques, revealing a mid Holocene age of 4.5 ka ± 0.092 (2σ). A ten year record has been analysed for stable isotopes, providing mean a $\delta^{18}O$ value of -4.82‰ ± 0.03‰ (2σ) and mean $\delta^{13}C$ of 1.12‰ ± 0.02‰ (2σ). These isotopes range from -3.47 to -5.45‰ and 3.43 to -0.49‰, respectively, with some values significantly more positive than expected. Diagenetic alteration due to subearial exposure, including secondary aragonite, dissolution, and secondary calcite, has been identified using X-ray diffraction (XRD), petrographic and scanning electron microscopy (SEM) analysis techniques, and interpreted to have been the dominant source of geochemical anomalies within the coral. Distinct zones of secondary aragonite viewed under SEM are likely to be responsible for the extreme positive isotopic shifts in the uppermost 4 cm of the specimen, with unrealistically cool sea surface temperatures (SSTs) of 18.5-25.2° C obtained using the temperature dependence equation calculated using a modern *Platygyra* coral. The remaining seven years of the record show SST fluctuations between 23.2-27.6° C. Mean annual SST in the southwestern Indo Pacific Warm Pool (IPWP) from 5.5-4.3 ka are believed to be 1.2 ± 0.3° C cooler than present (28° C), which indicates that the *P. pini* geochemical record has undergone diagenetic alteration of varying extents throughout the coral. However, seasonal fluctuations in $\delta^{18}O$ of ~ 0.5‰ reflect the range recorded in modern corals from the IPWP, suggesting that annual climate fluctuations change can be inferred. Interannual periodicity, similar to that of prevailing El Niño Southern Oscillation (ENSO) and Indian Ocean Dipole (IOD)-monsoon interaction, has been identified using spectral analysis. Although diagenesis is prevalent in this coral, preventing absolute SST evaluation, the dominant interannual variability and magnitude of seasonal isotopic fluctuations can be used to gain insights into the mid Holocene climate behaviour in the southern Indo-Pacific.

3.2 Introduction

Holocene fossil corals from tropical reefs provide geochemical archives of changing oceanic conditions during this over the last 10 ka. Seasonal fluctuations of SST and sea surface

salinity (SSS) have been inferred from isotopic records in genera such as *Porites* (Gagan et al., 2004), *Montastrea* (Swart et al., 1996) and *Pavona* (Dunbar et al., 1994) throughout the Pacific and Atlantic Oceans. Mayewski et al. (2004) describes three climatic phases during the Holocene, beginning with "glacial aftermath" from 9-8 ka, followed by "cool poles, dry tropics" between 6-1 ka, and current day conditions of "cool poles, wet tropics" beginning ~ 600 years ago. This pattern was revealed through analysis of ~ 50 globally distributed palaeoclimate records, showing that most events were characterised by polar cooling, tropical aridity, and major atmospheric circulation changes. An increase in $\delta^{18}O$ recorded in proxies suggest that from 5.5-4.3 ka the southwest and southeast margins of the IPWP were 1.2° C ± 0.3° cooler than present (Abram et al., 2009). Isotope records have inferred that a strong monsoon system has persisted throughout the Holocene (Stott et al., 2004) and ENSO periodicity has been identified from 5 ka, becoming much stronger after 3 ka (Gagan et al., 2004). Therefore, mid Holocene corals should are likely to record more positive isotope values than modern corals due to cooler climate conditions, and contain interannual periodicity consistent with modern ENSO.

P. pini corals are found throughout the Indo-Pacific and Central Pacific, forming massive or encrusting colonies in shallow reef environments (Fig. 3.1). Although less abundant in the tropical reef system than genera such as *Goniastrea* and *Porites* (Veron, 2000), its adaptation to colder water temperatures means it is prevalent in mid-latitude regions (Shimamura et al., 2008). This contrasts with *Porites*, which is restricted to areas of low latitude (Fig. 1.1). Mean annual extension rate has been estimated between 8.6 mm to 16.9 mm/year with an average of 13.3 mm/year (Shimamura et al., 2008), meaning it is slightly faster growing than *Porites*, which has been estimated as having a mean annual growth of 10.0 mm in shallow settings (Dullo, 2005). In an attempt to expand the current range of coral proxy records for the tropics, and determine whether coral samples containing moderate degrees of alteration can still be used to characterise climate fluctuations, two 4.5 ka *P. pini* corals from the southern IPWP were selected for analysis. Both corals (TL281 and LM33) have been exposed to subaearial weathering on an uplifted reef platform on the northern coast of Timor Leste (Fig. 3.2). The reef is now elevated ~ 1 m above high tide sea level and has been overlain by a conglomerate deposit (Fig. 3.3). Given that mid Holocene SSTs in the southwestern IPWP are shown to have been cooler than present, more positive isotopic values are expected to be seen in this coral record. However, the effects of diagenesis must also be taken into account,

with secondary aragonite and dissolution leading to enhanced positive values and cool SST artifacts, while secondary calcite causes negative shifts and warm SST artifacts in stable isotope values. Following extensive diagenetic analysis using XRD, petrographic and SEM techniques, LM33 was found to have extensive alteration throughout the entire skeleton and not used for further analysis. However, primary aragonite structures were identified in the uppermost 11 cm of the coral, interspersed with alteration, showing that coral TL289 contains variable diagenesis. For this reason, a selected section of this coral has been milled and analysed for stable isotopes, with results displaying promise that climate insights can be gained from diagenetically altered coral records.

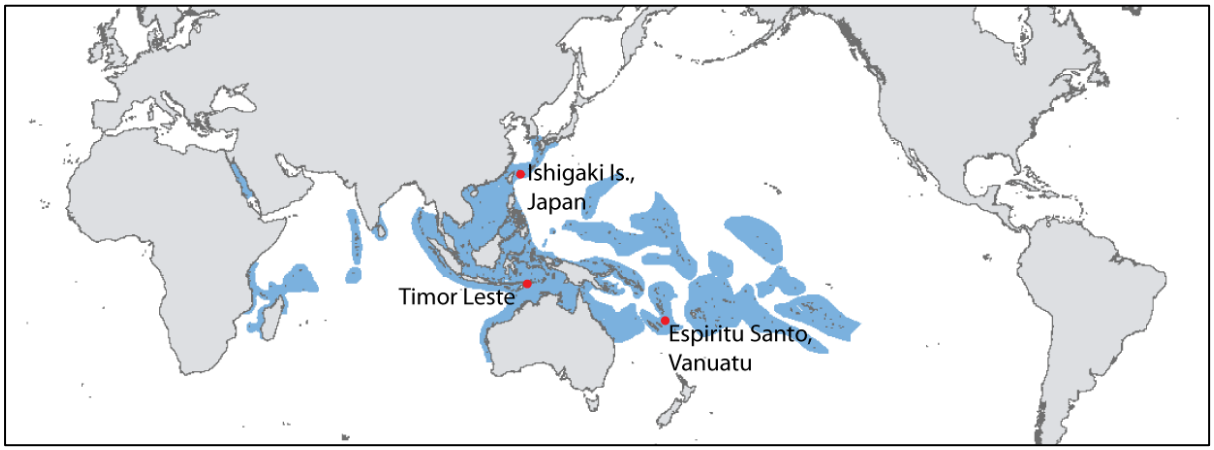

Fig. 3.1 Global distribution of *Platygyra pini*. Red circles indicate *Platygyra* records from Ishigaki Island, Japan, and Espiritu Santo, Vanuatu, and Timor Leste. Image sourced from Veron, 2000.

3.3 Methodology

Initially two 7mm slabs were cut from the centre of the each coral skeleton with a diamond wafer saw, cleaned with an ultrasonic probe to remove loose particles and surface contaminants, then X-rayed to identify annual density bands (Fig. 3.5). These bands revealed approximately 10 and 16 years of visible growth for LM33 and TL281, respectively. Growth rates are ~ 10 mm/yr in both corals, consistent with previous findings from Shimamura et al. (2008).

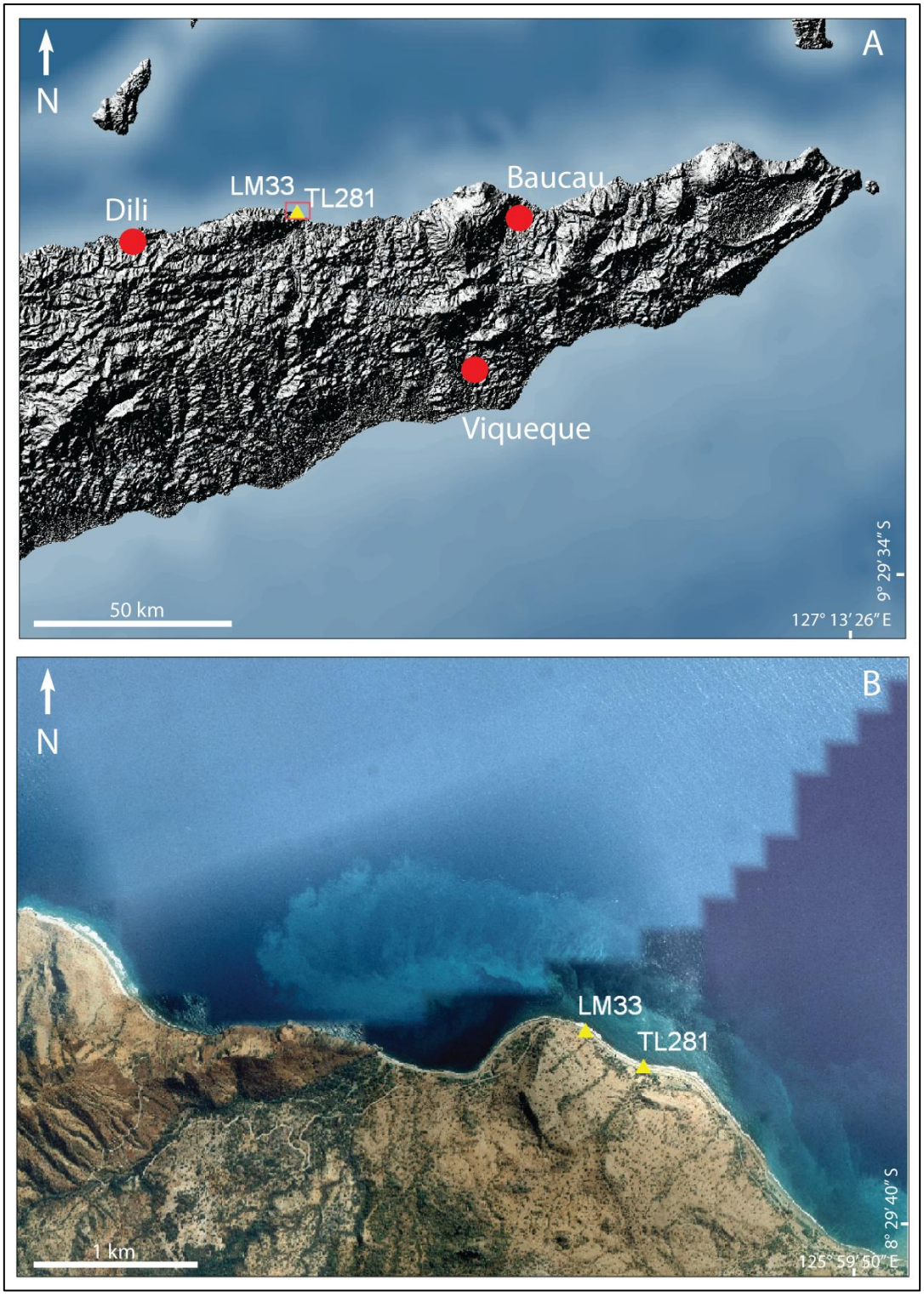

Fig. 3.2 (A) Location of Holocene fossil corals (LM33 and TL281) on the north coast of Timor Leste, (B) Zoomed in image of coastal platform which corals were collected from. Yellow triangles represent coral sample sites, red circles represent cities and townships, red square in map A indicates extent of map B.

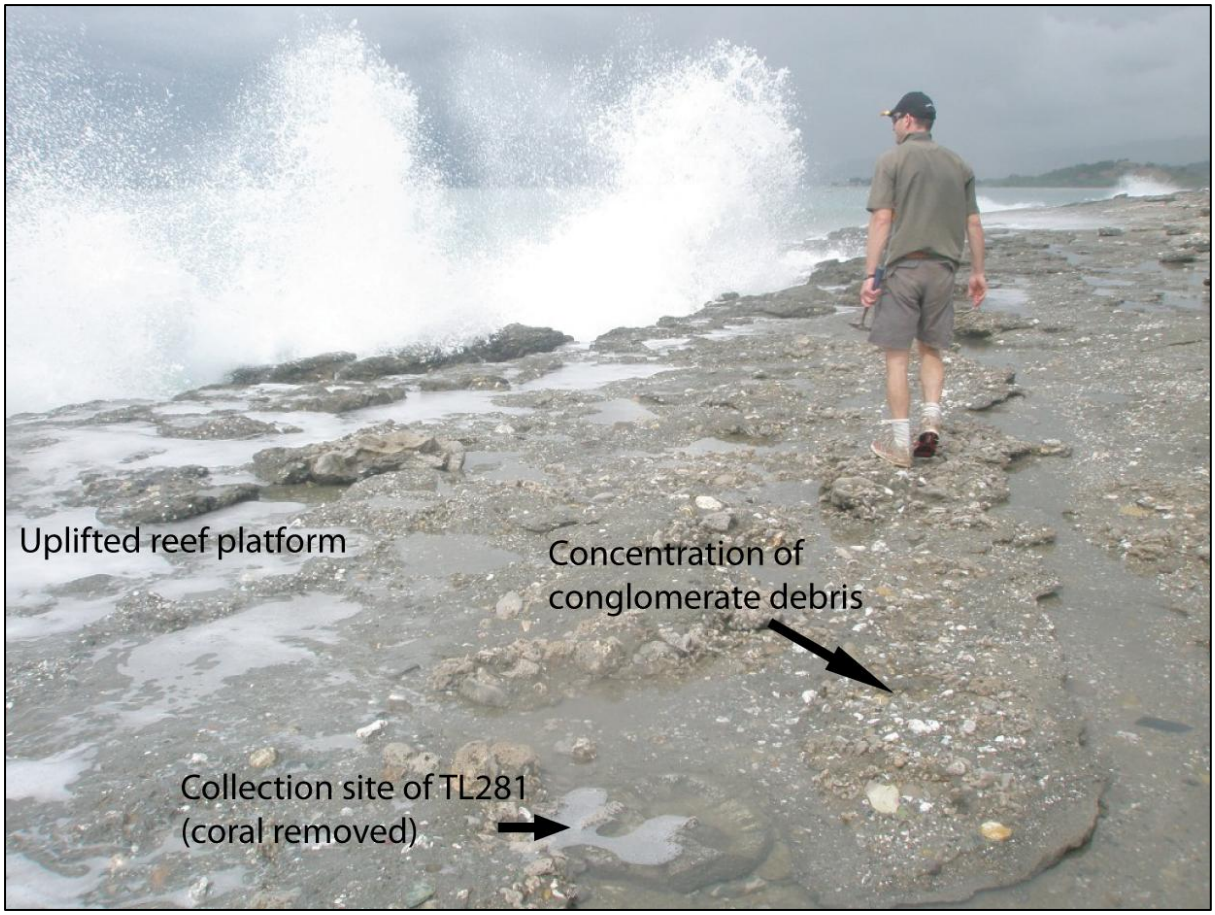

Fig. 3.3 Uplifted reef platform from which corals LM33 and TL281 were retrieved.

3.4 Screening for diagenesis

Due to aerial exposure and fossilised nature of these corals, they have experienced significant exposure to post depositional diagenetic alteration. While the reef was still submerged, phreatic marine diagenesis could have instigated secondary aragonite growth or dissolution. Later, when the reef was partially uplifted and in the tidal zone, marine vadose zone conditions could also have caused these types of alteration. Once the reef was fully emerged, the subaerial conditions and exposure to rainfall may have caused calcite growth or dissolution. Therefore, a thorough diagenetic screening process of XRD, petrographic analysis and SEM was conducted for these two mid Holocene corals.

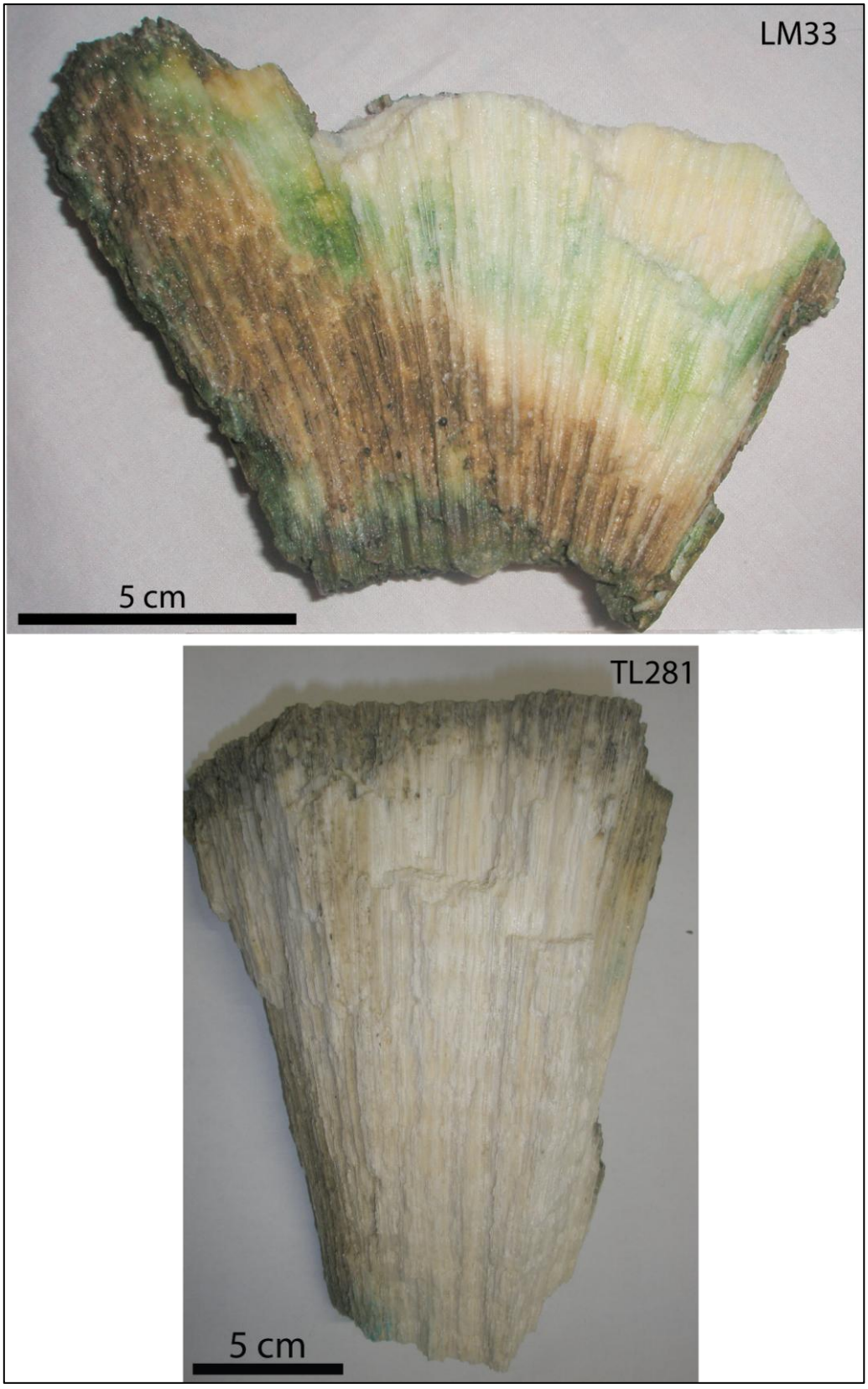

Fig. 3.4 Images of Holocene *Platygyra pini* corals shortly after collection from the raised reef platform. LM33 (top) and TL281 (bottom).

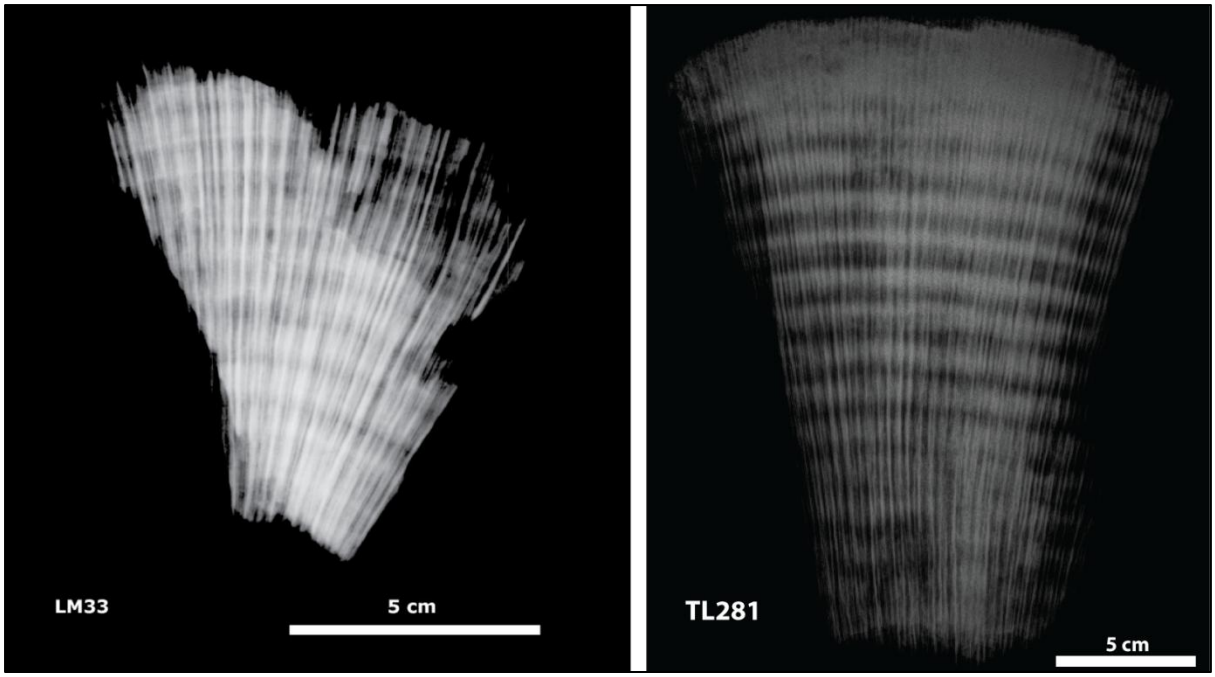

Fig. 3.5 X-ray images of *Platygyra pini* corals LM33 and TL281. Annual density bands visible, with 10 annual density band couplets seen in LM33 and 16 annual density band couplets seen in TL281.

3.4.1 XRD

Both corals were subject to a multi-sample screening process whereby an initial XRD sample was run, followed by five subsamples from each coral (Fig. 3.6). These were tested to determine the relative proportions of aragonite and calcite. Corals were cleaned with ultra-pure compressed air prior to sampling in order to remove any loose particles, and coral chunks collected with tweezers or hand dremel. Tweezers were cleaned with ethanol and dremel bit cleaned on a piece of granite between each sample to avoid cross contamination between samples. Samples were then crushed into powder using an agate mortar and pestle which was cleaned with ethanol between samples. Samples were scanned from 2θ of 3^0 to 50^0 using a Philips XRD at the University of Canterbury. Refer to Appendix Figure 3 through Appendix Figure 8 for diffractograms of each sample. The initial XRD results for LM33 and TL281 were 75% and 100% aragonite, respectively. However, subsequent subsamples of TL281 showed a range of aragonite percentages from 15 to 65%. LM33 had a range of 25 to 80% aragonite (Table 3.1). The high percentages of calcite indicate that neomorphism is likely to have occurred in these corals.

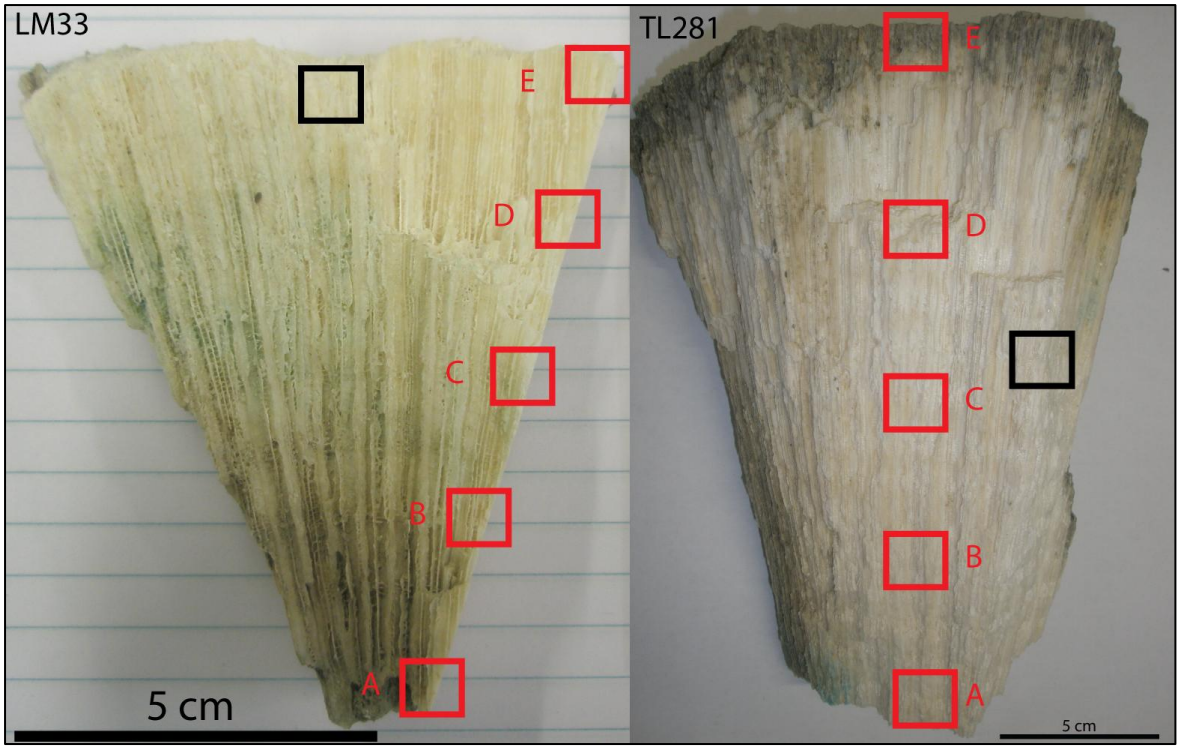

Fig. 3.6 Locations of XRD subsamples of LM33 and TL281. Black squares indicate locations of initial XRD samples, red labelled boxes indicate locations of sub-samples.

Table 3.1 XRD results for first and second screenings of Holocene corals LM33 and TL281.

Coral sample	Aragonite (%)	Calcite (%)
LM33	75	25
TL281	100	0
LM33A	65	35
LM33B	25	75
LM33C	55	45
LM33D	55	45
LM33E	80	20
TL281A	15	85
TL281B	20	80
TL281C	45	55
TL281D	65	35
TL281E	60	40

3.4.2 Petrographic analysis

LM33 was cut using a diamond wafer blade and two 7 mm slabs created. Due to its large size, TL281 could not be cut with the wafer blade, and was cut by a high pressure water jet creating two 7 mm slabs. After cleaning with an ultrasonic probe to remove loose particles and surface contaminants, one slab from each coral was prepared into a standard, 0.03 mm thick, 60 x 20 mm petrographic thin section for analysis under a Leica optical microscope.

Petrographic analysis of LM33 revealed a poorly preserved skeleton (Fig. 3.7 and Fig. 3.8). Throughout the basal, middle and upper zones of the coral there was extensive dissolution, overgrowths of calcite and micrite, as well as poor preservation of primary structures such as dissepiments. The petrographic analysis of this coral was in agreement with the XRD results, that diagenesis was too extensive to provide reliable geochemical data.

Petrographic analysis of TL281 revealed a mixture of reasonably well to poorly preserved primary aragonitic skeleton. The upper two thirds of the coral (Fig. 3.9 and Fig. 3.10) provided the most compelling evidence of pristine aragonite, with radiating sclerodermites, centres of calcification and dissepiments visible, and minimal algal borings or leaching observed. These primary textures have been described in modern and fossil *Porites* corals from PNG and Indonesia by McGregor and Abram (2008). However, the lowermost third of the coral (Fig. 3.11) has undergone extensive dissolution, with chalky zones masking the primary textures. Due to this observation, micromilling has been carried out on the upper two thirds (10 years) of the sample to determine whether a meaningful climate signal can be derived from a moderately altered section of coral.

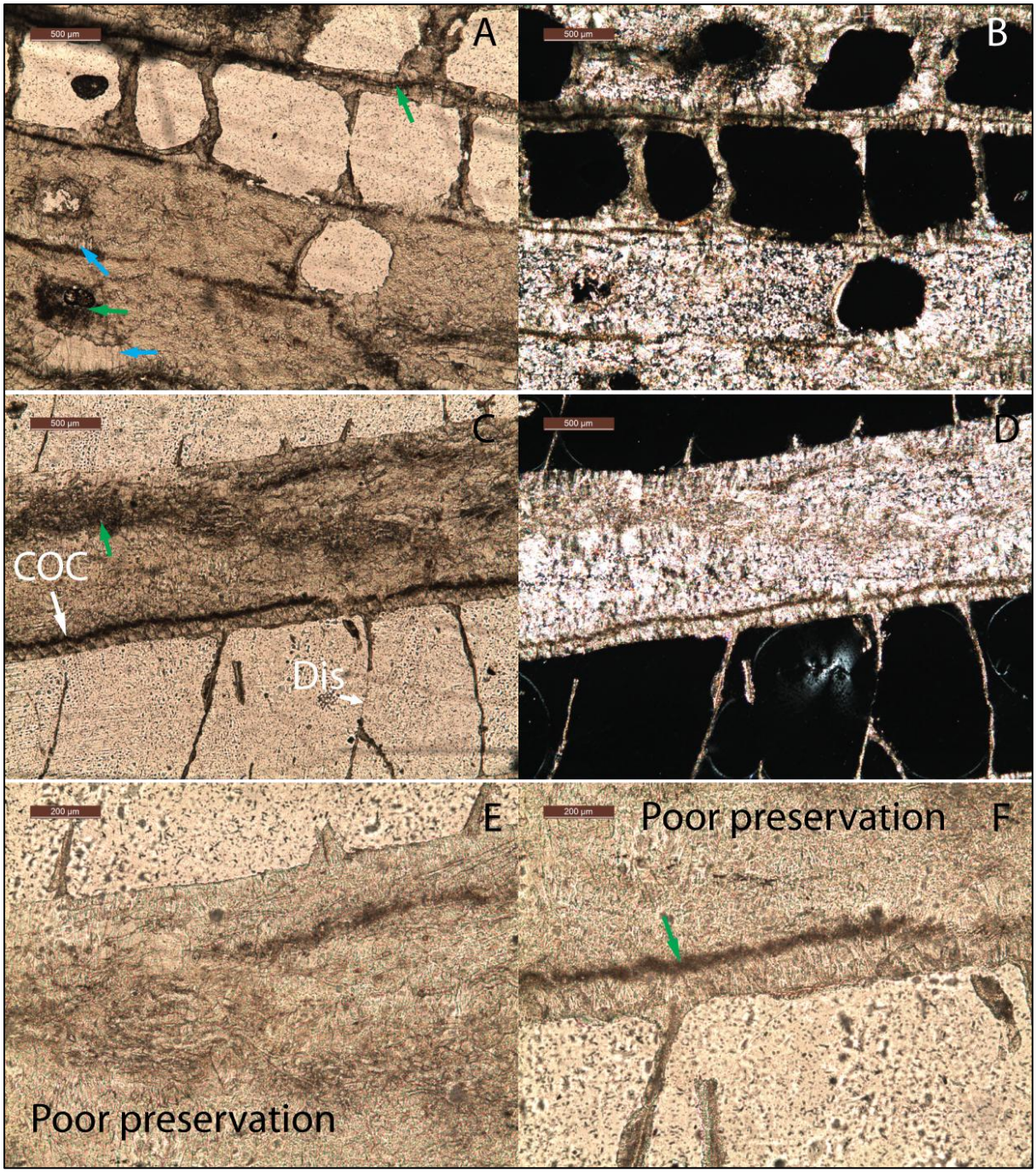

Fig. 3.7 Petrographic images of *P. pini* LM33, showing dissolution (green arrows), calcite (blue arrows), broken dissepiments (Dis), and overall poor preservation. Images B and D taken in CPL, all others taken in PPL.

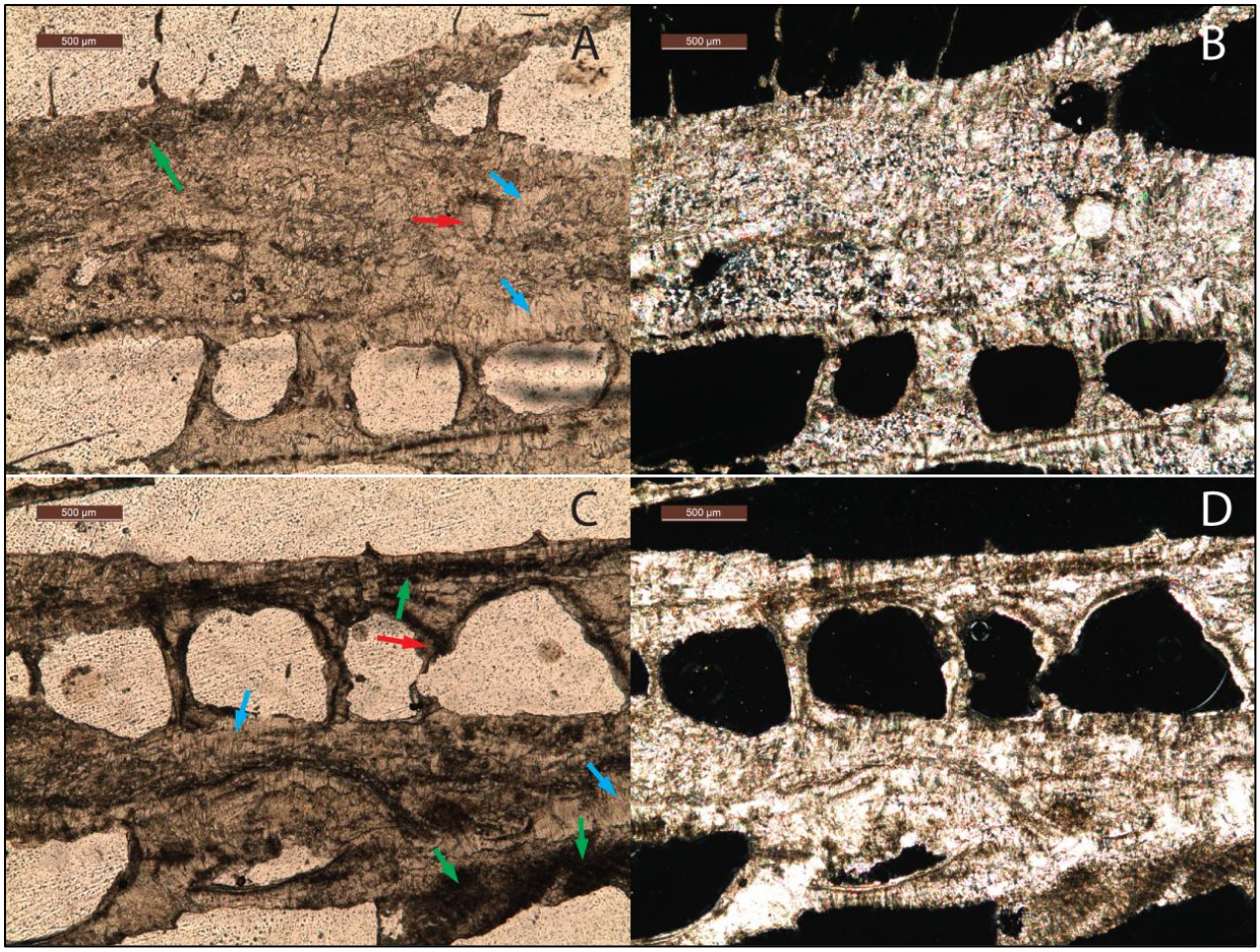

Fig. 3.8 Petrographic images of *P. pini* LM33, showing dissolution (green arrows), calcite (blue arrows), micritic overgrowths (red arrows), broken dissepiments (Dis), and overall poor preservation. Images A and C taken in PPL, images B and D taken in CPL.

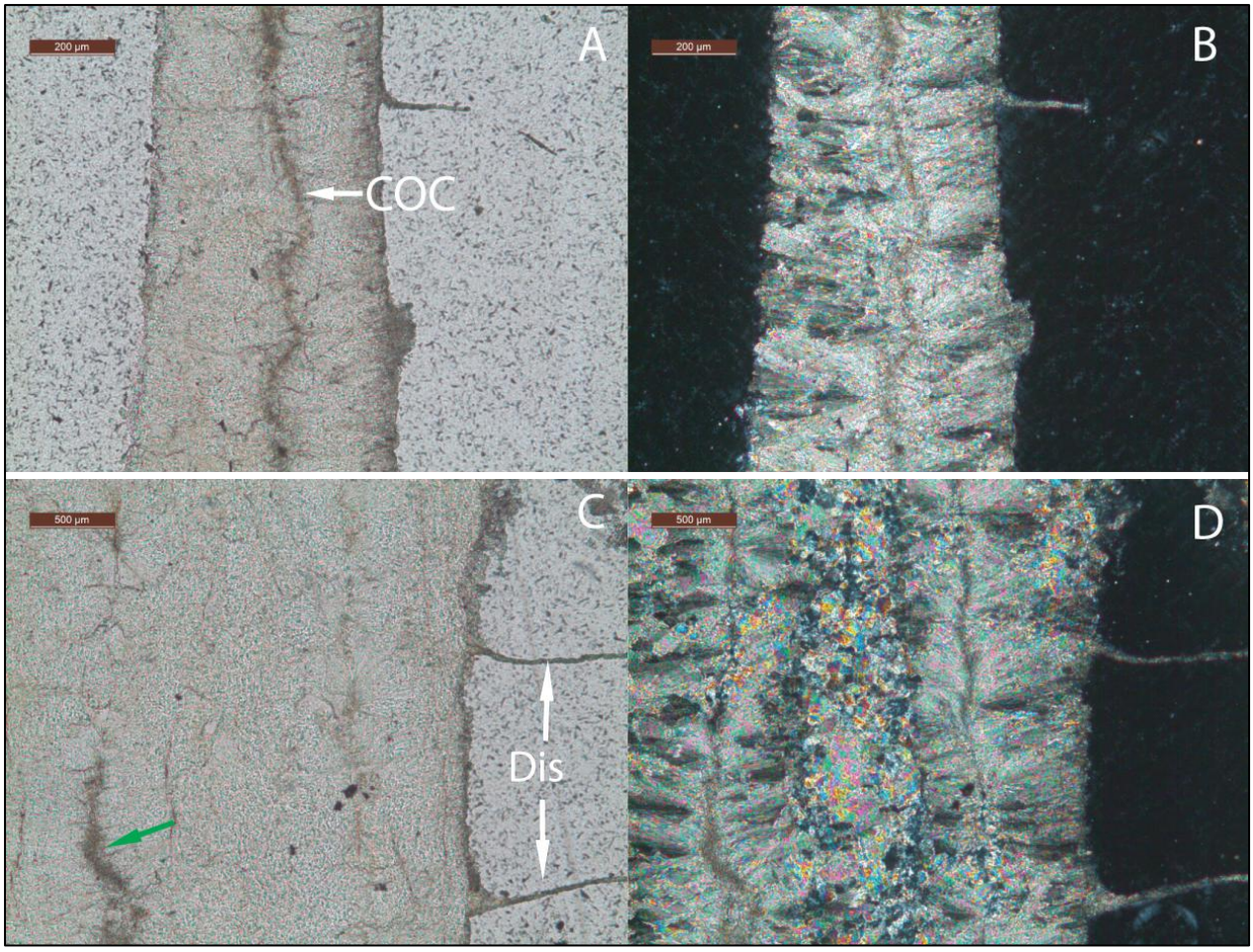

Fig. 3.9 Petrographic images of top (upper third) of *P. pini* TL281. Small amount of dissolution (green arrow) along COC visible in image C, otherwise well preserved primary aragonite septae and dissepiments (Dis). Images A and C taken in PPL, images B and D taken in CPL.

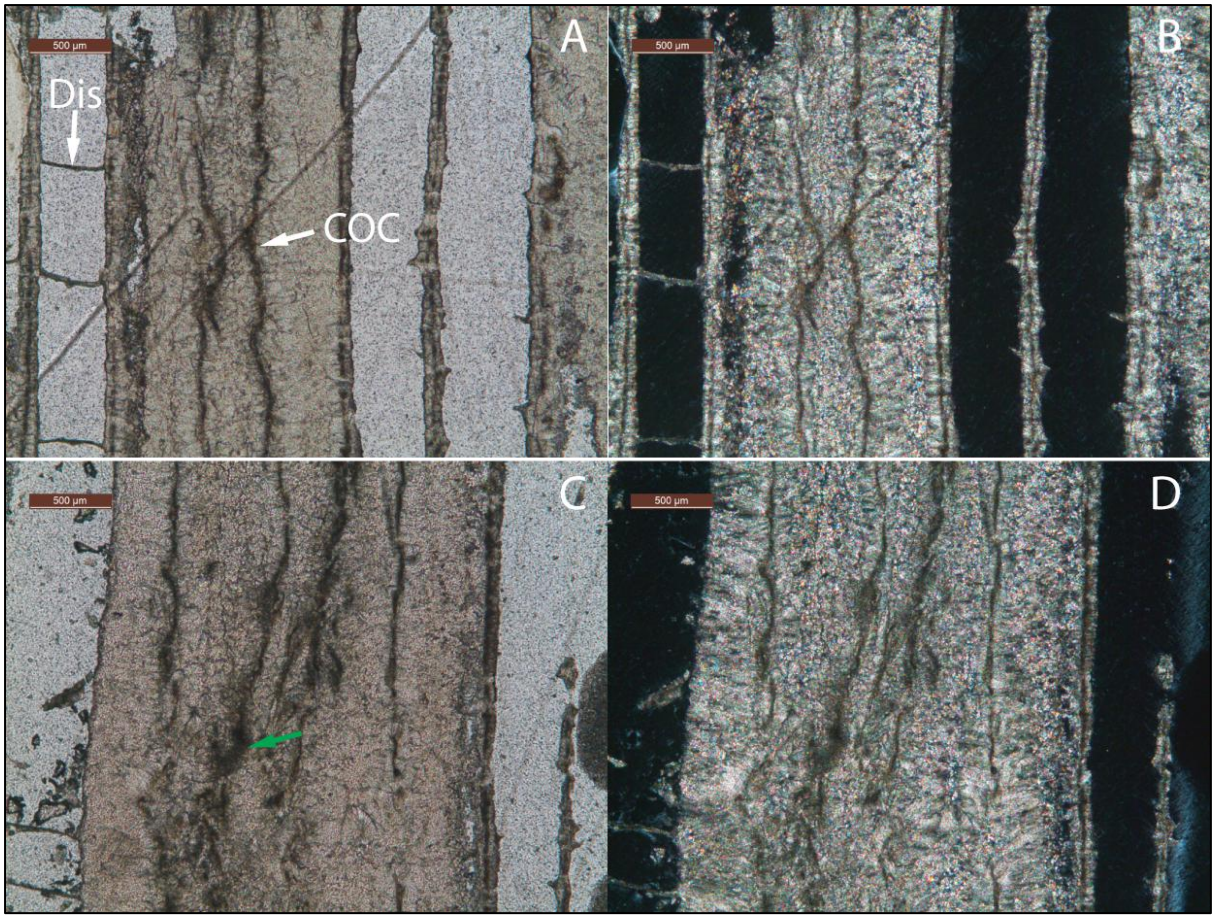

Fig. 3.10 Petrographic images of middle (middle third) of *P. pini* TL281. Small amount of dissolution (green arrow) along COC visible in image C and slightly darker COCs than in upper third of coral (Fig. 2.4), otherwise fairly well preserved primary aragonite septae. Images A and C taken in PPL, images B and D taken in CPL.

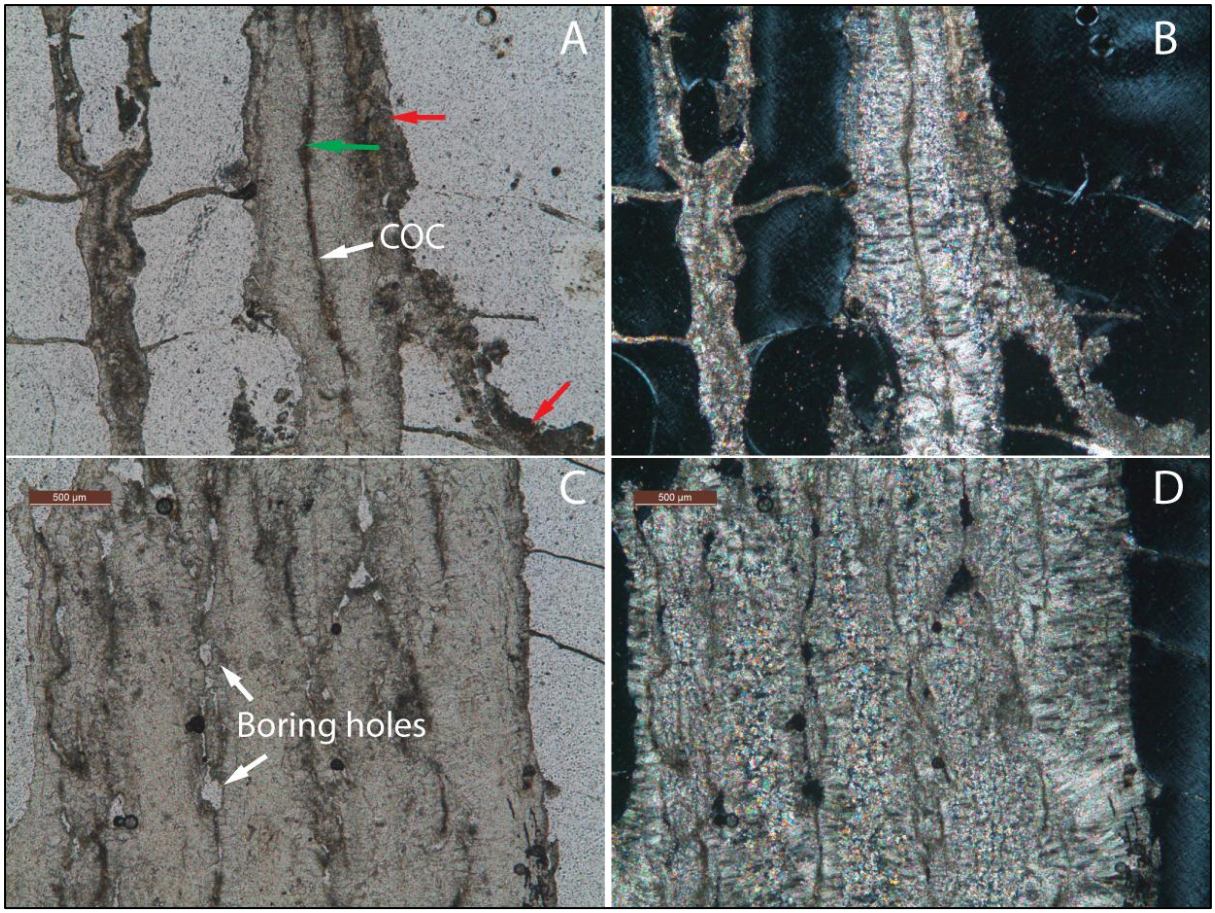

Fig. 3.11 Petrographic images of base (lowermost third) of *P. pini* TL281. Dissolution (green arrows), micritic overgrowths (red arrows) and boring holes visible. Much greater diagenesis in this zone of the coral than middle and uppermost zones. Images A and C taken in PPL, images B and D taken in CPL.

3.4.3 SEM

For SEM analyses, chunks of coral were mounted onto stubs that allowed analysis of both polished and broken surfaces under SEM (Fig. 3.12). Three main textures were used to distinguish areas of diagenesis, after Hendy et al., (2007) as described in Chapter 2. LM33 displays some preservation of structures, such as dissepiments, however this is not uniform throughout the coral. Rough overgrowths have replaced the original smooth coral surface in many areas. Secondary aragonite needles are located throughout the coral, and COCs are extremely altered. TL281 also displays some of these features. Poor preservation of septae is visible, as well as secondary aragonite and a significant amount of pitting of the coral surface, causing uneven and rough textures in pore spaces and along dissepiments.

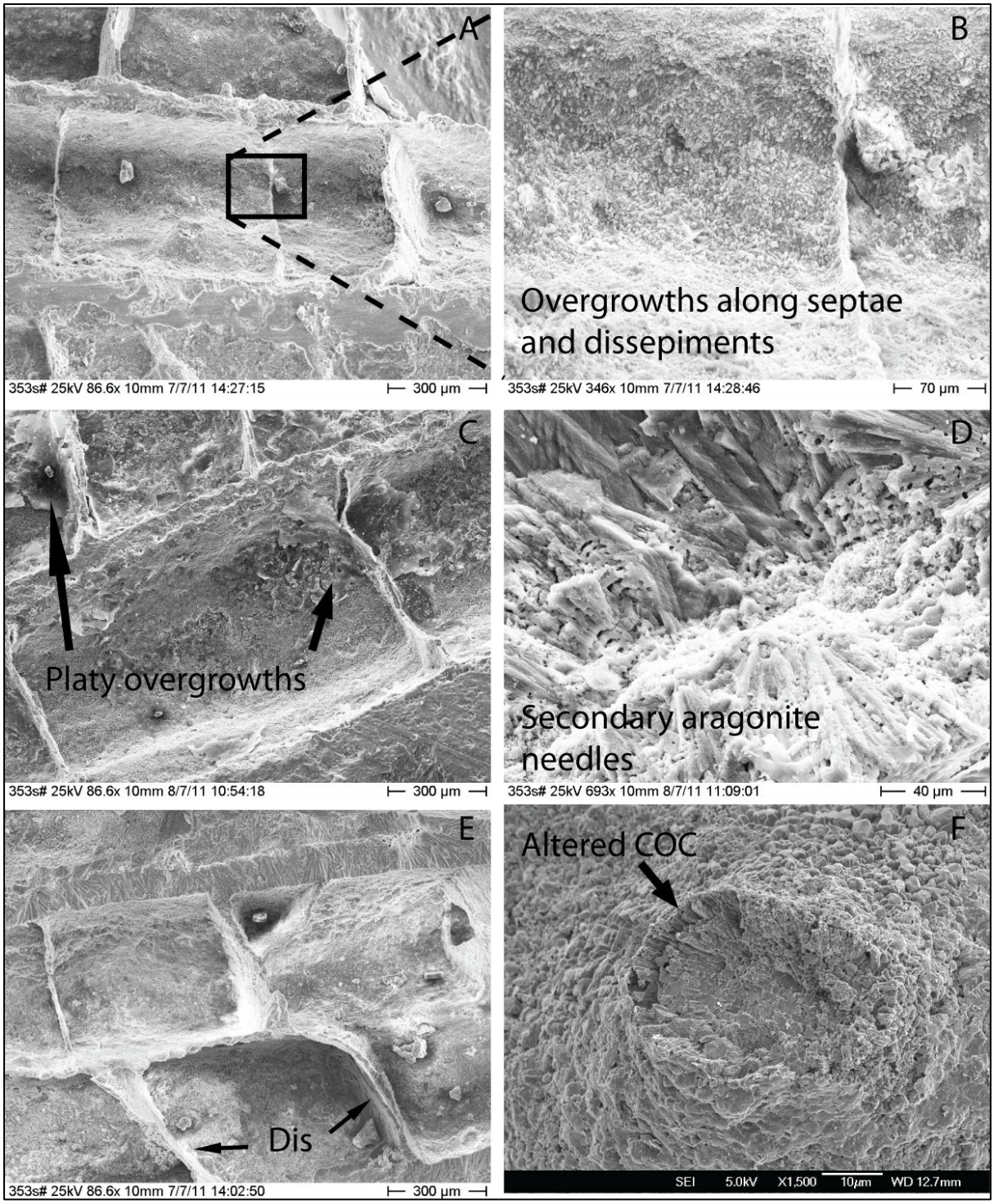

Fig. 3.12 SEM images of *P. pini* LM33. Although some areas of the coral show well preserved dissepiments, others display overgrowths, secondary aragonite and poorly preserved COCs. Images A and B are from the basal (oldest) zone, images C and D from the middle zone, and images E and F from the uppermost (youngest) zone of the coral.

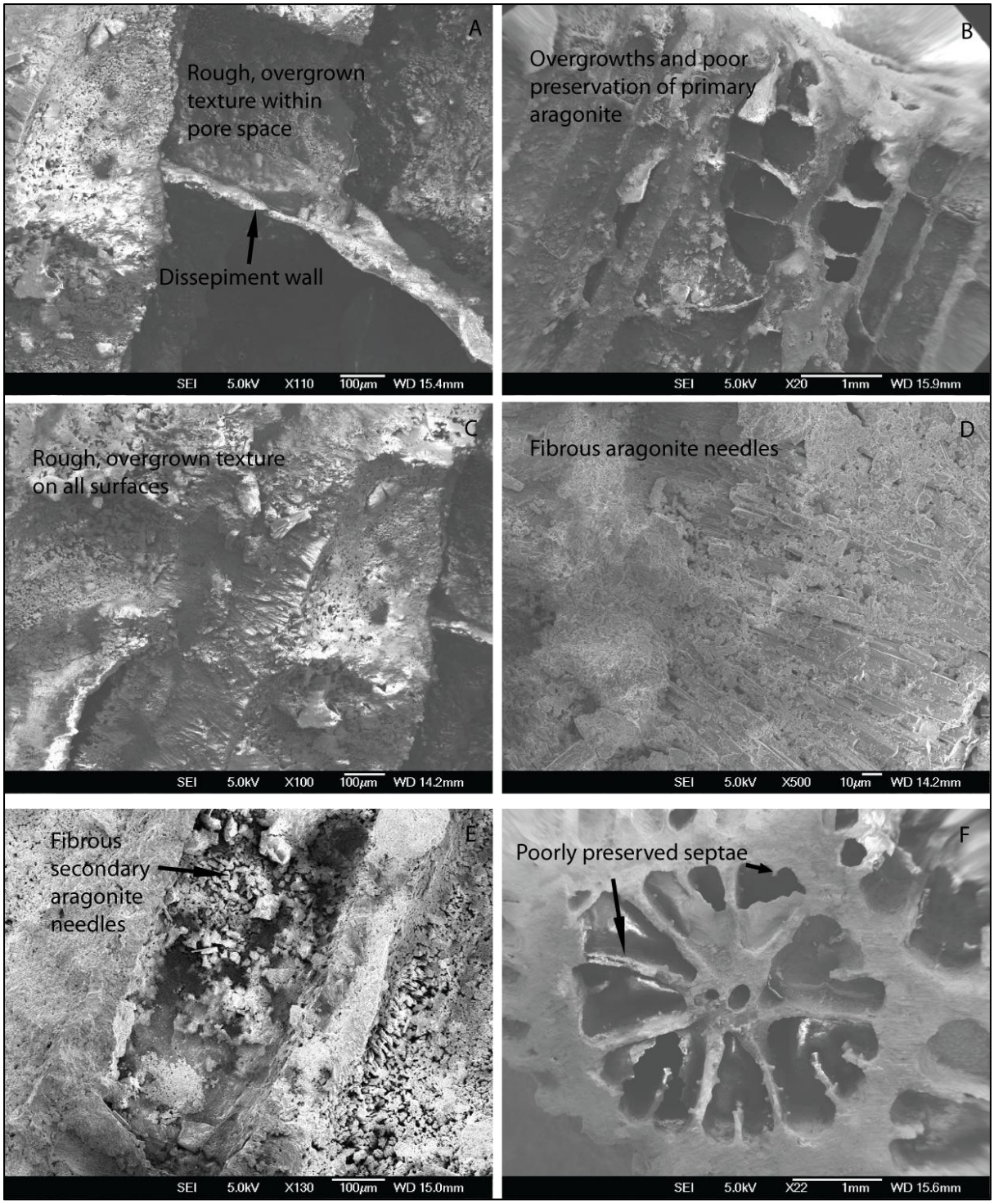

Fig. 3.13 SEM images of *P. pini* TL281, showing overgrowths, secondary aragonite and poorly preserved skeletal features. Images A, B, and C come from years five to seven of the milled coral, images D, E and F come from years eight to nine of the milled coral (depicted in Fig. 3.14)

3.5 Micromilling

Although XRD results for these two corals revealed that calcite had largely replaced the primary aragonite skeleton, the petrographic analysis of TL281 was in agreement with the XRD pattern of increasing preservation towards the youngest (uppermost) part of the coral. For this reason, micromilling has been carried out on the uppermost 10 years of TL281. LM33 has not been micromilled as the percentage of calcite is not a uniform gradation throughout the skeleton as found in TL281, and petrographic analysis did not reveal any well preserved areas of coral.

The remaining 7mm slab of TL281 was prepared for micromilling. This involved a second round of cleaning with an ultrasonic probe and determining the exact location of the annual density band couplets from the X-ray image. A hand dremel was used to cut away the skeleton to the very edge of a solid septal wall, along which a milling path was set up using a New Wave Micromill (Fig. 3.14). The five uppermost density band couplets were milled at approximately monthly resolution (0.08 mm spacing), with the following three couplets sampled at a higher resolution of approximately fortnightly resolution (0.04 mm spacing), with the following two couplets milled at the initial lower monthly resolution. This milling plan was designed to extract a highest resolution seasonal climate signal from the portion of the coral that is texturally consistent and best preserved, with the hope that geochemical changes reflect meaningful changes in seawater chemistry during the time of coral formation.

In an attempt to explain the reasons for variable rates of diagenesis throughout the coral, a schematic diagram has been prepared (Fig. 3.14). It shows that due to marine and freshwater pooling in the rock crevice in which the coral was located may have been the instrumental factor behind very high levels (80-85%) of calcite detected by XRD analysis in the lowermost third of the coral, as well as extensive secondary aragonite and dissolution detected in petrographic and SEM analyses. The schematic also displays that the upper ~ 2 cm of coral which is brown in colour, as opposed to creamy white, is likely to have been exposed to greater amounts of sedimentary infill and algal growth than the coral beneath. Light rainfall or ocean spray would also collect on the upper surface of the coral and cause increased diagenesis in this zone. These factors are attributed to the high levels of diagenesis detected in the lower third and uppermost 2 cm of the coral.

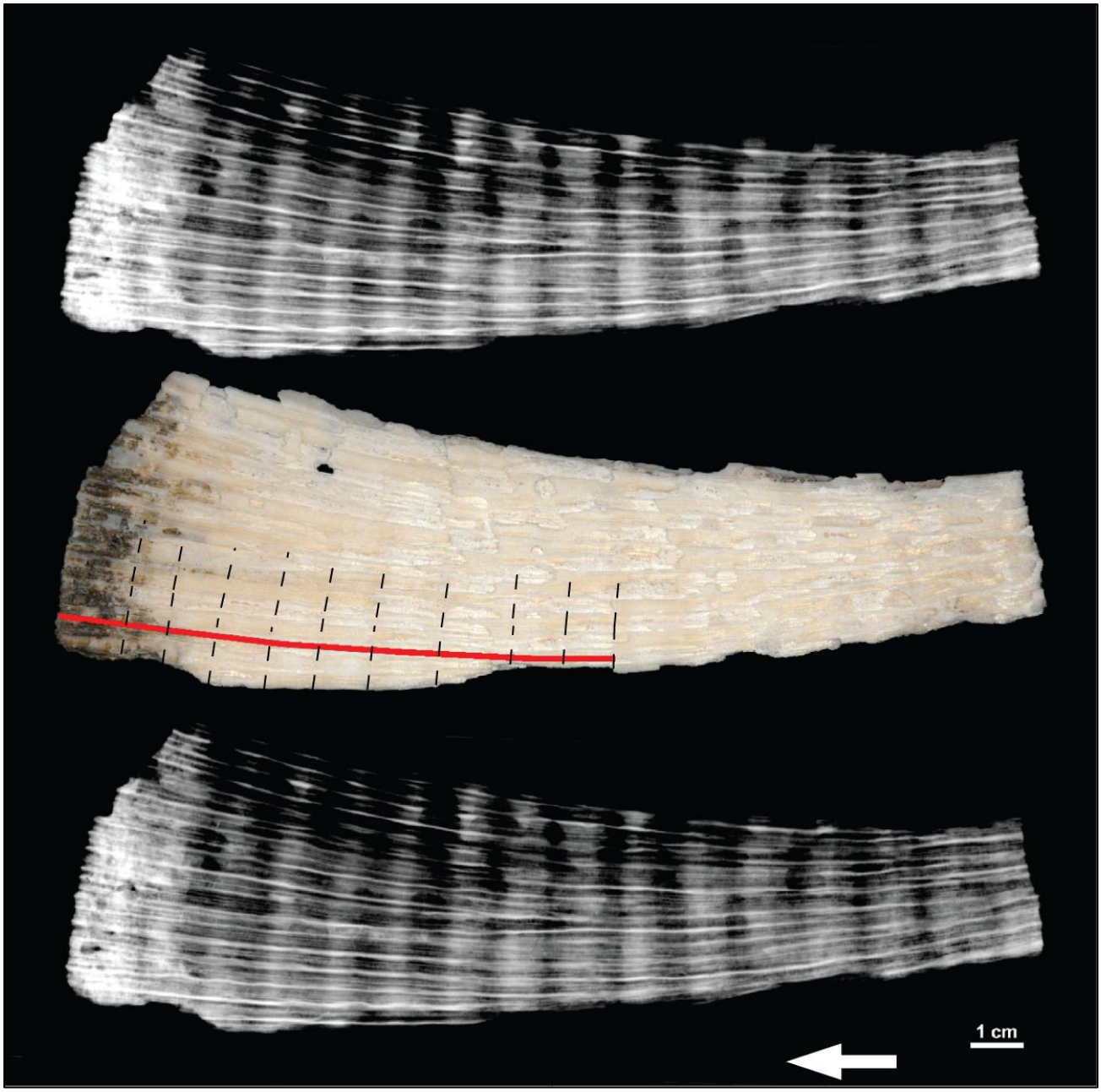

Fig. 3.14 Composite image showing *P. pini* TL281 7mm slab and X-ray images of each side of slab. Micromill path shown in red. Dashed lines indicated growth bands. Material beneath the micromill path was cut away with a hand dremel prior to milling. White arrow indicates younging direction.

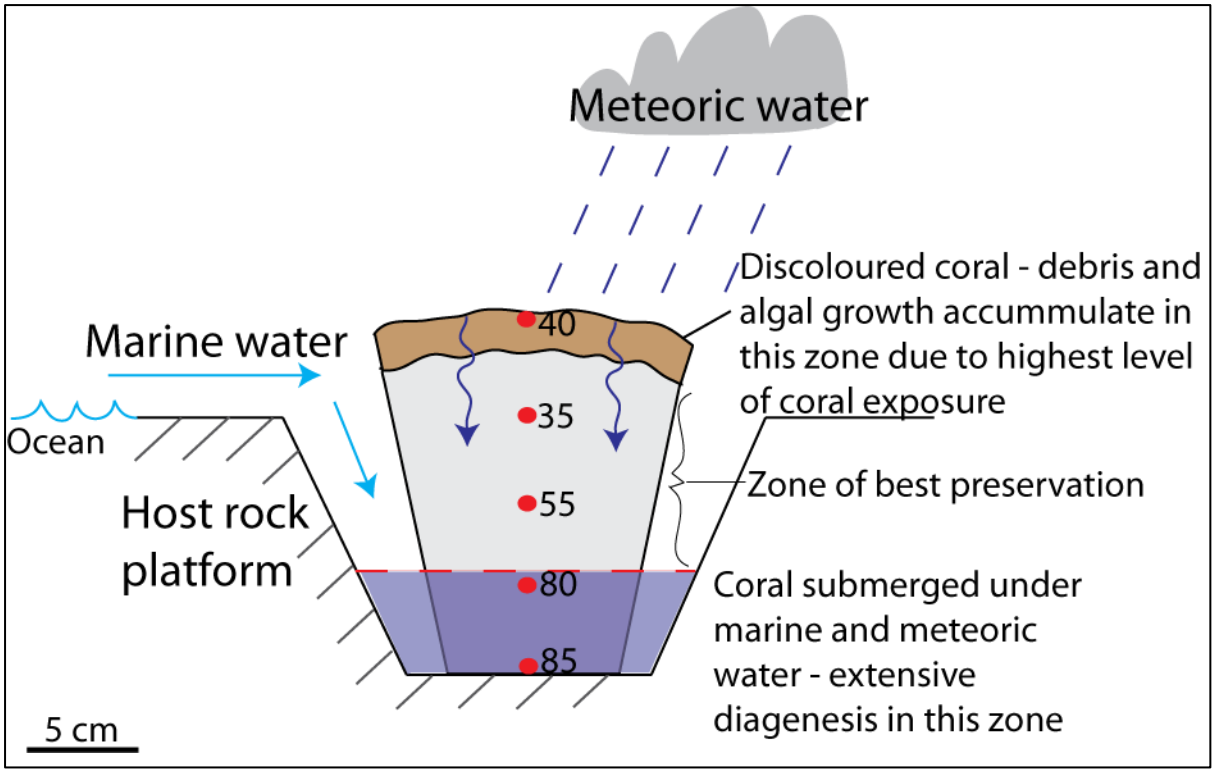

Fig. 3.15 Schematic diagram displaying the causes of diagenesic variability throughout the coral. Red circles indicate calcite percentages as determined by XRD analysis. Meteoric water could infiltrate through the coral (dark blue arrows), residing mostly in the uppermost section during light rainfall, and pooling in the rock crevice during heavy rainfall events leading to increased freshwater diagenesis in this zone. Wave impacts on the rock shelf (light blue arrows) could cause accumulation of seawater in the rock crevice, allowing increased marine diagenesis.

3.6 Results

Analyses of stable isotopes $\delta^{18}O$ and $\delta^{13}C$ have revealed average values of -4.82‰ and 1.12‰, respectively, with a range of -3.47‰ to -5.45‰ and 3.43‰a to -0.49‰, respectively. Raw isotopic data is presented in Fig. 3.16, with the sample number in the x-axis and isotopic values on the y-axis. Refer to Appendix Table 2 for raw isotopic data. Coral ages are discussed in terms of years of milled coral growth (MCG) i.e. the basal annual density band of the coral which has been milled is the oldest part of the coral, moving up the growth axis towards the top of the coral head through sequentially younger years MCG. Therefore, Year 1 MCG is the oldest, and Year 10 MCG is the youngest.

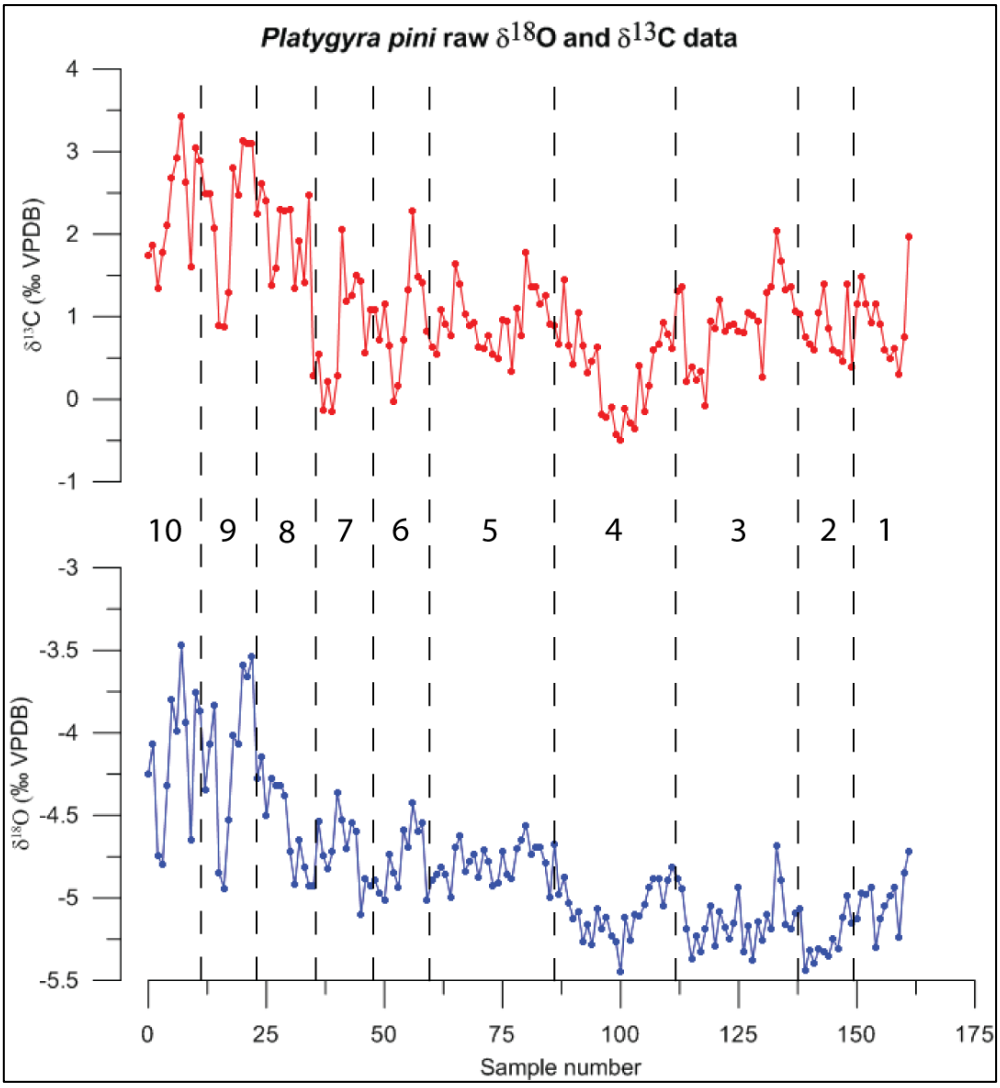

Fig. 3.16 Raw $\delta^{18}O$ and $\delta^{13}C$ data for *P. pini*. Years 1 to 10 MCG labelled along sampling axis. Wider spacing between years 3, 4 and 5 are due to the increased sampling resolution from monthly to fortnightly during this period.

Raw $\delta^{18}O$ and $\delta^{13}C$ values are also displayed in time, with years of coral growth sampled (1-10) in the x-axis (Fig. 3.17). A running mean of each data set has been included in the graph, to highlight periodicity. It must be noted that due to the coral being milled from the top to the base, Fig. 3.16 presents the data getting older to the right, whereas Fig. 3.17 shows younging to the right. Both data sets display a shift towards more positive values over time, with significant positive peaks in year 8 of both $\delta^{18}O$ and $\delta^{13}C$. These positive peaks are followed by a substantial negative shift. $\delta^{18}O$ peaks at -3.53‰ before rapidly dropping to -4.94‰, and $\delta^{13}C$ peaks at 1.24‰ before rapidly dropping to -2.90‰. These shifts represent the largest fluctuation in values for both data sets. As seen in the *G. retiformis* coral, the $\delta^{18}O$ and $\delta^{13}C$

values of *P. pini* display covariance when both overlain (Fig. 3.18), with an R^2 value of 0.6 (Fig. 3.19).

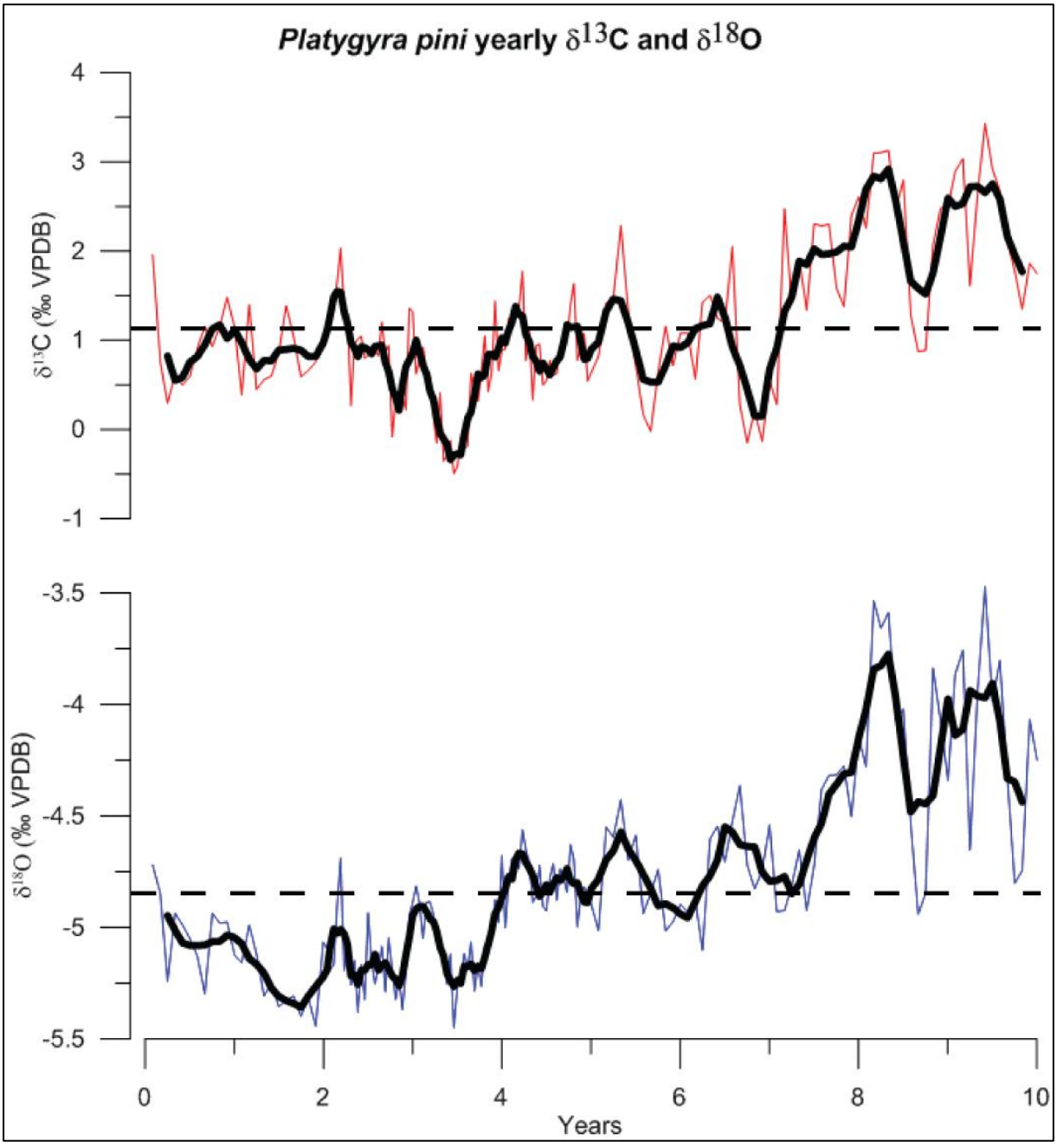

Fig. 3.17 *P. pini* stable isotope data as sampled through time (years 1-10.) Running average shown by thick black line. Horizontal dashed lines indicate average $\delta^{18}O$ of -4.82‰ and average $\delta^{13}C$ of 1.12‰.

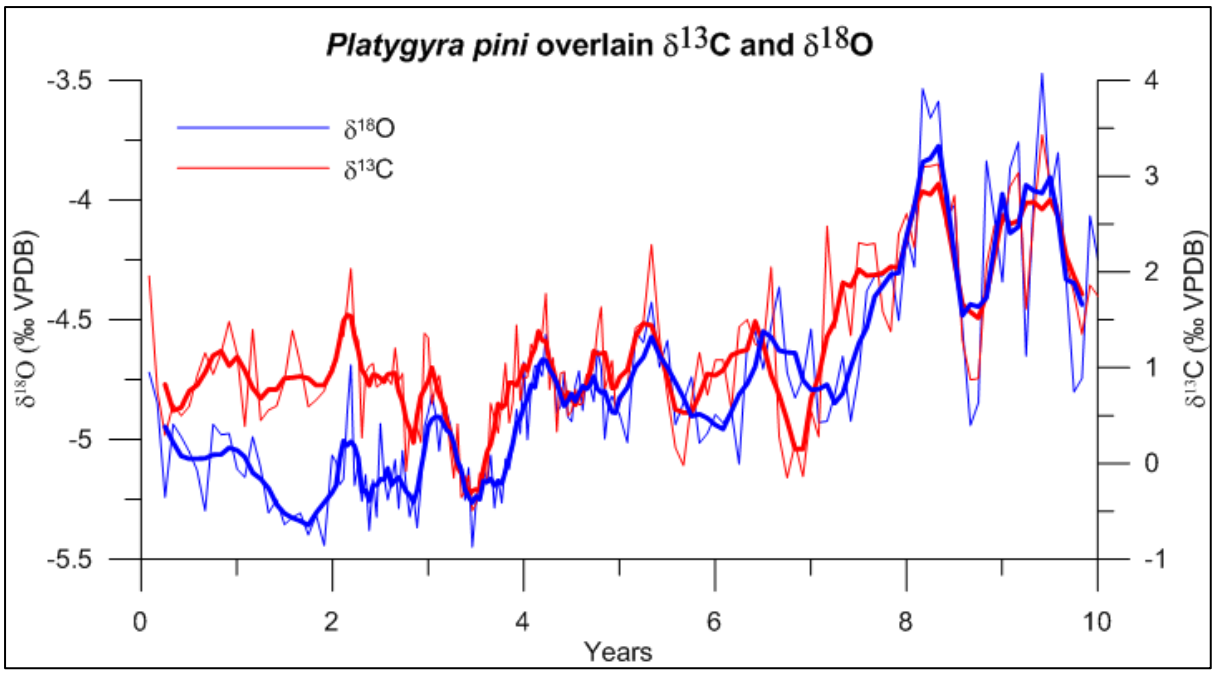

Fig. 3.18 Graph showing *P. pini* yearly raw and running mean average data overlain to exhibit the covariance of $\delta^{18}O$ and $\delta^{13}C$.

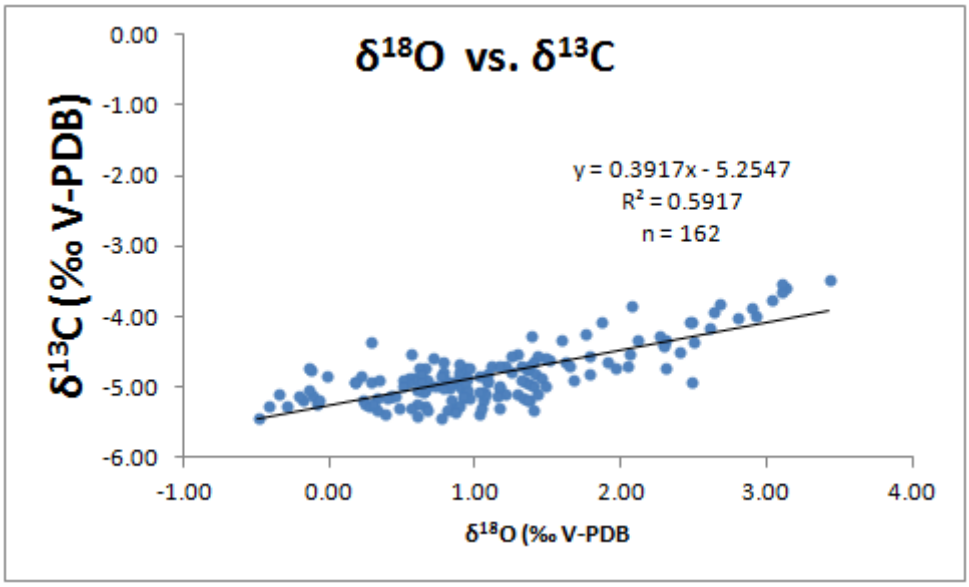

Fig. 3.19 $\delta^{18}O$ versus $\delta^{13}C$ scatter plot for all aragonite powders analysed. Covariance gives an R^2 value of 0.6 from 162 data points.

In order to statistically assess periodicity in the isotope data, spectral analysis and sinusoidal graphs of both $\delta^{18}O$ and $\delta^{13}C$ data have been generated using PAST. As seven out of the 10 years of the Holocene record were sampled at monthly resolution (Years 1, 2, 6, 7, 8, 9 and

10), the remaining three (Years 3, 4 and 5) were altered to monthly resolution so that the time spacing of the data was even before entering into PAST. This was achieved by determining the means between each two consecutive data points on average. When consecutive values were identical or very similar, one extra data point was incorporated in order to account for the additional three values from the fortnightly sampling which creates 26 data points, whereas monthly sampling creates only 12.

Using spectral analysis (Fig. 3.20), the peak frequency of monthly averaged $\delta^{18}O$ data is as follows;

$$Periodicity = \frac{1}{0.02101}$$

$$Periodicity = 47.596 \ \ months\ per\ cycle$$

During the 120 months of the 10 year time series, 2.5 of these 48 months cycles should be present. The sinusoidal model presents this poorly, even with a 48 month period selected (Fig. 3.21).

In contrast, the peak frequency of monthly averaged $\delta^{13}C$ data (Fig. 3.22) is;

$$Periodicity = \frac{1}{0.009454}$$

$$Periodicity = 105.775 \ \ months\ per\ cycle$$

Consistent with peak frequency results, the 105 month cycle is only detected once in the sinusoidal model (Fig. 3.8).

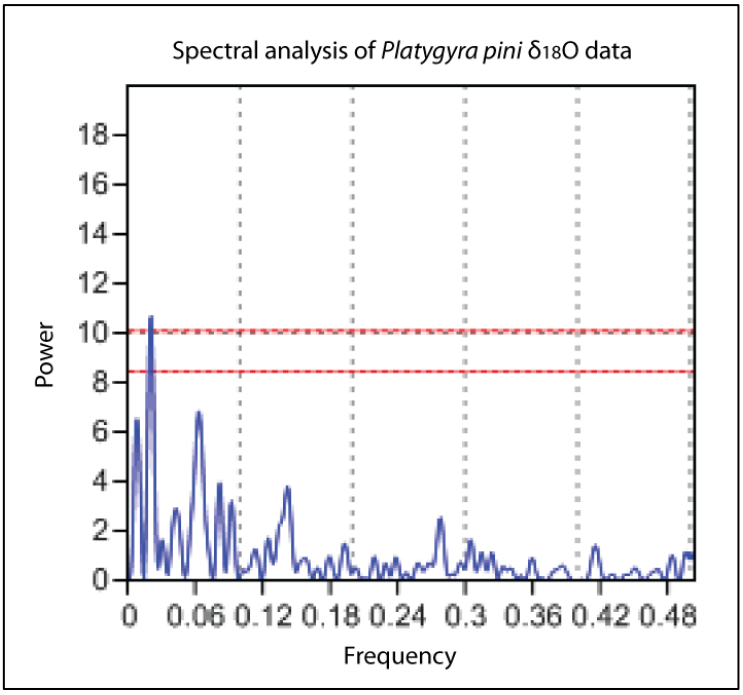

Fig. 3.20 Spectral analysis of monthly *P. pini* $\delta^{18}O$ data. The strongest peak in the spectrum is reported as 0.02101. The two dashed red lines are significance levels; the upper is $p<0.01$ and lower is $p<0.05$, with respect to white, uncorrelated noise.

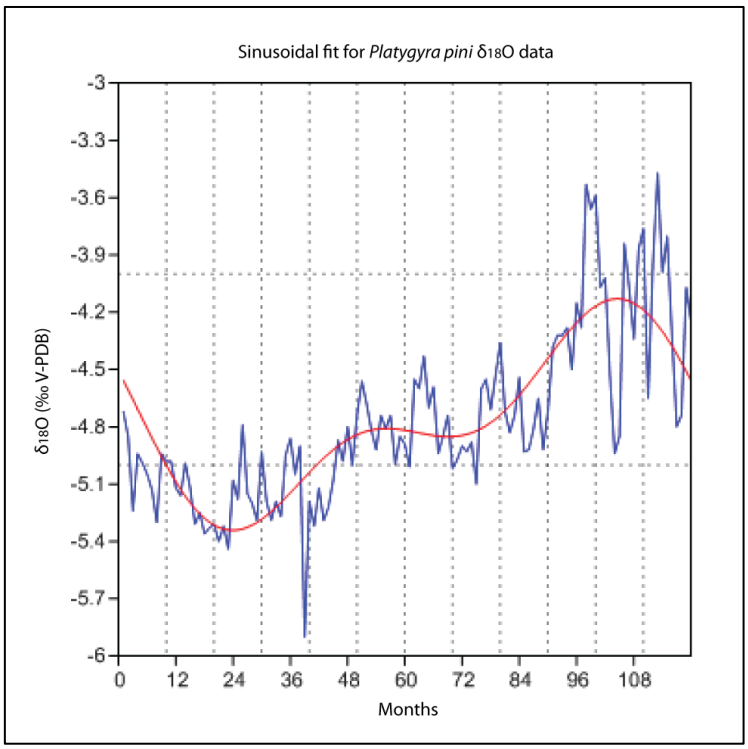

Fig. 3.21 Sinusoidal fit of monthly *P. pini* $\delta^{18}O$ data. $\delta^{18}O$ data is represented by the blue line, sinusoid is represented by the red line.

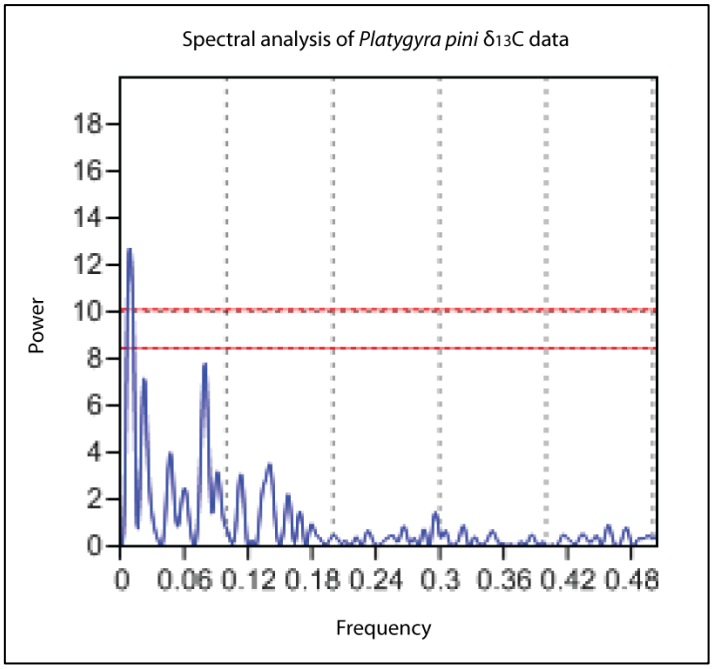

Fig. 3.22 Spectral analysis of monthly *P. pini* $\delta^{13}C$ data. The strongest peak in the spectrum is reported as 0.009454. The two dashed red lines are significance levels; the upper is $p<0.01$ and lower is $p<0.05$, with respect to white, uncorrelated noise.

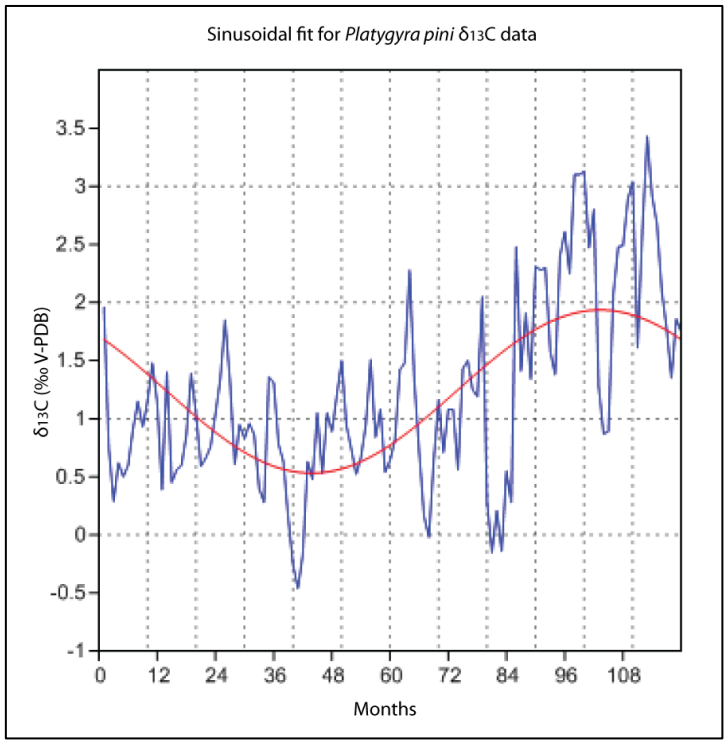

Fig. 3.23 Sinusoidal fit of monthly *P. pini* $\delta^{13}C$ data. 105 month periodicity displayed by sine curve. $\delta^{13}C$ data is represented by the blue line, sinusoid is represented by the red line.

3.6.1 U/Th results

Fossil coral samples were prepared by extracting sections of coral with sterile tweezers and storing each in a microcentrifuge tube. Samples weighed 50-100 micrograms. Seven samples were collected from the base to the top of each coral at evenly spaced intervals. Unfortunately, due to weathering, only one sample from each coral could be analysed. Fig. 3.24 displays the location of the sample that was used to date each coral. U/Th geochronology methods followed those outlined in Hellstrom et al. (2003), with analyses undertaken using a Nu Plasma multi-collector inductively-coupled plasma mass spectrometer (MC-ICP-MS). Coral samples were dissolved and equilibrated with a $^{229}Th/^{233}U$ mixed spike solution before U and Th were separated from the matrix using Eichrom TRU-Spec resin. The purified U/Th fraction was then introduced to the MC-ICP-MS via a Cetac Aridus membrane desolvator, giving total system efficiencies of ~ 0.3% for both elements. This technique has provided mid Holocene ages for the two corals (Table 3.2). LM33 is 4.538 ka (2σ% error of 0.104), and TL281 is 4.555 ka (2σ% error of 0.092). Although calcite and aragonite cements can significantly enrich coral $\delta^{234}U$, so that true coral ages are underestimated (Henderson et al., 1993), these U/Th dates are considered reliable as the ages are within initial $^{234}U/^{238}U$ range. (J. Hellstrom, Pers. Comm.).

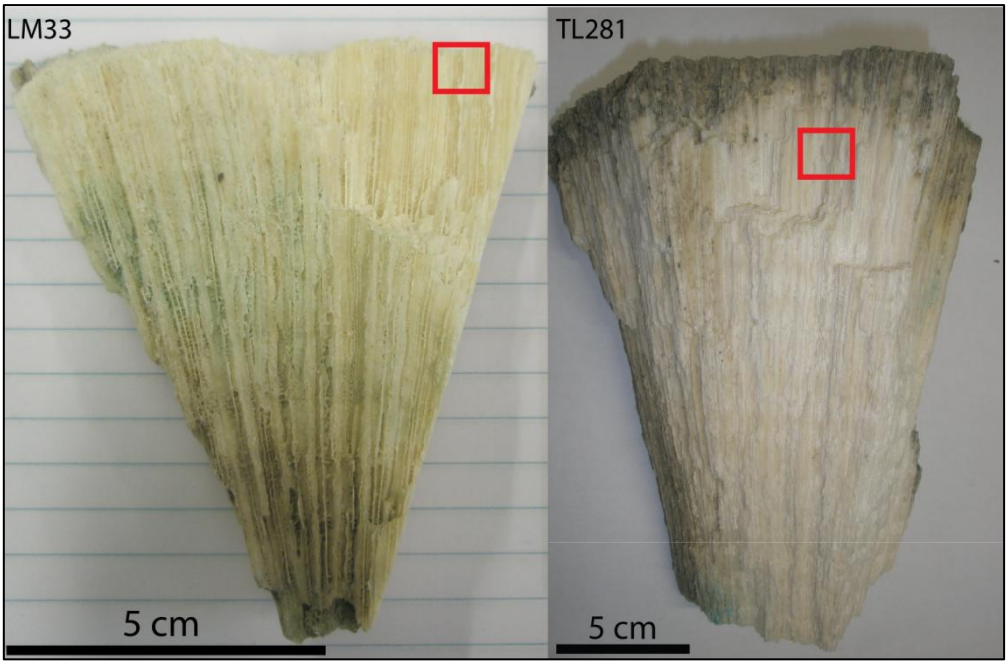

Fig. 3.24 Location of coral samples (red squares) providing U/Th dates in LM33 and TL281

Table 3.2 U/Th date results for Holocene corals LM33 and TL281

Sample	$^{234}U/^{238}U$	Error (2σ%)	$^{230}Th/^{238}U$	Error (2σ%)	$^{230}Th/^{232}Th$	$^{232}Th/^{238}U$	Error (2σ%)
LM33	1.1136	0.0043	0.0457	0.0010	126.3	0.000361	0.000009
TL281	1.1205	0.0026	0.0459	0.0009	456.4	0.000101	0.000003

All uncertainties and 9% confidence intervals and include allowances for external standard reproducibility and spike calibration uncertainty, although note that uncertainty in decay constants is not propagated. ($^{230}Th/^{238}U$) is determined using a mixed spike calibrated against a solution of HU-1; see Hellstrom (2003) for a detailed description of the method and results of standard analyses.

3.6.2 Mid Holocene SST reconstruction

A study using 48 modern and fossil corals from the Mentawai Island (Sumatra, Indonesia) and Muschu/Koil Islands (PNG) has enabled a reconstruction of oscillations in the extent of the IPWP since the mid-Holocene (Abram et al., 2009). Reliable SST estimates have been obtained using low resolution Sr/Ca analysis of fossil corals, with results indicating that the southwest margin of the IPWP was 1.2° C ± 0.3° C cooler than present between 5.5-4.3 ka. This corresponds to a mean SST of ~ 26-27° C. In order to determine whether the isotopic values obtained from *P. pini* are realistic, the temperature dependence equation for modern *Platygyra* calculated by Shimamura et al. (2008) has been applied to this coral. By quantifying the mid Holocene SSTs that these values necessitate, a greater understanding of the extent of geochemical alteration in the coral can be obtained. The temperature dependence equation is as follows:

$$T = -4.57(\delta^{18}O_c) + 2.65$$

This equation has been applied to fossil *P. pini* mean, minimum and maximum $\delta^{18}O$ values.

Mean $\delta^{18}O$:

$$T = -4.57(-4.82) + 2.65$$

$$= 24.6774$$

$$= 24.7° C$$

Minimum $\delta^{18}O$:

$$T = -4.57(-5.45) + 2.65$$

$$= 27.5565$$

$$= 27.6° C$$

Maximum $\delta^{18}O$:

$$T = -4.57(-3.47) + 2.65$$

$$= 18.5079$$

$$= 18.5° C$$

The SSTs deduced from *P. pini* using the *Platygyra* temperature dependence equation give a mean of 24.7° C, oscillating between 18.5° C and 27.6° C. It appears that diagenetic alteration of absolute isotopic values has indeed caused positive shifts and cool artifacts in the record, namely in years 7 to 10, where both $\delta^{18}O$ and $\delta^{13}C$ undergo a distinctly positive departure from mean values of -4.82‰ and 1.12‰, respectively. In this zone of the coral, where SSTs are modelled as low as 18.5° C, extensive secondary aragonite has been identified in SEM (Fig. 3.13). Years 5-6 vary between 23.2° C and 25.0° C. When comparing to the suite of coral data that has provided constraints on mid Holocene cooling in the southwest IPWP (Abram et al., 2009), it is apparent that temperatures this cool are unrealistic for this site. However, the record from years 1-4 provides more reasonable results with SST fluctuations between 24.7° C and 27.6° C, but diagenetic textures are also identified in this section of the coral. In comparison, the modern *Platygyra* corals from Ishigaki Island and Espiritu Santo provide mean SSTs of 25.9° C and 25.4° C, respectively, when the temperature dependence equation is applied. The annual mean SST for Ishigaki Island is within the 24-26° C isopleth, however Espiritu Santo is within the 26-28° C isopleth, meaning that this temperature dependence equation must be altered slightly in order for accurate results to be obtained from low latitude corals. This reinforces the need for a modern *Platygyra* calibration for the southern Indo-Pacific region.

3.7 Discussion

Initial assessment of the stable isotope results shows a data set that becomes increasingly positive through time, with positive covariance of $\delta^{18}O$ and $\delta^{13}C$ throughout. If the coral was pristine, the positive shift would be interpreted as the display of gradually cooling SSTs, and covariance as the result of a combination of kinetic and metabolic effects acting equally upon the oxygen and carbon isotopes, as described by McConnaughey (1989). The isotopic values in this coral are noticeably higher than those from the modern *Platygyra* from Ishigaki Island and *Porites* from Espiritu Santo (Table 3.3), but there is minimal relevance in comparing these data sets, because of their distal locations from this study site and as mid Holocene SSTs in the southern IPWP were cooler than present (Abram et al., 2009), so are expected to be more positive than modern records. Sun et al. (2005) found that the $\delta^{18}O$ record of a 4.4 ka *Porites* from the South China Sea is ~ 0.6‰ higher than that of a modern coral from the same location, suggesting that the $\delta^{18}O$ of surface seawater was higher by at least 0.5‰ relative to modern values. As such, it seems feasible that ^{18}O enrichment due to freshening in the Indo-Pacific at this time of cooler oceans and strengthening monsoon rainfall could be partially responsible for the values recorded in the *P. pini* coral. However, since this coral has been affected by diagenesis, the results must be treated with caution.

3.7.1 Influence of diagenesis on isotopes

XRD scanning revealed high proportions (~ 80%) of calcite in the lower third of the coral, reducing to ~ 40% in the upper third. When thin sections of the coral were petrographically analysed, it was reinforced that the lower third of the coral is extremely altered and confirmed that extensive alteration has taken place throughout the coral. However, the upper two thirds of the coral, specifically the top 11 cm, has retained signatures of primary growth textures, including well preserved COCs, septae and dissepiments. Abnormally dark areas indicative of dissolution were present throughout this 11 cm section, but not to the same extent as the lowermost section of the coral. Secondary aragonite was detected using SEM, with fibrous needles typical of recrystallisation seen in pore spaces and along septal and dissepiment walls. Given this identification of dissolution and secondary aragonite, it would be expected that isotopic values would be more positive in this coral than in pristine *Platygyra* samples. Secondary aragonite and dissolution have been seen to create cool SST artifacts in modern corals, which are caused due to the forcing of a positive shift in isotope values (McGregor and Abram, 2008). Early marine diagenesis has been identified as a driver for this process

(Bar-Matthews et al., 1993), which probably occurred while the reef was submerged and the coral pore spaces completely saturated with water. The absence of distinct zones of calcite when examined in thin section and using the SEM is also supported when interpreting isotopic values, as calcite has the effect of forcing negative isotopic shifts in corals, leading to warm SST artifacts (McGregor and Abram, 2008). Comparison to modern and fossil *Platygyra* records (Table 3.3) suggests that this record is altered, as $\delta^{18}O$ ($\delta^{13}C$) isotope values are 0.6‰ to 1.2‰ (0.86‰ to 2.55‰) more positive than maximum values. Qu (2007) explains that 20% secondary aragonite within a coral causes a shift to 0.5‰ higher $\delta^{18}O$, which is reflected by these figures. Yet the XRD results showing 55%, 35% and 45% calcite for the three uppermost subsamples of this coral must also be acknowledged. Calcite growth is known to occur through subaerial exposure (McGregor and Abram, 2008), a process which has obviously taken place since the reef has been emergent above high tide sea level. There are no drastically negative isotope excursions, and the highest SSTs produced using the Shimamura et al. (2008) equation are not unrealistically warm. Clearly, more geochemical analysis is required to determine the exact influence of secondary calcite growth on this coral.

The amplitude of isotopic fluctuation throughout the time series gives an indication of the level of diagenesis present throughout the 11 cm milled zone. There is a steady increase in $\delta^{18}O$ values from year 0 to year 10 of the record. During years 0-4 the values fluctuate between ~ -5.0‰ to -5.5 ‰, followed by a sharp step to fluctuations between -5.0‰ to -4.5‰ from years 4-7. From here, the fluctuations become much more exaggerated, with peaks and troughs of almost 1.5‰ recorded by two distinct cycles during years 7-10. This indicates that the top (youngest) three years of the coral have undergone more extensive levels of diagenesis that the coral below, as this amplitude is distinctly larger than the previous seven years of the record. When inspecting the entire coral specimen (Fig. 3.24) it is obvious that sedimentary infill and alteration affecting the top 1-2 cm has caused discolouration of the originally cream coloured coral to a dark brown. This immediately suggests that primary aragonite has been drastically altered and recrystallised, and corroborates with the sharp increase in the magnitude of the isotopic fluctuation. In the $\delta^{13}C$ record, values fluctuate between ~ 1.5‰ and 0.0‰ for a long portion of the record (years 0-7). However, as seen in the $\delta^{18}O$ record, a substantial shift to positive values of ~ 1.5‰ to 3.0‰ occurs during years 7-10. This provides further evidence for intense dissolution and secondary aragonite growth in the uppermost ~ 4 cm of the coral.

Table 3.3 Isotopic range and means from *Platygyra* corals, highlighting the relative positivity of *P. pini* values.

Coral location	$\delta^{18}O$ range (‰ V-PDB)	Mean $\delta^{18}O$ (‰ V-PDB)	$\delta^{13}C$ range (‰ V-PDB)	Mean $\delta^{13}C$ (‰ V-PDB)	Author
Timor Leste (*P. pini*)	-3.47 to -5.45	-4.82	3.43 to -0.49	1.12	(Moody et al., 2012)
Timor Leste (*P. lamellina*)	-4.67 to -5.48	-5.08	0.88 to -1.12	-0.34	(Moody et al., 2012)
Vanuatu (*P. lamellina*)	-4.07 to -5.75	-4.98	2.57 to -1.55	0.01	(Quinn et al., 1993; 1996)
Japan (*Platygyra sp.*)	-4.2 to -6.0	-5.10	no data	no data	(Shimamura et al., 2008)

3.7.2 Isotopic fluctuations and Periodicity

Within the geochemical record of this coral, diagenesis prohibits our ability to use $\delta^{18}O$ values to determine absolute SST information, yet periodicity appears to be retained to some extent, allowing an insight into mid Holocene climate behaviour. Rather than a quantitative assessment of absolute SST values, this record provides a qualitative insight into the scale of SST fluctuations (i.e. Δ‰ from peaks to troughs) of the waters of Ombai Strait during this time period. The magnitude of seasonal $\delta^{18}O$ fluctuations in the *P. pini* is ~ 0.4‰. This is very similar to the modern *Porites* from West Timor (Cahyarini et al., 2008), which shows fluctuations of 0.4-0.7‰ except for one anomalous fluctuation of 1.6‰. A similar magnitude is recorded in 7.6-5.4 ka *Porites* records from PNG (McGregor and Gagan, 2004), with fluctuations of ~ 0.2‰. In contrast, the modern *Platygyra* from Ishigaki Island (Shimamura et al., 2008) and mid Holocene fossil *Porites* records from the South China Sea (Sun et al., 2005) show a larger Δ‰ between peaks and troughs. Both provide consistent records with fluctuations between 1.5-2.0‰, likely due to the greater seasonal SST fluctuations in the northern parts of the IPWP.

Abram et al. (2009) suggest that mid-Holocene cooling at their study sites in Indonesia and PNG was related to contractions of the southeastern and southwestern margins of the IPWP. Such contractions would have been associated with the more northerly position of the Inter-

tropical Convergence Zone (ITCZ) that accompanied mid-Holocene strengthening of the Asian summer monsoon. Intervals of a strengthened Asian monsoon and cooling in the southwestern IPWP during the mid-Holocene appear to correspond with a more positive IOD-like mean configuration across the tropical Indian Ocean, suggesting that the Asian monsoon–IOD interaction that exists at interannual time scales also persists over centennial to millennial scales (Abram et al., 2009). They postulate that associated mean changes in the Pacific ENSO modes may have also occurred during the mid-Holocene. Therefore an interannual periodicity should be present in this coral record. Spectral analysis has indeed detected interannual periodicity of 48 and 105 months in the $\delta^{18}O$ and $\delta^{13}C$ records, respectively. These 4 and 8.75 year cycles are likely to be the result of the interaction between climatic processes such as the Asian monsoon and IOD, or an ENSO-driven signal. It is unusual that there is a 4.75 year difference between these two periodicities, and suggests that diagenesis has caused isotopic shifts which have produced skewed periodicity data. Nevertheless, the retention of an interannual periodicity which aligns with known climatic processes occurring in the region during the mid Holocene presents new insights and shows that corals displaying diagenetic alteration may in fact be able to contribute to palaeoclimate proxy records.

3.8 Conclusion and implications

This 4.5 ka *P. pini* coral shows both preservation of climatic signals and the influence of diagenetic alteration in its isotopic record. Careful examination of diagenetic zones and a preliminary mid Holocene SST calculation has highlighted areas within the coral where the geochemical signal has been overprinted and is unreliable, as well as zones where some palaeoclimate inferences may be possible. Mean isotopic values of -4.82‰ ($\delta^{18}O$) and 1.12‰ ($\delta^{13}C$) are more positive than modern *Platygyra* values, which is to be expected due to the ~ 1.2° C cooler SSTs that were prevalent in the mid Holocene in the southwest Indo-Pacific. However, there are certainly zones of the geochemical record that have been influenced by diagenesis, with SST interpretation reiterating the fact that diagenetic screening is a crucial aspect to in all studies using corals as climate proxies. The preservation of interannual periodicity in the record displays the potential use of slightly altered fossil corals as qualitative climate archives, where absolute climate data such as SST and SSS cannot be ascertained, but broader scale climate behaviour can. This study is the first to implement a fossil *Platygyra* coral as climate proxy, and provides encouraging results that this genus is

indeed capable of recording a useful geochemical signal. Due to its broad latitudinal range, emphasis should be placed upon further detailed studies which will allow the development of *Platygyra* corals as reliable palaeoclimate proxies.

4 Oceanographic insights from the Indo-Pacific Warm Pool using a terminal Pliocene *Platygyra lamellina* coral

4.1 Abstract

A *Platygyra lamellina* coral was recovered from the Pliocene Viqueque Megasequence (VM) in Timor Leste, and dated using U/Pb techniques to obtain an age of 2.7 Ma ± 0.34 (2σ). After rigorous diagenetic screening using X-ray diffraction (XRD), petrographic, and scanning electron microscopy (SEM) examination, stable isotope analyses have yielded the first results from an Indo-Pacific, terminal Pliocene coral. Mean $\delta^{18}O$ and $\delta^{13}C$ values of -5.08‰ and -0.34‰, respectively, and ranges of -4.67‰ to -5.48‰ and 0.88‰ to -1.12‰ were obtained. These isotopic values correlate well with a modern *Platygyra* coral from Ishigaki Island, Japan, which has a mean $\delta^{18}O$ of -5.1‰ and a range of -4.2‰ to -6.0‰. They also emulate those seen in modern *Platygyra* samples from locations around the Central- and Indo-Pacific. Spectral analysis has revealed peak frequencies of 0.08263 and 0.08051 for $\delta^{18}O$ and $\delta^{13}C$, corresponding to 12.1 and 12.4 months per cycle, respectively. This provides statistically robust evidence that the five year long record displays strong annual periodicity, and gives a seasonal record for the terminal Pliocene. Palaeo-sea surface temperatures (SSTs) have been derived using the temperature dependence equation calculated from the Ishigaki Island coral. A mean SST of 25.9° C for the Timor region aligns with Mg/Ca records that show SSTs were ~ 2-3° C cooler than present between 3.3-2.5 Ma in the Indo Pacific Warm Pool (IPWP).

4.2 Introduction

The use of fossil corals as geochemical archives of past ocean temperatures and salinities contributes significantly to the understanding of past climate conditions. The most commonly used and well understood coral genus in both modern and fossil realms is *Porites* (McGregor et al., 2011). This technique is normally restricted to the past 130,000 years as aragonite coral skeletons undergo rapid diagenetic alteration (Brachert et al., 2006), as seen in the mid Holocene *P. pini* coral (Chapter 3). However, fossil corals from the Caribbean have provided insights into climatic variation, ocean composition and chronostratigraphy from the Pliocene to the Eocene (Brachert et al., 2006; Ivany et al., 2004; Mackenzie et al., 1997; Roulier and Quinn, 1995). Until very recently no such record existed for the Indo-Pacific

region. The previous extent of the fossil coral palaeoclimate record dated back to a 124 ka *Porites* coral from North Sulawesi, Indonesia (Hughen et al., 1999), and a 130 ka record from a *Porites* coral from Papua New Guinea (PNG) (Tudhope et al., 1995). Both records use coral $\delta^{18}O$ to trace El Niño Southern Oscillation (ENSO) behaviour through the last glacial-interglacial cycle. The fossil coral retrieved from an uplifted reef on Bunaken Island, North Sulawesi provides a 65 year long time series that reveals ENSO variability on a temporal and geochemical scale similar to the modern instrumental record, and fossil corals from PNG suggest that ENSO may be stronger now than at any other time over the past 150 ka (Hughen et al., 1999). Yet new insights from a stratigraphically constrained 3.5-3.8 Ma outcrop in the Phillipines containing two pristine fossil *Porites* provide 35 year long records displaying the first proxy evidence of ENSO-like interannual variability occurring during the Pliocene Warm Period (PWP) which spanned 5-3 Ma (Watanabe et al., 2011). This contradicts previous studies that suggest permanent El-Niño-like conditions during this time (Wara et al., 2005), and provides the first detailed Pliocene ENSO record from the region. Further proxy records are needed to help clarify the onset of ENSO and other climate processes currently operating in the Indo-Pacific. Analyses of foraminiferal assemblages within sediment cores from locations throughout the Indo-Pacific (Gallagher et al., 2009) have provided indications that the Indonesian Throughflow (ITF) experienced restriction between 4-1.6 Ma. This is supported by deep sea drilling programme (DSDP) cores in the region, which provide time constraints on the timing of Indonesian Seaway narrowing (Srinivasan and Sinha, 1998). The absence of early Pliocene taxon from all Indian Ocean sites suggests the Indonesian Seaway became an effective biogeographic barrier to planktic formaninifera at the beginning of the Pliocene (Srinivasan and Sinha, 1998), yet the exchange of surface waters via the ITF persisted over this time. The sediment record can be expanded upon with histories gathered from high resolution seasonal records of mean temperature and salinity fluctuations using Pliocene corals. This presents exciting possibilities to provide insights into this period of global climate using corals *Platygyra* collected from the VM of Timor Leste.

A modern *Platygyra* coral has been investigated by Shimamura et al. (2008) to determine its ability to accurately record modern climate signals. Their findings confirm that this genus is an excellent climate proxy, with a strong temperature dependence and high extension rate making it ideal for isotopic analysis. Importantly, this genus has a much wider spatial distribution than *Porites* (Fig. 4.1), suggesting that *Platygyra* skeletons can be used as a

palaeo-SST proxy from tropical to mid-latitude regions (Shimamura et al., 2008). Previously, Quinn et al., (1996; 1993) analysed a *P. lamellina* coral head from Espiritu Santo Island in Vanuatu, to find that cross spectral analysis of $\delta^{18}O$ and $\delta^{13}C$ indicated a strong concentration of variance at the quasi-biennial (~ 2 years) and ENSO (~ 4-5 years) frequency bands. Importantly, these studies show that this genus is capable of accurately recording climate behaviour. Weber and Woodhead (1972) also studied *Platygyra* corals, recording mean $\delta^{18}O$ values for samples located throughout the Pacific, Indo-Pacific, and Indian Oceans (Fig. 4.1), which provide further constraints on isotope values that are expected from the terminal Pliocene sample. It is apparent that further studies using this genus will allow for a more detailed global climate record to be captured.

A suite of both *Platygyra* and *Porites* corals were retrieved from the Pliocene VM; a package of turbidites and poorly sorted debris flow paraconglomerates (Quigley et al., 2012) now exposed on the island of Timor in the Indonesian region (Fig. 4.2). A section of the VM rich in corals has been dubbed "Coral Gorge", where uplifted turbidite deposits have allowed excellent preservation of some of these ~ 2.7 Ma corals. After a rigorous diagenetic screening process, the pristine *Platygyra lamellina* coral (TL289) was analysed for stable isotopes, providing the first detailed five year record of terminal Pliocene age from the southern Indo-Pacific.

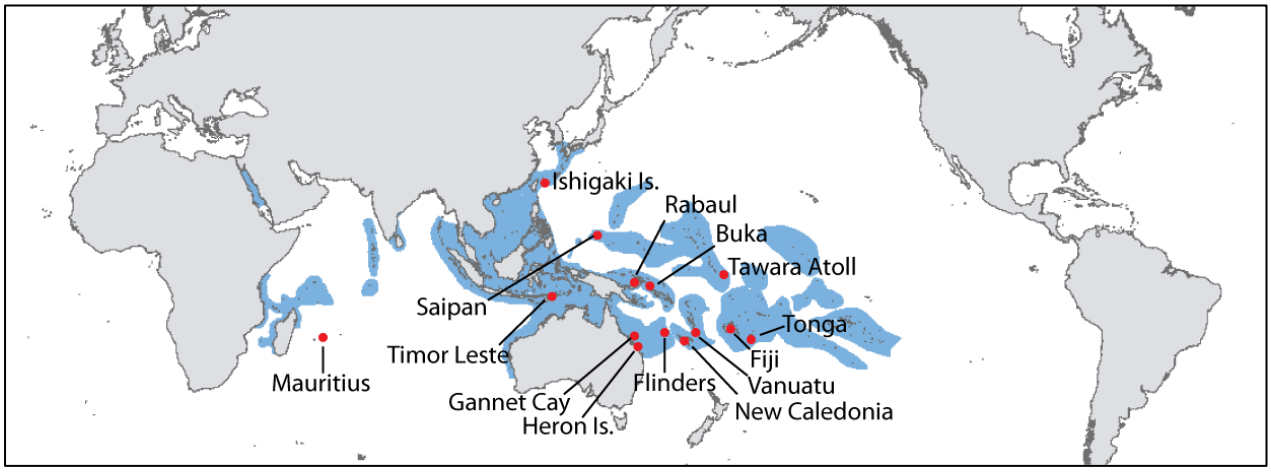

Fig. 4.1 Global distribution of *P. lamellina*, showing broader latitudinal range than *Porites*. Red circles indicate sites where modern *Platygyra* corals have been studied and data is compared with *P. lamellina* in this study. Modified from Veron, 2000.

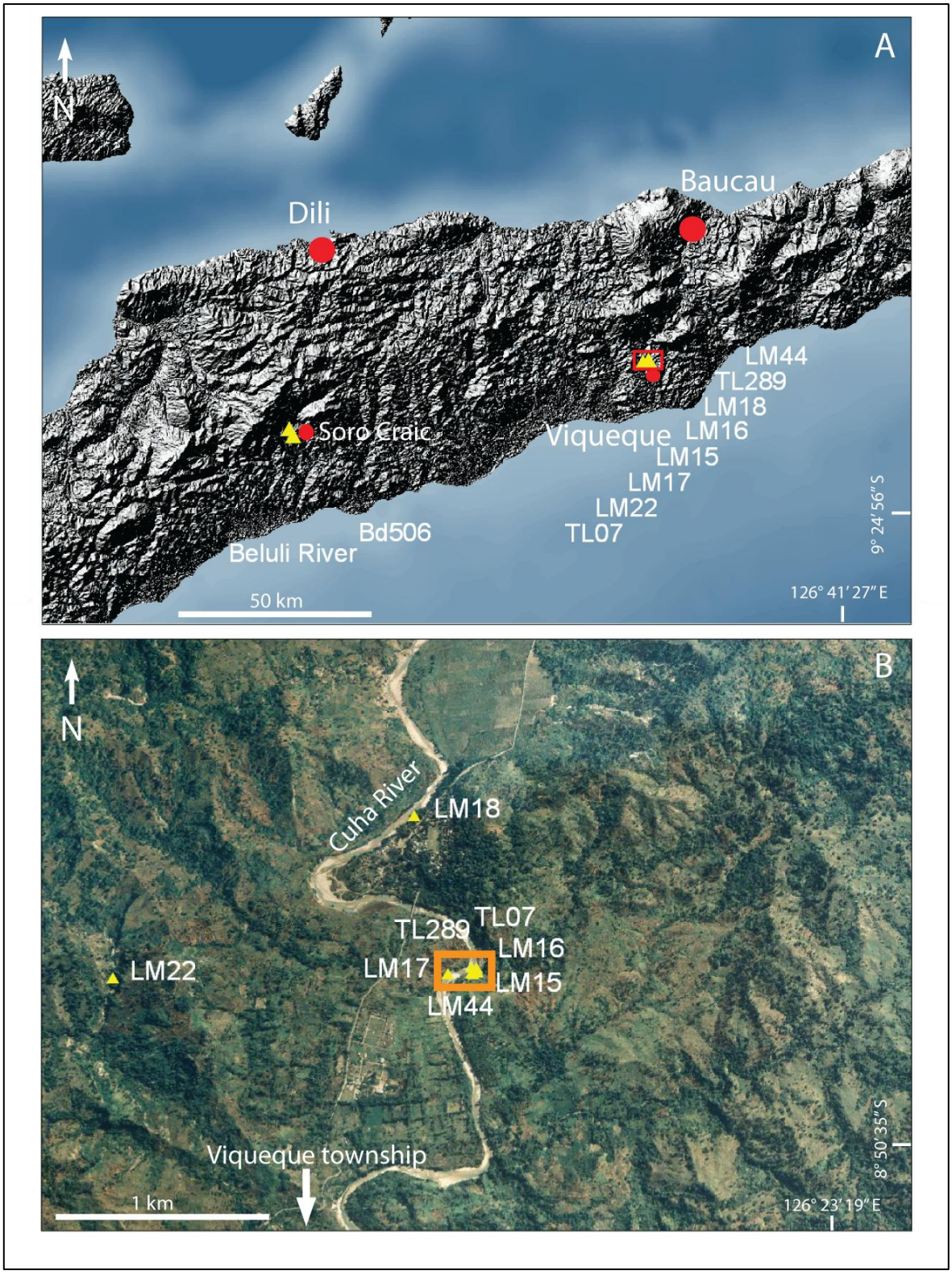

Fig. 4.2 (A) Location of fossil corals in Timor Leste, (B) Higher resolution image of coral gorge, Cuha River. Yellow triangles indicate coral collection sites, red square in map A indicates extent of map B, orange square indicates location of coral gorge, red circles indicate cities and townships.

4.2.1 Viqueque Megasequence

The VM is a sedimentary unit of Upper Miocene to Upper Pliocene age (Audley-Charles, 1968b) located at the central, southern and north-eastern basins of Timor Leste. It consists of basal conglomerates, sandstones, siltstones, mudstones, marls, and chalks, (Audley-Charles, 1968b). Deposition occurred during the emergence of Timor, with foraminiferal assemblages indicating the deposit is 5.6-5.2 Ma at the base, younging upwards to an age of 3.1-1.9 Ma at the top (Haig and McCartain, 2007). An intact detrital coral, found in the uppermost 50 m in Coral Gorge (Fig. 4.3, Fig. 4.4 C), has been dated using U/Pb techniques, providing a terminal Pliocene age of 2.6 Ma (P. pini, TL07; Quigley et al., 2012). This provides further constraints on the age of the deposit. The entire 450 m section is depicted in a stratigraphic log (Fig. 4.4 A), with a larger scale stratigraphic log detailing the lithology of the Coral Gorge section, from where multiple fossil corals were collected. Fig. 4.4 B depicts this fining upwards sequence of very coarse pebble to fine pebble conglomerate, containing sedimentary rip up clasts and entrained fossil corals. These corals exhibit varying degrees of preservation, although some have remained pristine (e.g. TL289). Chapter 3 reveals the extent to which relatively short periods of subaerial exposure can cause extensive diagenetic alteration of a coral, therefore it is likely that the well preserved fossil corals collect from this outcrop were living at the time they were entrained within the deposit, and a lack of subaerial exposure has allowed them to retain their primary aragonite skeletons. These fossils provide perfect specimens to examine for a more detailed understanding of the terminal Pliocene climate in the Indo-Pacific. Debris flows are likely to have been triggered coseismically (Goldfinger et al., 2003) or during storm events, and when travelling across the shelf would have entrained living or recently living corals from within the reef, before being deposited on the sea floor (Fig. 4.5). In addition to coral, large amounts of organic material has also been entrained in these turbidite deposits (Fig. 4.6), which is characteristic of a seismically generated turbidite (Goldfinger, 2009). The impact of a turbidite deposit cascading down on top of non-lithified sediments is likely to have caused agitation, resulting in sedimentary rip up deposits being incorporated into the turbidite, as seen in coral gorge (Fig. 4.4 D).

Fig. 4.3 Coral Gorge in the Cuha River north of the Viqueque township. *P. pini* coral (LM15) circled in red. Photo taken looking upstream (north).

Fig. 4.4 (Next page) Stratigraphic log of the entire 450 m Northern Cuha section (A), with a blow up of an 8 m section from Coral Gorge (B). Description of fining upwards sequence, containing extensive sedimentary rip ups and fossil corals. (C) *Goniopora* (LM17) detrital coral in VM. Conglomerate consists of granule to medium pebble size, sub-rounded to rounded clasts. (D) Sandstone rip up (~ 100 cm x 60 cm) within turbidite deposit, consisting of granule to cobble size, sub-rounded clasts with multiple sandstone and mudstone rip ups and entrained corals present. Northern Cuha stratigraphic log modified from Quigley et al., 2012.

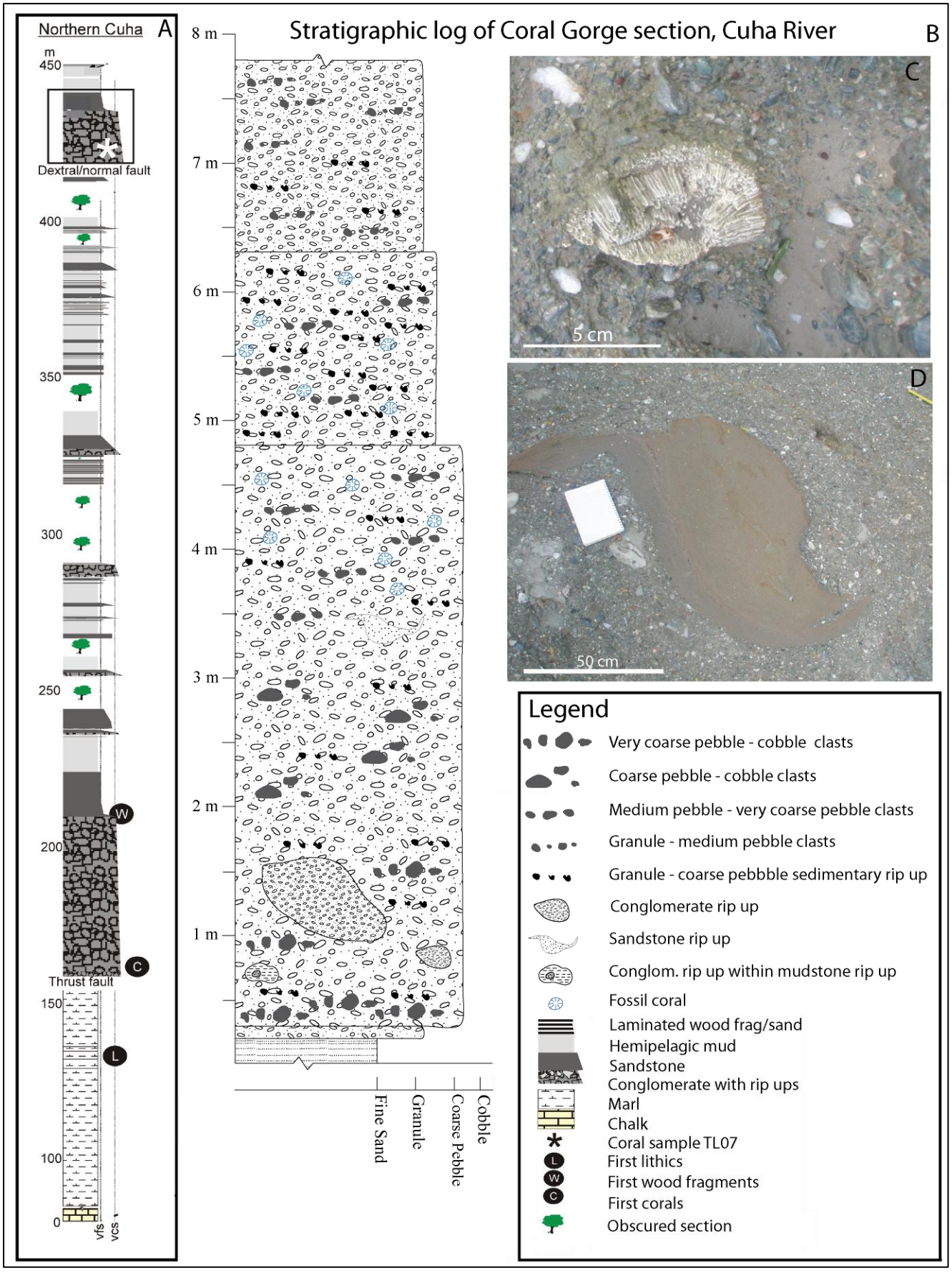
Northern Cuha
A
m
450
400
350
300
250
200
150
100
0
Dextral/normal fault
Thrust fault
W
C
L
vfs
vcs
Stratigraphic log of Coral Gorge section, Cuha River
B
8 m
7 m
6 m
5 m
4 m
3 m
2 m
1 m
Fine Sand
Granule
Coarse Pebble
Cobble
C
5 cm
D
50 cm
Legend
Very coarse pebble - cobble clasts
Coarse pebble - cobble clasts
Medium pebble - very coarse pebble clasts
Granule - medium pebble clasts
Granule - coarse pebbble sedimentary rip up
Conglomerate rip up
Sandstone rip up
Conglom. rip up within mudstone rip up
Fossil coral
Laminated wood frag/sand
Hemipelagic mud
Sandstone
Conglomerate with rip ups
Marl
Chalk
Coral sample TL07
First lithics
First wood fragments
First corals
Obscured section

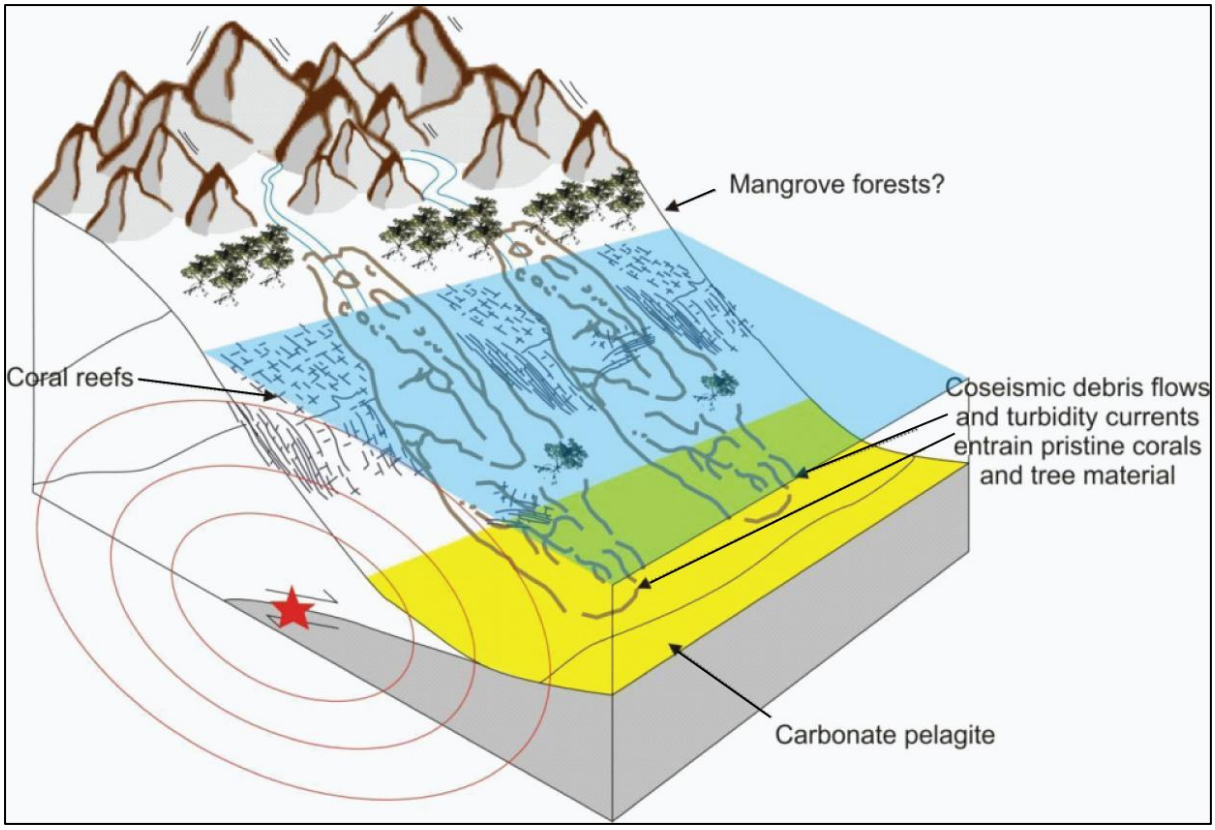

Fig. 4.5 Model of processes which deposited the Viqueque Megasequence and entrained Pliocene corals. Figure courtesy of Brendan Duffy.

Fig. 4.6 Fossilised log showing the large size and excellent preservation of some organic detritus entrained within VM. Photo courtesy of Dr. Mark Quigley.

4.3 Methodology

Multiple fossil corals were retrieved with hammer and chisel from VM outcrops in the Cuha River to the north of the township of Viqueque, and further east in the Soro Craic region (Fig. 4.2). Most corals were identified as *Porites sp.*, however there were also a variety of other intertidal reef corals (Fig. 4.7, Fig. 4.8 and Fig. 4.9). *P. lamellina* (TL289) was among these corals.

4.3.1 Screening for diagenesis

Due to the fossilised nature of these corals, it is likely they have experienced some of the effects of diagenesis. In order to eliminate unsuitable corals from further analysis, the three step screening programme was applied to all fossil corals.

4.3.1.1 XRD

All fossil corals were subject to a first-pass screening process of single samples tested using XRD to determine whether they contained any calcite (Table 4.1). Corals were cleaned with ultra-pure compressed air prior to sampling in order to remove any loose particles, and coral chunks collected with tweezers or hand dremel. Tweezers were cleaned with ethanol and dremel bit cleaned on a piece of granite between each sample to avoid cross contamination between samples. Samples were then crushed into powder using an agate mortar and pestle which was cleaned with ethanol between samples. Samples were scanned from 2θ of 3^0 to 50^0 using a Philips XRD at the University of Canterbury. Refer to Appendix Figure 9 through Appendix Figure 18 for diffractograms of these corals. Although many of the corals indicated 100% aragonite composition, many were too friable to successfully work with. Therefore, from this initial screening and taking into account skeletal robustness and apparent preservation, corals LM15, LM16b, TL07 and TL289 were selected for further analysis. The location of XRD subsamples taken from each coral is shown in Fig. 4.10, Fig. 4.11, Fig. 4.12 and Fig. 4.13. A second XRD screening of the four selected corals was completed, with subsamples along growth axes of each of the corals providing more detailed information about preservation (Table 4.2).

Table 4.1 Fossil coral identification, location, elevation, host lithological and preliminary XRD information.

Coral sample	**LM15**	**LM16b**	**LM17**	**LM18**	**LM18a**	**LM18b**	**LM18c**	**LM22a**
Species	*Platygyra pini*	*Porites sp.*	*Goniopora sp.*	*Porites sp.*	*Porites sp.*	*Porites sp.*	*Porites sp.*	*Acropora sp.*
Location	126.3 E 8.8 S	126.3 E 8.8 S	126.3 E 8.8 S	126.2 E 8.4 S	126.2 E 8.4 S	126.2 E 8.4 S	126.2 E 8.4 S	126.2 E 8.5 S
Elevation (m)	66	66	66	79	79	79	79	118
Host lithology	VM	VM	VM	VM	VM	VM	VM	VM
XRD (% aragonite: % calcite)	100:0	60:40	95:05	100:0	100:0	100:0	100:0	90:10

Coral sample	**LM22b**	**LM44**	**Beluli River A**	**Beluli River B**	**Beluli River C**	**TL07**	**TL289**
Species	*Porites sp.*	*Porites sp.*	*Porites sp.*	*Porites sp.*	*Porites sp.*	*Platygyra pini*	*Platygyra lamellina*
Location	126.2 E 8.5 S	126.3 E 8.8 S	125.3 E 9.0 S	125.3 E 9.0 S	125.3 E 9.0 S	126.3 E 8.8 S	126.3 E 8.8 S
Elevation (m)	118	66	232	232	232	66	66
Host lithology	VM	VM	VM	VM	VM	VM	VM
XRD (% aragonite: % calcite)	95:5	100:0	100:0	100:0	100:0	100:0	100:0

Table 4.2 XRD results for subsampled corals LM15, LM16b, TL07 and TL289

Coral sample	Aragonite (%)	Calcite (%)
LM15A	100	Trace
LM15B	100	0
LM15C	100	0
LM15D	100	0
LM15E	100	0
LM16A	100	0
LM16B	100	0
LM16C	100	0
LM16D	100	0
LM16D	100	0
LM16E	100	Trace
TL07 Part 1	100	0
TL07 Part 2	100	0
TL289A	100	0
TL289B	100	0
TL289C	100	0
TL289D	100	0

Fig. 4.7 Fossil coral images of corals Beluli River A and B, from the Soro Craic region, and corals LM15, LM16a, LM17 and LM16a from coral gorge, Cuha River. Both locations are outcrops of the Viqueque Megasequence.

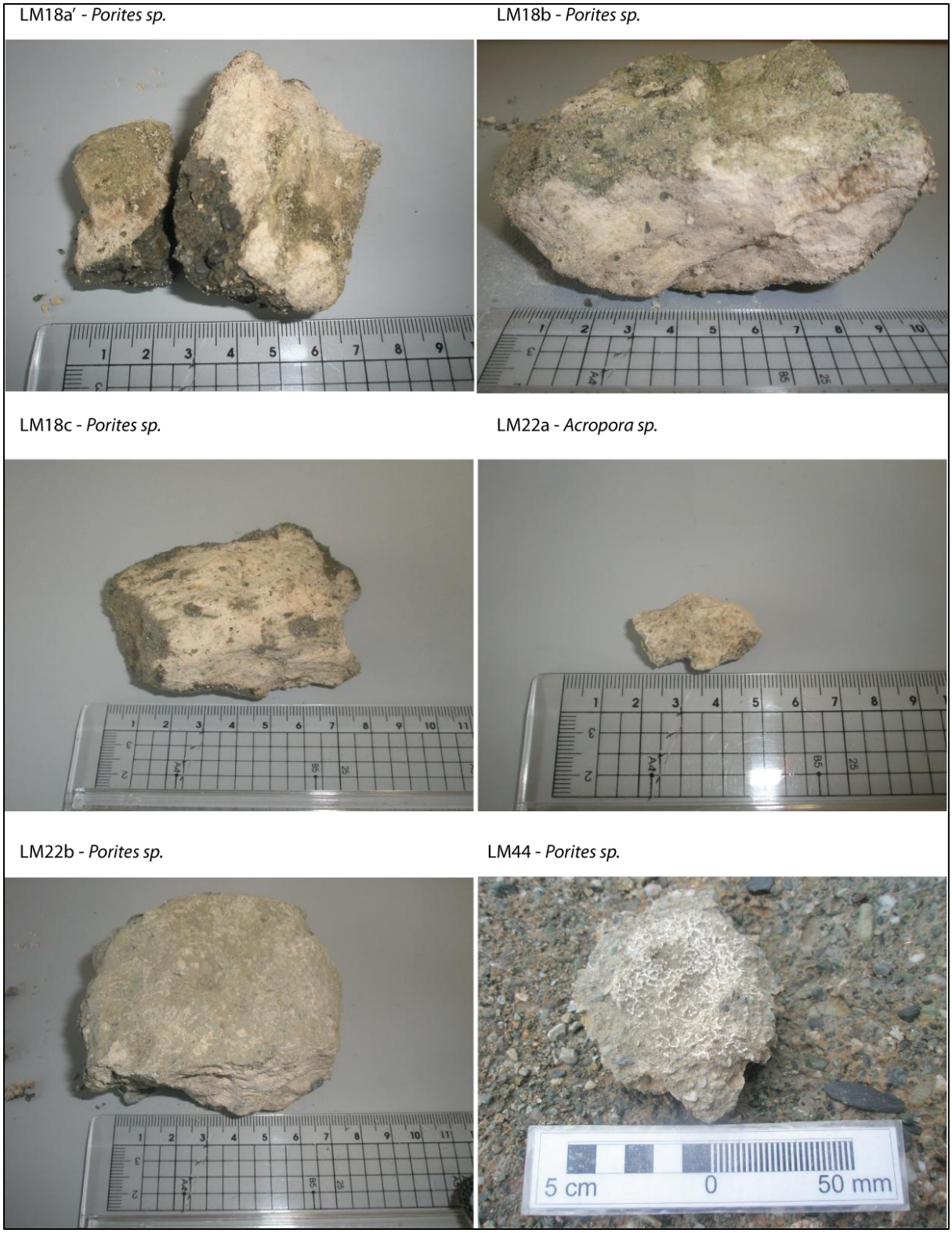

Fig. 4.8 Fossil coral images of corals LM18a', LM18b, LM18c, LM22a, LM22b and LM44 from coral gorge in the Cuha River.

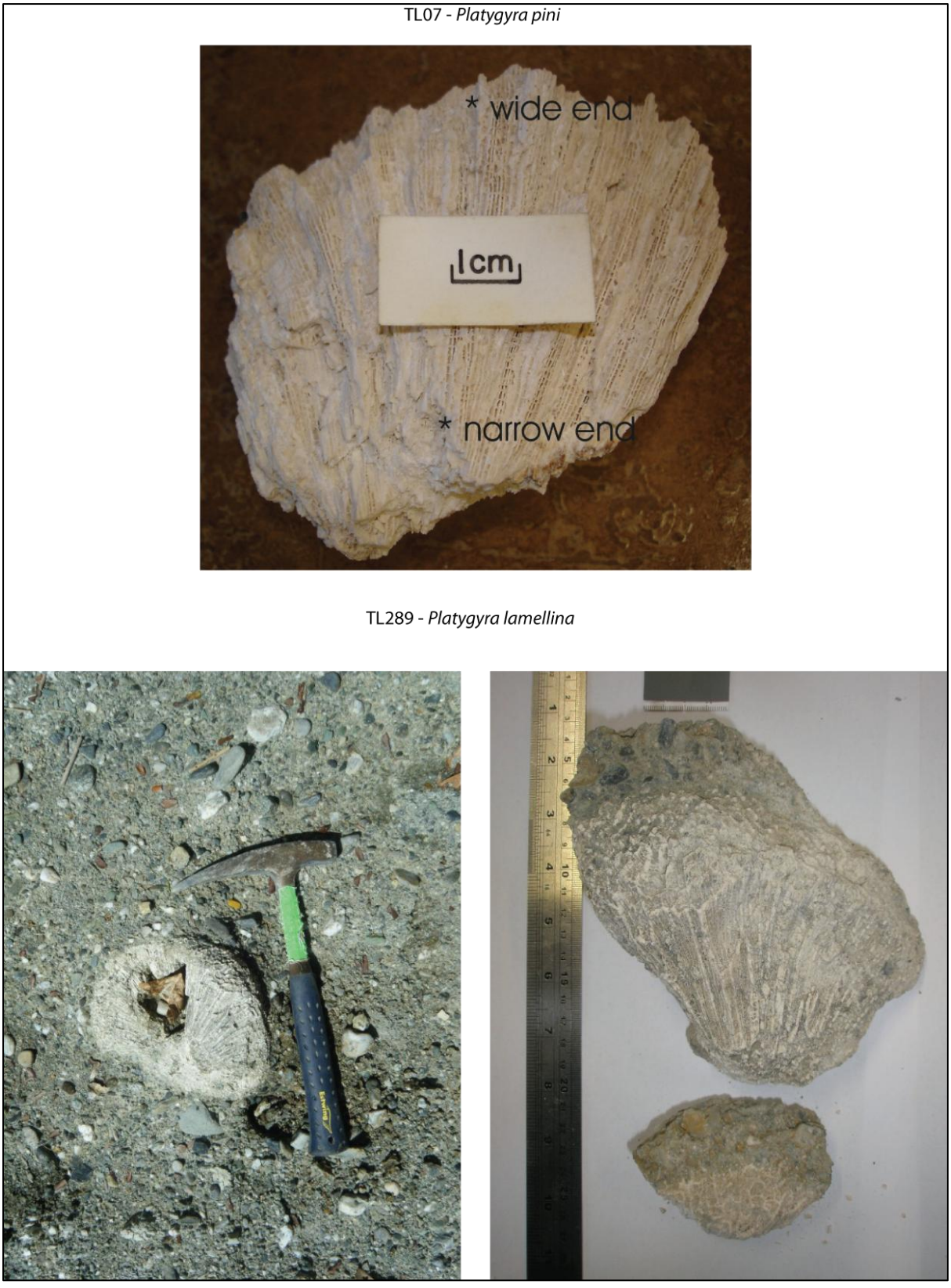

Fig. 4.9 Fossil coral images of corals TL07 and TL289 from coral gorge in the Cuha River.

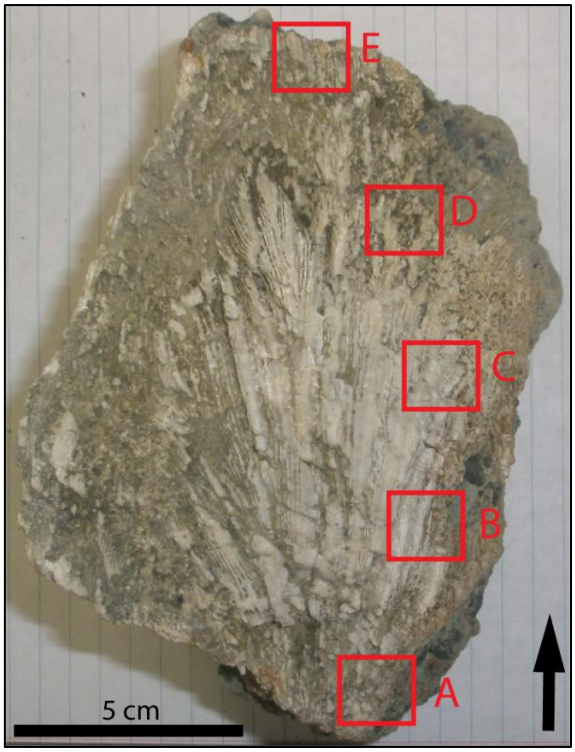

Fig. 4.10 Location of XRD subsamples on coral LM15. Arrow indicates younging direction.

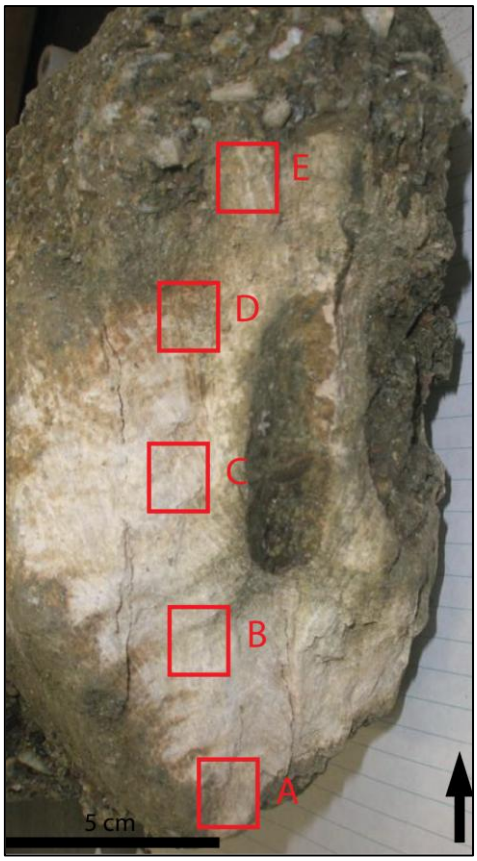

Fig. 4.11 Location of XRD subsamples on coral LM16b. Arrow indicates younging direction.

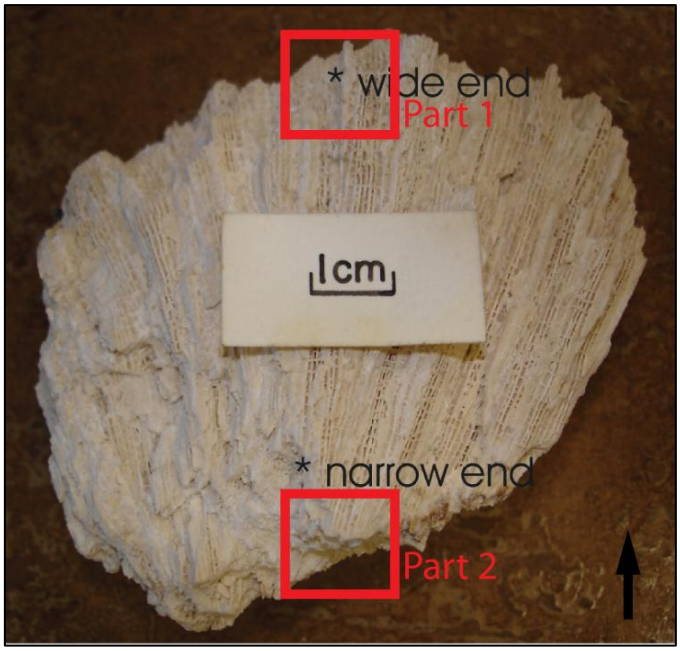

Fig. 4.12 Location of XRD subsamples for coral TL07. Arrow indicates younging direction.

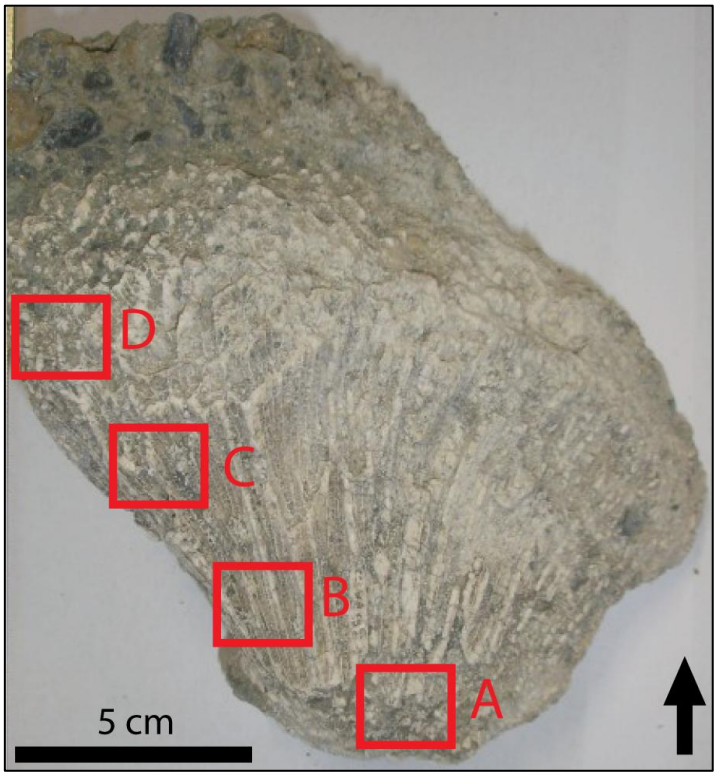

Fig. 4.13 Location of XRD subsamples for coral TL289. Arrow indicates younging direction.

4.3.2 Embedding

Due to their extremely friable nature, the fossil corals LM15, LM16b, TL07 and TL289 were embedded in epoxy resin before conducting further lab work (Fig. 4.14, Fig. 4.15, Fig. 4.16, Fig. 4.17). K-142 resin was used, as it has been tested and does not react with the phosphoric acid used in the Kiel mass spectrometer at NIWA, Wellington (Dr. H. Neil, pers. comm.). Prior to embedding, coral samples were broken in half along the axes of maximum growth, so that there is a portion of untreated coral to work with in future studies if required. Resin was poured over the corals and allowed to set in a vacuum, meaning the resin would infiltrate the pore space as much as possible to give maximum strength to the skeleton. Once set, the corals were dried in an oven at 50°C overnight before two 7 mm slabs were cut from each portion of embedded coral with a diamond wafer blade. These slabs were then cleaned with an ultrasonic probe to remove loose particles and surface contaminants before being used for further analysis. Cutting into the LM15 sample revealed conglomerate inclusions within the coral skeleton, which are likely due to the infilling of borings made by lithophagan bivalves, which occurs frequently in both modern and fossil reef corals (Professor T. Brachert, Pers. Comm.). These bore holes in the coral skeleton have probably been infilled with conglomerate during entrainment within the turbidite deposit.

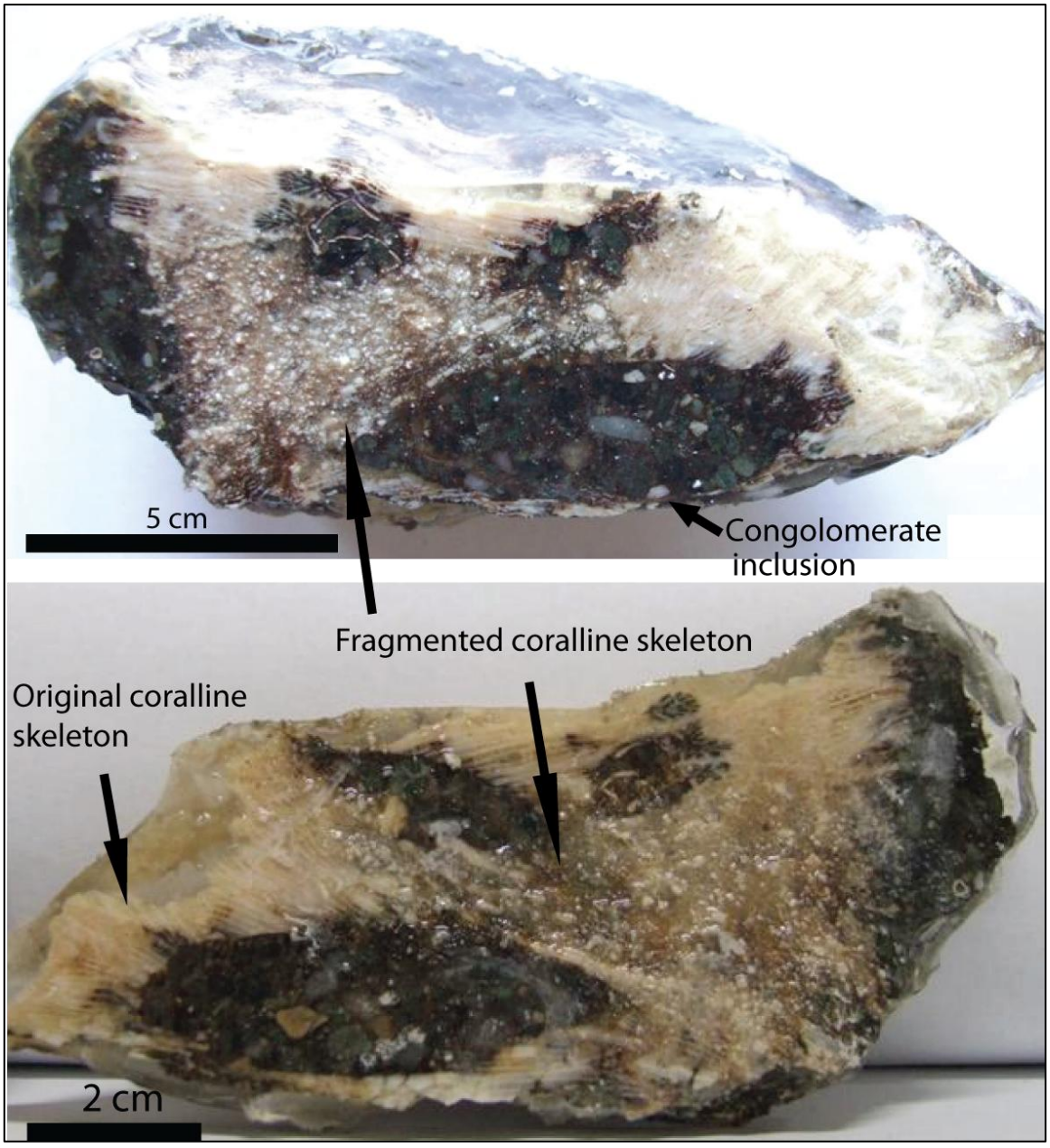

Fig. 4.14 LM15 *P. pini* coral embedded in epoxy resin and slabbed, showing internal conglomerate clasts and collapsed coralline structure.

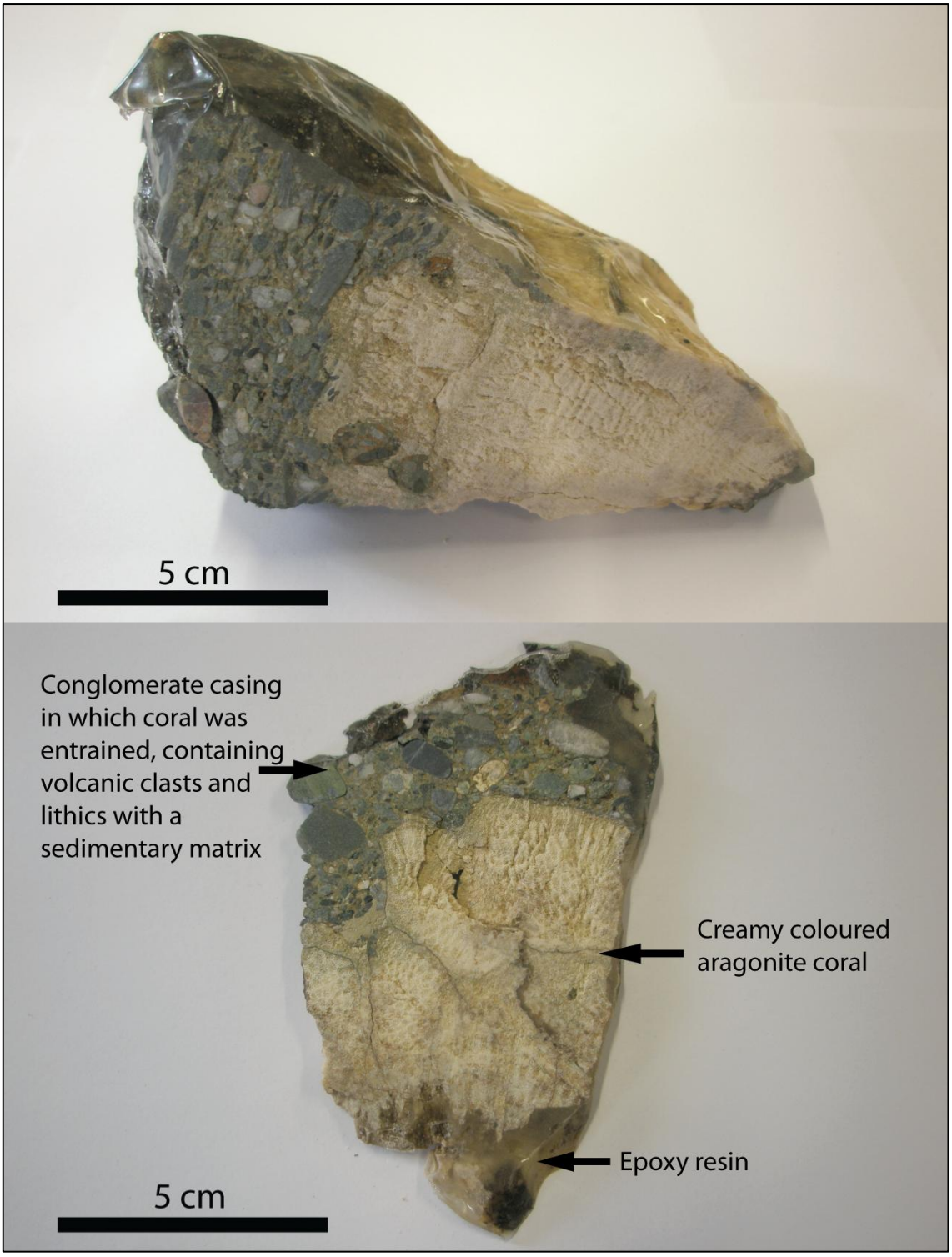

Fig. 4.15 LM16b *Porites* coral embedded in epoxy resin. (Top) main portion of embedded coral, (bottom) 7 mm coral slab.

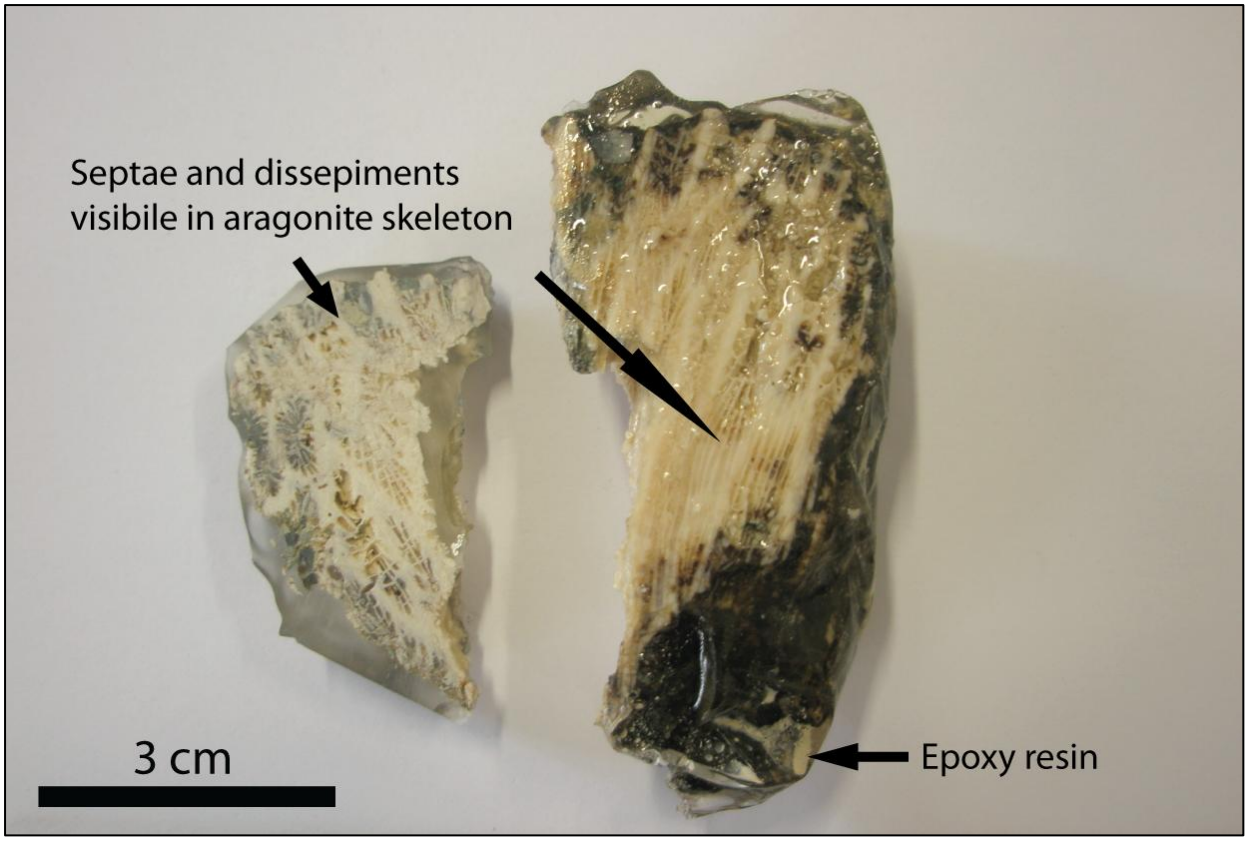

Fig. 4.16 TL07*P. pini* coral embedded in epoxy resin. (Left) 7 mm coral slab, (right) larger portion of embedded coral.

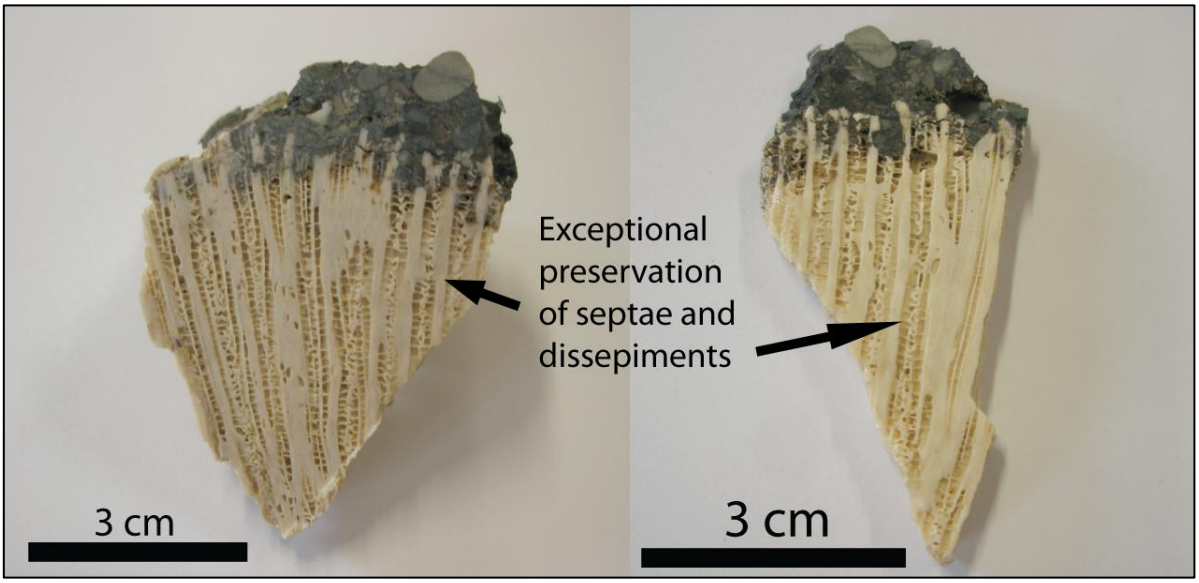

Fig. 4.17 TL289 *P. lamellina* coral embedded in epoxy resin. (Left) larger portion of coral, (right) 7 mm coral slab post-micromilling.

4.3.3 Petrographic analyses

From each of the corals, one of the two 7 mm slabs was prepared into a standard 0.03 mm thick, 60 x 20 mm petrographic thin section for analysis under a Leica optical microscope. In LM15, LM16b and TL07, this revealed extensive dissolution and some micritic overgrowths (Fig. 4.18 and Fig. 4.19). LM16b displayed an extensively pitted texture showing almost total dissolution across the entire coral skeleton. This is reflected by the chalky texture of the specimen. LM15 and TL07 have extremely darkened COCs indicative of high levels of dissolution in these particular zones. Although some primary features such as non-altered COCs and daily growth lines were visible in LM15 and TL07, the overall amount of diagenesis was too high and the corals too poorly preserved for any further analysis to be worthwhile. Analysis of TL289 revealed primary aragonitic textures as described by McGregor and Abram (2008) and provided compelling evidence of pristine aragonite, with radiating sclerodermites, centres of calcification and dissepiments visible, and minimal algal borings, leaching or micritic overgrowths observed (Fig. 4.20), and was thus chosen for further analysis.

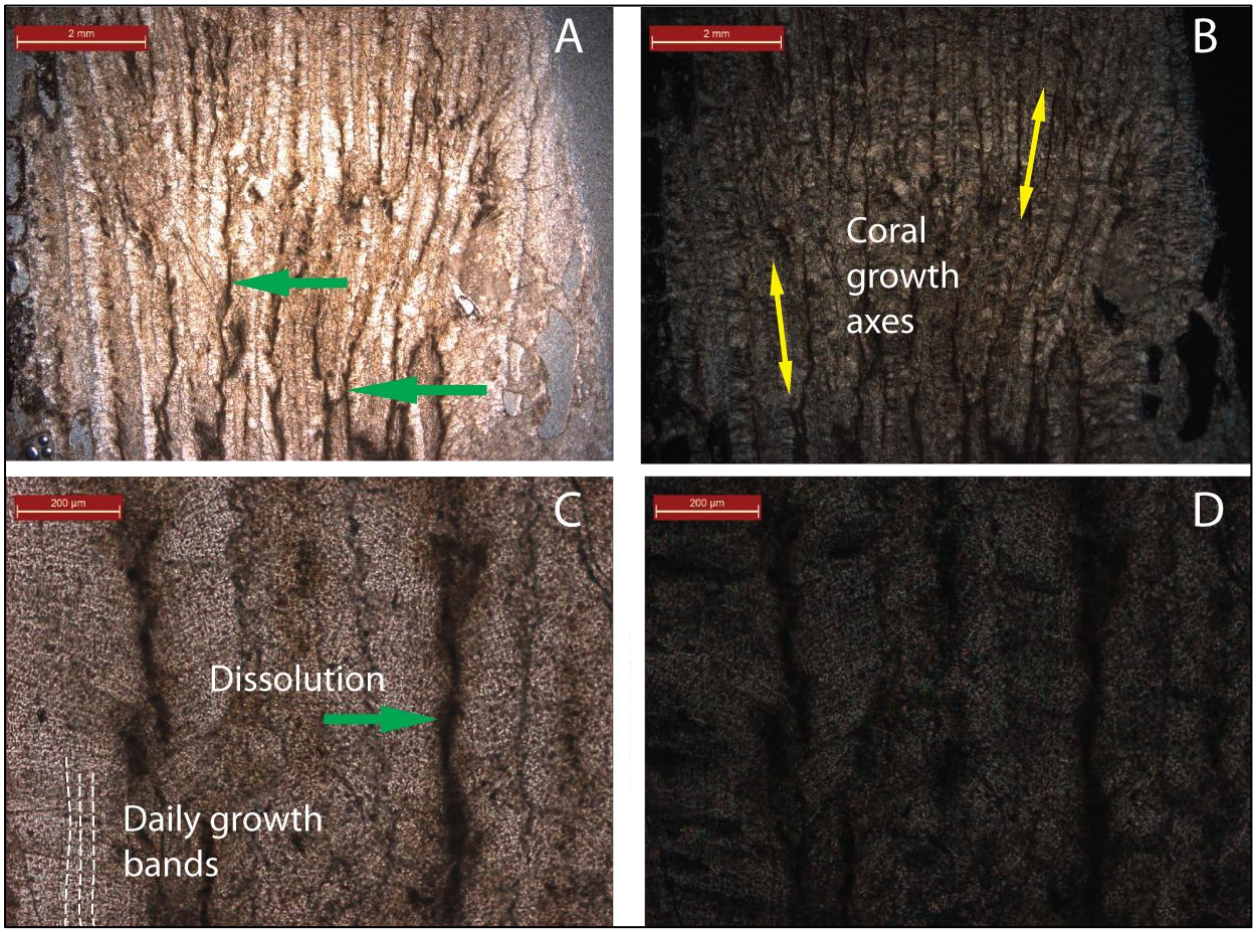

Fig. 4.18 (Previous page) Petrographic images of fossil coral LM15. Green arrows show dissolution along COCs, yellow double-ended arrows indicate growth axes of corals, and white dashed lines indicate daily growth bands. Images A and C are PPL, images B and D are CPL.

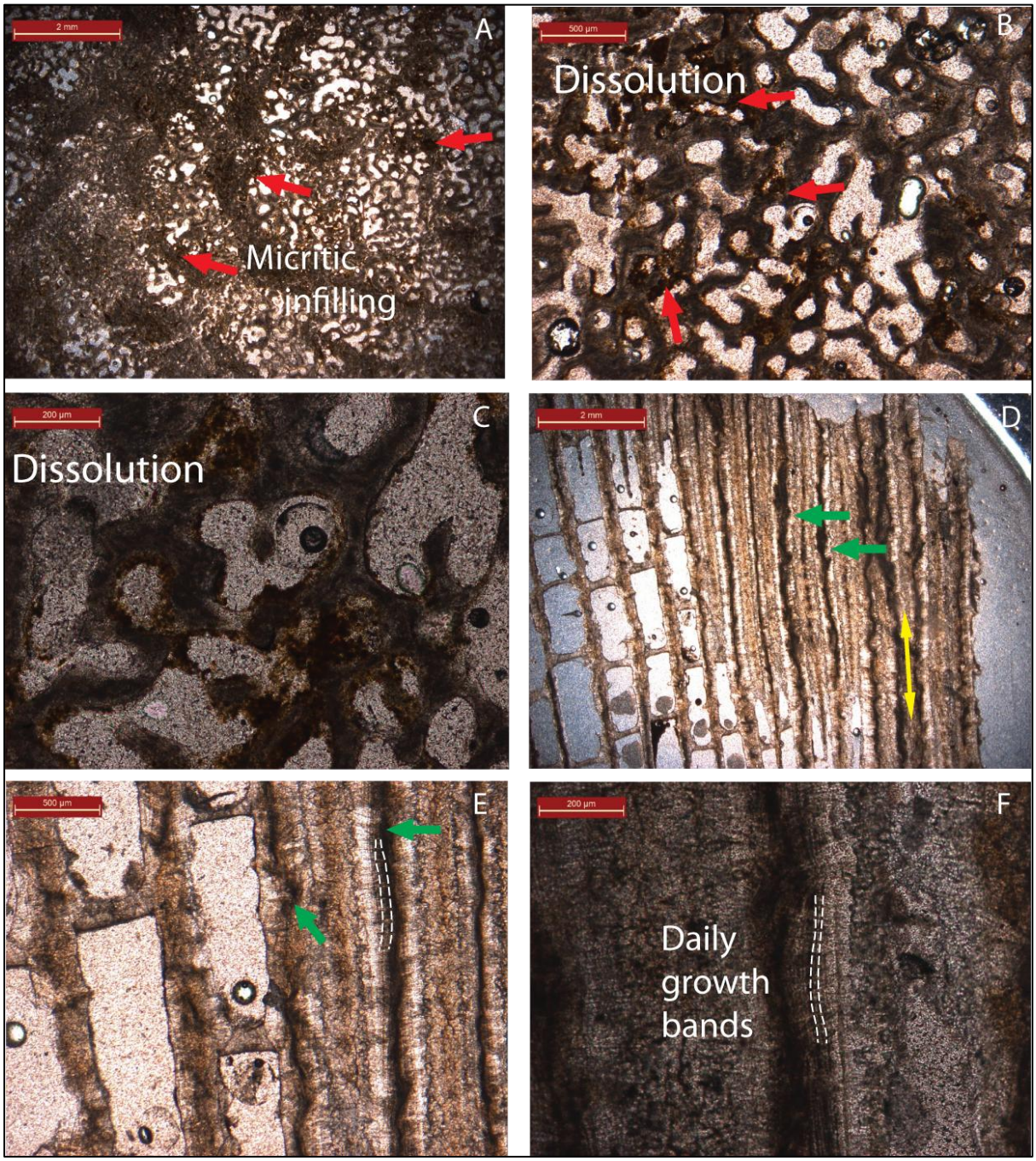

Fig. 4.19 Petrographic images of fossil corals LM16b and TL07. Green arrows show dissolution along COCs, red arrows indicate micritic infilling, yellow double-ended arrows indicate growth axes of corals, and white dashed lines indicate daily growth bands. Images A, B and C are LM16b (all PPL

images) with pitted texture exhibiting extensive dissolution. Images D-F are TL07 (all PPL), with extensive dissolution along COCs, however daily growth lines (a primary texture) still visible.

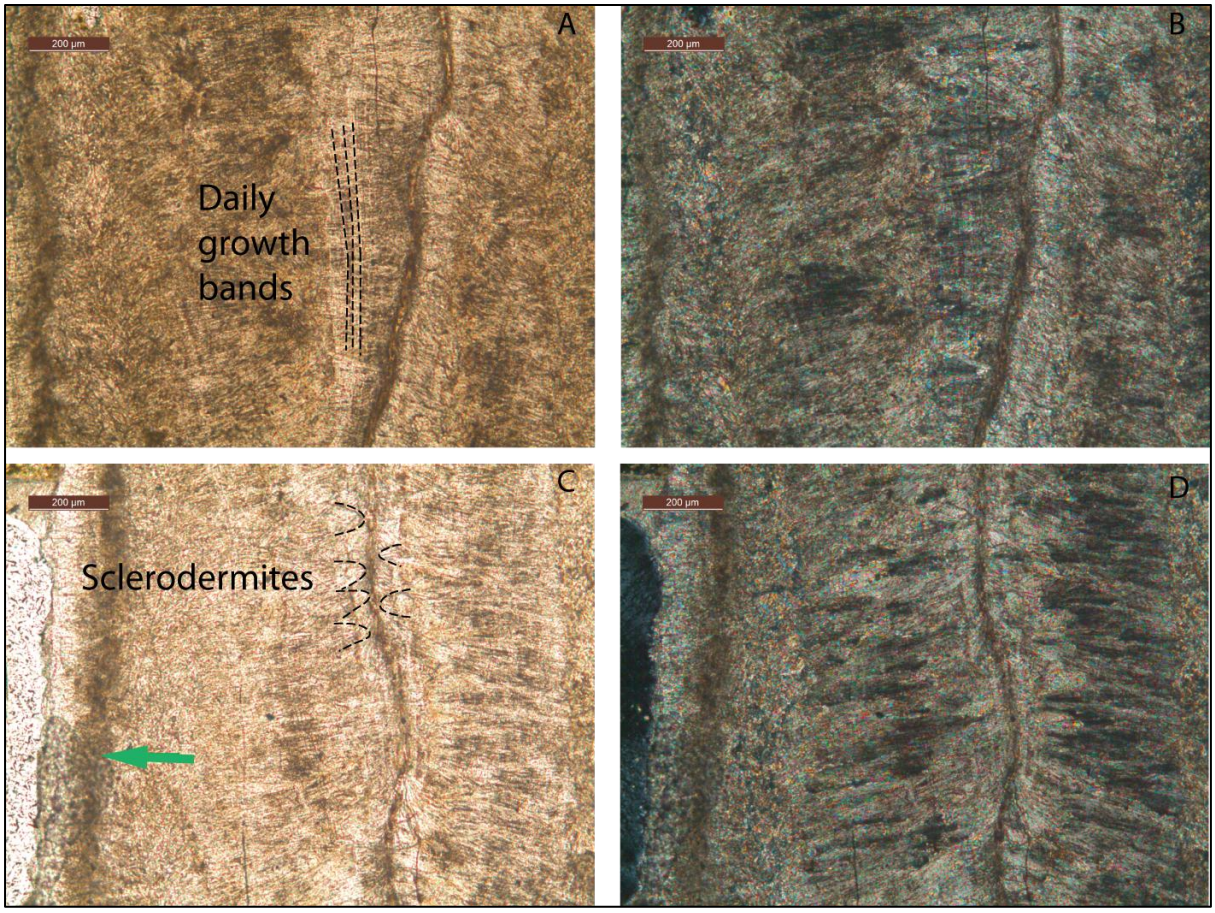

Fig. 4.20 Petrographic images of fossil coral TL289. Green arrows show dissolution along COCs, red arrows indicate micritic infilling, straight black dashed lines indicate daily growth bands, curved black dashed lines indicate sclerodermites. Images A and C taken in PPL, images B and D taken in CPL.

Fig. 4.21 Petrographic images of fossil coral TL289. Green arrows show dissolution along COCs, red arrows indicate micritic infilling, and straight black dashed lines indicate daily growth bands. Images A and C taken in PPL, images B and D taken in CPL.

4.3.4 SEM

SEM analyses for the fossil corals were limited, as their friability prevented chunks of coral being easily mounted onto stubs. Only LM15 and TL289 were robust enough to mount prior to being embedded, and the textures visible on the broken surfaces corroborated with the dissolution seen in thin section. LM15 exhibited growth of fibrous, needle-like secondary aragonite crystals on COCs, as described by Allison et al., (2007) and Hendy et al., (2007) (Fig. 4.22), as well as micro-boring holes and a rough, uneven overgrowth texture replacing what would have originally been smooth, pristine coral aragonite. In stark contrast, TL289 shows exceptional preservation, with pristine coral faces visible. Smooth septae, dissepiments and pore spaces show no signs of diagenesis, and represent primary aragonite growth textures.

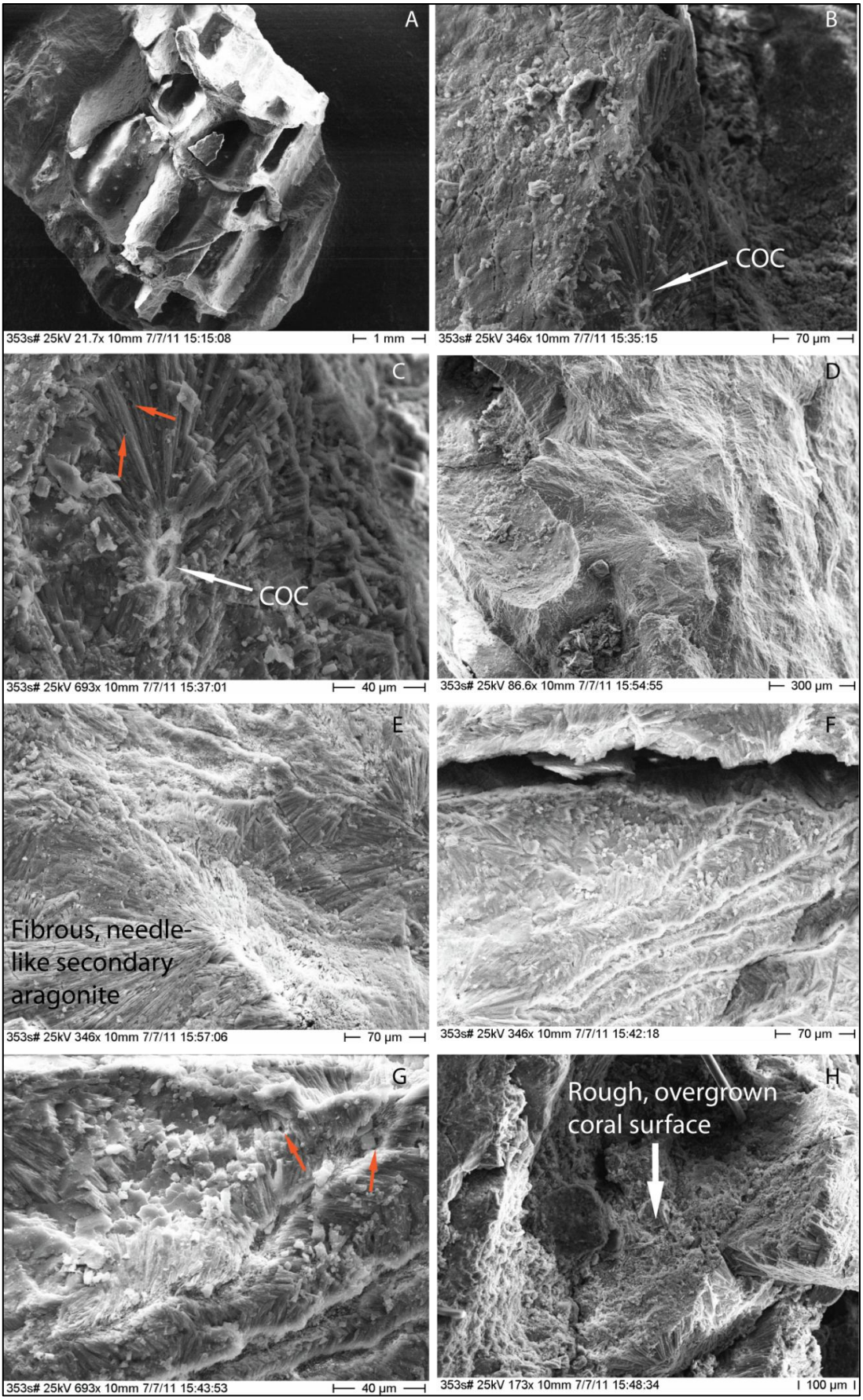
A
353s# 25kV 21.7x 10mm 7/7/11 15:15:08
1 mm
B
COC
353s# 25kV 346x 10mm 7/7/11 15:35:15
70 µm
C
COC
353s# 25kV 693x 10mm 7/7/11 15:37:01
40 µm
D
353s# 25kV 86.6x 10mm 7/7/11 15:54:55
300 µm
E
Fibrous, needle-like secondary aragonite
353s# 25kV 346x 10mm 7/7/11 15:57:06
70 µm
F
353s# 25kV 346x 10mm 7/7/11 15:42:18
70 µm
G
353s# 25kV 693x 10mm 7/7/11 15:43:53
40 µm
H
Rough, overgrown coral surface
353s# 25kV 173x 10mm 7/7/11 15:48:34
100 µm

Fig. 4.22 (Previous page) SEM images of LM15 coral. Orange arrows indicate micro-boring. Extensive growth of fibrous, needle-like secondary aragonite needles. Pitted and overgrown skeletal surface representing extensive dissolution and diagenesis.

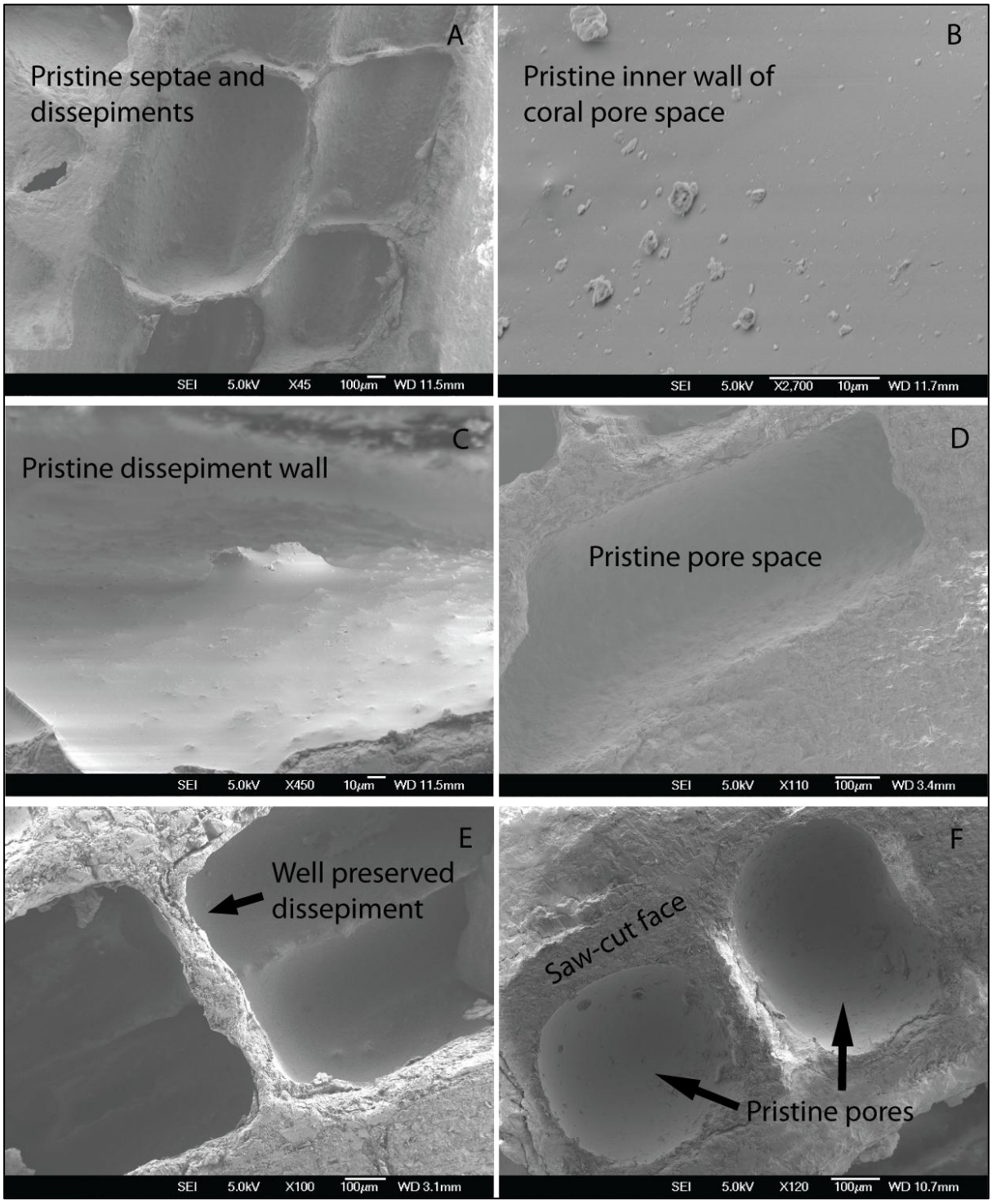

Fig. 4.23 SEM images of TL289 coral. Pristine coral with well preserved septae, dissepiments and pores are visible. Little to no overgrowths or alteration is present. Images A, B and C are from the

central third of the coral. Images D, E and F are from the upper third of the coral. Images A, B and C come from years two and three of the coral sample, and images D, E and F come from years four and five of the coral sample (refer to Fig. 4.24).

4.3.5 X-RAY AND MICROMILLING

After passing the diagenetic screening tests, TL289 was selected for micromilling. A 7mm slab was prepared for milling, involving a second round of cleaning with an ultrasonic probe before taking X-ray images to determine the exact location of the annual density band couplets (Fig. 4.24). The X-ray images clearly showed 7 annual density band couplets, meaning the coral was approximately 7 years old. A thick, pristine septa was selected for milling, and a hand dremel used to cut away the coral skeleton to the very edge of a solid septal wall. A milling path was set up along the septa using the New Wave Micromill facility at NIWA, Wellington. Petrographic analysis revealed the upper ~ 5 years of the coral to have primary textures such as radiating sclerodermites, centres of calcification, daily growth bands and dissepiments visible, as well as minimal algal borings and leaching observed, but some dissolution visible in the lowermost two years of growth. Therefore, only the uppermost 5 years of the coral have been milled. The uppermost density band couplet was milled at approximately monthly resolution of 12 samples (0.3 mm spacing), with the following three couplets sampled at a higher resolution of approximately fortnightly resolution of 26 samples (0.2 mm spacing), and the lowermost couplet milled at monthly resolution (0.3 mm spacing). Annual density bands visible in X-ray allow the estimation of a growth rate of ~ 5 mm/yr, which is less than the rate of 8.6-16.9 mm/yr identified by Shimamura et al. (2008), but closer to the rate of 7-9 mm/yr identified in a modern *P. lamellina* by Quinn et al. (1993).

Fig. 4.24 (Next page) Coral TL289 X-ray images showing 7 years of growth (white dashed lines indicate growth lines) and micromilling path (outlined by red dashed line). Black lines in the micromilling path indicated the yearly growth bands. Black arrow indicates younging direction of coral.

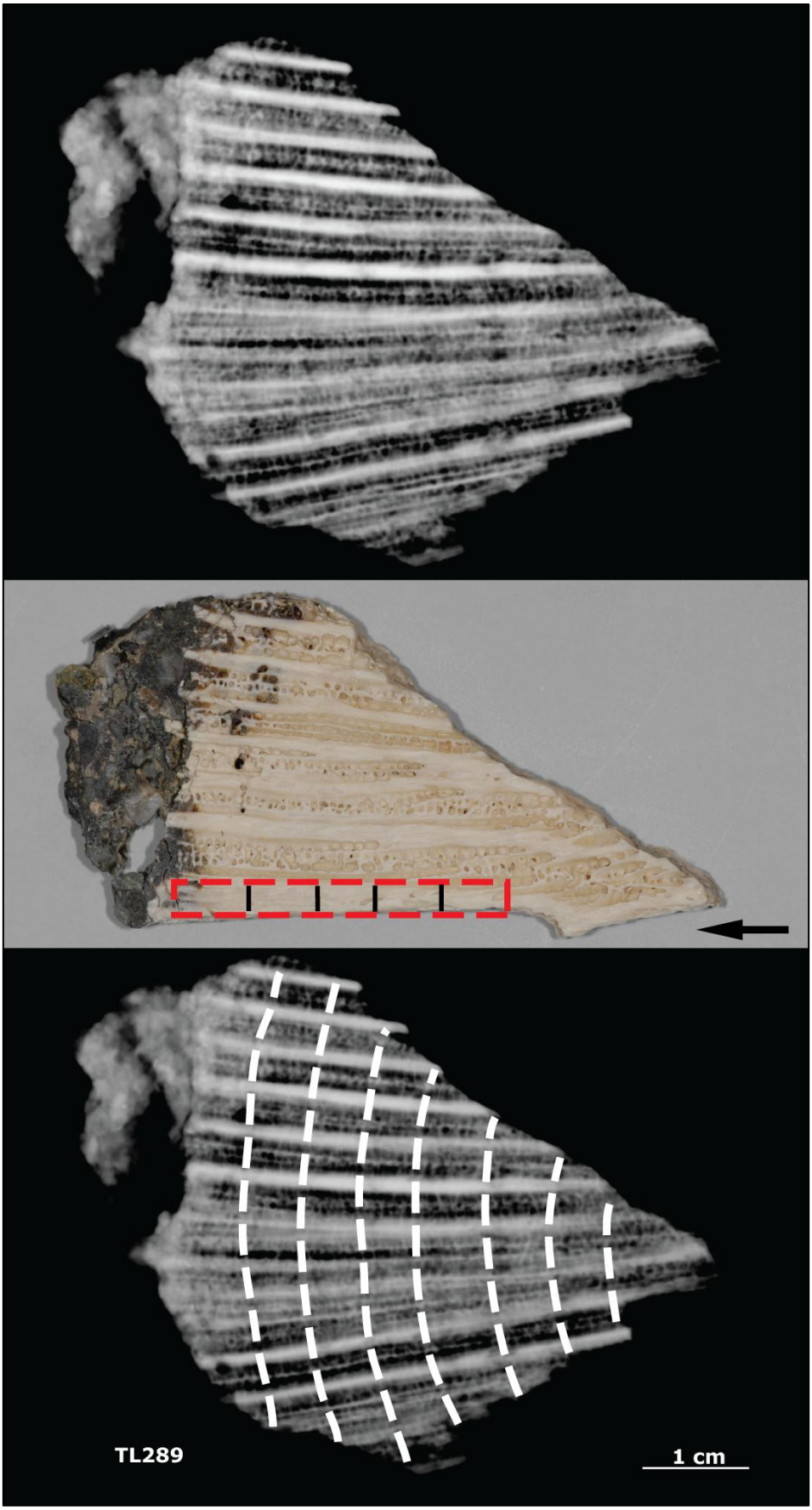
TL289
1 cm

4.3.6 U/Pb DATING

U/Pb geochronology methods followed those outlined in Woodhead et al. (2006), and U/Th geochronology methods followed those outlined in Hellstrom et al. (2003). Fossil coral samples were prepared by extracting sections of coral with sterile tweezers and storing each in a microcentrifuge tube. Samples for U/Pb (U/Th) analysis weighed 100-200 (50-100) micrograms. Between five and seven samples were collected from each coral, depending on the size of the coral, and were collected from the base to the top at evenly spaced intervals. For U/Pb analysis, samples were dissolved and spiked with a mixed $^{233}U/^{205}Pb$ tracer, then U and Pb separated using conventional ion exchange techniques and isotopic ratios were plotted in a $^{238}U/^{206}Pb$-$^{207}Pb/^{206}Pb$ inverse concordia ("Terra Wasserburg") plot (Fig. 4.25) and corrected for initial disequilibrium in the ^{238}U and ^{235}U decay chains (Table 4.3). An age of 2.67 ± 0.34 Ma has been obtained. This age is considered reliable as the data points form a high quality isochron, indicative of closed system behaviour (J. Woodhead, Pers. Comm.) U/Th has also been conducted (Table 4.4), confirming that there has been no departure from secular equilibrium within the coral and that the U/Pb age is reliable. Although TL289 is the only coral to have been selected for stable isotopic analysis, all samples were prepared for dating to ensure that as many coral ages as possible were obtained. Refer to Appendix Table 4 for detailed information of samples collected for dating.

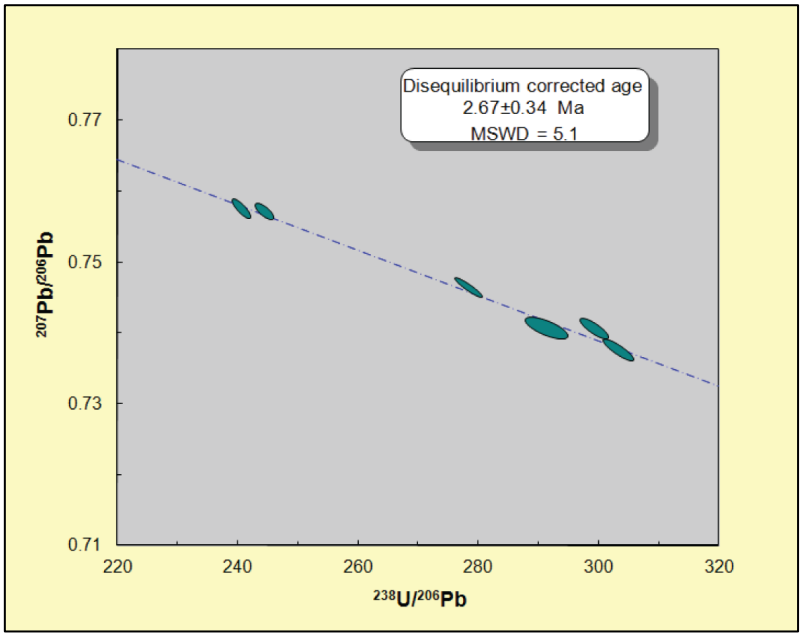

Fig. 4.25 U/Pb isochron for TL289 showing an age of 2.67 ± 0.34 Ma. Data point error ellipses are 2σ.

Table 4.3 TL289 raw U/Pb data

$^{238}U/^{206}Pb$	Error (2σ%)	$^{207}Pb/^{206}Pb$	Error (2σ%)	Error correlation
303.01	0.68	0.7376	0.175	-0.87
291.22	0.99	0.7406	0.175	-0.72
298.99	0.64	0.7405	0.162	-0.83
240.45	0.55	0.7575	0.150	-0.83
244.28	0.51	0.7570	0.127	-0.74
278.09	0.67	0.7464	0.150	-0.93

Table 4.4 TL289 raw U/Th data

Sample	$^{234}U/^{238}U$	Error (2σ%)	$^{230}Th/^{238}U$	Error (2σ%)	$^{230}Th/^{232}Th$	$^{232}Th/^{238}U$	Error (2σ%)	Age (ka)	Error (2σ%)
TL289_2	1.0095	0.002	1.0054	0.0027	198.0	0.005077	0.000026	**532.413**	57.448

4.3.7 Pliocene SST reconstruction for Timor Leste

Shimamura et al. (2008) have provided a new *Platygyra* calibration from specimens located in the mid-latitude, cooler waters of Ishigaki Island, Japan. Skeletal $\delta^{18}O$ ratio ($\delta^{18}O_c$) provided evidence that this genera is a robust palaeo-SST proxy as it shows clear seasonality corresponding to SST variation, with temperature dependence estimated at -0.219‰/^{0}C

Their temperature dependence equation is;

$$T = -4.57(\delta^{18}O_c) + 2.65$$

This agrees well with previously reported values of -0.27 (Weber and Woodhead, 1972) and -0.22 (Quinn et al., 1996; 1993). This equation has been applied to fossil *P. lamellina* mean, minimum and maximum $\delta^{18}O$ values

Mean $\delta^{18}O$:

$$T = -4.57(-5.08) + 2.65$$

$$= 25.8656$$

$$= 25.9° C$$

Minimum $\delta^{18}O$:

$$T = -4.57(-5.48) + 2.65$$

$$= 23.9919$$

$$= 24.0° C$$

Maximum $\delta^{18}O$:

$$T = -4.57(-4.67) + 2.65$$

$$= 27.6936$$

$$= 27.7° C$$

These values provide the first insights into late Pliocene SSTs in the Timor region. Using this equation, the results give an SST range of 24-27.7° C and mean of 25.9° C. Late Pliocene SST has been reconstructed using *Globigerinoides ruber* Mg/Ca records from Ocean Drilling Program (ODP) Site 1143 in the southern South China Sea (Tian et al., 2006). This reconstruction shows that SST varied within a range of 31° C and 26.4° C between 3.3-2.5 Ma, with more than half the record cooler than 28.4° C. This is in agreement with the ODP site 806 in the open western Pacific where Mg/Ca records from *G. sacculifer* indicate 2° C cooler SSTs than present in the western equatorial Pacific ocean from 5.3-1.7 Ma (Wara et al., 2005). Although these two ODP sites are further north and east than Timor (Fig. 4.26), they provide SST constraints for the Indo-Pacific, and the reconstructions fit reasonably well with the *P. lamellina* SST proxy for Timor Leste indicating SSTs were ~ 3° C cooler than at present. Accuracy could be improved using a temperature dependence equation from modern *Platygyra* coral located in the southern Indo-Pacific, but until a modern calibration from this region is complete, this provides preliminary analysis is the best that can be achieved.

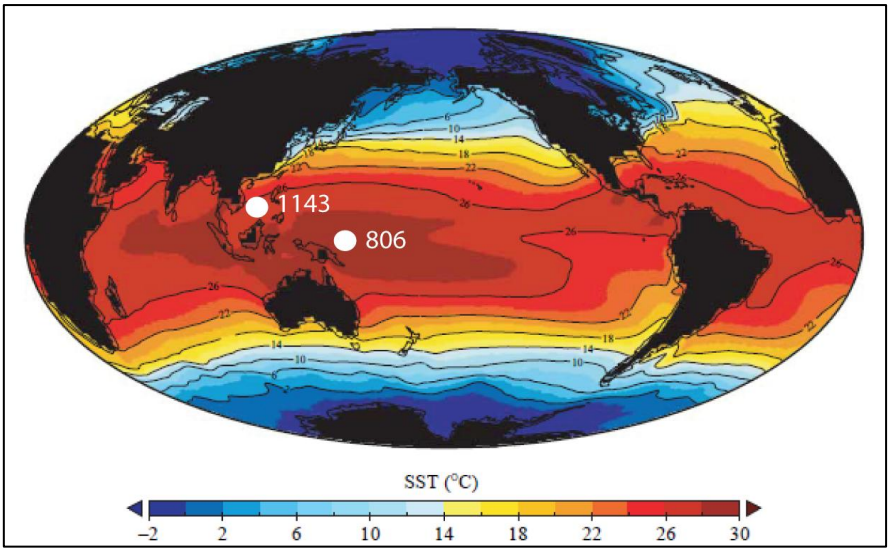

Fig. 4.26 Modern mean annual SSTs, with IPWP extent shown by pool of greater than 28° C. ODP sites 1143 in the southern South China Sea and 806 in the western equatorial Pacific marked by white circles.

4.4 Results

4.4.1 Stable isotopes

Analyses of stable isotopes $\delta^{18}O$ and $\delta^{13}C$ have revealed mean values of -5.08‰ and -0.34‰, with ranges of -4.67‰ to -5.48‰ and 0.88‰ to -1.12‰, respectively (Appendix Table 3). Raw isotopic data is presented in Fig. 4.27, with the sample number in the x-axis and isotopic values on the y-axis. In general, the results for both isotopes fluctuate steadily, with three noticeable positive peaks of $\delta^{13}C$ between sample numbers 0-10, 90-100 and 110-120. $\delta^{18}O$ has one noticeable peak between samples 60-70. It is interesting to note that none of these positive peaks are seen in both data sets simultaneously. Coral ages are discussed in terms of years of milled coral growth (MCG) i.e. the basal annual density band of the coral which has been milled is the oldest part of the coral, moving up the growth axis towards the top of the coral head through sequentially younger years MCG. Therefore, Year 1 MCG is the oldest, and Year 5 MCG is the youngest.

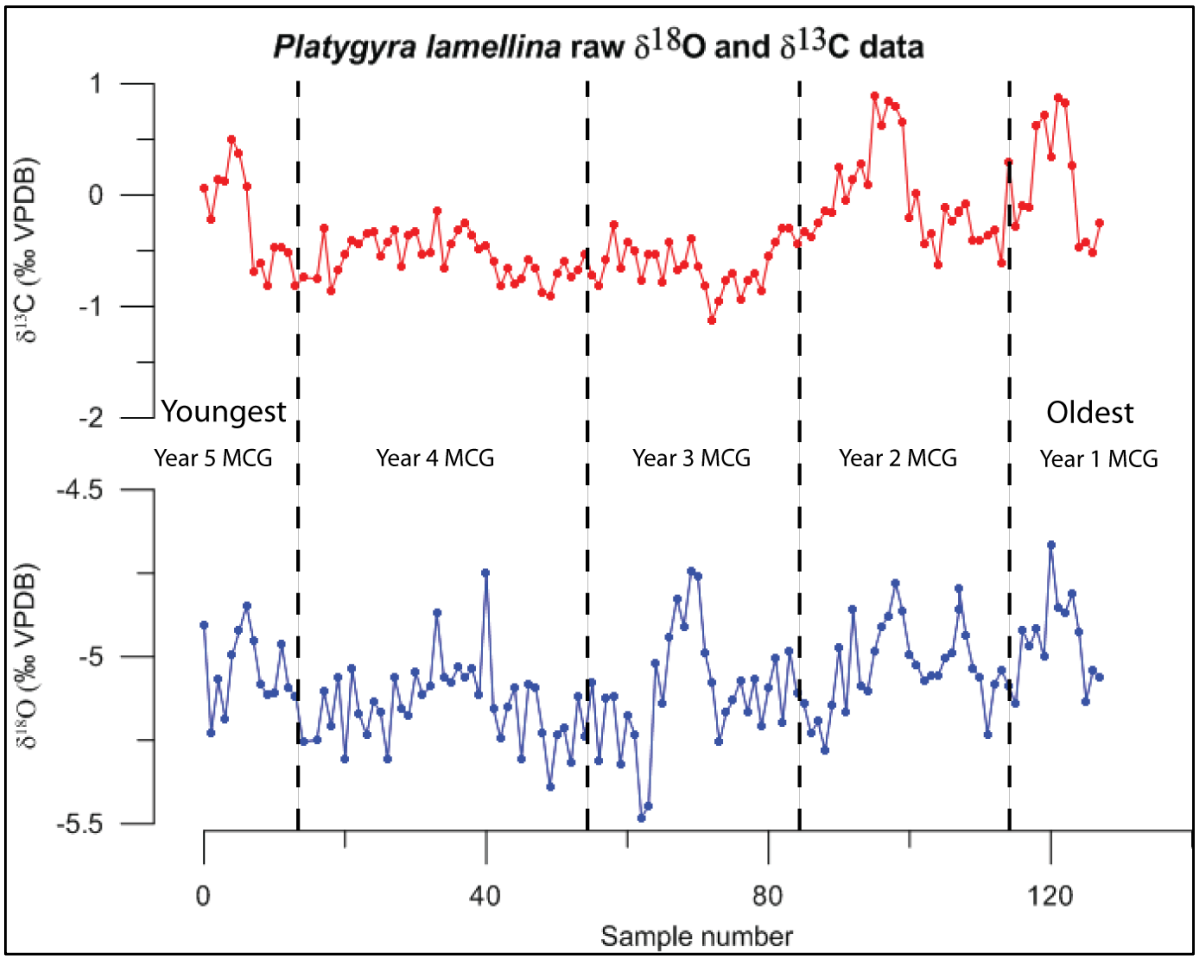

Fig. 4.27 Raw $\delta^{18}O$ and $\delta^{13}C$ data for *P. lamellina* coral. Distinct peaks between samples 0-10, 60-70 and 110-120 of $\delta^{13}C$, and between samples 60-70 of $\delta^{18}O$.

Raw $\delta^{18}O$ and $\delta^{13}C$ values are also displayed in time, with years of coral growth sampled (1-5) in the x-axis (Fig. 4.28). A running mean of each data set has been included in the graph, to highlight periodicity. It must be noted that due to the coral being milled from the top to the base, Fig. 4.27 presents the data getting older to the right, whereas Fig. 4.28 shows younging to the right. The $\delta^{13}C$ record commences with two sharp, positive peaks in the first two years of the record. Values spike from -0.51‰ to 0.88‰ over five months in the first peak, then decline to the mean value of -0.34‰, before reaching another peak of 0.88‰. From here, values experience a large decline to -1.12‰ over a ~ 10 month period. This is followed by two isolated, plateau-style peaks, each spanning ~ 6 months, however these do not exceed -0.14‰. The $\delta^{13}C$ climbs once again into positive values with a sharp increase from -0.82‰ to 0.50‰ over a ~ 3 month period at the end of the five year record.

The $\delta^{18}O$ record also displays distinct peaks and troughs, with variations between these of ~ 1‰ in magnitude. Years 1 and 5 each display a single, smooth positive peak during the middle of the year, whereas years 2, 3 and 4 each have two individual peaks. In year 2, these peaks are almost of equal magnitude, reaching -4.80‰ and -4.78‰. In contrast, the first of the two peaks seen in years 3 and 4 are both of much smaller magnitude than the secondary peaks. The maximum values for peaks in year two are -4.98‰ and -4.75‰, with -5.08‰ and -4.75‰ in year three.

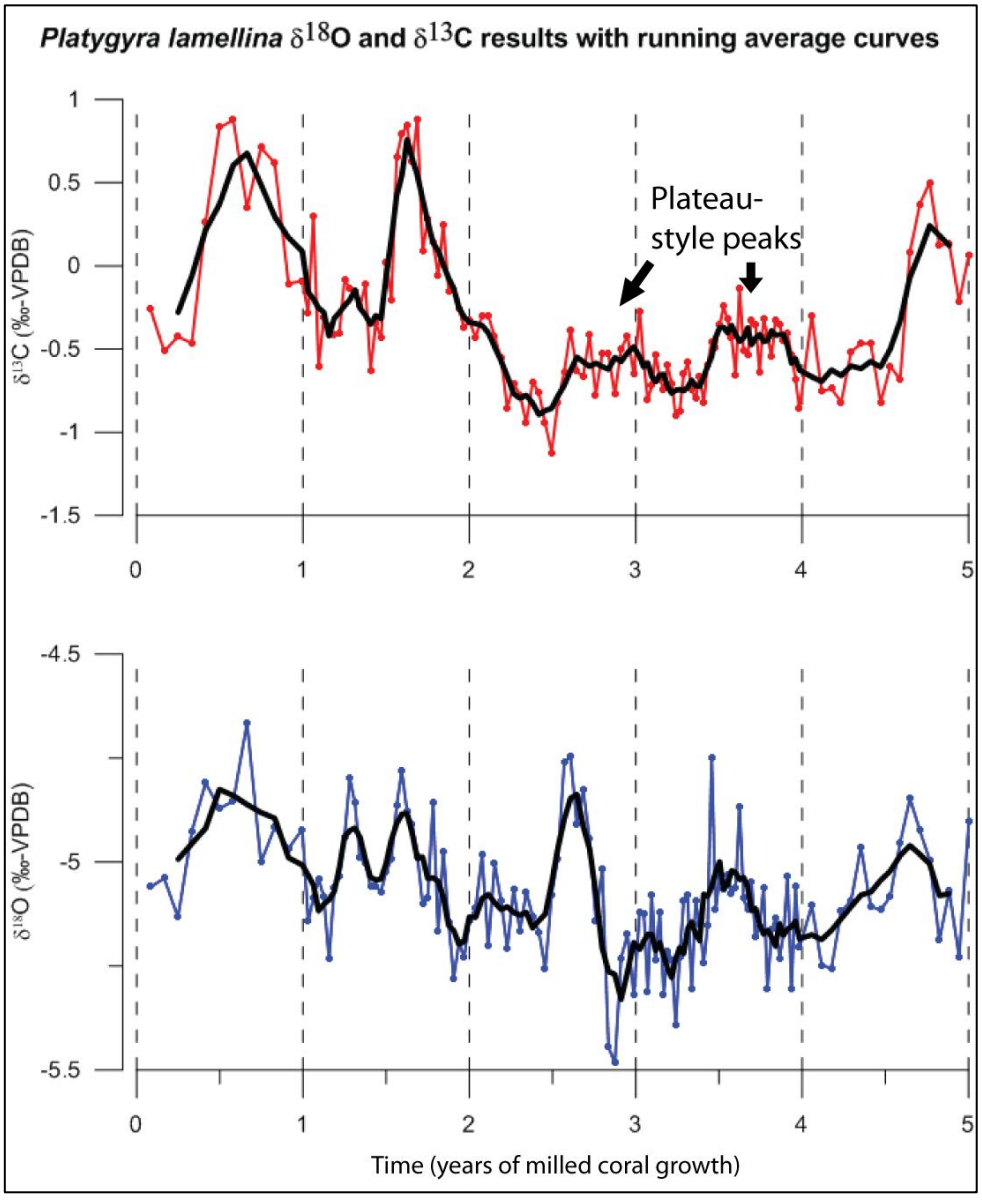

Fig. 4.28 *P. lamellina* stable isotope data as sampled through time (years 1-5.) Running average shown by thick black line. Vertical dashed lines indicate yearly boundaries. Horizontal dashed lines indicate mean $\delta^{18}O$ of -5.08‰ and mean $\delta^{13}C$ of -0.34‰.

To examine the relationship between $\delta^{18}O$ and $\delta^{13}C$ the data sets are overlain (Fig. 4.29) and plotted against one another, giving an R^2 value of 0.28 (Fig. 4.30). This shows that covariance of $\delta^{18}O$ and $\delta^{13}C$ is not as strong in *P. lamellina* as in *P. pini* or *G. retiformis*.

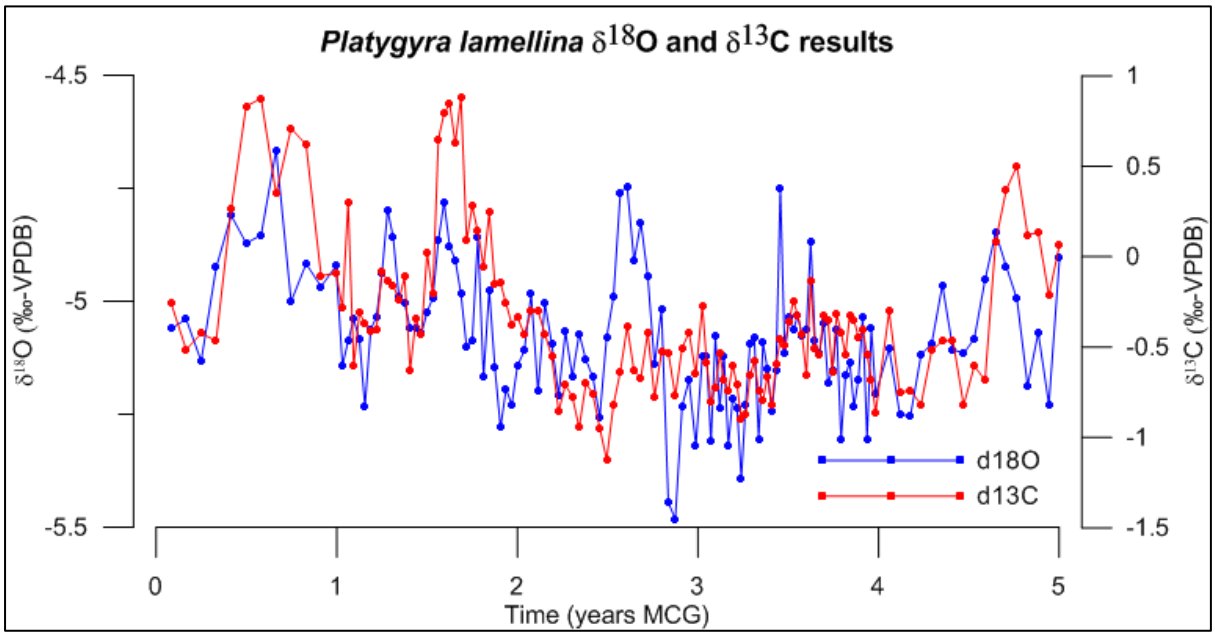

Fig. 4.29 Graph showing *P. lamellina* yearly raw data overlain to exhibit the covariance of $\delta^{18}O$ and $\delta^{13}C$.

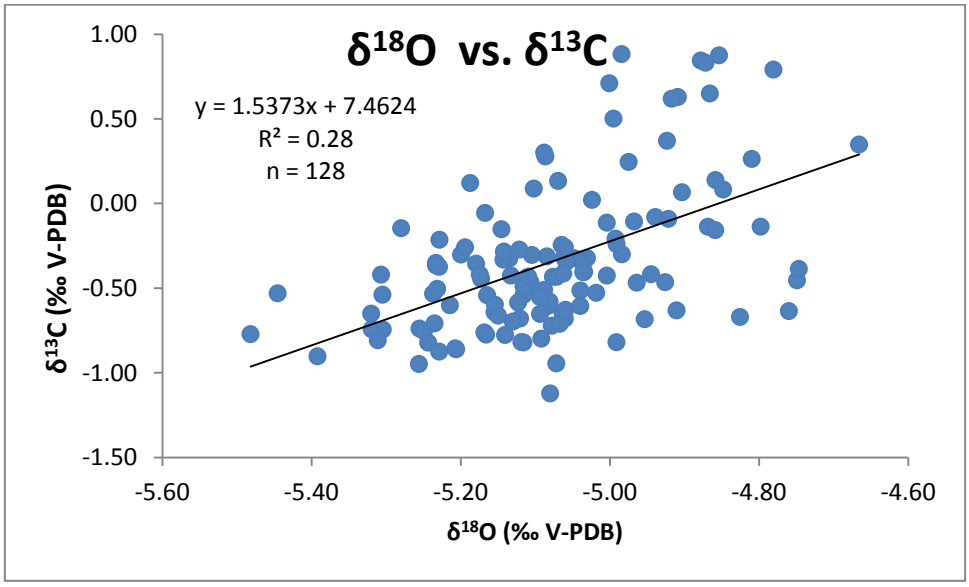

Fig. 4.30 $\delta^{18}O$ versus $\delta^{13}C$ scatter plot for all aragonite powders analysed. Weak covariance represented by an R^2 value of 0.28 from 128 data points.

In order to statistically assess periodicity in the isotope data, spectral analysis (Fig. 4.31 and Fig. 4.33) and sinusoidal models (Fig. 4.32 and Fig. 4.34) of both $\delta^{18}O$ and $\delta^{13}C$ data have been generated using PAST. The peak frequency of monthly averaged $\delta^{18}O$ data is as follows;

$$Periodicity = \frac{1}{0.08263}$$

$$Periodicity = 12.102 \ \ months\ per\ cycle$$

This is very similar to the peak frequency found using monthly averaged $\delta^{13}C$ data;

$$Periodicity = \frac{1}{0.08051}$$

$$Periodicity = 12.420 \ \ months\ per\ cycle$$

Annual periodicity, such as that which is often seen in *Porites*, was also recorded by the modern *Platygyra* coral from Ishigaki Island, Japan (Shimamura et al., 2008), 250 km due east of Taiwan (124° E, 24° N). In the Ishigaki Island coral record, negative $\delta^{18}O$ peaks correspond to summer conditions, as is expected owing to the temperature influence on $\delta^{18}O$ isotopes in corals. Sinusoidal graphs reflect these spectral analysis findings, with sine curves each matching a 12 month period, highlighting the 5 cycles traced through the record.

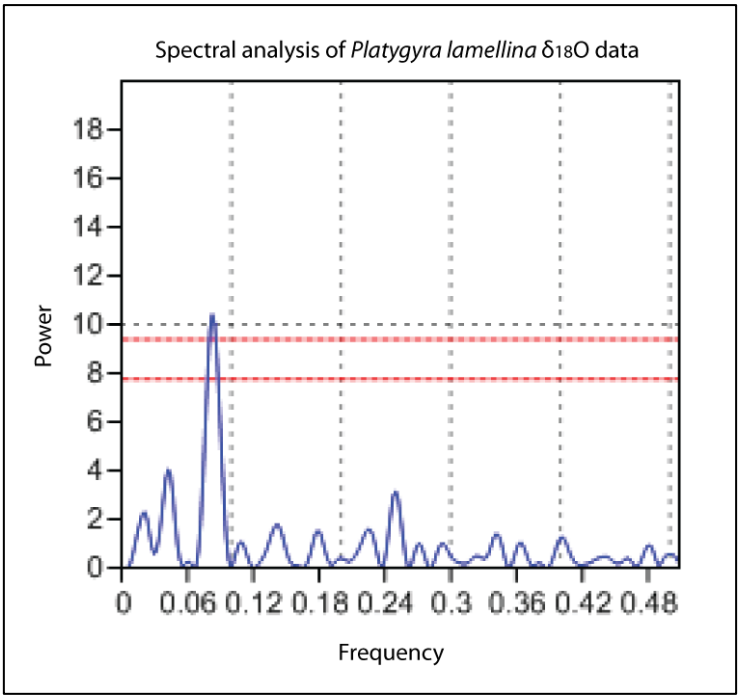

Fig. 4.31 Spectral analysis of monthly *P. lamellina* $\delta^{18}O$ data. The strongest peak in the spectrum is reported as 0.08263. The two dashed red lines are significance levels; the upper is $p<0.01$ and lower is $p<0.05$, with respect to white, uncorrelated noise.

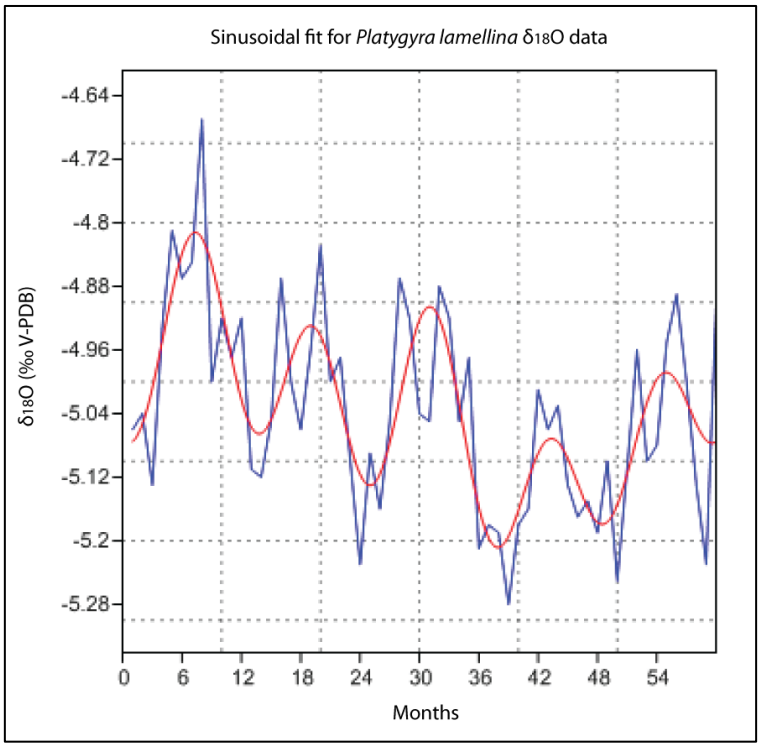

Fig. 4.32 Sinusoidal fit of monthly *P. lamellina* $\delta^{18}O$ data. $\delta^{18}O$ data represented by blue line is, sinusoid represented by red line. One sine curve is seen to correlate with 12 months.

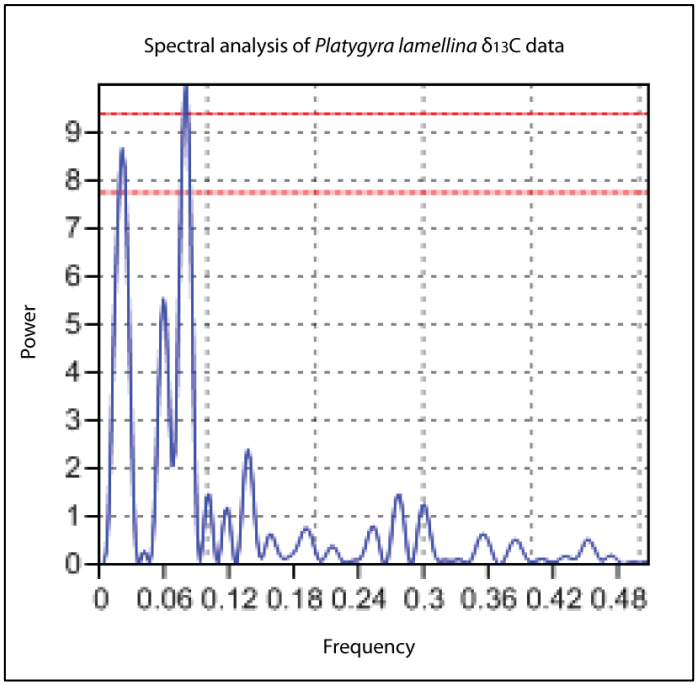

Fig. 4.33 Spectral analysis of monthly *P. lamellina* $\delta^{13}C$ data. The strongest peak in the spectrum is reported as 0.08051. The two dashed red lines are significance levels; the upper is $p<0.01$ and lower is $p<0.05$, with respect to white, uncorrelated noise.

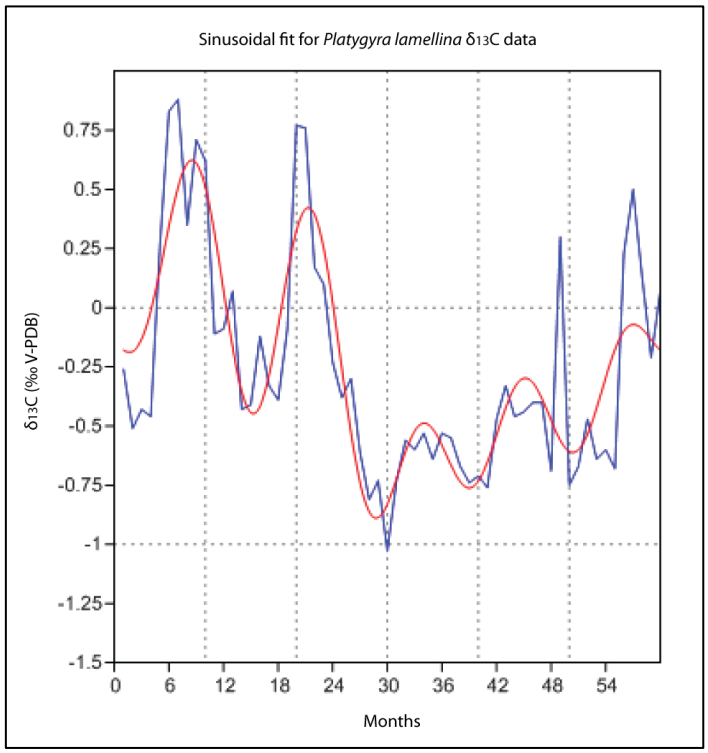

Fig. 4.34 Sinusoidal fit of monthly *P. lamellina* $\delta^{13}C$ data. $\delta^{13}C$ data represented by blue line is, sinusoid represented by red line. One sine curve is seen to correlate with 12 months.

4.5 Discussion

4.5.1 Oxygen and carbon isotopes

The geochemical record from this 2.7 Ma *P. lamellina* fossil coral provides new insights into terminal Pliocene climate conditions. Its isotope results are consistent with data from *Platygyra* corals from throughout the Pacific and Indonesian regions (Table 4.5), yet annual isotopic range is narrower. A modern sample from Ishigaki Island, Japan, was found to have a mean $\delta^{18}O$ value of -5.1‰ with a range of -4.2‰ to -6.0‰. This gives a range of 1.8‰, whereas the *P. lamellina* has a narrower range of 0.81‰. Previous studies have shown that coral growth rate and skeletal form can contribute to $\delta^{18}O$ offsets of 0.4‰ for corals in the same location (Felis and Paetzold, 2003; Guilderson and Schrag, 1999; Leder et al., 1996), therefore it is likely that the latitudinal difference of 32° between the two sites is a contributing factor of this 1.01‰ variability. Ishigaki Island is located at the northern most zone of the IPWP, where SSTs are on the boundary of the 28° C isopleths and progressively cool northward. It is possible that values more positive than -4.67‰ could be attributed to cooler SSTs during the winter months relative to winter SSTs in Timor. A 173-year long record of a modern *P. lamellina* from Vanuatu in the tropical south Pacific also revealed similar stable isotope values to this fossil. Mean $\delta^{18}O$ was -4.98‰, with a range of -4.07‰ to -7.85‰. Mean $\delta^{13}C$ was 0.01‰, with a range of 2.57‰ to -1.55‰ (Quinn et al., 1993). A study of 114 *Platygyra* specimens from different localities throughout the Pacific and Indian Oceans provides further examples of mean $\delta^{18}O$ for this genus (Weber and Woodhead, 1972); Heron Island (-4.29‰), Gannet Cay (-4.44‰), Fiji (-5.08‰), New Caledonia (-4.61‰), Flinders (-3.7‰), Saipan (-5.18‰), Tarawa Atoll (-5.25‰), Rabaul (-5.50‰), Buka (-5.36‰), Tonga (-4.41‰) and Mauritius (-4.68‰) (Fig. 4.1). Comparison to these previous *Platygyra* studies show that the fossil *P. lamellina* stable isotope results are well within range of documented modern examples, and appear to record fluctuations in oxygen and carbon isotopes in a similar manner to their modern counterparts.

SST reconstructions using the modern *Platygyra* temperature dependence equation provide the first palaeo-SST insights into terminal Pliocene ocean conditions in the IPWP. When comparing to ODP data from the South China Sea and western Pacific, the coral derived SST values of 24.0-27.7° C represent further evidence of the inferred 2-3° C cooler conditions. With modern mean annual SSTs of ~ 28° C in the oceans surrounding Timor, the mean

palaeo-SST of 25.9° C suggests that this late Pliocene (3.3-2.5 Ma) cool episode also prevailed throughout the southwest Indo-Pacific. Reliable coral archives of this age are rare, further illustrating that the corals entrained within the VM on Timor Leste provide a unique opportunity to gain detailed insights into oceanographic conditions of the Indonesian Seaway during an important period of global climate change.

The maximum $\delta^{18}O$ of the fossil *P. lamellina* (-5.48‰) is noted to be ~ 0.5‰ more positive than the Ishigaki Island modern *Platygyra* (-6.0‰). The isotopic composition of seawater during the Pliocene is predicted to have had an oscillation of ~ 0.5‰ due to cooler conditions due to near total glaciation of Antartica (Zachos et al., 2001), which is likely to be an influencing factor. However, the minimum *P. lamellina* $\delta^{18}O$ value of -4.67‰ is 0.45‰ more positive than the modern minimum of -4.2‰, so this slightly larger oscillation of values may simply be due to differences in ambient $\delta^{18}O_{sw}$ at each locality, as there is 32° latitude of difference between the two sites.

Table 4.5 Mean isotopic values from *Platygyra* coral studies. Results from Weber and Woodhead, 1972, grouped as Australia include Heron Island and Gannet Cay; Central Pacific includes New Caledonia, Flinders, Saipan, Tarawa Atoll, and Tonga; and Indo-Pacific includes Rabaul and Buka.

Coral location	Mean $\delta^{18}O$ (‰ V-PDB)	Mean $\delta^{13}C$ (‰ V-PDB)	Lifespan	Length of record (years)	Author
Timor Leste	-5.08	-0.34	2.7 Ma	5	(Moody et al., 2012)
Japan	-5.10	No data	1995-2005	11	(Shimamura et al., 2008)
Vanuatu	-4.98	0.01	1806-1978	173	(Quinn et al., 1993; 1996)
Australia	-4.36	No data	No data	No data	(Weber and Woodhead, 1972)
Central Pacific	-4.71	No data	No data	No data	(Weber and Woodhead, 1972)
Indo-Pacific	-5.43	No data	No data	No data	(Weber and Woodhead, 1972)

4.5.2 ENSO

The presence of a dominant annual cycle documents the effects of seasonal SST and SSS fluctuations of ambient seawater conditions. There is no indication of an interannual ENSO

signal, however the five year record is too short to confirm that there is no ENSO behaviour present at the time the coral was living. It has been documented that *Platygyra* corals can record both seasonal and ENSO periodicity, as provided by records from Shimamura et al. (2008) and Quinn et al. (1996; 1993). Seasonal SST fluctuation is accountable for the annual periodicity at Ishigaki Island (Shimamura et al., 2008), whereas the most prominent spectral peaks in the Espirito Santo coral are at 14-15 and 7 years, as well as the annual cycle (Quinn et al., 1996; 1993). The three spectral peaks shows that the coral is not only recording seasonal SST fluctuations but also decadal scale climate variability, proving that strong ENSO behaviour can be preserved in this coral genus. If a longer record can be obtained from the *P. lamellina* coral in future studies, the presence or absence of ENSO-like climatic behaviour may be able to be detected.

4.5.3 Geological setting

The geological setting from which this fossilised coral has been retrieved provides a unique "time-capsule" of Pliocene climate. The uplift of the VM means that these entrained corals can be collected in situ which presents an advantage over more technical ocean drilling, and by implementing a rigorous diagenetic screening process, pristine corals can be selected for analysis. Fossil corals located in uplifted reefs have often been severely exposed to post depositional diagenesis, such as marine and fresh water phreatic and vadose zone alteration. This is seen in the 4.5 ka *P. pini* corals, which now display extensive secondary aragonite growth and diagenesis. This strongly suggests that the *P. lamellina* coral did not experience significant subaerial exposure and was likely still living in the reef environment when it became entrained within the VM. The U/Pb age supports the 3.1-1.9 Ma stratigraphic age of the section provided by foraminifera (Haig and McCartain, 2007), further justifying that the coral has not been exposed to alteration, and increasing temporal resolution of the timing of tectonic uplift to post 2.7 Ma.

4.6 Implications and conclusions

The preservation of this 2.7 Ma coral reveals new evidence of climate behaviour in the Indo-Pacific. The stable isotope record provides the first coral record of terminal Pliocene age from the region, with both annual periodicity detected using spectral analysis and mean $\delta^{18}O$ values corroborating with a modern *Platygyra* record. The cyclical isotope pattern is representative of seasonal climate behaviour, where peak SST values are recorded during

summer months, a relationship which is also distinct in modern studies. Preliminary terminal Pliocene SST data has been provided for the southern Indo-Pacific, showing mean temperatures of 25.9° C. As cooler temperatures of ~ 2° C have been observed in Mg/Ca records from this time period, the palaeo-SSTs obtained using the modern *Platygyra* temperature dependence equation for this fossil coral are shown to be realistic. The possibility to determine precise SST fluctuations from the Indonesian Seaway at 2.7 Ma provides unique insights into the changes occurring in the ITF during seaway narrowing.

The broad latitudinal distribution of *Platygyra* corals, as explained by Shimamura et al. (2008), means that these corals represent an exclusive opportunity to gain insights into climate behaviour of not only the tropics, but also the mid latitudes. The recognition that fossil samples, such as TL289, can be geochemically preserved means that archives of mid latitude climate through the Holocene, Pleistocene and Pliocene is possible using this genus. This provides an exciting possibility for extending the range and time span of coral records well beyond that which is presently documented.

4.6.1 Future work

Determining a $\delta^{18}O$-palaeotemperature equation for a modern *Platygyra* from Timor would allow further increase the reliability of palaeo-SST models obtained from fossil corals of the VM. This could then be compared to inferred SST values from sedimentary and foraminiferal records, strengthening the dependability of proxies. Gaining a record longer 10 years, preferably 20-30 years, from Pliocene corals entrained in the VM would allow the analysis of interannual variability. This could then be used to infer the presence or absence of ENSO in the terminal Pliocene at this site.

Thesis Conclusions

This thesis has shed new light of the use of living and fossil corals from the Timor region as climate proxies. Stable isotopic investigations have provided the first ever analysis of the *G. retiformis* species, and first insights into fossil specimens of the *Platygyra* genus. The abundance of *G. retiformis* and broad latitudinal range of *Platygyra* mean these corals are particularly important to examine. They have the ability to increase the spatial concentration of climate records currently provided by *Porites* throughout the tropical Pacific, and crucially, to maximise the latitudinal extent over which detailed climate records can be retrieved. The importance of understanding past climatic shifts and trends is a vital part of our understanding of the present climate and how it may change in the future.

G. retiformis appears to correlate to multiple climate indices throughout its 4.5 year record. Interpretation of the data shows that variation of SST and precipitation due to the interaction between ENSO and the monsoon system is the most likely cause for isotopic fluctuation. Quasi-biennial periodicity has previously been detected in coral records, meaning that this species is a candidate for further identification of coupled climate interactions which have significant effects on the global climate system. This species' abundance throughout the tropical Pacific means that when its geochemical systematic are thoroughly understood and it is applied as a climate proxy, the spatial resolution of climate data will increase dramatically. Fossil samples are also prolific throughout raised reefs in PNG, so there is also wide scope for palaeoclimate reconstruction using this species.

The diagenetically altered *P. pini* coral record displays positive isotopic values relative to modern and fossil *Platygyra* corals. These anomalies are consistent with the effects of diagenesis in corals, specifically secondary aragonite and dissolution. Yet mean annual SSTs in the southern Indo-Pacific were 1.2° C cooler in the mid Holocene, meaning that unaltered geochemical records would also display relatively positive isotopic values. SST interpretation using the modern *Platygyra* temperature dependence equation explicitly shows that diagenesis in the uppermost 4 cm of the coral has caused unrealistically cool temperatures as low as 18.5° C. However, the mean and maximum annual SSTs of 24.7° C and 27.6° C are much more realisitic, albeit slightly cooler than predicted. This analysis, along with interannual periodicity and a ~ 0.4‰ amplitude of seasonal fluctuations shows that general features of mid Holocene climate have been preserved. The impacts of

diagenesis in this species have not previously been assessed, and this study shows that corals which have experienced diagenesis should not be discarded as useful climate proxies. They cannot provide absolute isotopic or SST values, but signals of the climate processes driving the geochemical record can be retained, thus providing important insights into local and regional climate behaviour throughout the time the coral was living.

The discovery of strong annual periodicities in the Pliocene coral indicates dominant seasonal climate dynamics in this region. However, a five year time slice is not a long enough record to detect interannual variability characteristic of ENSO, so assumptions cannot be made as to whether this record was being influenced by ENSO-like conditions. The isotopic record allows the first terminal Pliocene SST reconstruction, providing temperatures that are consistent with 2-3° C cooler conditions in this region from 3.3-2.5 Ma. This coral record is in good agreement with the modern *Platygyra* records from Ishigaki Island and Epsiritu Santo, providing further evidence that this genus should undergo extensive investigations in order to determine reliable temperature dependence equations from a range of locations. This would allow full utilisation of this coral which is particularly well suited to climate proxy applications across a much broader latitudinal range than the presently used *Porites* genus.

By investigating the preservation and isotope signals of these corals collected from Timor Leste, the aim to maximise the temporal and spatial resolution of data capture, and improve the understanding of coral climate records throughout this region has been wholly achieved. These three species have been identified as promising climate proxies, which will provide robust climate data on modern to Pliocene timescales.

References

Abram, N.J., McGregor, H.V., Gagan, M.K., Hantoro, W.S., and Suwargadi, B.W., 2009, Oscillations in the southern extent of the Indo-Pacific Warm Pool during the mid-Holocene: Quaternary Science Reviews, v. 28, p. 2794-2803.

Al-Rousan, S., Felis, T., Manasrah, R., and Al-Horani, F., 2007, Seasonal variations in the stable oxygen isotopic composition in Porites corals from the northern Gulf of Aqaba, Red Sea: Geochemical Journal, v. 41, p. 333-340.

Alibert, C., and McCulloch, M.T., 1997, Strontium/calcium ratios in modern Porites corals from the Great Barrier Reef as a proxy for sea surface temperature: calibration of the thermometer and monitoring of ENSO: Paleoceanography, v. 12, p. 345-363.

Allison, N., Finch, A.A., Webster, J.M., and Clague, D.A., 2007, Palaeoenvironmental records from fossil corals: The effects of submarine diagenesis on temperature and climate estimates: Geochimica et Cosmochimica Acta, v. 71, p. 4693-4703.

Asami, R., Yamada, T., Iryu, Y., Meyer, C.P., Quinn, T.M., and Paulay, G., 2004, Carbon and oxygen isotopic composition of a Guam coral and their relationships to environmental variables in the western Pacific: Palaeogeography, Palaeoclimatology, Palaeoecology, v. 212, p. 1-22.

Audley-Charles, M.G., 1968a, The Geology of Portugese Timor: London, Geological Society of London.

Audley-Charles, M.G., 1968b, The geology of Portuguese Timor: Memoirs of the Geological Society of London, v. 4.

Audley-Charles, M.G., 1986, Rates of Neogene and Quaternary tectonic movements in the southern Banda Arc based on micropalaeontology: Journal of the Geological Society, v. 143, p. 161-175.

Audley-Charles, M.G., 2011, Tectonic post-collision processes in Timor, *in* Hall, R., Cottam, M.A., and Wilson, M.E.J., eds., The SE Asian Gateway: History and Tectonics of the Australia-Asia Collision, Volume 355: London, Geological Society Special Publications, p. 241-266.

Bar-Matthews, M., Wasserburg, G.J., and Chen, J.H., 1993, Diagenesis of fossil coral skeletons: Correlation between trace elements, textures, and 234 U/238 U: Geochimica et Cosmochimica Acta, v. 57, p. 257-276.

Barnett, J., Dessai, S., and Jones, R., 2003, Climate Change In Timor Leste: Science, Impacts, Policy and Planning, Briefing to Government, civil society, and donors, RDTL., University of Melbourne and CSIRO.

Bathurst, R.G.C., 1975, Carbonate sediments and their diagenesis: Developments in Sedimentology v. 12.

Beck, J.W., Récy, J., Taylor, F., Edwards, R.L., and Cabioch, G., 1997, Abrupt changes in early Holocene tropical sea surface temperature derived from coral records: Nature, v. 385, p. 705-707.

Bock, Y., Prawirodirdjo, L., Genrich, J.F., Stevens, C.W., McCaffrey, R., Subarya, C., Puntodewo, S.S.O., and Calais, E., 2003, Crustal motion in Indonesia from Global Positioning System measurements: Journal of Geophysical Research B: Solid Earth, v. 108.

Boekschoten, G.J., Best, M.B., Oosterbaan, A., and Molenkamp, F.M., 1989, Past corals and recent reefs in Indonesia: Netherlands Journal of Sea Research, v. 23, p. 117-122.

Brachert, T.C., Reuter, M., Felis, T., Kroeger, K.F., Lohmann, G., Micheels, A., and Fassoulas, C., 2006, Porites corals from Crete (Greece) open a window into Late Miocene (10 Ma) seasonal and interannual climate variability: Earth and Planetary Science Letters, v. 245, p. 81-94.

Bromfield, K., and Pandolfi, J.M., 2011, Regional patterns of evolutionary turnover in Neogene coral reefs from the central Indo-West Pacific Ocean: Evolutionary Ecology, p. 1-17.

Cahyarini, S.Y., Pfeiffer, M., Timm, O., Dullo, W.C., and Schönberg, D.G., 2008, Reconstructing seawater [delta] 18O from paired coral [delta] 18O and Sr/Ca ratios: Methods, error analysis and problems, with examples from Tahiti (French Polynesia) and Timor (Indonesia): Geochimica et Cosmochimica Acta, v. 72, p. 2841-2853.

Cane, M.A., 2005, The evolution of El Niño, past and future: Earth and Planetary Science Letters, v. 230, p. 227-240.
Cane, M.A., and Molnar, P., 2001, Closing of the Indonesian seaway as a precursor to east African aridification around 3–4 million years ago: Nature, v. 411, p. 157-162.
Carter, D.J., Audley-Charles, M.G., and Barber, A.J., 1976, Stratigraphical analysis of island arc-continental margin collision in eastern Indonesia: Journal of the Geological Society of London, v. 132, p. 179-198.
Carton, J.A., Chepurin, G., and Cao, X., 2000a, A simple ocean data assimilation analysis of the global upper ocean 1950-95. Part II: Results: Journal of physical oceanography, v. 30, p. 311-326.
Carton, J.A., Chepurin, G., Cao, X., and Giese, B., 2000b, A simple ocean data assimilation analysis of the global upper ocean 1950–95. Part I: Methodology.
Charles, C., Hunter, D., and Fairbanks, R.G., 1997, Interaction between the ENSO and the Asian monsoon in a coral record of tropical climate: Science, v. 277, p. 925.
Chiang, H.W., Chen, Y.G., Fan, T.Y., and Shen, C.C., 2010, Change of the ENSO-related [delta] 18O-SST correlation from coral skeletons in northern South China Sea: A possible influence from the Kuroshio Current: Journal of Asian Earth Sciences, v. 39, p. 684-691.
Chivas, A., 2012, AQUA Biennial Conference: Lake Tekapo, New Zealand.
Cobb, K.M., Charles, C.D., Cheng, H., and Edwards, R.L., 2003, El Nino/Southern Oscillation and tropical Pacific climate during the last millennium: Nature, v. 424.
Cohen, A.L., and McConnaughey, T.A., 2003, Geochemical perspectives on coral mineralization: Reviews in mineralogy and geochemistry, v. 54, p. 151.
Cole, J., 1996, Coral records of climate change: Understanding past variability in the tropical ocean-atmosphere: NATO ASI Series I Global Environmental Change, v. 41, p. 331-354.
Correge, T., 2006, Sea surface temperature and salinity reconstruction from coral geochemical tracers: Palaeogeography, Palaeoclimatology, Palaeoecology, v. 232, p. 408-428.
deMenocal, P.B., 2004, African climate change and faunal evolution during the Pliocene-Pleistocene: Earth and Planetary Science Letters, v. 220, p. 3-24.
DeMets, C., Gordon, R.G., Argus, D.F., and Stein, S., 1994, Effect of recent revisions to the geomagnetic reversal time scale on estimates of current plate motions: Geophysical Research Letters, v. 21, p. 2191-2194.
Denniston, R.F., Asmerom, Y., Polyak, V.Y., McNeill, D.F., Klaus, J.S., Cole, P., and Budd, A.F., 2008, Caribbean chronostratigraphy refined with U-Pb dating of a Miocene coral: Geology, v. 36, p. 151.
Druffel, E.R.M., 1997, Geochemistry of corals: Proxies of past ocean chemistry, ocean circulation, and climate: Proceedings of the National Academy of Sciences of the United States of America, v. 94, p. 8354.
Dullo, W.C., 2005, Coral growth and reef growth: a brief review: Facies, v. 51, p. 33-48.
Dunbar, R.B., and Cole, J.E., 1999, Annual Records of Tropical Systems (ARTS): PAGES Workshop Rep. Ser., v. 99.
Dunbar, R.B., Wellington, G.M., Colgan, M.W., and Glynn, P.W., 1994, Eastern Pacific sea surface temperature since 1600 AD: The 18O record of climate variability in Galápagos corals: Paleoceanography, v. 9, p. 291-315.
Edinger, E.N., and Risk, M.J., 1994, Oligocene-Miocene extinction and geographic restriction of Caribbean corals: roles of turbidity, temperature, and nutrients: Palaios, p. 576-598.
Edwards, R.L., Chen, J.H., and Wasserburg, G.J., 1987, U-238-U-234-Th-230-Th-232 systematics and the precise measurement of time over the past 500,000 years: Earth and Planetary Science Letters, v. 81, p. 175-192.
Fairbanks, R.G., and Dodge, R.E., 1979, Annual periodicity of the 18 O/16 O and 13 C/12 C ratios in the coral Montastrea annularis: Geochimica et Cosmochimica Acta, v. 43, p. 1009-1020.
Fairbanks, R.G., Evans, M.N., Rubenstone, J.L., Mortlock, R.A., Broad, K., Moore, M.D., and Charles, C.D., 1997, Evaluating climate indices and their geochemical proxies measured in corals: Coral Reefs, v. 16, p. 93-100.

Fedorov, A.V., Dekens, P.S., McCarthy, M., Ravelo, A.C., deMenocal, P.B., Barreiro, M., Pacanowski, R.C., and Philander, S.G., 2006, The Pliocene Paradox (Mechanisms for a Permanent El Nino): Science, v. 312.

Felis, T., and Paetzold, J., 2003, Climate Records from Corals: Berlin, Springer-Verlag.

Gagan, M.K., Ayliffe, L.K., Beck, J.W., Cole, J.E., Druffel, E.R.M., Dunbar, R.B., and Schrag, D.P., 2000, New views of tropical paleoclimates from corals: Quaternary Science Reviews, v. 19, p. 45-64.

Gagan, M.K., Ayliffe, L.K., Hopley, D., Cali, J.A., Mortimer, G.E., Chappell, J., McCulloch, M.T., and Head, M.J., 1998, Temperature and surface-ocean water balance of the mid-Holocene tropical western Pacific: Science, v. 279, p. 1014.

Gagan, M.K., Chivas, A.R., and Isdale, P.J., 1994, High-resolution isotopic records from corals using ocean temperature and mass-spawning chronometers: Earth and Planetary Science Letters, v. 121, p. 549-558.

Gagan, M.K., Hendy, E.J., Haberle, S.G., and Hantoro, W.S., 2004, Post-glacial evolution of the Indo-Pacific warm pool and El Nino-Southern Oscillation: Quaternary International, v. 118, p. 127-143.

Gallagher, S., Wallace, M., Li, C., Kinna, B., Bye, J., Akimoto, K., and Torii, M., 2009, Neogene history of the West Pacific Warm Pool, Kuroshio and Leeuwin currents: Paleoceanography, v. 24.

Getty, S.R., Asmerom, Y., Quinn, T.M., and Budd, A.F., 2001, Accelerated Pleistocene coral extinctions in the Caribbean Basin shown by uranium-lead (U-Pb) dating: Geology, v. 29, p. 639.

Goldfinger, C., 2009, Sub-Aqueous Paleoseismology: International Geophysics, v. 95, p. 119-170.

Goldfinger, C., Nelson, C.H., and Johnson, J.E., 2003, Deep-water turbidites as Holocene earthquake proxies: the Cascadia subduction zone and northern San Andreas fault systems: Annals of Geophysics, v. 46.

Gordon, A.L., and Fine, R.A., 1996, Pathways of water between the Pacific and Indian oceans in the Indonesian seas: Nature, v. 379, p. 146-149.

Gordon, A.L., Giulivi, C.F., and Ilahude, A.G., 2003, Deep topographic barriers within the Indonesian seas: Deep Sea Research Part II: Topical Studies in Oceanography, v. 50, p. 2205-2228.

Gordon, A.L., Susanto, D.R., and Vranes, K., 2004, Cool Indonesian Throughflow as a consequence of restricted surface layer flow: Nature, v. 425, p. 824-828.

Guilderson, T.P., and Schrag, D.P., 1998, Abrupt shift in subsurface temperatures in the tropical Pacific associated with changes in El Niño: Science, v. 281, p. 240.

Guilderson, T.P., and Schrag, D.P., 1999, Reliability of coral isotope records from Pacific warm pool: A comparison using age-optimized records: Paleoceanography, v. 14, p. 457-464.

Haig, D.W., and McCartain, E., 2007, Carbonate pelagites in the post-Gondwana succession (Cretaceous - Neogene) of East Timor: Australian Journal of Earth Sciences, v. 54, p. 875-897.

Harris, R.A., 1991, Temporal distribution of strain in the active Banda orogen: a reconciliation of rival hypotheses: Journal of Southeast Asian Earth Sciences, v. 6, p. 373-386.

Hellstrom, J., 2003, Rapid and accurate U/Th dating using parallel ion-counting multi-collector ICP-MS: J. Anal. At. Spectrom., v. 18, p. 1346-1351.

Henderson, G.M., Cohen, A.S., and Onions, R.K., 1993, U-234/U-238 ratios and TH-230 ages for Hateruma Atoll corals - implications for coral diagenesis and seawater U-234/U-238 ratios: Earth and Planetary Science Letters, v. 115, p. 65-73.

Hendy, E.J., Gagan, M.K., Lough, J.M., McCulloch, M., and deMenocal, P.B., 2007, Impact of skeletal dissolution and secondary aragonite on trace element and isotopic climate proxies in Porites corals: Paleoceanography, v. 22.

Highsmith, R.C., 1979, Coral growth rates and environmental control of density banding: Journal of Experimental Marine Biology and Ecology, v. 37, p. 105-125.

Hudson, J.H., Shinn, E.A., Halley, R.B., and Lidz, B., 1976, Sclerochronology: a tool for interpreting past environments: Geology, v. 4, p. 361.

Hughen, K.A., Schrag, D.P., Jacobsen, S.B., and Hantoro, W., 1999, El Nino during the last interglacial period recorded by a fossil coral from Indonesia: Geophysical Research Letters, v. 26, p. 3129-3132.
IPCC, 2007, Climate Change 2007: Working Group I: The Physical Science Basis, IPCC Fourth Assessment Report.
Ivany, L.C., Peters, S.C., Wilkinson, B.H., Lohmann, K.C., and Reimer, B.A., 2004, Composition of the early Oligocene ocean from coral stable isotope and elemental chemistry: Geobiology, v. 2, p. 97-106.
Jochum, M., Fox-Kemper, B., Molnar, P.H., and Shields, C., 2009, Differences in the Indonesian seaway in a coupled climate model and their relevance to Pliocene climate and El Nino: Paleoceanography, v. 24, p. PA1212.
Juillet-Leclerc, A., Thiria, S., Naveau, P., Delcroix, T., Le Bec, N., Blamart, D., and Correge, T., 2006, SPCZ migration and ENSO events during the 20th century as revealed by climate proxies from a Fiji coral: Geophys. Res. Lett, v. 33, p. L17710.
Karas, C., Nürnberg, D., Gupta, A.K., Tiedemann, R., Mohan, K., and Bickert, T., 2009, Mid-Pliocene climate change amplified by a switch in Indonesian subsurface throughflow: Nature Geoscience, v. 2, p. 434-438.
Keep, M., and Haig, D.W., 2010, Deformation and exhumation in Timor: Distinct stages of a young orogeny: Tectonophysics, v. 483, p. 93-111.
Kenyon, C.S., 1974, Stratigraphy and sedimentology of the Late Miocene to Quaternary deposits in Timor. [PhD thesis], University of London.
Kirono, D., 2010, Climate change in Timor-Leste–a brief overview on future climate projections, National Research Flagships Climate Adaptation, CSIRO.
Lea, D.W., Shen, G.T., and Boyle, E.A., 1989, Coralline barium records temporal variability in Equatorial Pacific upwelling.: Nature, v. 340, p. 373-376.
Leder, J.J., Swart, P.K., Szmant, A.M., and Dodge, R.E., 1996, The origin of variations in the isotopic record of scleractinian corals: I. Oxygen: Geochimica et Cosmochimica Acta, v. 60, p. 2857-2870.
Linsley, B.K., Rosenthal, Y., and Oppo, D.W., 2010, Holocene evolution of the Indonesian throughflow and the western Pacific warm pool: Nature Geoscience.
Mackenzie, G., Veauvy, C.M., and Swart, P.K., 1997, Climatic variation in the early to middle Eocene using the stable isotopic composition of coral skeletons, Volume 29, p. 395.
Mayewski, P.A., Rohling, E.E., Curt Stager, J., Karlen, W., Maasch, K.A., David Meeker, L., Meyerson, E.A., Gasse, F., van Kreveld, S., and Holmgren, K., 2004, Holocene climate variability: Quaternary Research, v. 62, p. 243-255.
McConnaughey, T., 1989, 13C and 18O isotopic disequilibrium in biological carbonates: I. Patterns: Geochimica et Cosmochimica Acta, v. 53, p. 151-162.
McCulloch, M., Mortimer, G., Esat, T., Xianhua, L., Pillans, B., and Chappell, J., 1996, High resolution windows into early Holocene climate: Sr/Ca coral records from the Huon Peninsula: Earth and Planetary Science Letters, v. 138, p. 169-178.
McCulloch, M.T., Gagan, M.K., Mortimer, G.E., Chivas, A.R., and Isdale, P.J., 1994, A high-resolution Sr/Ca and [delta] 18O coral record from the Great Barrier Reef, Australia, and the 1982-1983 El Niño: Geochimica et Cosmochimica Acta, v. 58, p. 2747-2754.
McGregor, H.V., and Abram, N.J., 2008, Images of diagenetic textures in Porites corals from Papua New Guinea and Indonesia: Geochemistry Geophysics Geosystems, v. 9, p. Q10013.
McGregor, H.V., Fischer, M.J., Gagan, M.K., Fink, D., and Woodroffe, C.D., 2011, Environmental control of the oxygen isotope composition of Porites coral microatolls: Geochimica et Cosmochimica Acta.
McGregor, H.V., and Gagan, M.K., 2003, Diagenesis and geochemistry of porites corals from Papua New Guinea:: Implications for paleoclimate reconstruction: Geochimica et Cosmochimica Acta, v. 67, p. 2147-2156.

McGregor, H.V., and Gagan, M.K., 2004, Western Pacific coral d18O records of anomalous Holocene variability in the El Nino–Southern Oscillation: Geophysical Research Letters, v. 31, p. L11204.
Meehl, G.A., 1987, The annual cycle and interannual variability in the tropical Pacific and Indian Ocean regions: Monthly Weather Review, v. 115, p. 27-50.
Meehl, G.A., 1994, Coupled land-ocean-atmosphere processes and South Asian monsoon variability: Science, v. 266, p. 263.
Molnar, P., and Cane, M.A., 2007, Early Pliocene (pre–Ice Age) El Niño–like global climate: Which El Niño?: Geosphere, v. 3, p. 337.
Montaggioni, L.F., and Braithwaite, C.J.R., 2009, Quarternary Coral Reef Systems: history, development processes and controlling factors: Oxford, Elsevier.
Morey, S.L., Shriver, J.F., and O'Brien, J.J., 1999, The effects of Halmahera on the Indonesian throughflow: Journal of geophysical research, v. 104, p. 23281.
Nguyen, N., Shulmeister, J., Duffy, B., and Quigley, M., In prep, Palynological insights into the uplift of Timor and implications for the onset of a modern ENSO climate.
NOAA, 2012, Global Climate Change Indicators, National Climatic Data Center.
Nugroho, H., Harris, R., Lestariya, A.W., and Maruf, B., 2009, Plate Boundary Reorganization in the Active bandA Arc-Continent Collision: Insights from New GPS Measurements: Tectonophysics, v. 479, p. 52-65.
Oomori, T., Kaneshima, K., Nakamura, Y., and Kitano, Y., 1983, Seasonal variation of minor elements in coral skeletons: Galaxea, v. 1, p. 77-86.
Price, N.J., and Audley-Charles, M.G., 1983, Plate rupture by hydraulic fracture resulting in overthrusting: Nature, v. 306, p. 572-575.
Price, N.J., and Audley-Charles, M.G., 1987, Tectonic collision processes after plate rupture: Tectonophysics, v. 140, p. 121-129.
Qu, D.-C., 2007, Late Quarternary climate in the Indo-Pacific Warm Pool reconstructed from the raised coral reefs of Sumba, Indonesia: Canberra, Australian National University.
Qu, T., Du, Y., Strachan, J., Meyers, G., and Slingo, J., 2005, Sea surface temperature and its variability in the Indonesian region: Oceanography, v. 18.
Quigley, M., Duffy, B., Woodhead, J., Hellstrom, J., Moody, L., Horton, T., Suares, J., Fernandez, L., and Haig, D., 2012, U/Pb dating of a terminal Pliocene coral from the Indonesian Seaway: Marine Geology.
Quinn, T.M., Crowley, T.J., and Taylor, F.W., 1996, New stable isotope results from a 173-year coral from Espiritu Santo, Vanuatu: Geophysical Research Letters, v. 23, p. 3413-3416.
Quinn, T.M., Taylor, F.W., and Crowley, T.J., 1993, A 173 year stable isotope record from a tropical south pacific coral: Quaternary Science Reviews, v. 12, p. 407-418.
Rasmusson, E.M., and Carpenter, T.H., 1983, The relationship between eastern equatorial Pacific sea surface temperatures and rainfall over India and Sri Lanka: Monthly Weather Review, v. 111, p. 517-528.
Ravelo, A.C., Andreasen, D.H., Lyle, M., Olivarez Lyle, A., and Wara, M.W., 2004, Regional climate shifts caused by gradual global cooling in the Pliocene epoch: Nature, v. 429, p. 263-267.
Rayner, N., Parker, D., Horton, E., Folland, C., Alexander, L., Rowell, D., Kent, E., and Kaplan, A., 2003, Global analyses of sea surface temperature, sea ice, and night marine air temperature since the late nineteenth century: J. Geophys. Res, v. 108, p. 4407.
Reed, K.E., 1997, Early hominid evolution and ecological change through the African Plio-Pleistocene* 1: Journal of Human Evolution, v. 32, p. 289-322.
Roulier, L.M., and Quinn, T.M., 1995, Seasonal-to decadal-scale climatic variability in southwest Florida during the middle Pliocene: Inferences from a coralline stable isotope record: Paleoceanography, v. 10, p. 429-443.
Rutherford, E., Burke, K., and Lytwyn, J., 2001, Tectonic history of Sumba Island, Indonesia, since the Late Cretaceous and its rapid escape into the forearc in the Miocene: Journal of Asian Earth Sciences, v. 19, p. 453-479.

Sandiford, M., 2008, Seismic moment release during slab rupture beneath the Banda Sea: Geophysical Journal International, v. 174, p. 659-671.
Scholz, D., and Mangini, A., 2007, How precise are U-series coral ages?: Geochimica et cosmochimica acta, v. 71, p. 1935-1948.
Schott, F.A., and McCreary, J.P., 2001, The monsoon circulation of the Indian Ocean: Progress In Oceanography, v. 51, p. 1-123.
Shen, G., Boyle, E., and Lea, D., 1987, Cadmium in corals as a tracer of historical upwelling and industrial fallout.
Shimamura, M., Hyeong, K., Yoo, C.M., Watanabe, T., Irino, T., and Jung, H.S., 2008, High resolution stable isotope records of sclreractinian corals near Ishigaki Island: Their implication as a potential paleoclimatic recorder in middle latitude regions: Geosciences Journal, v. 12, p. 25-31.
Silenzi, S., Bard, E., Montagna, P., and Antonioli, F., 2005, Isotopic and elemental records in a non-tropical coral (Cladocora caespitosa): Discovery of a new high-resolution climate archive for the Mediterranean Sea: Global and Planetary Change, v. 49, p. 94-120.
Spero, H.J., Bijma, J., Lea, D.W., and Bemis, B.E., 1997, Effect of seawater carbonate concentration on foraminiferal carbon and oxygen isotopes: Nature, v. 390, p. 497-500.
Sprintall, J., John, H.S., Karl, K.T., and Steve, A.T., 2009, Indonesian Throughflow, Encyclopedia of Ocean Sciences: Oxford, Academic Press, p. 237-243.
Sprintall, J., Potemra, J.T., Hautala, S.L., Bray, N.A., and Pandoe, W.W., 2003, Temperature and salinity variability in the exit passages of the Indonesian Throughflow: Deep Sea Research Part II: Topical Studies in Oceanography, v. 50, p. 2183-2204.
Srinivasan, M.S., and Sinha, D.K., 1998, Early Pliocene closing of the Indonesian Seaway: evidence from north-east Indian Ocean and Tropical Pacific deep sea cores: Journal of Asian Earth Sciences, v. 16, p. 29-44.
Stoll, H.M., and Schrag, D.P., 1998, Effects of Quaternary sea level cycles on strontium in seawater: Geochimica et Cosmochimica Acta, v. 62, p. 1107-1118.
Stott, L., Cannariato, K., Thunell, R., Haug, G.H., Koutavas, A., and Lund, S., 2004, Decline of surface temperature and salinity in the western tropical Pacific Ocean in the Holocene epoch: Nature, v. 431, p. 56-59.
Sun, D., Gagan, M.K., Cheng, H., Scott-Gagan, H., Dykoski, C.A., Edwards, R.L., and Su, R., 2005, Seasonal and interannual variability of the Mid-Holocene East Asian monsoon in coral $d^{18}O$ records from the South China Sea: Earth and Planetary Science Letters, v. 237, p. 69-84.
Swart, P.K., and Coleman, M.L., 1980, Isotopic data for scleractinian corals explain their palaeotemperature uncertainties.
Swart, P.K., Dodge, R.E., and Hudson, H.J., 1996, A 240-year stable oxygen and carbon isotopic record in a coral from south Florida: implications for the prediction of precipitation in southern Florida: Palaios, p. 362-375.
Tian, J., Pak, D.K., Wang, P., Lea, D., Cheng, X., and Zhao, Q., 2006, Late Pliocene monsoon linkage in the tropical South China Sea: Earth and Planetary Science Letters, v. 252, p. 72-81.
Tudhope, A.W., Chilcott, C.P., McCulloch, A.T., Cook, E.R., Chappell, J., Ellam, R.M., Lea, D.W., Lough, J.M., and Shimmield, G.B., 2001, Variability in the El Nino-Southern Oscillation Through a Glacial-Interglacial Cycle: Science, v. 291.
Tudhope, A.W., Shimmield, G.B., Chilcott, C.P., Jebb, M., Fallick, A.E., and Dalgleish, A.N., 1995, Recent changes in climate in the far western equatorial Pacific and their relationship to the Southern Oscillation; oxygen isotope records from massive corals, Papua New Guinea: Earth and Planetary Science Letters, v. 136, p. 575-590.
van Marle, L.J., 1991, Late Cenozoic palaeobathymetry and geohistory analysis of Central West Timor, eastern Indonesia: Marine and Petroleum Geology, v. 8, p. 22-34.
Veevers, J.J., Falvey, D.A., and Robins, S., 1978, Timor trough and australia: Facies show topographic wave migrated 80 km during the past 3 m.y: Tectonophysics, v. 45, p. 217-227.
Veron, J.E.N., 2000, Corals of the World: Townsville MC, Qld, Australia, Australian Institute of Marine Science.

Wang, C., 2002, Atmospheric circulation cells associated with the El Niño-Southern Oscillation: Journal of Climate, v. 15, p. 399-419.
Wara, M.W., Ravelo, A.C., and Delaney, M.G., 2005, Permanent El Nino-like Conditions During the Pliocene Warm Period: Science, v. 309, p. 758.
Watanabe, T., Gagan, M.K., Corrége, T., Scott-Gagan, H., Cowley, J., and Hantoro, W.S., 2003, Oxygen isotope systematics in Diploastrea heliopora: new coral archive of tropical paleoclimate: Geochimica et Cosmochimica Acta, v. 67, p. 1349-1358.
Watanabe, T., Suzuki, A., Minobe, S., Kawashima, T., Kameo, K., Minoshima, K., Aguilar, Y.M., Wani, R., Kawahata, H., and Sowa, K., 2011, Permanent El Nino during the Pliocene warm period not supported by coral evidence: Nature, v. 471, p. 209-211.
Watanabe, T., Winter, A., Oba, T., Anzai, R., and Ishioroshi, H., 2002, Evaluation of the fidelity of isotope records as an environmental proxy in the coral Montastraea: Coral Reefs, v. 21, p. 169-178.
Weber, J.N., and Woodhead, P.M.J., 1970, Carbon and oxygen isotope fractionation in the skeletal carbonate of reef-building corals: Chemical Geology, v. 6, p. 93-117.
Weber, J.N., and Woodhead, P.M.J., 1972, Temperature dependence of oxygen-18 concentration in reef coral carbonates: Journal of geophysical research, v. 77, p. 463-473.
Webster, P.J., and Yang, S., 1992, Monsoon and ENSO: Selectively interactive systems: Quarterly Journal of the Royal Meteorological Society, v. 118, p. 877-926.
Winter, A., Ishioroshi, H., Watanabe, T., Oba, T., and Christy, J., 2000, Caribbean sea surface temperatures: Two to three degrees cooler than present during the Little Ice Age: Geophysical Research Letters, v. 27, p. 3365-3368.
Woodhead, J., Hellstrom, J., Maas, R., Drysdale, R., Zanchetta, G., Devine, P., and Taylor, E., 2006, U-Pb geochronology of speleothems by MC-ICPMS: Quaternary Geochronology, v. 1, p. 208-221.
Wynn, J.G., 2004, Influence of Plio-Pleistocene aridification on human evolution: evidence from paleosols of the Turkana Basin, Kenya: American Journal of Physical Anthropology, v. 123, p. 106-118.
Zachos, J., Pagani, M., Sloan, L., Thomas, E., and Billups, K., 2001, Trends, rhythms, and aberrations in global climate 65 Ma to present: Science, v. 292, p. 686.

Appendix A: Diffractograms

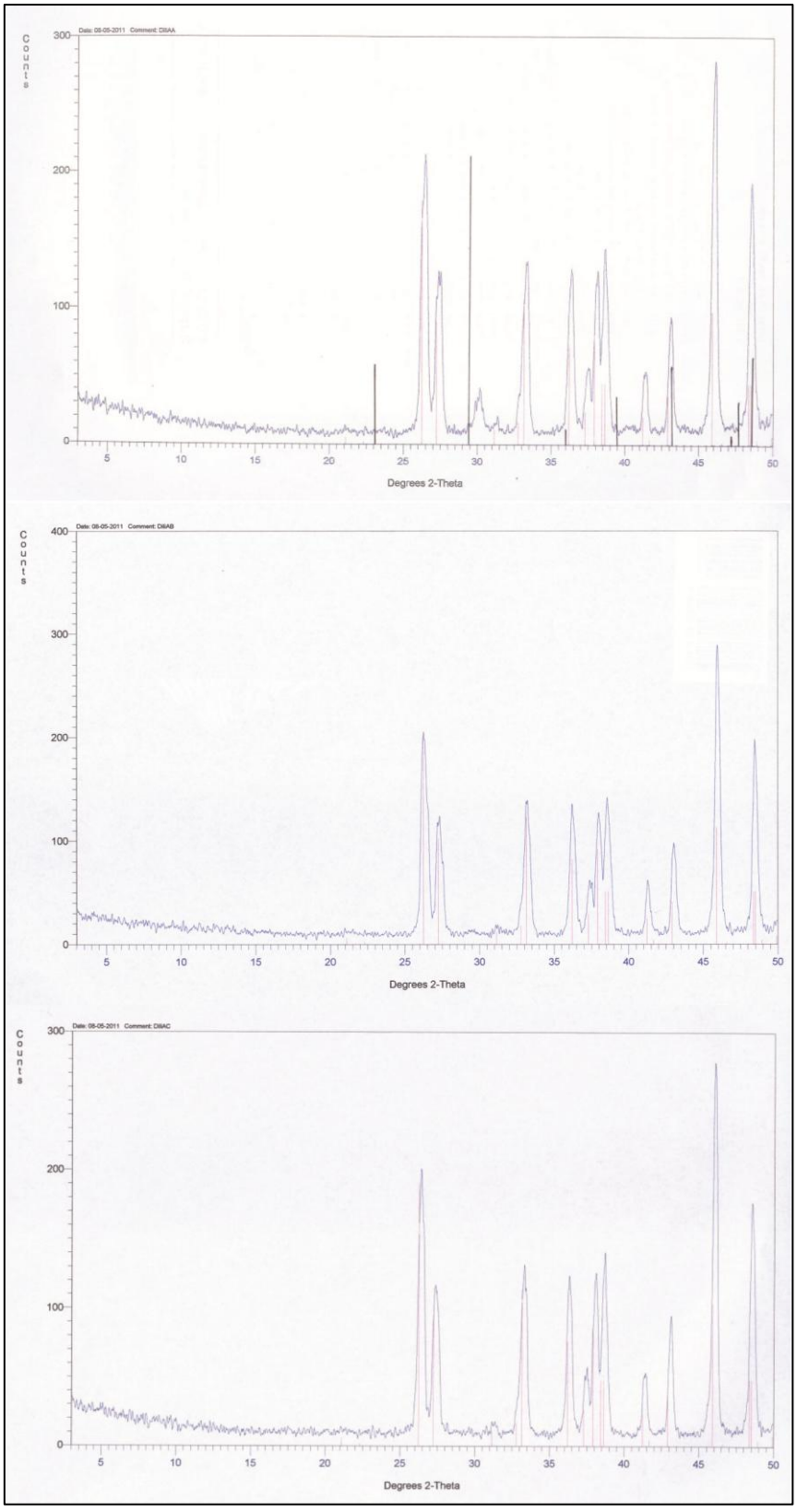

Appendix Figure 1 XRD diffractograms of *G. retiformis*. Samples from top to bottom: Dili A_A (with trace calcite), Dili A_B, Dili A_C. Aragonite shown in pink, calcite shown in black

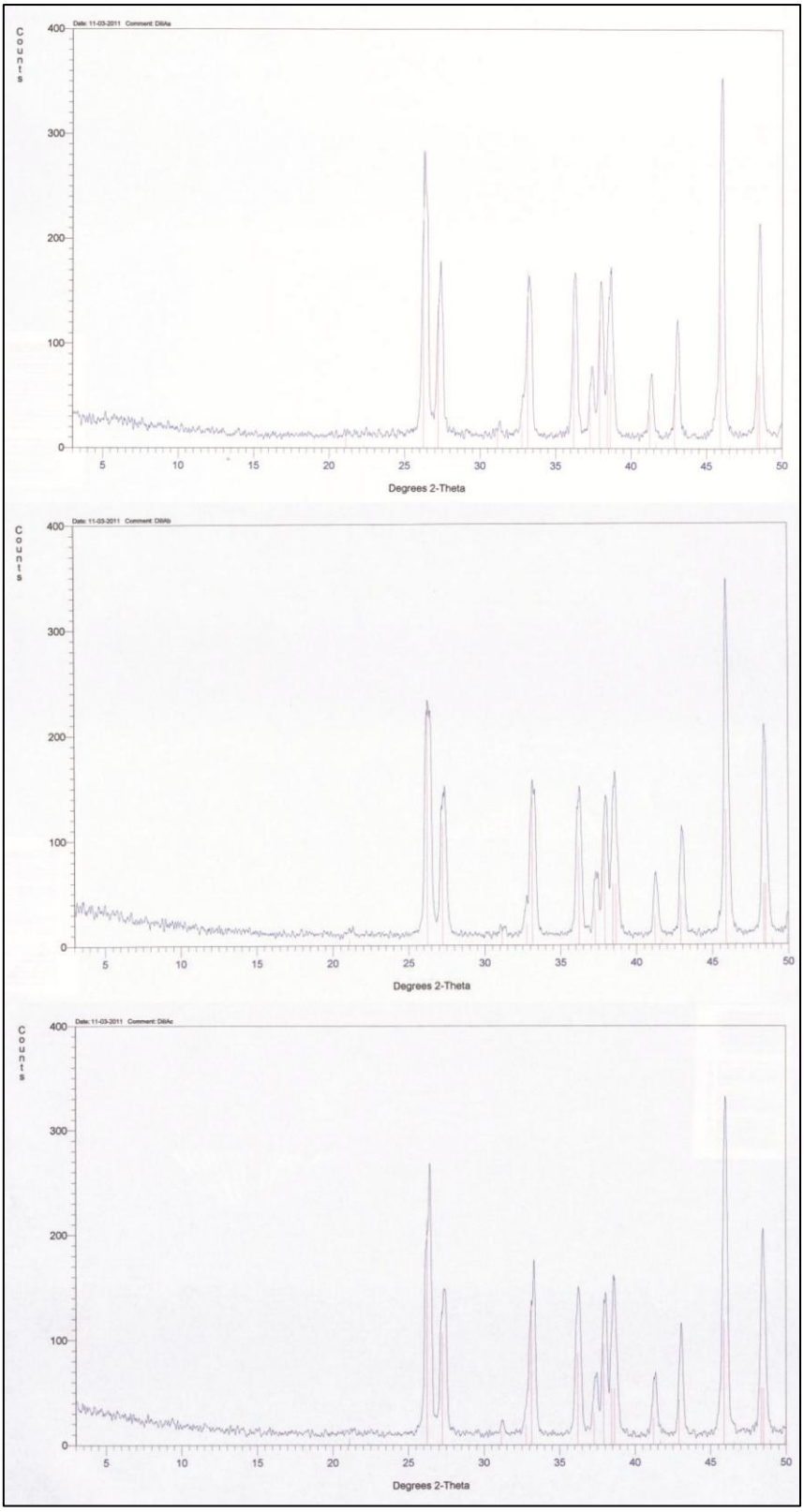

Appendix Figure 2 XRD diffractograms of *G. retiformis* with no trace calcite present (second run). Samples from top to bottom: Dili A_a, Dili A_b, Dili A_c.

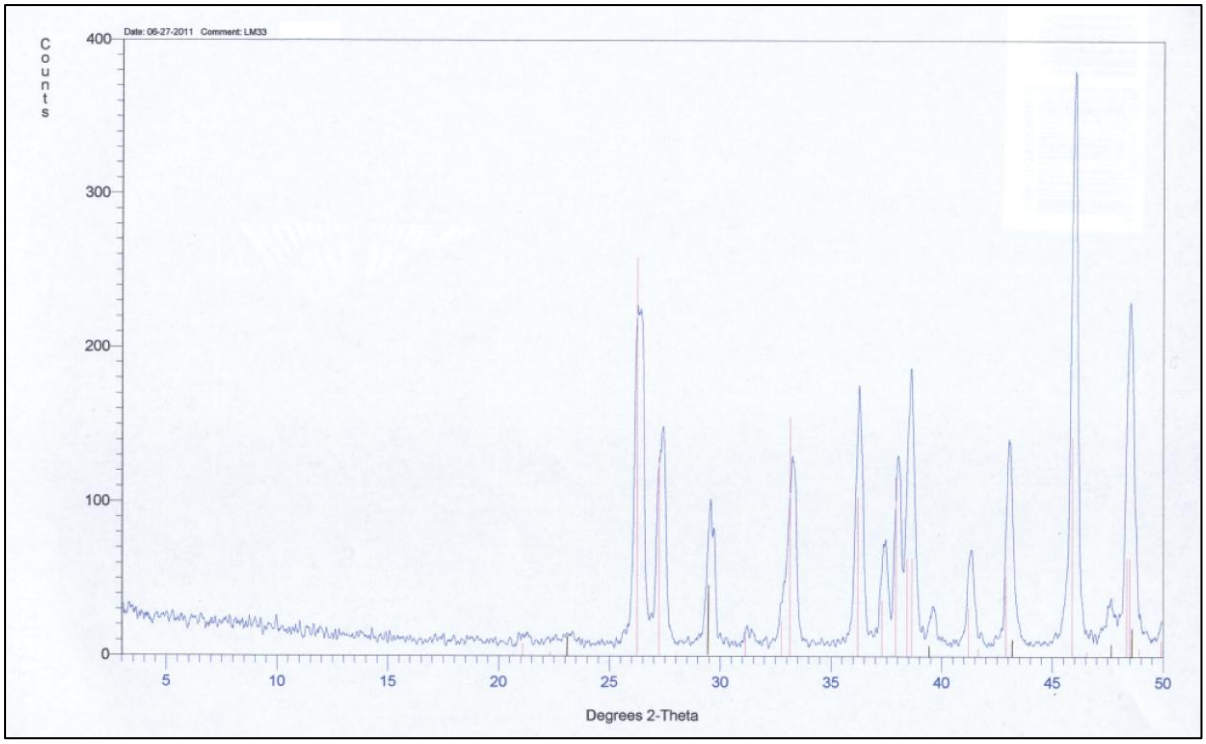

Appendix Figure 3 Preliminary XRD assessment of LM33. Aragonite shown in pink, calcite shown in black.

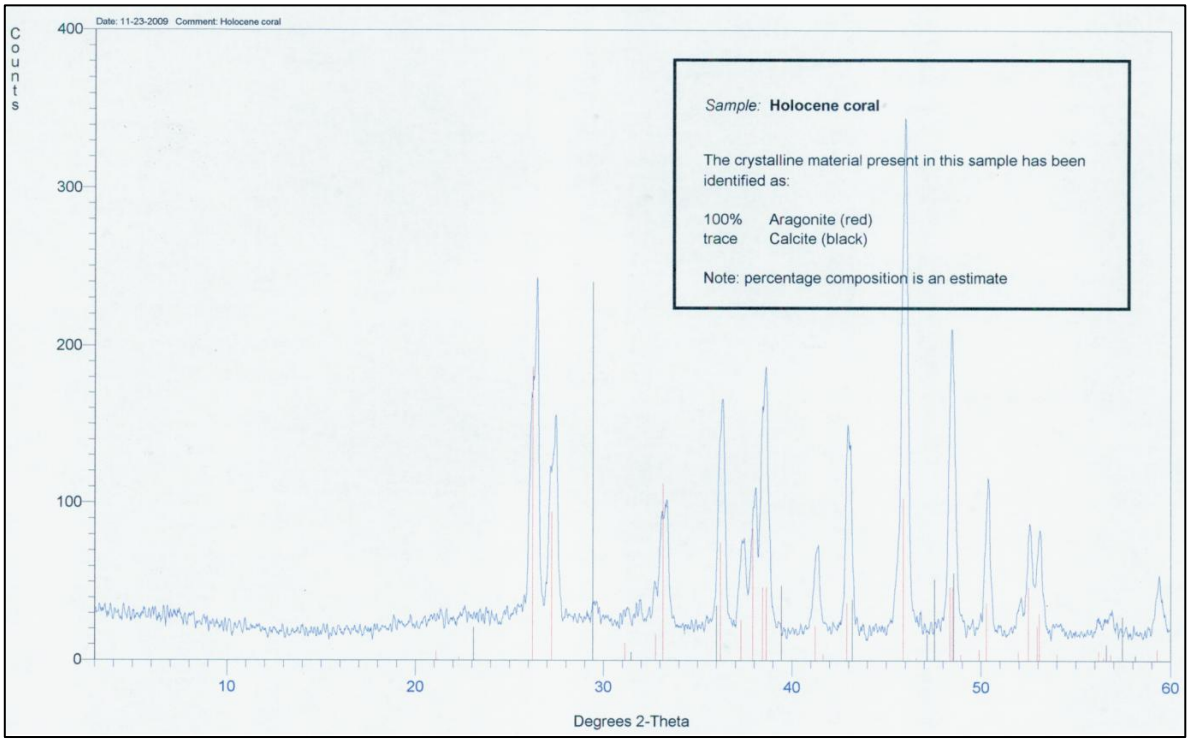

Appendix Figure 4 Preliminary XRD assessment of TL281. Aragonite shown in pink, calcite shown in black.

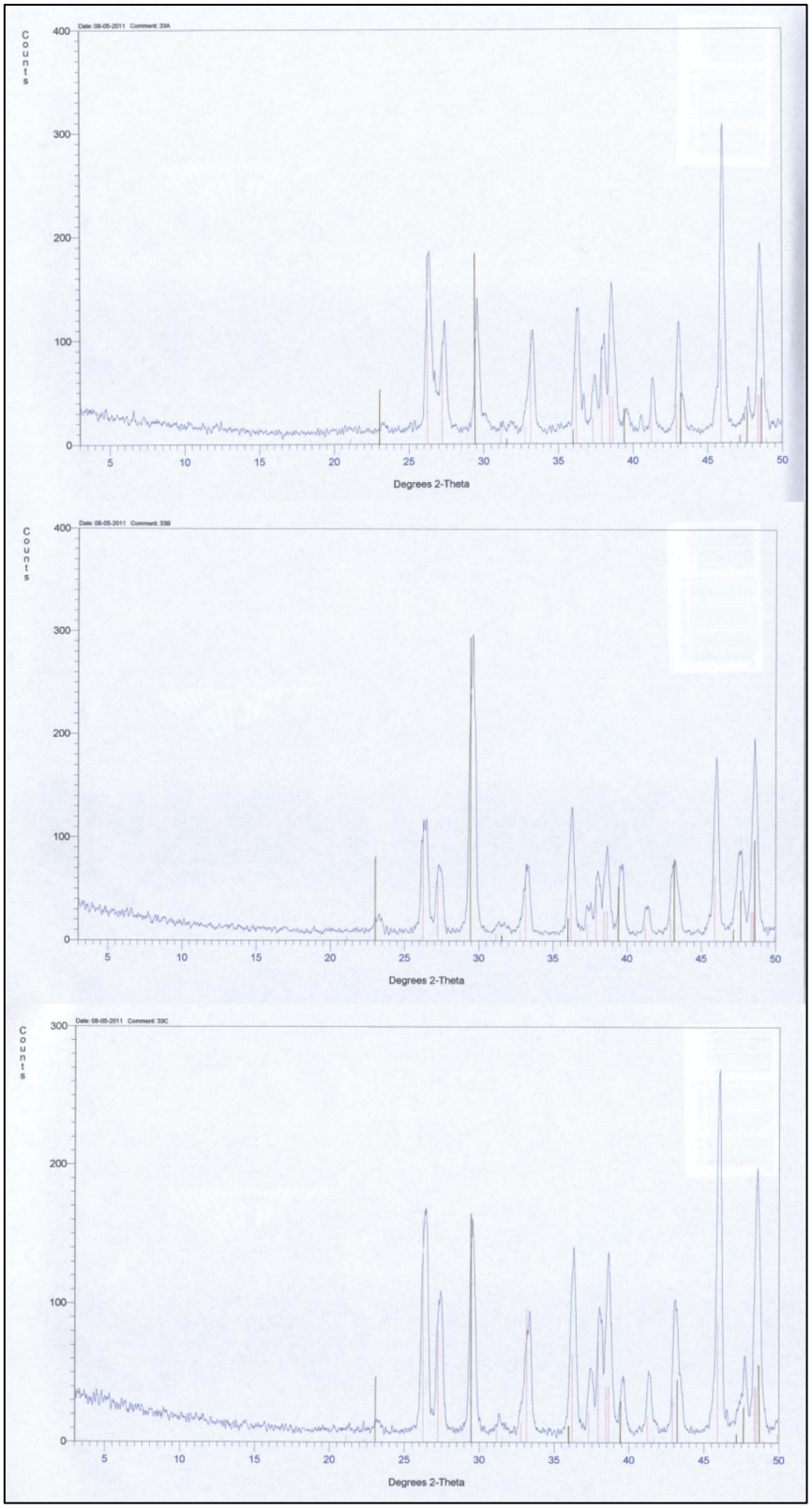

Appendix Figure 5 XRD diffractograms of LM33. Samples from top to bottom: LM33A, LM33B and LM331C. Aragonite shown in pink, calcite shown in black.

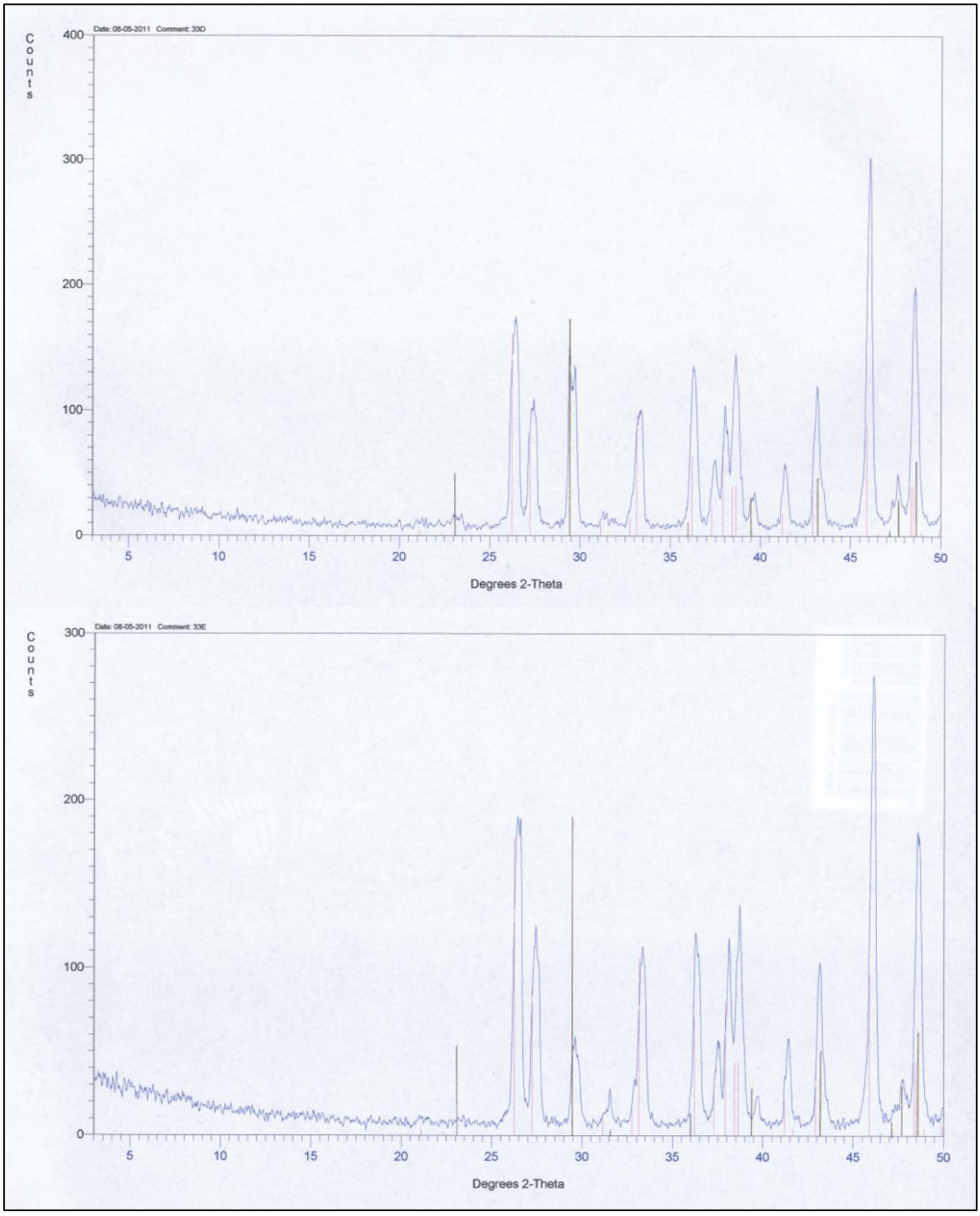

Appendix Figure 6 XRD diffractograms of LM33. Samples from top to bottom: LM33D and LM331E. Aragonite shown in pink, calcite shown in black.

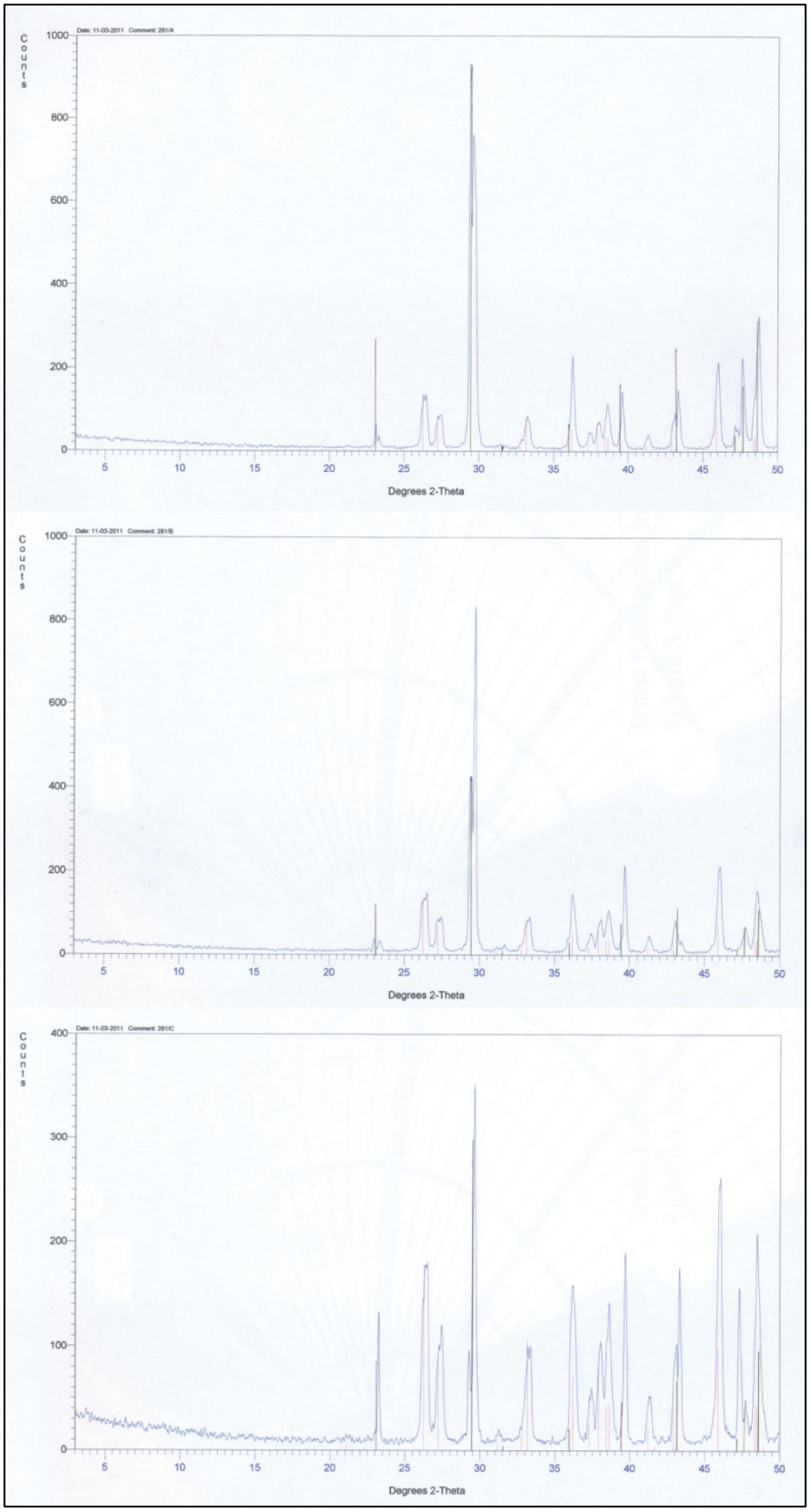

Appendix Figure 7 XRD diffractograms of TL281. Samples from top to bottom: TL281A, TL281B and TL281C. Aragonite shown in pink, calcite shown in black.

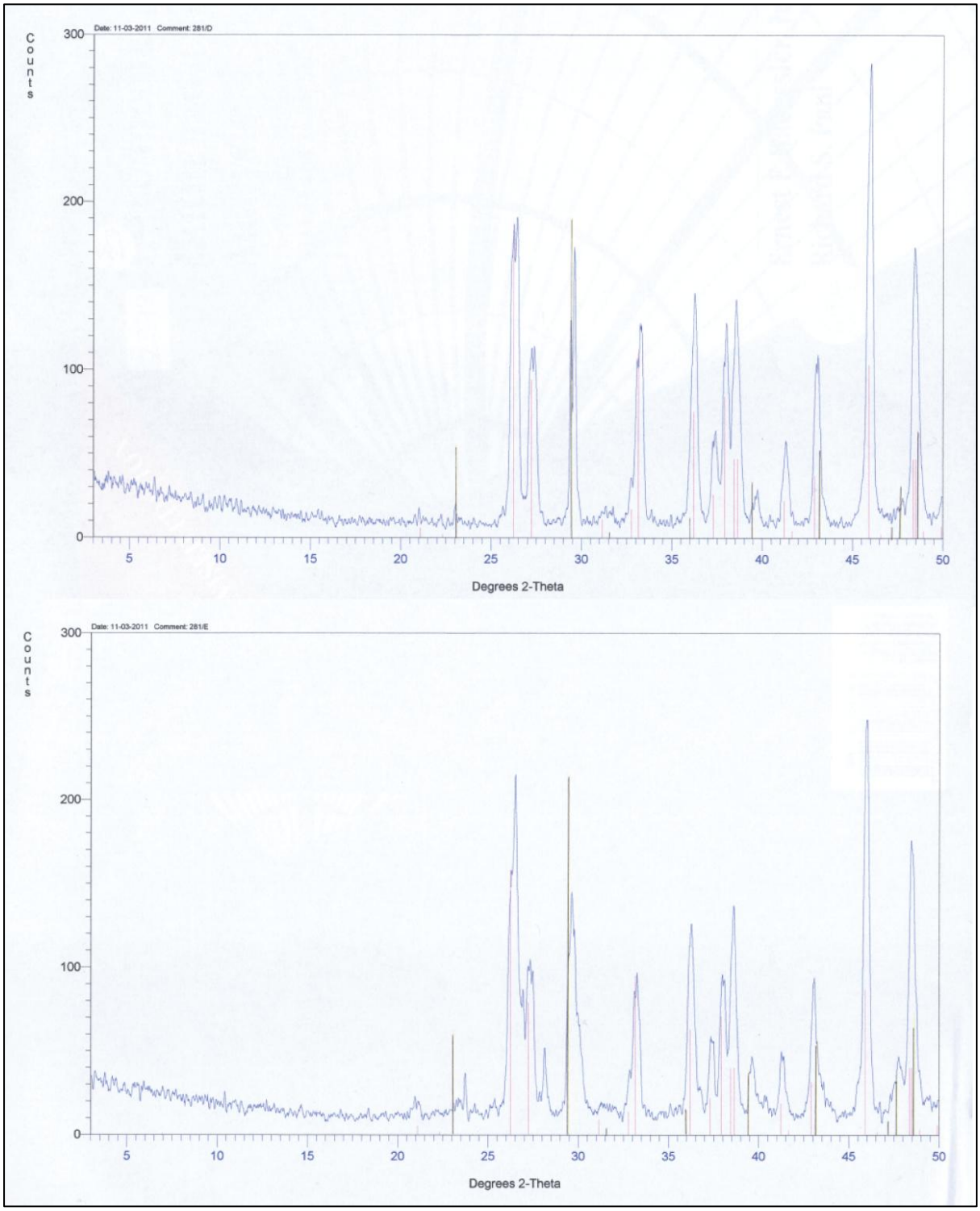

Appendix Figure 8 XRD diffractograms of TL281. Samples from top to bottom: TL281D and TL281E. Aragonite shown in pink, calcite shown in black.

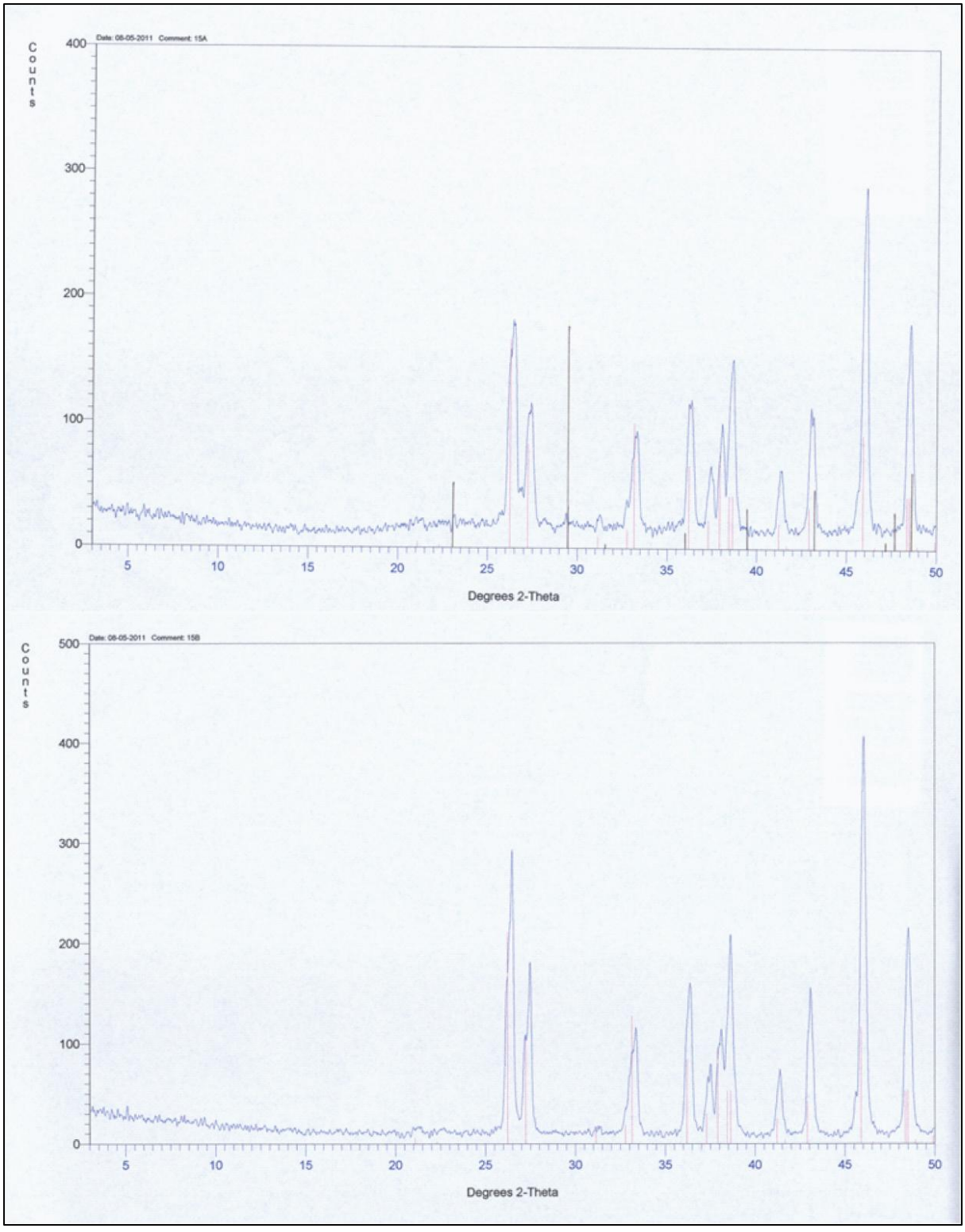

Appendix Figure 9 LM15A and LM15B XRD diffractograms, with trace calcite in LM15A shown by black lines

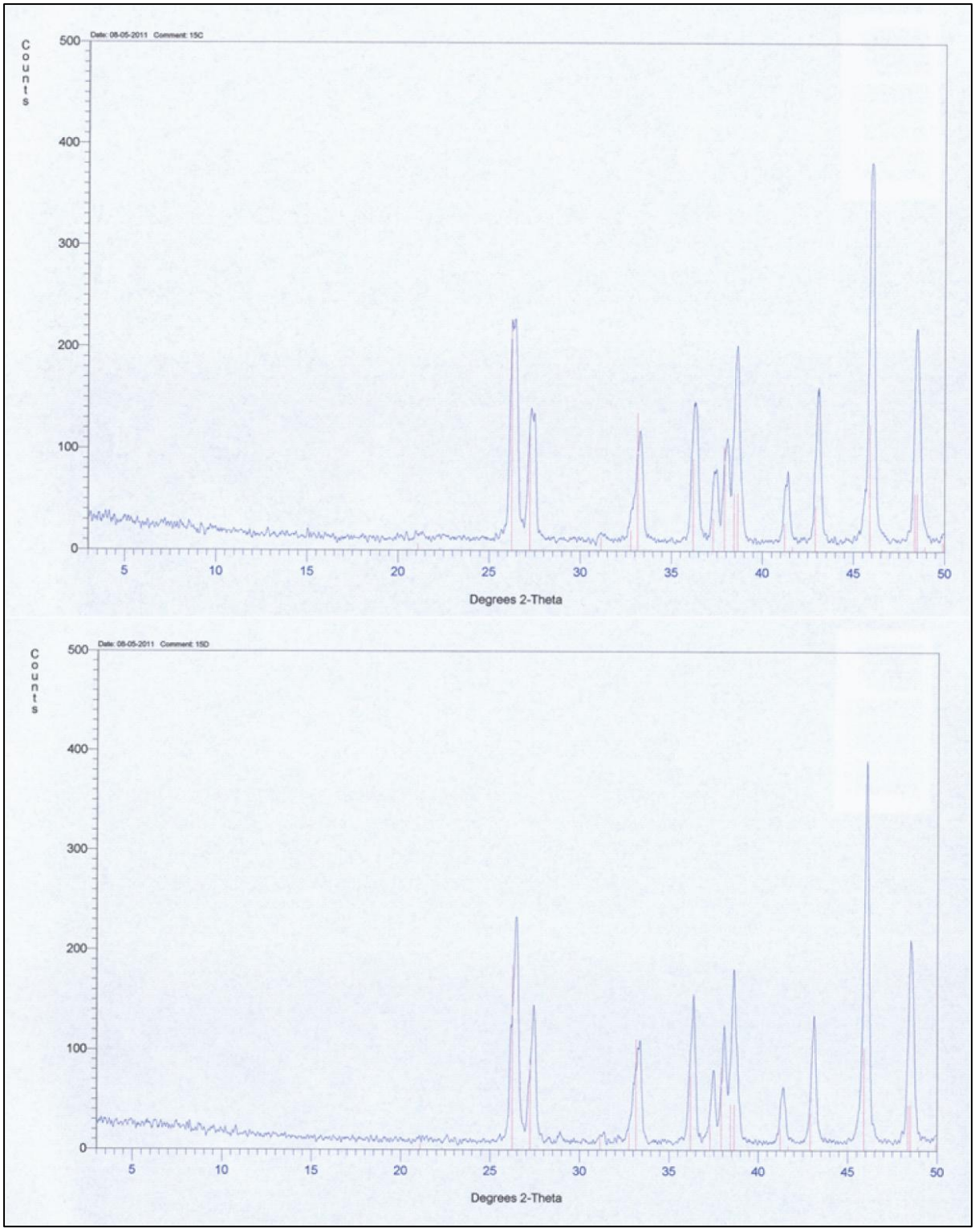

Appendix Figure 10 LM15C and LM15D XRD diffractograms

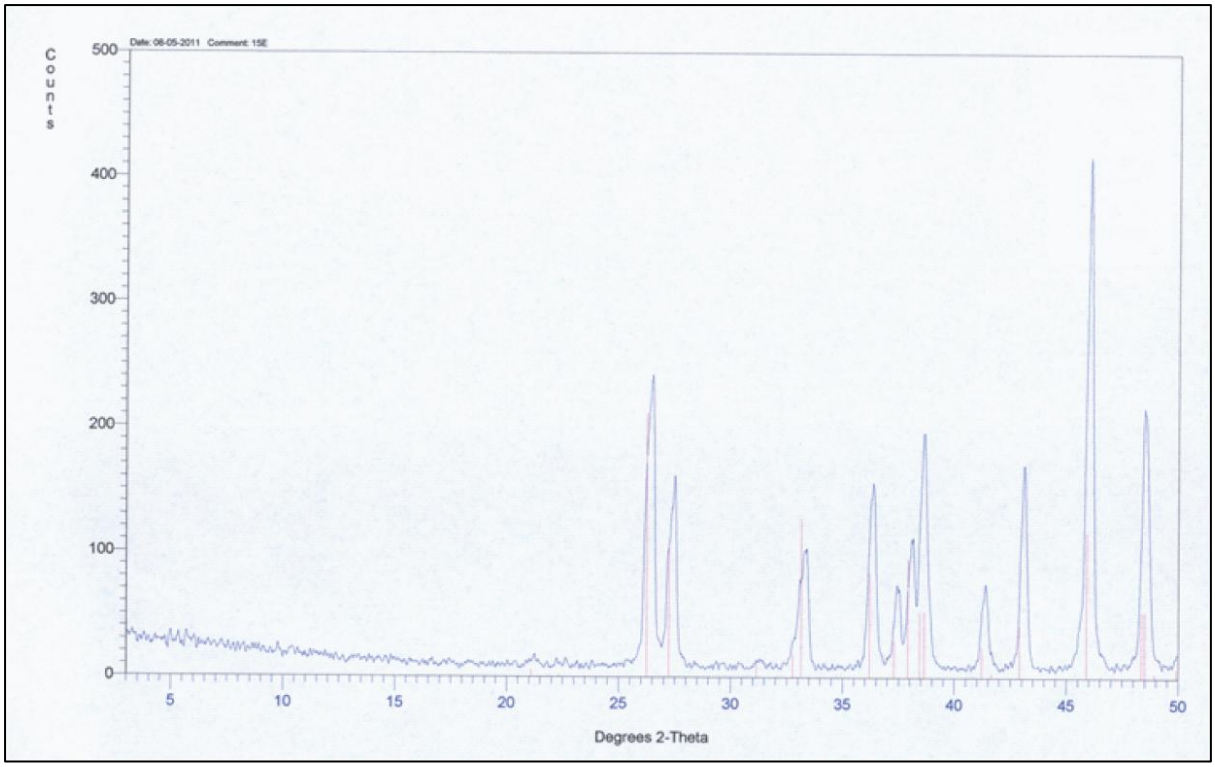

Appendix Figure 11 LM15E XRD diffractogram.

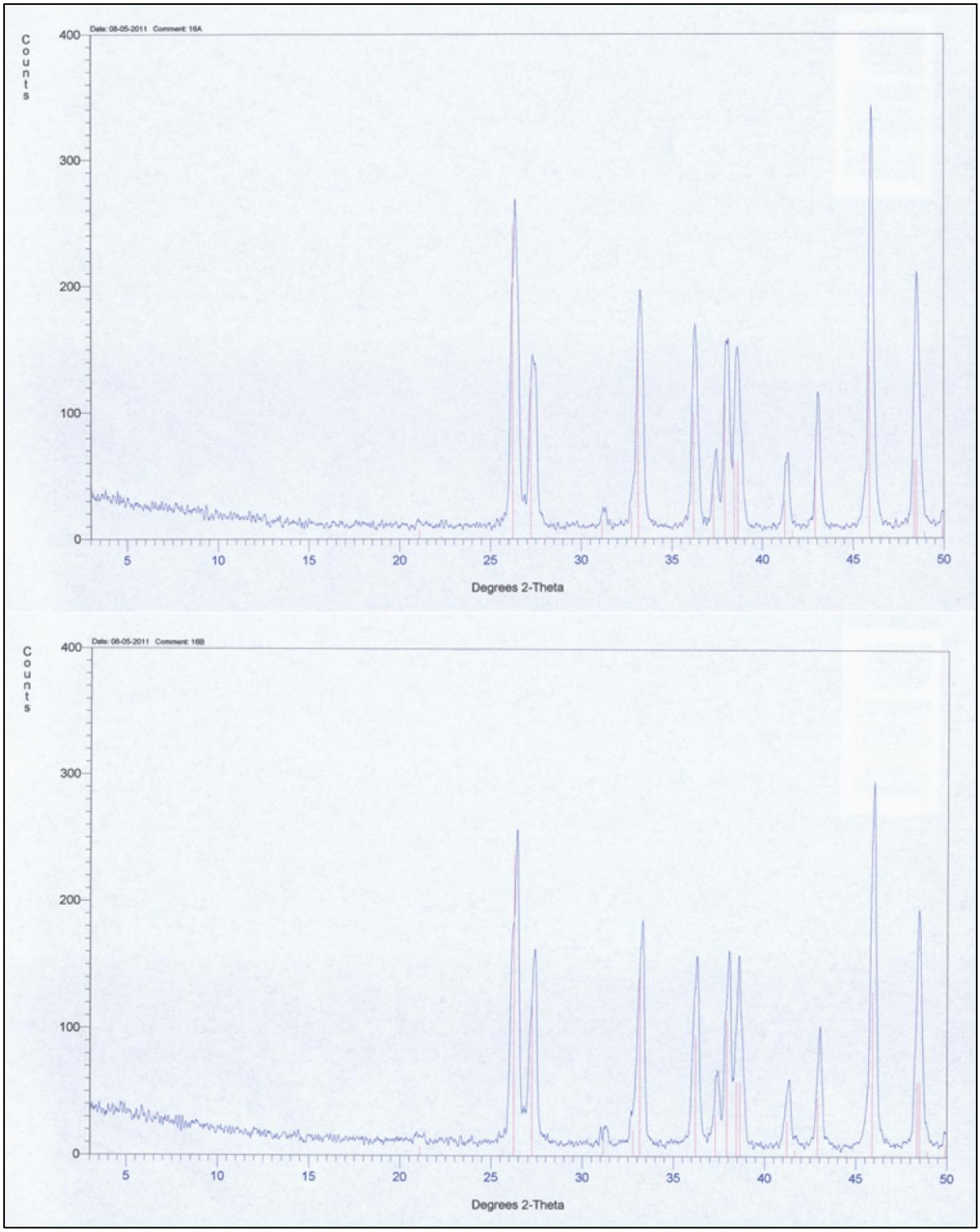

Appendix Figure 12 LM16A and LM16B XRD diffractograms.

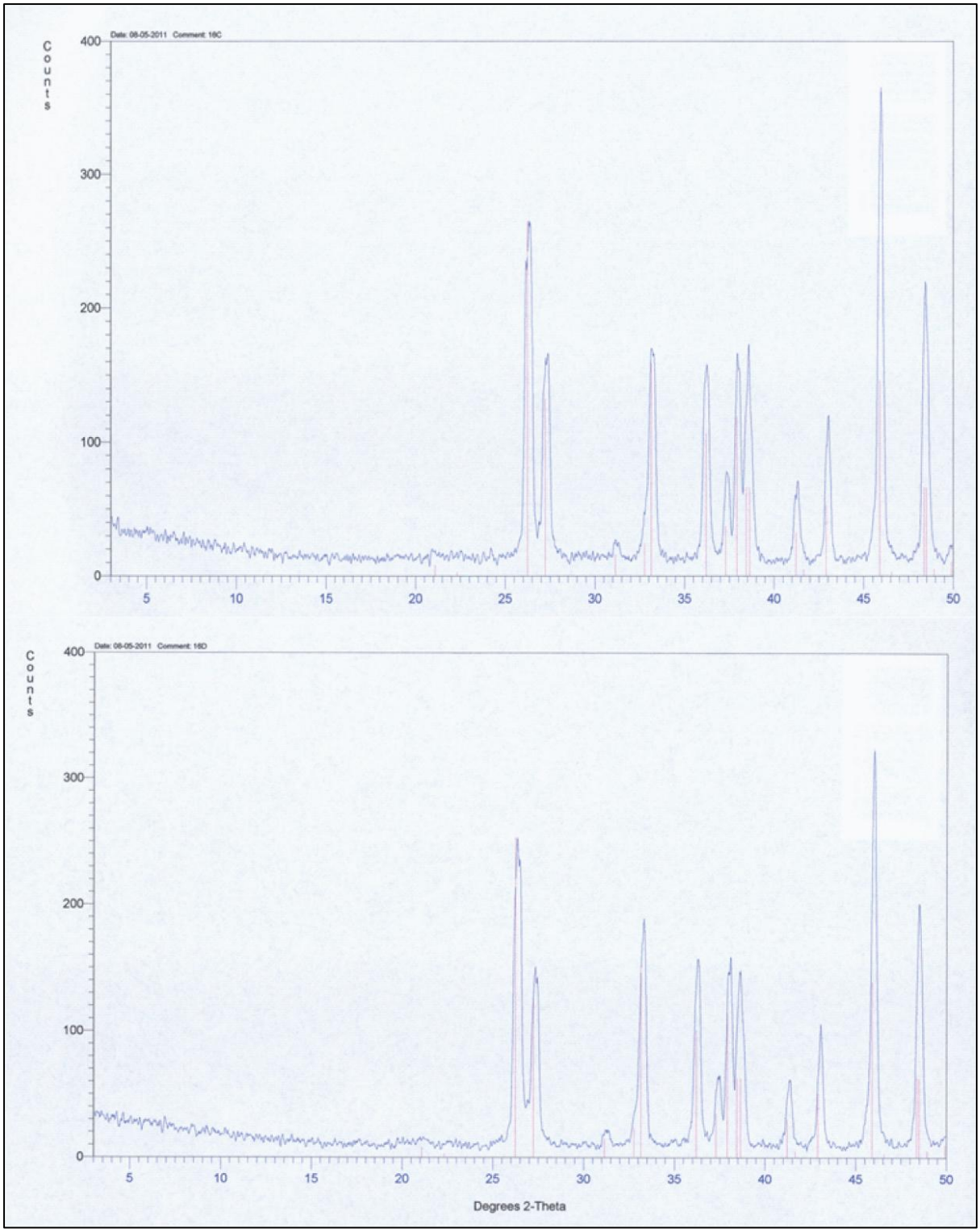

Appendix Figure 13 LM16C and LM16D XRD diffractograms.

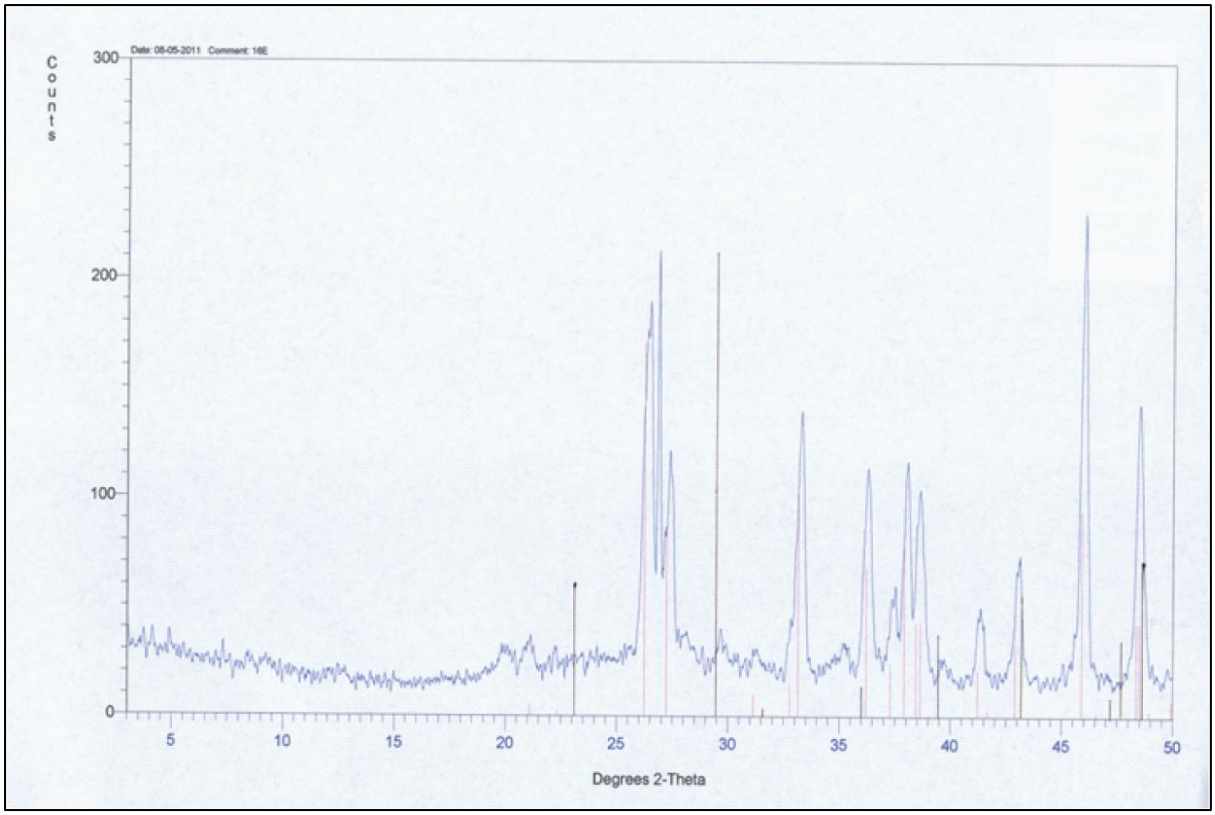

Appendix Figure 14 LM16E XRD diffractogram with trace calcite shown by black lines.

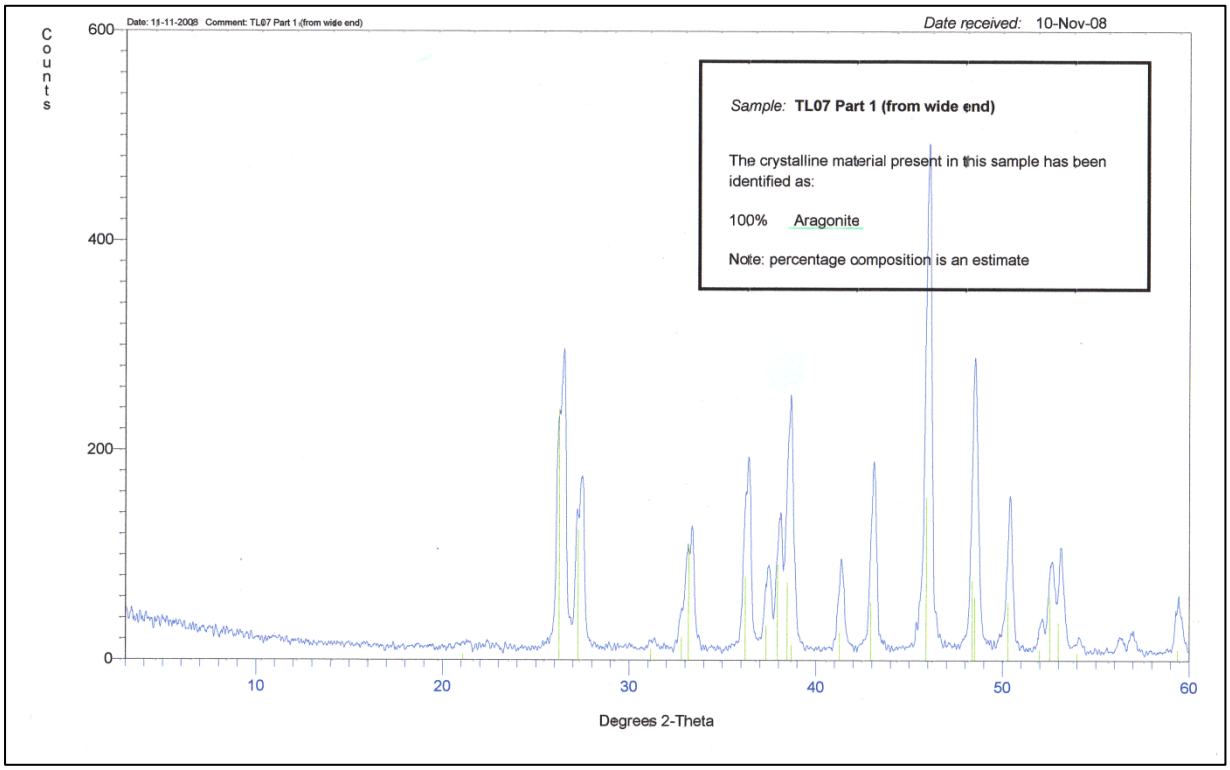

Appendix Figure 15 TL07 Part 1 XRD diffractogram.

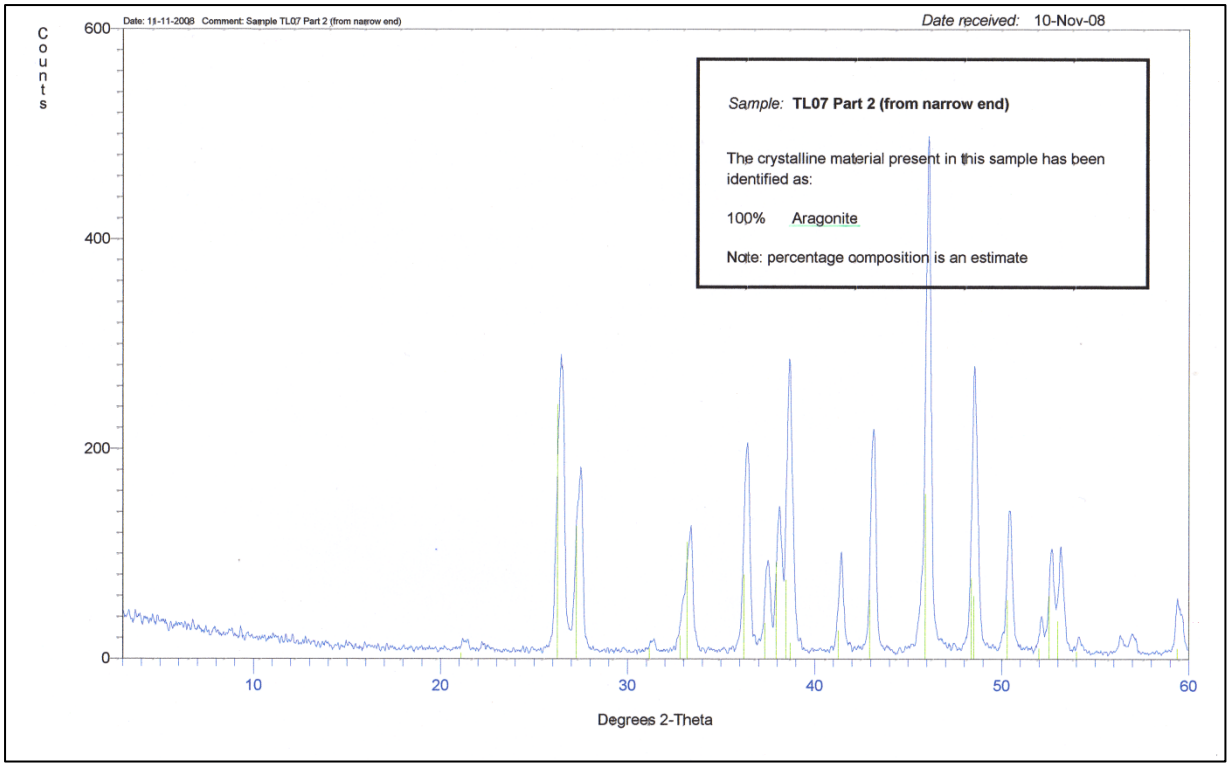

Appendix Figure 16 TL07 Part 2 XRD diffractogram.

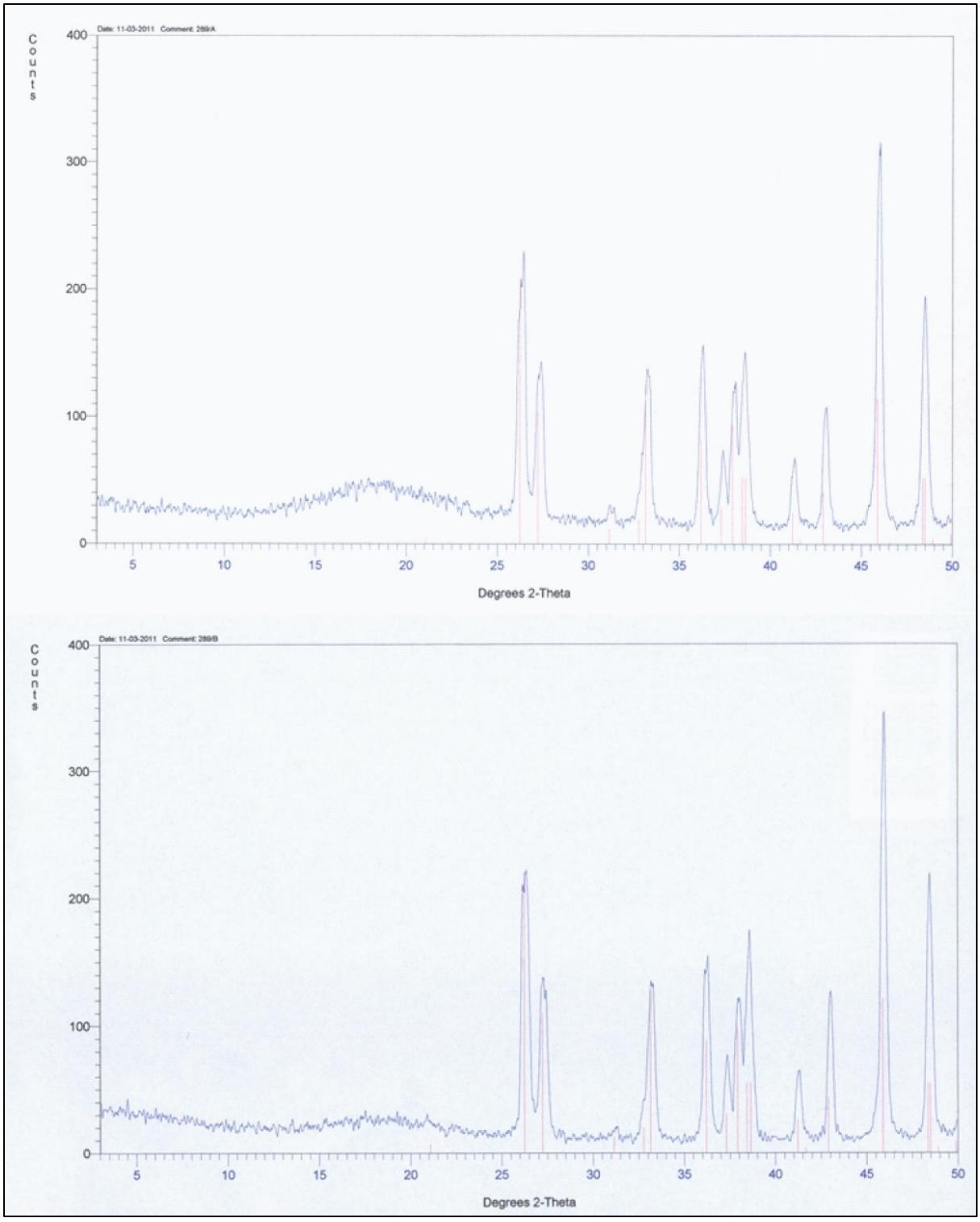

Appendix Figure 17 TL289A and TL289B XRD diffractograms.

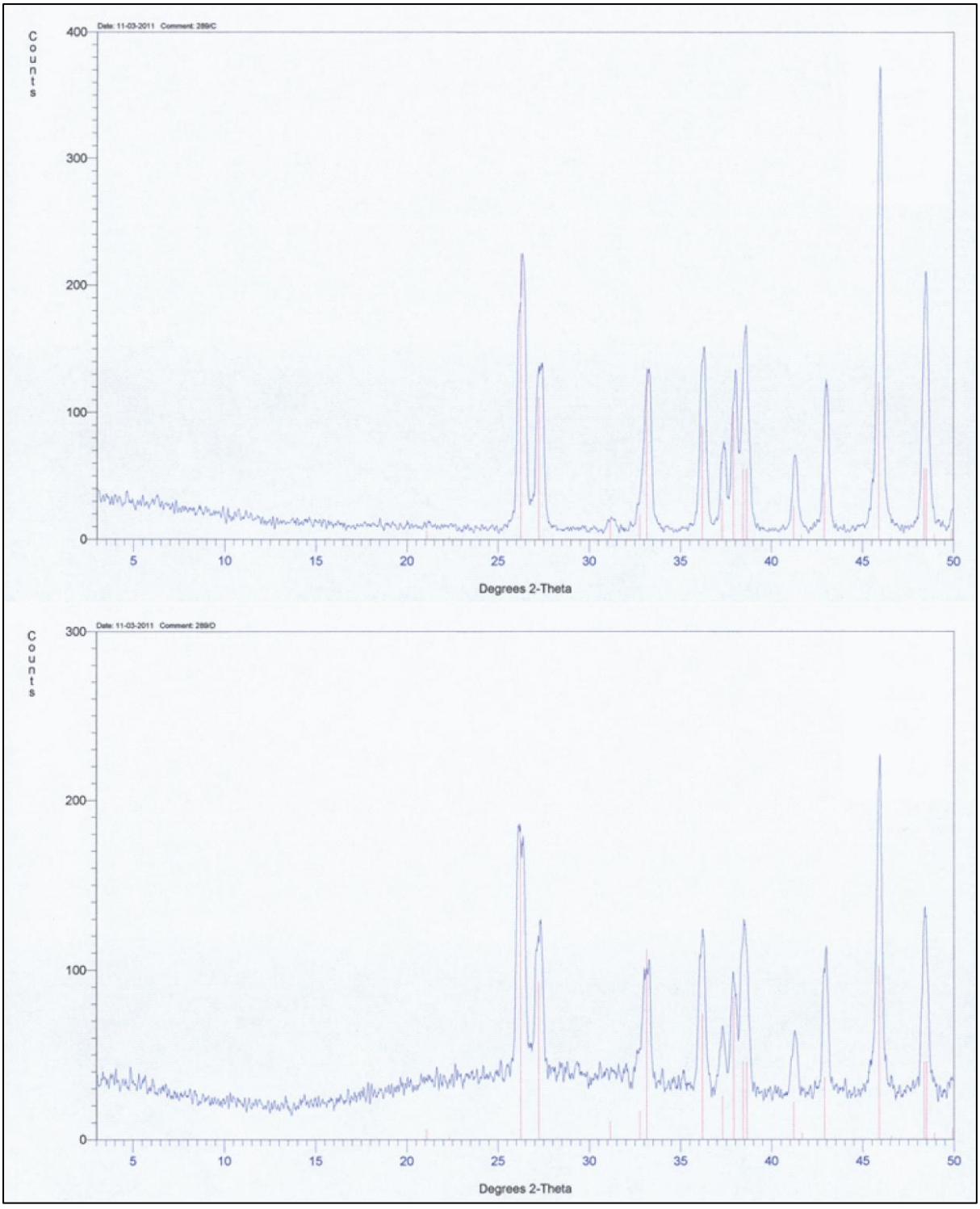

Appendix Figure 18 TL289C and TL289D XRD diffractograms.

Appendix B: Stable isotope results

Appendix Table 1 Raw isotopic data ($\delta^{18}O$ and $\delta^{13}C$) for *Goniastrea retiformis* coral, Dili A.

Sample	$\delta^{13}C$	$\delta^{18}O$	SA44[V]	ST44[V]	Balance	volt <1.0
0	-0.43	-5.36	2.67	3.00	0.89	
1	-0.52	-5.24	2.74	3.08	0.89	
2	-1.57	-5.53	1.30	1.38	0.94	
3	-1.32	-5.46	1.50	1.61	0.93	
4	-1.77	-5.63	1.51	1.63	0.93	
5	-1.59	-5.76	1.46	1.57	0.93	
6	-1.78	-5.62	2.88	3.29	0.88	
7	-1.41	-5.50	1.52	1.65	0.92	
8	-1.72	-5.68	1.93	2.12	0.91	
9	-1.76	-5.61	1.34	1.43	0.94	
10	-1.73	-5.72	2.33	2.59	0.90	
11	-1.38	-5.47	1.36	1.50	0.91	
12	-1.23	-5.57	1.27	1.36	0.94	
13	-1.22	-5.46	1.93	2.11	0.92	
14	-1.34	-5.50	1.38	1.53	0.90	
15	-1.36	-5.51	1.55	1.68	0.93	
16	-1.89	-5.45	1.38	1.48	0.93	
18	-1.69	-5.38	2.06	2.27	0.91	
19	-1.31	-5.27	1.42	1.70	0.84	
20	-1.53	-5.29	1.54	1.67	0.92	
21	-0.60	-5.32	2.31	2.56	0.90	
22	-1.67	-5.18	2.42	2.69	0.90	
23	-1.68	-5.43	2.24	2.49	0.90	
24	-0.66	-5.30	2.08	2.30	0.90	
25	-0.94	-5.21	2.42	2.70	0.89	
26	0.58	-4.98	2.89	3.30	0.88	
27	-0.28	-5.19	1.94	2.12	0.92	
28	-0.32	-5.18	1.65	1.80	0.92	
29	-0.21	-5.14	1.73	1.89	0.92	
30	-0.46	-5.21	1.41	1.51	0.93	
31	-0.20	-5.43	2.60	2.95	0.88	
32	-1.08	-5.26	2.02	2.23	0.91	
33	-1.14	-5.12	1.64	1.78	0.92	
34	-1.68	-5.35	2.04	2.24	0.91	
35	-1.20	-5.24	2.02	2.23	0.91	
36	0.70	1.90	0.13	0.36	0.35	-0.87
36	0.20	-4.90	1.04	1.09	0.95	repeat
37	-0.05	-5.19	1.54	1.88	0.82	
38	-0.66	-5.40	2.56	2.90	0.88	
39	-0.07	-5.18	2.42	2.70	0.90	
40	-0.70	-5.23	2.17	2.40	0.91	

Sample	$\delta^{13}C$	$\delta^{18}O$	SA44[V]	ST44[V]	Balance	volt <1.0
41	-0.74	-5.22	1.66	1.80	0.92	
42	-0.74	-5.31	1.22	1.30	0.94	
43	-0.98	-5.44	2.53	2.85	0.89	
44	-0.41	-5.11	1.22	1.30	0.94	repeat
44	-0.65	-5.04	0.40	0.45	0.90	-0.60
45	-1.96	-5.88	2.67	3.05	0.88	
46	-1.50	-5.99	2.42	2.73	0.89	
47	-0.92	-5.94	1.83	2.00	0.91	
48	-0.19	-5.40	1.41	1.51	0.93	
49	-1.03	-5.46	2.07	2.28	0.91	
50	-0.28	-5.65	1.83	2.00	0.91	
51	-2.00	-6.00	2.51	2.65	0.95	
52	-1.62	-5.96	1.67	1.72	0.97	
53	-2.48	-6.01	1.59	1.63	0.97	
54	-2.19	-6.11	1.50	1.54	0.98	
55	-2.21	-5.97	1.97	2.05	0.96	
56	-2.03	-5.97	1.82	1.88	0.96	
57	-2.02	-6.13	2.69	2.88	0.94	
59	-1.73	-6.04	2.01	2.09	0.96	
60	-1.41	-6.09	2.98	3.20	0.93	
62	-1.29	-6.06	2.27	2.39	0.95	
63	-1.07	-5.44	0.62	0.54	1.16	-0.38
64	-1.07	-5.44	0.59	0.54	1.11	-0.41
65	-0.51	-4.99	0.51	0.45	1.15	-0.59
67	-0.30	-4.62	0.44	0.37	1.20	-0.56
69	-0.79	-5.38	1.96	2.15	0.91	
70	-1.49	-5.51	2.71	3.06	0.89	
71	-1.49	-5.45	1.73	1.88	0.92	
72	-1.97	-5.48	1.38	1.48	0.93	
73	-2.28	-5.59	1.96	2.15	0.92	
74	-2.53	-5.82	1.52	1.64	0.93	
75	-2.14	-5.60	2.48	2.80	0.88	
76	-2.27	-5.54	2.10	2.35	0.89	
77	-1.97	-5.50	1.74	1.89	0.92	
78	-2.25	-5.45	1.69	1.84	0.92	
79	-2.46	-5.39	1.85	2.03	0.91	
80	-2.13	-5.51	1.44	1.54	0.93	
81	-1.73	-5.28	2.20	2.48	0.89	
82	-1.75	-5.34	2.26	2.52	0.90	
83	-2.20	-5.44	2.63	3.05	0.86	
84	-0.79	-5.16	2.94	3.34	0.88	
85	-0.45	-5.11	2.11	2.34	0.90	

Sample	$\delta^{13}C$	$\delta^{18}O$	SA44[V]	ST44[V]	Balance	volt <1.0
86	-0.24	-5.25	1.56	1.69	0.92	
87	1.21	-5.02	2.26	2.51	0.90	
88	0.76	-4.98	2.45	2.76	0.89	
89	1.57	-4.99	1.53	1.65	0.92	
90	1.17	-5.12	2.05	2.28	0.90	
91	0.85	-5.09	2.59	2.94	0.88	
92	0.72	-5.01	2.81	3.17	0.88	
93	1.10	-4.96	2.57	2.89	0.89	
94	0.19	-5.28	1.71	1.87	0.92	
95	0.08	-5.07	2.81	3.23	0.87	

All values reported relative to vPDB, where $\delta^{13}C$ has a value of +1.95‰ and $\delta^{18}O$ has a value of -2.20‰ for NBS19 calcite. Internal precision of measurements is 0.02-0.08‰ for $\delta^{18}O$ and 0.01-0.06‰ for $\delta^{13}C$, external precision is 0.03‰ for $\delta^{18}O$ and 0.02‰ for $\delta^{13}C$, relative to vPDB.

Appendix Table 2 Raw isotopic data ($\delta^{18}O$ and $\delta^{13}C$) for *Platygyra pini* coral, TL281.

Sample	$\delta^{13}C$	$\delta^{18}O$	SA44[V]	ST44[V]	Balance	volt <1.0
0	1.75	-4.25	2.28	2.38	0.96	
1	1.86	-4.07	1.21	1.21	1.00	
2	1.35	-4.74	1.82	1.88	0.97	
3	1.78	-4.80	2.30	2.41	0.96	
4	2.10	-4.32	2.59	2.73	0.95	
5	2.68	-3.80	1.65	1.60	1.03	
6	2.92	-3.99	2.78	2.94	0.95	
7	3.43	-3.47	2.11	2.32	0.91	
8	2.63	-3.94	1.52	1.55	0.98	
9	1.61	-4.65	1.64	1.70	0.96	
9	1.41	-4.75	2.96	3.34	0.89	repeat
10	3.04	-3.76	2.90	3.11	0.93	
11	2.89	-3.87	1.66	1.70	0.97	
12	2.49	-4.34	2.10	2.19	0.96	
13	2.48	-4.07	1.97	2.04	0.96	
14	2.07	-3.84	2.17	2.26	0.96	
15	0.89	-4.85	1.58	1.62	0.98	
16	0.87	-4.94	1.24	1.24	0.99	
17	1.28	-4.53	1.84	2.01	0.91	
18	2.80	-4.02	1.54	1.67	0.92	
19	2.47	-4.07	1.48	1.59	0.93	
20	3.13	-3.59	1.39	1.49	0.93	
21	3.10	-3.66	2.02	2.21	0.91	
22	3.10	-3.53	2.47	2.76	0.89	
23	2.25	-4.28	1.21	1.30	0.93	
23	2.52	-4.46	2.61	2.92	0.90	repeat
24	2.61	-4.15	1.58	1.70	0.92	
25	2.40	-4.50	2.25	2.48	0.91	
26	1.38	-4.28	1.83	2.00	0.91	
27	1.58	-4.32	1.36	1.46	0.93	
28	2.30	-4.32	2.09	2.31	0.91	
29	2.28	-4.38	1.38	1.49	0.93	
30	2.31	-4.72	1.72	1.87	0.92	
31	1.34	-4.92	1.92	2.10	0.91	
32	1.91	-4.65	1.63	1.77	0.92	
33	1.41	-4.81	1.25	1.33	0.94	
34	2.48	-4.92	2.32	2.56	0.90	
35	0.28	-4.93	2.61	2.98	0.88	

Sample	$\delta^{13}C$	$\delta^{18}O$	SA44[V]	ST44[V]	Balance	volt <1.0
36	0.55	-4.54	0.92	0.95	0.96	-0.08
37	-0.14	-4.74	1.31	1.41	0.93	
38	0.21	-4.83	2.21	2.46	0.90	
39	-0.15	-4.72	1.10	1.15	0.95	
40	0.28	-4.36	0.84	0.86	0.97	-0.16
41	2.05	-4.53	2.27	2.51	0.90	
42	1.19	-4.71	1.75	1.91	0.92	
43	1.25	-4.55	1.28	1.36	0.94	
44	1.50	-4.60	1.54	1.67	0.93	
45	1.43	-5.10	2.50	2.80	0.89	
46	0.56	-4.88	1.54	1.67	0.92	
47	1.08	-4.93	1.48	1.59	0.93	
48	1.08	-4.90	1.25	1.33	0.94	
49	0.71	-4.97	1.32	1.41	0.93	
50	1.16	-5.02	2.33	2.58	0.90	
51	0.64	-4.74	1.96	2.16	0.91	
52	-0.02	-4.85	2.54	2.82	0.90	
53	0.16	-4.94	2.23	2.47	0.90	
54	0.71	-4.59	1.55	1.67	0.93	
55	1.32	-4.70	2.64	3.01	0.88	
56	2.28	-4.43	2.29	2.54	0.90	
57	1.48	-4.60	1.47	1.58	0.93	
58	1.42	-4.55	1.27	1.35	0.94	
59	0.82	-5.01	1.46	1.57	0.93	
60	0.64	-4.89	1.27	1.35	0.94	
61	0.54	-4.86	1.31	1.40	0.93	
62	1.08	-4.82	1.29	1.38	0.93	
63	0.91	-4.86	1.44	1.55	0.93	
64	0.77	-5.00	1.60	1.73	0.92	
65	1.63	-4.70	1.81	1.98	0.92	
66	1.39	-4.63	1.26	1.34	0.94	
67	1.03	-4.84	1.21	1.29	0.94	
68	0.89	-4.78	1.91	2.10	0.91	
69	0.93	-4.74	1.74	1.89	0.92	
70	0.63	-4.88	1.65	1.79	0.92	
71	0.61	-4.71	1.44	1.55	0.93	
72	0.78	-4.78	2.44	2.73	0.89	
73	0.55	-4.93	2.30	2.55	0.90	
74	0.50	-4.91	2.26	2.50	0.90	

Sample	$\delta^{13}C$	$\delta^{18}O$	SA44[V]	ST44[V]	Balance	volt <1.0
75	0.96	-4.72	1.34	1.43	0.93	
76	0.94	-4.86	2.65	2.97	0.89	
77	0.33	-4.89	2.48	2.77	0.90	
78	1.10	-4.71	2.81	3.15	0.89	
79	0.77	-4.65	1.54	1.68	0.91	
80	1.77	-4.56	2.67	2.98	0.89	
81	1.36	-4.74	1.59	1.72	0.92	
82	1.36	-4.69	1.59	1.72	0.92	
83	1.16	-4.69	1.83	2.00	0.91	
84	1.25	-4.79	2.21	2.44	0.91	
85	0.90	-5.00	1.44	1.55	0.93	
86	0.89	-4.68	1.22	1.30	0.94	
87	0.66	-4.98	2.71	3.03	0.89	
88	1.44	-4.87	2.08	2.28	0.91	
89	0.65	-5.03	1.55	1.67	0.92	
90	0.42	-5.12	1.26	1.34	0.94	
91	1.05	-5.08	2.12	2.33	0.91	
92	0.65	-5.27	1.55	1.68	0.93	
93	0.32	-5.17	2.02	2.22	0.91	
94	0.46	-5.29	1.91	2.09	0.91	
95	0.63	-5.06	1.72	1.87	0.92	
96	-0.19	-5.19	1.66	1.80	0.92	
97	-0.22	-5.12	1.34	1.44	0.93	
98	-0.10	-5.23	1.25	1.33	0.94	
99	-0.42	-5.27	1.57	1.70	0.92	
100	-0.49	-5.45	2.60	2.92	0.89	
101	-0.12	-5.12	2.10	2.31	0.91	
102	-0.29	-5.25	1.60	1.74	0.92	
103	-0.36	-5.11	1.63	1.77	0.92	
104	0.41	-5.11	1.51	1.63	0.93	
105	-0.15	-5.04	2.02	2.22	0.91	
106	0.16	-4.94	2.57	2.87	0.90	
107	0.60	-4.88	2.65	2.97	0.89	
108	0.66	-4.89	1.70	1.84	0.92	
109	0.92	-5.05	1.47	1.61	0.91	
110	0.79	-4.89	2.36	2.62	0.90	
111	0.62	-4.81	1.38	1.48	0.93	
112	1.31	-4.89	1.32	1.41	0.94	
113	1.36	-4.95	2.89	3.25	0.89	
114	0.22	-5.19	1.44	1.55	0.93	

Sample	$\delta^{13}C$	$\delta^{18}O$	SA44[V]	ST44[V]	Balance	volt <1.0
115	0.38	-5.37	1.57	1.70	0.92	
116	0.24	-5.23	1.82	1.99	0.91	
117	0.33	-5.32	2.29	2.53	0.91	
118	-0.08	-5.19	1.59	1.74	0.92	
119	0.94	-5.05	1.16	1.23	0.94	
120	0.86	-5.29	2.62	2.92	0.90	
121	1.21	-5.08	2.85	3.20	0.89	
122	0.83	-5.18	2.86	3.21	0.89	
123	0.89	-5.25	2.85	3.20	0.89	
124	0.91	-5.15	1.29	1.38	0.94	
125	0.83	-4.93	1.57	1.70	0.92	
126	0.80	-5.32	1.99	2.19	0.91	
127	1.04	-5.17	1.33	1.42	0.94	
128	1.01	-5.38	2.33	2.59	0.90	
129	0.95	-5.15	2.45	2.73	0.90	
130	0.27	-5.26	1.87	2.05	0.91	
131	1.29	-5.10	2.66	2.98	0.89	
132	1.37	-5.19	1.48	1.59	0.93	
133	2.04	-4.69	2.31	2.56	0.90	
133	1.98	-4.76	1.96	2.15	0.91	repeat
134	1.67	-4.89	2.63	2.94	0.89	
135	1.33	-5.17	1.55	1.68	0.92	
136	1.35	-5.19	3.01	3.41	0.88	
137	1.06	-5.10	2.44	2.99	0.81	
138	1.03	-5.07	0.88	0.91	0.97	-0.12
139	0.76	-5.44	2.05	2.26	0.91	
140	0.66	-5.32	1.56	1.73	0.90	
141	0.59	-5.40	1.53	1.65	0.93	
142	1.04	-5.31	1.48	1.60	0.93	
143	1.39	-5.33	2.31	2.56	0.90	
144	0.86	-5.36	2.00	2.19	0.91	
145	0.60	-5.25	2.49	2.78	0.90	
146	0.56	-5.31	1.65	1.79	0.92	
147	0.45	-5.12	1.58	1.72	0.92	
148	1.40	-4.99	1.43	1.54	0.93	
149	0.39	-5.16	1.56	1.69	0.92	
150	1.14	-5.12	2.12	2.34	0.91	
151	1.48	-4.98	2.81	3.16	0.89	
152	1.15	-4.98	1.43	1.54	0.93	
153	0.93	-4.94	1.26	1.34	0.94	

Sample	$\delta^{13}C$	$\delta^{18}O$	SA44[V]	ST44[V]	Balance	volt <1.0
154	1.15	-5.30	1.84	2.01	0.92	
155	0.91	-5.13	2.15	2.37	0.91	
156	0.60	-5.05	1.71	1.86	0.92	
157	0.50	-4.99	1.65	1.81	0.92	
158	0.62	-4.94	1.54	1.66	0.93	
159	0.29	-5.24	2.60	2.90	0.90	
160	0.75	-4.85	1.14	1.21	0.95	
161	1.96	-4.72	1.86	2.03	0.92	

All values reported relative to vPDB, where $\delta^{13}C$ has a value of +1.95‰ and $\delta^{18}O$ has a value of -2.20‰ for NBS19 calcite. Internal precision of measurements is 0.02-0.08‰ for $\delta^{18}O$ and 0.01-0.06‰ for $\delta^{13}C$, external precision is 0.03‰ for $\delta^{18}O$ and 0.02‰ for $\delta^{13}C$, relative to vPDB.

Appendix Table 3 Raw stable isotope ($\delta^{18}O$ and $\delta^{13}C$) data for *Platygyra lamellina*, coral TL289.

Sample	$\delta^{13}C$	$\delta^{18}O$	SA44[V]	ST44[V]	Balance	volt <1.0
0	0.07	-4.90	2.42	2.70	0.90	
1	-0.21	-5.23	1.56	1.69	0.92	
2	0.13	-5.07	2.00	2.19	0.91	
3	0.12	-5.19	1.82	1.98	0.92	
4	0.50	-5.00	1.45	1.56	0.93	
5	0.37	-4.92	3.16	3.65	0.87	
6	0.08	-4.85	1.79	1.95	0.92	
7	-0.68	-4.95	2.16	2.40	0.90	
8	-0.60	-5.08	2.39	2.68	0.89	
9	-0.82	-5.12	2.39	2.70	0.88	
10	-0.46	-5.11	2.47	2.75	0.90	
11	-0.47	-4.96	2.19	2.42	0.90	
12	-0.52	-5.09	2.78	3.14	0.89	
13	-0.82	-5.12	2.11	2.33	0.91	
14	-0.74	-5.26	1.92	2.12	0.90	
15	-0.51	-3.96	0.62	0.60	1.04	-0.38
16	-0.75	-5.25	2.64	3.02	0.88	
17	-0.30	-5.10	2.79	3.15	0.88	
18	-0.86	-5.21	2.40	2.72	0.88	
19	-0.68	-5.06	2.74	3.13	0.87	
20	-0.54	-5.30	1.79	1.96	0.91	
21	-0.40	-5.03	2.48	2.82	0.88	
22	-0.44	-5.17	1.74	1.89	0.92	
23	-0.35	-5.23	1.81	2.00	0.90	
24	-0.32	-5.13	2.35	2.62	0.90	
25	-0.54	-5.16	2.28	2.53	0.90	
26	-0.42	-5.31	1.76	1.92	0.92	
27	-0.32	-5.06	1.70	1.85	0.92	
28	-0.64	-5.15	1.50	1.62	0.93	
29	-0.35	-5.18	1.74	1.90	0.92	
30	-0.32	-5.05	1.91	2.09	0.91	
31	-0.54	-5.12	2.77	3.18	0.87	
32	-0.51	-5.09	1.84	2.02	0.91	
33	-0.14	-4.87	1.58	1.71	0.92	
34	-0.65	-5.06	1.60	1.73	0.92	
35	-0.43	-5.08	1.95	2.14	0.91	
36	-0.32	-5.03	2.32	2.58	0.90	
37	-0.24	-5.06	3.02	3.47	0.87	
38	-0.36	-5.04	1.78	1.96	0.91	
39	-0.49	-5.12	1.46	1.58	0.93	
40	-0.45	-4.75	1.64	1.78	0.92	
41	-0.60	-5.15	2.26	2.55	0.88	

Sample	$\delta^{13}C$	$\delta^{18}O$	SA44[V]	ST44[V]	Balance	volt <1.0
42	-0.82	-5.24	1.64	1.78	0.92	
43	-0.66	-5.15	1.98	2.17	0.91	
44	-0.80	-5.09	1.97	2.17	0.91	
45	-0.74	-5.30	1.86	2.04	0.91	
46	-0.58	-5.08	2.54	2.88	0.88	
47	-0.65	-5.09	2.64	3.00	0.88	
48	-0.87	-5.23	1.87	2.07	0.90	
49	-0.90	-5.39	1.87	2.06	0.91	
50	-0.71	-5.23	2.50	2.79	0.89	
51	-0.60	-5.21	2.15	2.39	0.90	
52	-0.74	-5.32	2.79	3.17	0.88	
53	-0.68	-5.12	1.92	2.13	0.90	
54	-0.53	-5.24	2.69	3.05	0.88	
55	-0.72	-5.08	2.42	2.71	0.89	
56	-0.81	-5.31	2.02	2.28	0.89	
57	-0.58	-5.12	1.97	2.16	0.91	
58	-0.27	-5.12	2.04	2.25	0.91	
59	-0.65	-5.32	2.09	2.31	0.90	
60	-0.42	-5.17	1.72	1.88	0.92	
61	-0.50	-5.23	2.59	2.93	0.88	
62	-0.77	-5.48	2.32	2.63	0.88	
63	-0.53	-5.45	2.10	2.36	0.89	
64	-0.53	-5.02	3.15	3.60	0.87	
65	-0.78	-5.14	1.53	1.66	0.93	
66	-0.42	-4.94	2.75	3.17	0.87	
67	-0.67	-4.83	2.56	2.89	0.89	
68	-0.63	-4.91	1.56	1.69	0.92	
69	-0.39	-4.75	1.77	1.94	0.91	
70	-0.64	-4.76	2.27	2.55	0.89	
71	-0.82	-4.99	1.41	1.52	0.93	
72	-1.12	-5.08	1.37	1.52	0.90	
73	-0.95	-5.26	1.72	1.88	0.92	
74	-0.76	-5.17	1.86	2.04	0.91	
75	-0.70	-5.13	2.60	2.92	0.89	
76	-0.94	-5.07	2.20	2.43	0.91	
77	-0.77	-5.17	1.44	1.55	0.93	
78	-0.71	-5.07	2.41	2.72	0.89	
79	-0.86	-5.21	1.38	1.48	0.93	
80	-0.55	-5.09	1.40	1.51	0.93	
81	-0.43	-5.00	1.37	1.47	0.93	
82	-0.30	-5.20	2.20	2.44	0.90	
83	-0.30	-4.98	2.76	3.11	0.89	

Sample	$\delta^{13}C$	$\delta^{18}O$	SA44[V]	ST44[V]	Balance	volt <1.0
84	-0.43	-5.11	3.00	3.41	0.88	
85	-0.33	-5.14	2.35	2.63	0.89	
86	-0.37	-5.23	1.43	1.54	0.93	
87	-0.26	-5.19	1.59	1.73	0.92	
88	-0.15	-5.28	1.90	2.09	0.91	
89	-0.15	-5.15	1.85	2.02	0.92	
90	0.25	-4.97	1.64	1.78	0.92	
91	-0.06	-5.17	3.09	3.52	0.88	
92	0.14	-4.86	1.73	1.89	0.92	
93	0.28	-5.09	1.89	2.08	0.91	
94	0.09	-5.10	2.02	2.23	0.91	
95	0.88	-4.98	2.63	3.00	0.88	
96	0.63	-4.91	1.40	1.50	0.93	
97	0.85	-4.88	2.16	2.43	0.89	
98	0.79	-4.78	2.03	2.23	0.91	
99	0.65	-4.87	2.39	2.87	0.83	
100	-0.21	-4.99	2.21	2.47	0.90	
101	0.02	-5.02	2.63	3.00	0.88	
102	-0.43	-5.07	2.18	2.45	0.89	
103	-0.34	-5.06	1.76	1.93	0.91	
104	-0.63	-5.06	2.39	2.66	0.90	
105	-0.11	-5.00	2.66	2.98	0.89	
106	-0.24	-4.99	1.74	1.89	0.92	
107	-0.16	-4.86	2.15	2.37	0.91	
107	-0.14	-4.80	2.19	2.41	0.91	
108	-0.08	-4.94	2.18	2.41	0.90	
109	-0.41	-5.04	2.19	2.42	0.90	
110	-0.41	-5.06	1.56	1.69	0.92	
111	-0.36	-5.23	1.38	1.49	0.93	
112	-0.31	-5.08	2.67	3.00	0.89	
113	-0.61	-5.04	1.89	2.08	0.91	
114	0.30	-5.09	1.72	1.87	0.92	
115	-0.28	-5.14	1.41	1.52	0.93	
116	-0.09	-4.92	2.46	2.74	0.90	
117	-0.11	-4.97	2.22	2.47	0.90	
118	0.62	-4.92	2.37	2.64	0.90	
119	0.71	-5.00	1.51	1.63	0.93	
120	0.35	-4.67	2.41	2.72	0.89	
121	0.88	-4.85	2.37	2.64	0.90	
122	0.83	-4.87	1.30	1.38	0.94	
123	0.26	-4.81	2.05	2.26	0.91	
124	-0.46	-4.93	1.50	1.62	0.93	

Sample	$\delta^{13}C$	$\delta^{18}O$	SA44[V]	ST44[V]	Balance	volt <1.0
125	-0.43	-5.13	1.54	1.66	0.92	
126	-0.51	-5.04	1.66	1.79	0.93	
127	-0.26	-5.06	1.34	1.46	0.92	

All values reported relative to vPDB, where $\delta^{13}C$ has a value of +1.95‰ and $\delta^{18}O$ has a value of -2.20‰ for NBS19 calcite. Internal precision of measurements is 0.02-0.08‰ for $\delta^{18}O$ and 0.01-0.06‰ for $\delta^{13}C$, external precision is 0.03‰ for $\delta^{18}O$ and 0.02‰ for $\delta^{13}C$, relative to vPDB.

Appendix C: U/Pb and U/Th dating

Appendix Table 4 U/Pb and U/Th samples of fossil corals

Coral sample	U/Pb	U/Th
LM15	LM15/a, LM15/b, LM15/c, LM15/d, LM15/e, LM15/f, LM15/g	LM15/1, LM15/2, LM15/3, LM15/4, LM15/5, LM15/6, LM15/7
LM16a	LM16a/a, LM16a/b, LM16a/c, LM16a/d, LM16a/e	LM16a/1, LM16a/2, LM16a/3, LM16a/4, LM16a/5
LM16b	LM16b/a, LM16b/b, LM16b/c, LM16b/d, LM16b/e, LM16b/f, LM16b/g	LM16b/1, LM16b/2, LM16b/3, LM16b/4, LM16b/5, LM16b/6, LM16b/7
LM17	LM17/a, LM17/b, LM17/c, LM17/d, LM17/e	LM17/1, LM17/2, LM17/3, LM17/4, LM17/5
LM18a	LM18a/a, LM18a/b, LM18a/c, LM18a/d, LM18a/e	LM18a/1, LM18a/2, LM18a/3, LM18a/4, LM18a/5
LM18b	LM18b/a, LM18b/b, LM18b/c, LM18b/d, LM18b/e	LM18b/1, LM18b/2, LM18b/3, LM18b/4, LM18b/5
LM18c	LM18c/a, LM18c/b, LM18c/c, LM18c/d, LM18c/e	LM18c/1, LM18c/2, LM18c/3, LM18c/4, LM18c/5
LM22b	LM22b/a, LM22b/b, LM22b/c, LM22b/d, LM22b/e	LM22b/1, LM22b/2, LM22b/3, LM22b/4, LM22b/5
TL07	TL01/a, TL07/b, TL07/c, TL07/d, TL07/e, TL07/f	TL01/1, TL07/2, TL07/3, TL07/4, TL07/5, TL07/6
TL289	TL289/a, TL289/b, TL289/c, TL289/d, TL289/e, TL289/f, TL289/g	TL289/1, TL289/2, TL289/3, TL289/4, TL289/5, TL289/6, TL289/7
Beluli River A	BRA/a, BRA/b, BRA/c, BRA/d, BRA/e	BRA/1, BRA/2, BRA/3, BRA/4, BRA/5
Beluli River B	BRB/a, BRB/b, BRB/c, BRB/d, BRB/e	BRB/1, BRB/2, BRB/3, BRB/4, BRB/5
Beluli River C	BRC/a, BRC/b, BRC/c, BRC/d, BRC/e	BRC/1, BRC/2, BRC/3, BRC/4, BRC/5